Flows in porous channels

Harwin, Damien Anthony

Award date:
2007

Awarding institution:
University of Bath

Flows in Porous Channels

submitted by

Damien Anthony Harwin

for the degree of Doctor of Philosophy

of the

University of Bath

Department of Mathematical Sciences

July 2007

ProQuest LLC
789 East Eisenhower Parkway
P.O. Box 1346
Ann Arbor, MI 48106-1346

Table of Contents

List of Figures

Acknowledgements

I must first thank God for sending his only Son Jesus Christ into the world to die for me so that I might be set free from my sins and have the opportunity of a restored personal relationship with the Father. Through all of my studies I have been encouraged by the Holy Spirit and have sought to be all that God has called me to be as a Christian.

I would like to thank my wife Petra for all her love, support and patience throughout the course of my studies. She has been through all the different emotions that postgraduate study brings during her own doctorate; for her to stand by me while I complete my studies has been a source of encouragement, physically, emotionally and spiritually. I also thank my family: Dad and Mum, Simon, Barry and Stella, Nan, Adam and Heidi, Benjamin and Elisha for all their love, support, concerns, willingness to listen (even when it doesn't make sense), enjoyable times away from Bath and, in the case of Benjamin and Elisha, just being kids who accept you just as you are and who want to know when Uncle Damo is visiting again. I would also like to thank all my friends from Bath City Church over the years, with whom I have shared my experiences and from whom I have again and again received prayers, fellowship and encouragement: Haydn and Muriel, Jo, Nathaniel, Maurice and Penny, John and Alyssa, Jessica, James and Sally, Abigail, Harry, John and Katherine, Graham, Peter and Denise, Chris and Leigh, Daniel, Samantha, Neil and Joy, Eamonn and Louise, Lynette, Lilian and Dhana, Peter and Zhvina, Hannah, John and Sue, Abigail and Sharon.

I would like to thank my supervisor, Jonathan Evans, for his guidance throughout my studies. I would also thank my colleagues, some of whom are long gone and some who are still on the way to their doctorate: Steve, Jörg, Jf, Paul, Andy, André, Jenny, Patrick, Matt, James, Doku, Lorina, Eugen, Barrie, Duncan, Jason, Vicky and Zoë. Also a great amount of thanks is due to all the administrative and computer support staff who work behind the scenes to make the Department such an enjoyable place to work.

Summary

This thesis considers the problem of the steady flow of an incompressible non-Newtonian viscous fluid through a channel with porous walls, under conditions of suction or injection through the walls and possibly in the presence of a temperature gradient. The non-Newtonian viscosity function is either of power-law type or has an exponential dependence upon the temperature within the channel. Solutions of similarity type are sought for the stream function and asymptotic results are presented. Numerical solutions of the reduced similarity equation system are performed and initial linear stability calculations are given.

Chapter 1

Introduction

1.1 Applications

The instance of laminar flow through a channel with porous walls is an idealisation of the flow behaviour that occurs in the real world in corresponding geometries. It can be used to model processes such as transpiration cooling, where the walls of a pipe or channel containing heated fluid are protected from overheating by passing cooler fluid over the exterior surface of the pipe or channel; another application is to model the fluid flow occurring during the separation of isotopes of Uranium-235 and Uranium-238 by gaseous diffusion in order to produce fuel for nuclear reactors; controlling boundary layer flow over aircraft wings by injection or suction of fluid out of or into the wing, or as part of a model for flow past a membrane or filter. Whereas some of these can be situations where one or both of the walls of the channel are porous, a motivation for [Cox91a] is that in an experimental situation, having both walls porous means that experimental equipment would obstruct the observation of any flow within the channel; having one transparent solid wall would allow observations to be made. The fluid flow underlying gaseous diffusion for nuclear fuel was the motivation for Berman's 1953 paper [Ber53] that describes the problem that now bears his name.

The variation of viscosity with respect to temperature or shearing within a flow situation is one way of reconciling the difference between mathematical models and reality. A fluid model with constant viscosity is not a good choice for describing flows which have some microstructure or other material property that may change with temperature e.g. industrial lubricants, polymers. It may be the case that the viscosity of the material will decrease with increasing temperature, and so a constant viscosity model may predict inaccurate results in experiments. In addition, the flowing materials may have a nonlinear relationship between their viscosity and applied shear, e.g. shear-

thickening, where the viscosity increases with shear-rate so that it becomes harder to deform the material under the same rate of applied shearing, or shear-thinning, (which is the opposite effect) where the viscosity decreases as the shear-rate increases, so it become easier to deform the material under the same rate of shearing. Materials with these nonlinear and complex behaviours can only be modelled approximately and so there will be many different models which could be chosen to describe their viscosities.

1.2 Problem formulation

We wish to consider the steady two-dimensional laminar flow of an incompressible viscous fluid within a channel. The fluid is assumed to be of a non-Newtonian type, with a viscosity that may depend upon both the stresses and temperature effects that the fluid is experiencing. The channel can have uniformly porous walls or a single porous wall through which fluid may be withdrawn or introduced. In addition a temperature difference may be imposed between the walls of the channel. The effects of viscous generation of heat due to internal friction are neglected in this work.

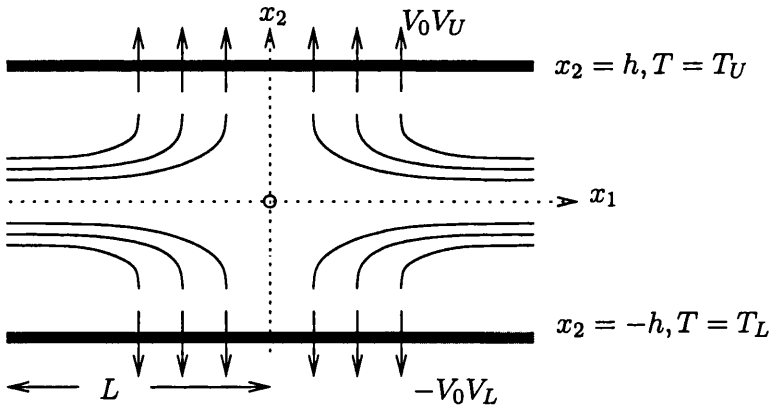

Figure 1.2.1. Channel geometry for both the one and two porous walled cases.

A Cartesian (x_1, x_2) coordinate system is set up within the channel with the x_1 axis located midway between, and parallel to, the channel walls, which are at $x_2 = \pm h$. The upper wall is held at a constant temperature T_U and the lower wall is held at a constant temperature T_L.

The main dimensional equations that will govern the fluid flow and temperature

$\mathbf{u}(x_1, x_2, t) = (q_1(x_1, x_2, t),\ q_2(x_1, x_2, t))$	fluid velocity vector
$T(x_1, x_2, t)$	temperature
$p(x_1, x_2, t)$	fluid pressure
$x_1,\ x_2,\ t$	coordinate directions and time
ρ	fluid density (constant)
k	fluid thermal conductivity (constant)
c	specific heat of fluid (constant)
$\kappa = \frac{k}{\rho c}$	fluid thermal diffusivity (constant)
$\mu(\Pi_d, T)$	shear rate and temperature dependent fluid viscosity
$\Pi_A = \frac{1}{2}(A_{ii}A_{jj} - A_{ij}A_{ji})$	second invariant of tensor A
$\sigma_{ij} = -p\delta_{ij} + T_{ij}$	Cauchy stress tensor ($i, j \in \{1, 2\}$) being the sum of the fluid pressure and the deviatoric stress tensor
$T_{ij} = 2\mu d_{ij}$	deviatoric stress tensor (zero when no shear stresses acting)
$\delta_{ij} = \begin{cases} 1, & i = j \\ 0, & i \neq j \end{cases}$	Kronecker delta tensor ($i, j \in \{1, 2\}$)
$d_{ij} = \frac{1}{2}\left(\frac{\partial q_i}{\partial x_j} + \frac{\partial q_j}{\partial x_i}\right)$	symmetric rate of deformation tensor ($i, j \in \{1, 2\}$)
Φ	function describing the rate of viscous dissipation of energy as heat

Table 1.1. List of notation.

profile can be stated as follows,

$$\frac{\partial q_i}{\partial x_i} = 0, \tag{1.2.1}$$

$$\rho\left(\frac{\partial q_i}{\partial t} + q_j\frac{\partial q_i}{\partial x_j}\right) = \frac{\partial \sigma_{ij}}{\partial x_j}, \tag{1.2.2}$$

$$\sigma_{ij} = \sigma_{ji}, \tag{1.2.3}$$

$$\rho c\left(\frac{\partial T}{\partial t} + q_i\frac{\partial T}{\partial x_i}\right) = \frac{\partial}{\partial x_i}\left(k\frac{\partial T}{\partial x_i}\right) + \Phi, \tag{1.2.4}$$

$$\Phi = \sigma_{ij}d_{ij}, \tag{1.2.5}$$

where the notation is defined in Table 1.1. These equations represent the conservation of mass in a fluid particle, conservation of linear momentum, conservation of angular momentum, conservation of energy and finally the definition of the rate of viscous dissipation of energy as heat. In stating these we have assumed that the density of the fluid is constant and that there are no body forces acting upon the fluid as a whole (e.g. gravity). In addition, the temperature equation has been stated with the assumption that the total internal energy of the fluid does not explicitly depend upon any kinematic quantity, e.g. the strain-rate or stress tensor, but it may depend upon the pressure and temperature.

The conservation of mass statement can be interpreted as the identity[1]

$$I_d = d_{ii} = 0. \tag{1.2.6}$$

It remains to specify the form of the viscosity function before stating the final set of dimensional governing equations for the problem. Let us assume that the dependencies upon temperature and shear rate factor into the form

$$\mu = F_1(T)F_2(\Pi_d). \tag{1.2.7}$$

The second factor, $F_2(\Pi_d)$, describes the variation of the viscosity with shear rate. A commonly used model is the power-law model,

$$F_2 = K\left|\Pi_d\right|^{n-1}, \tag{1.2.8}$$

where the second tensor invariant Π_d is defined in Table 1.1. The nondimensional exponent n determines the type of fluid under consideration. The parameter K is the

[1]The summation convention is adopted, whereby repeated indices indicate summation over the possible values of that index. In this case the index i may take the values $1, 2$.

Material	Consistency index K (Pas^n)	n	Shear rate range (s^{-1})
Ball-point pen ink	10	0.85	$10^0 - 10^3$
Fabric conditioner	10	0.6	$10^0 - 10^2$
Polymer melt	10000	0.6	$10^2 - 10^4$
Molten chocolate	50	0.5	$10^{-1} - 10$
Synovial fluid	0.5	0.4	$10^{-1} - 10^2$
Toothpaste	300	0.3	$10^0 - 10^3$
Skin cream	250	0.1	$10^0 - 10^2$
Lubricating grease	1000	0.1	$10^{-1} - 10^2$
Conc. corn starch solution	0.131	1.72	10^0

Table 1.2. Typical values of the power-law parameters of common materials for a particular range of shear rates. Collated from [BHW89, page 22], [Ste96, page 80].

consistency index and has units of Pas^n. If $n = 1$ the Newtonian fluid model is recovered, where K assumes the role of the dynamic fluid viscosity. If $0 < n < 1$ then the fluid is said to be shear-thinning and the viscosity decreases as the rate of shear increases. If $n > 1$ then the fluid is shear-thickening and the viscosity decreases as the shear rate increases. Shear-thinning fluids are more common than shear-thickening fluids, and shear-thinning fluids are usually found in industrial applications such as lubricants. Some typical values of the exponent n and consistency index K are shown in Table 1.2, the data being reproduced from the work of Barnes, Hutton and Walters [BHW89, page 22] and Steffe [Ste96, page 80]. Both K and n are in general temperature dependent, but the temperature dependence of n is so weak that it is acceptable to use a constant n, [BAH87, page 210]. The temperature dependence of K can be absorbed into the first functional factor of μ, and so we consider K constant here.

The first factor, $F_1(T)$, describes the dependence of the viscosity upon the fluid temperature. It it usual that the viscosity will decrease monotonically as the temperature increases. It is generally found that the temperature dependence produces a linear shift a_T in the value of the viscosity when plotting the logarithm of the viscosity versus the logarithm of the shear rate [BAH87, page 139], [Tan00, page 459]. This shift can be expressed as the following ratio,

$$a_T = \frac{\mu(T)T_0\rho_0}{\mu(T_0)T\rho} = \frac{\mu(T)T_0}{\mu(T_0)T} \quad (\text{as } \rho \text{ is constant}). \tag{1.2.9}$$

This can then be rearranged to give an expression for the overall viscosity at temperature T given a reference value at temperature T_0. An initial functional form for the

temperature dependence is provided by the Andrade model (also referred to as the Arrhenius model) [BAH87, page 140],[Tan00, page 451] and is given by

$$\mu = \text{const} * \exp\left(\frac{E}{RT}\right) = \exp\left(\frac{E}{RT_0}\right) \exp\left(\frac{E}{R}\left(\frac{1}{T} - \frac{1}{T_0}\right)\right), \tag{1.2.10}$$

where E is the activation energy of the fluid molecules (different for each fluid), R is the universal gas constant ($8.314 J/(Kmol)$), T is the absolute temperature of the fluid and T_0 is a reference temperature. However, for small temperature variation, this can be approximated and we will consider two common functional forms: one exponential and one algebraic. In both cases the viscosity decreases monotonically as the temperature increases. In this situation we can omit the small ratio T_0/T in a_T as it is approximately unity. More specifically we take

$$F_1(T) = \exp\left(\frac{E}{RT_0}\right) \exp\left(\frac{E}{R}\left(\frac{1}{T} - \frac{1}{T_0}\right)\right), \tag{1.2.11}$$

$$\approx \begin{cases} \exp\left(\frac{E}{RT_0}\right) \exp\left(\frac{E}{RT_0}\left(\frac{T_0 - T}{T}\right)\right), \\ \left(1 + \frac{E}{RT_0}\right)\left(1 + \frac{E}{RT_0}\frac{T_0 - T}{T}\right). \end{cases} \tag{1.2.12}$$

The final functional dependence of the viscosity upon temperature and shear rate is of the form

$$\mu = F_1(T) K \left|\Pi_d\right|^{n-1}. \tag{1.2.13}$$

In summary, the dimensional set of governing partial differential equations that are to be solved for the fluid flow and temperature problems are

$$\frac{\partial q_1}{\partial x_1} + \frac{\partial q_2}{\partial x_2} = 0, \tag{1.2.14a}$$

$$\rho \frac{Dq_1}{Dt} = -\frac{\partial p}{\partial x_1} + \frac{\partial}{\partial x_1}\left(2\mu \frac{\partial q_1}{\partial x_1}\right) + \frac{\partial}{\partial x_2}\left(\mu \frac{\partial q_1}{\partial x_2}\right) + \frac{\partial}{\partial x_2}\left(\mu \frac{\partial q_2}{\partial x_1}\right), \tag{1.2.14b}$$

$$\rho \frac{Dq_2}{Dt} = -\frac{\partial p}{\partial x_2} + \frac{\partial}{\partial x_1}\left(\mu \frac{\partial q_2}{\partial x_1}\right) + \frac{\partial}{\partial x_1}\left(\mu \frac{\partial q_1}{\partial x_2}\right) + \frac{\partial}{\partial x_2}\left(2\mu \frac{\partial q_2}{\partial x_2}\right), \tag{1.2.14c}$$

$$\rho c \frac{DT}{Dt} = k \frac{\partial^2 T}{\partial x_1^2} + k \frac{\partial^2 T}{\partial x_2^2} + \Phi, \tag{1.2.14d}$$

$$\Phi = \sigma_{ij} d_{ij} = \left(-p\delta_{ij} + T_{ij}\right) d_{ij} =$$

$$2\mu \left\{ \left(\frac{\partial q_1}{\partial x_1}\right)^2 + \frac{1}{2}\left(\frac{\partial q_1}{\partial x_2}\right)^2 + \frac{\partial q_1}{\partial x_2}\frac{\partial q_2}{\partial x_1} + \frac{1}{2}\left(\frac{\partial q_2}{\partial x_1}\right)^2 + \left(\frac{\partial q_2}{\partial x_2}\right)^2 \right\}, \tag{1.2.14e}$$

$$\text{on } x_2 = +h: \quad q_1(x_1, h, t) = 0, \quad q_2(x_1, h, t) = V_0 V_U(x_1), \quad T = T_U, \tag{1.2.14f}$$

$$\text{on } x_2 = -h: \quad q_1(x_1, -h, t) = 0, \quad q_2(x_1, -h, t) = -V_0 V_L(x_1), \quad T = T_L, \tag{1.2.14g}$$

where the symbol $\frac{D}{Dt}$ denotes the material derivative and is defined to be

$$\frac{D}{Dt}(\cdot) = \frac{\partial}{\partial t}(\cdot) + (\boldsymbol{u} \cdot \nabla)(\cdot), \qquad \nabla = \left(\frac{\partial}{\partial x_1}, \frac{\partial}{\partial x_2}\right). \tag{1.2.15}$$

The boundary conditions being applied are that of no-slip, an upper- and lower-wall normal fluid speed (which may be position dependent) and an upper- and lower-wall temperature profile. We restrict attention to temperature profiles that are constant with respect to longitudinal position. The final parameter, E, is defined to be

$$E = 1 - V_L(x_1)/V_U(x_1) \quad (\text{thus } V_L(x_1) = (1-E)V_U(x_1)) \tag{1.2.16}$$

and allows a degree of problem selection: if $E = 0$ we have the two porous walled problem as stated above; if $E = 1$ we obtain a problem where there is no fluid motion through the lower wall; finally if $0 < E < 1$ there are different rates of fluid extraction or injection through the walls. We require $V_U(x_1)$ and $V_L(x_1)$ to be non-negative functions and so the sign of V_0 controls whether fluid is being introduced to or removed from the channel through the porous walls. We restrict our attention to $E \in [0,1]$ and so have $0 \leq V_L(x_1) \leq V_U(x_1)$; if $E \in (-\infty, 0]$ then $0 \leq V_U(x_1) \leq V_L(x_1)$ would hold and if $E \notin (-\infty, 1]$ then channel cross-flow would occur as the non-negativity conditions upon $V_L(x_1)$ and $V_U(x_1)$ would no longer hold. In this work we are not considering channel cross-flow situations and choose to limit consideration to $E \in [0,1]$, although the expanded range $E \in [-1,1]$ could in principle be considered in the same way.

1.3 Problem nondimensionalisation

The next step is to nondimensionalise the system in order that terms may be consistently compared. It is not possible to make comparisons prior to nondimensionalisation because each quantity in the system has a physical dimension and it is nonsensical to compare quantities of differing physical dimension. Once these dimensions have been removed the sizes of the nondimensional terms may be estimated and progress may be made to simplify the governing system, where possible. The nondimensionalisation process is the first step in refining a model by being able to identify the processes that are most influential upon the system given the values of the parameters at that time.

Typical values for characteristic dimensions are chosen in accordance with the problem in hand. In this case we nondimensionalise the system with the following changes

of variables:

$$x_1 = L\bar{x},\ x_2 = h\bar{y},\ q_1 = \frac{V_0 V_U L}{h}\bar{u},\ q_2 = V_0 V_U \bar{v},\ t = \frac{h}{V_0 V_U}\bar{t},$$
$$\mu = \underbrace{M_0 K \left|\frac{V_0 V_U L}{2h^2}\right|^{n-1}}_{=\mu_0}\bar{\mu},\ p = \rho V_0^2 V_U^2 P\bar{p},\ T = T_0 + \underbrace{\Delta_T}_{=T_L - T_U}\bar{\theta}, \tag{1.3.1}$$

where h is a characteristic channel half-width, Δ_T a characteristic temperature difference $T_L - T_U$ across the channel width, μ_0 denotes the fluid viscosity at temperature T_0 (and shear rate h/V_0V_U if applicable) and $\varepsilon = h/L$ is the aspect ratio of the channel. The characteristic fluid velocity is taken to be V_0V_U, where V_U is a non-negative constant characteristic fluid speed and the sign of V_0 determines whether there is suction or injection occurring. The pressure has been scaled with inertia and an additional parameter P, which can be chosen to find consistent scalings for the different regimes under consideration.

The nondimensionalisation for the viscosity is obtained by expanding the definition of μ and requiring that the nondimensional viscosity $\bar{\mu}$ is $\mathcal{O}(1)$. The reference value of T_0 is chosen to be T_U, the temperature of the upper wall, and then the temperature problem is that of a cooler upper wall than lower wall if $\Delta_T > 0$ (the heated channel problem) and a hotter upper wall than lower wall if $\Delta_T < 0$ (cooled channel problem). Using $M(T)$ to denote the generic temperature dependence for convenience, the nondimensionalisation for the viscosity is found after the following manipulation,

$$\begin{aligned}
\mu &= M(T)K\left|-\frac{1}{2}\left(\left(\frac{\partial q_1}{\partial x_1}\right)^2 + \frac{1}{2}\left(\frac{\partial q_1}{\partial x_2}\right)^2 + \frac{\partial q_1}{\partial x_2}\frac{\partial q_2}{\partial x_1} + \frac{1}{2}\left(\frac{\partial q_2}{\partial x_1}\right)^2 + \left(\frac{\partial q_2}{\partial x_2}\right)^2\right)\right|^{\frac{n-1}{2}} \\
&= M(T)K\left|\frac{1}{2}\frac{V_0^2V_U^2}{h^2}\right|^{\frac{n-1}{2}}\left|\left(\frac{\partial \bar{u}}{\partial \bar{x}}\right)^2 + \frac{1}{2}\frac{L^2}{h^2}\left(\frac{\partial \bar{u}}{\partial \bar{y}}\right)^2 + \frac{\partial \bar{u}}{\partial \bar{y}}\frac{\partial \bar{v}}{\partial \bar{x}} + \frac{1}{2}\frac{h^2}{L^2}\left(\frac{\partial \bar{v}}{\partial \bar{x}}\right)^2 + \left(\frac{\partial \bar{v}}{\partial \bar{y}}\right)^2\right|^{\frac{n-1}{2}} \\
&= M(T)K\left|\frac{1}{2}\frac{V_0^2V_U^2L^2}{h^4}\right|^{\frac{n-1}{2}}\left|\frac{h^2}{L^2}\left(\frac{\partial \bar{u}}{\partial \bar{x}}\right)^2 + \frac{1}{2}\left(\frac{\partial \bar{u}}{\partial \bar{y}}\right)^2 + \frac{h^2}{L^2}\frac{\partial \bar{u}}{\partial \bar{y}}\frac{\partial \bar{v}}{\partial \bar{x}} + \frac{1}{2}\frac{h^4}{L^4}\left(\frac{\partial \bar{v}}{\partial \bar{x}}\right)^2 + \frac{h^2}{L^2}\left(\frac{\partial \bar{v}}{\partial \bar{y}}\right)^2\right|^{\frac{n-1}{2}} \\
&= M(T)K\left|\frac{V_0^2V_U^2L^2}{4h^4}\right|^{\frac{n-1}{2}}\left|\left(\frac{\partial \bar{u}}{\partial \bar{y}}\right)^2 + \mathcal{O}\left(\frac{h^2}{L^2}\right)\right|^{\frac{n-1}{2}} \\
&\approx M_0K\left|\frac{V_0^2V_U^2L^2}{4h^4}\right|^{\frac{n-1}{2}} M(\bar{\theta})\left|\left(\frac{\partial \bar{u}}{\partial \bar{y}}\right)^2\right|^{\frac{n-1}{2}}
\end{aligned}$$

where M_0 is the contribution to the reference viscosity μ_0 at fixed temperature T_0 and $M(\bar{\theta})$ is the nondimensional temperature dependent contribution to the viscosity. The

nondimensional quantities M_0 and $M(\bar{\theta})$ are found to be

$$\text{either } M(T) = \mathrm{e}^{\frac{E}{RT_0}}\mathrm{e}^{\frac{E}{RT_0^2}(T-T_0)} = \mathrm{e}^{\frac{E}{RT_0}}\mathrm{e}^{-\frac{E\Delta_T}{RT_0^2}\bar{\theta}} = M_0^e M^e(\bar{\theta}), \tag{1.3.2a}$$

$$\text{or } M(T) = \left(1+\frac{E}{RT_0}\right)\left(1-\frac{E\Delta_T\bar{\theta}}{RT_0^2}\right) = M_0^a M^a(\bar{\theta}), \tag{1.3.2b}$$

and we then take either M_0^a and $M^a(\bar{\theta})$ or M_0^e and $M^e(\bar{\theta})$ for M_0 and $M(\bar{\theta})$ respectively.

The governing equations are now expressed as

$$\frac{V_0V_U}{h}\frac{\partial\bar{u}}{\partial\bar{x}} + \frac{V_0V_U}{h}\frac{\partial\bar{v}}{\partial\bar{y}} = 0, \tag{1.3.3a}$$

$$\frac{\rho V_0^2V_U^2L}{h^2}\frac{D\bar{u}}{D\bar{t}} = -\frac{\rho V_0^2V_U^2}{L}P\frac{\partial\bar{p}}{\partial\bar{x}} + \frac{V_0V_UM_0K}{Lh}\left|\frac{V_0^2V_U^2L^2}{4h^4}\right|^{\frac{n-1}{2}}\frac{\partial}{\partial\bar{x}}\left(2\bar{\mu}\frac{\partial\bar{u}}{\partial\bar{x}}\right)$$
$$+\frac{V_0V_UM_0KL}{h^3}\left|\frac{V_0^2V_U^2L^2}{4h^4}\right|^{\frac{n-1}{2}}\frac{\partial}{\partial\bar{y}}\left(\bar{\mu}\frac{\partial\bar{u}}{\partial\bar{y}}\right) + \frac{V_0V_UM_0K}{Lh}\left|\frac{V_0^2V_U^2L^2}{4h^4}\right|^{\frac{n-1}{2}}\frac{\partial}{\partial\bar{y}}\left(\bar{\mu}\frac{\partial\bar{v}}{\partial\bar{x}}\right), \tag{1.3.3b}$$

$$\frac{\rho V_0^2V_U^2}{h}\frac{D\bar{v}}{D\bar{t}} = -\frac{\rho V_0^2V_U^2}{h}P\frac{\partial\bar{p}}{\partial\bar{y}} + \frac{V_0V_UM_0K}{L^2}\left|\frac{V_0^2V_U^2L^2}{4h^4}\right|^{\frac{n-1}{2}}\frac{\partial}{\partial\bar{x}}\left(\bar{\mu}\frac{\partial\bar{v}}{\partial\bar{x}}\right)$$
$$+\frac{V_0V_UM_0K}{h^2}\left|\frac{V_0^2V_U^2L^2}{4h^4}\right|^{\frac{n-1}{2}}\frac{\partial}{\partial\bar{x}}\left(\bar{\mu}\frac{\partial\bar{u}}{\partial\bar{y}}\right) + \frac{V_0V_UM_0K}{h^2}\left|\frac{V_0^2V_U^2L^2}{4h^4}\right|^{\frac{n-1}{2}}\frac{\partial}{\partial\bar{y}}\left(2\bar{\mu}\frac{\partial\bar{v}}{\partial\bar{y}}\right), \tag{1.3.3c}$$

$$\frac{\rho cV_0V_U\Delta_T}{h}\frac{D\bar{\theta}}{D\bar{t}} = \frac{k\Delta_T}{L^2}\frac{\partial^2\bar{\theta}}{\partial\bar{x}^2} + \frac{k\Delta_T}{h^2}\frac{\partial^2\bar{\theta}}{\partial\bar{y}^2} + \bar{\Phi}, \tag{1.3.3d}$$

$$\bar{\Phi} = 2\frac{V_0^2V_U^2M_0K}{h^4}\left|\frac{V_0^2V_U^2L^2}{4h^4}\right|^{\frac{n-1}{2}}\bar{\mu}\left\{\frac{h^2}{L^2}\left(\frac{\partial\bar{u}}{\partial\bar{x}}\right)^2 + \frac{1}{2}\left(\frac{\partial\bar{u}}{\partial\bar{y}}\right)^2 + \frac{h^2}{L^2}\frac{\partial\bar{u}}{\partial\bar{y}}\frac{\partial\bar{v}}{\partial\bar{x}}\right.$$
$$\left.+\frac{1}{2}\frac{h^4}{L^4}\left(\frac{\partial\bar{v}}{\partial\bar{x}}\right)^2 + \frac{h^2}{L^2}\left(\frac{\partial\bar{v}}{\partial\bar{y}}\right)^2\right\}, \tag{1.3.3e}$$

$$\text{on } \bar{y}=+1: \quad \bar{u}=0, \quad \bar{v}=V(\bar{x}), \quad \bar{\theta}=0, \qquad (\text{where } V(\bar{x}) = V_U(\bar{x})/V_U) \tag{1.3.3f}$$

$$\text{on } \bar{y}=-1: \quad \bar{u}=0, \quad \bar{v}=(-1+E)V(\bar{x}), \quad \bar{\theta}=1. \tag{1.3.3g}$$

We now define the nondimensional groups

- $\mathrm{Re} = \rho V_0V_Uh \Big/ \left(M_0K\left|\frac{V_0V_UL}{2h^2}\right|^{n-1}\right)$, the Reynolds number, comparing the effects of inertia and viscosity;
- $\mathrm{Pe} = \frac{\rho cV_0V_Uh}{k}$, the Péclet number, comparing the convective and thermal conductive length scales;

- $\mathrm{Pr} = \frac{\mathrm{Pe}}{\mathrm{Re}} = \frac{cM_0K\left|\frac{V_0V_UL}{2h^2}\right|^{n-1}}{k}$, the Prandtl number, comparing the relative effects of thermal conductivity and inertia;
- $\mathrm{Br} = \frac{M_0KV_0^2V_U^2L^2\left|\frac{V_0V_UL}{2h^2}\right|^{n-1}}{k\Delta_Th^2}$, the Brinkman number, comparing the thermal effects from the heat produced by viscous dissipation against the effects of heat conduction;
- $\mathrm{Na} = \frac{V_0^2V_U^2\left|\frac{d\mu}{dT}\right|_{T=T_0}}{k}$, the Nahme-Griffith number, comparing the heat generated by viscous dissipation against the temperature change required to change the viscosity substantially;
- $\beta = \frac{\mathrm{Na}}{\mathrm{Br}} = \Delta_T\left|\frac{\frac{d\mu}{dT}}{\mu}\right|_{T=T_0}$, which measures the sensitivity of the viscosity to changes in temperature.

In the cases of the full Andrade model with the algebraic and exponential approximations (1.2.12), the sensitivity parameter β has the common value of

$$\beta = \frac{E\Delta_T}{RT_0^2}.$$

In both the algebraic and exponential cases we make the assumption that

$$\frac{\mu(\beta T)}{\mu(\beta \cdot 1)} = \mathcal{O}(1) \text{ as } \beta \to \infty \text{ for } T = \mathcal{O}(1), \tag{1.3.4}$$

and we define $\mu_0 = \mu(\beta)$ and $\mu_0 \ll 1$, where μ has been evaluated with a typical shear rate for the fluid. The $\beta \to \infty$ limit corresponds to a biviscosity fluid model, that is a fluid which has two distinct values for its viscosity.

Using these nondimensional groups, we may rewrite the governing equations in the

form

$$\frac{\partial \bar{u}}{\partial \bar{x}} + \frac{\partial \bar{v}}{\partial \bar{y}} = 0, \tag{1.3.5a}$$

$$\mathrm{Re}\frac{D\bar{u}}{D\bar{t}} = -\mathrm{Re}\varepsilon^2 P\frac{\partial \bar{p}}{\partial \bar{x}} + \varepsilon^2\frac{\partial}{\partial \bar{x}}\left(2\bar{\mu}\frac{\partial \bar{u}}{\partial \bar{x}}\right) + \frac{\partial}{\partial \bar{y}}\left(\bar{\mu}\frac{\partial \bar{u}}{\partial \bar{y}}\right) + \varepsilon^2\frac{\partial}{\partial \bar{y}}\left(\bar{\mu}\frac{\partial \bar{v}}{\partial \bar{x}}\right), \tag{1.3.5b}$$

$$\mathrm{Re}\varepsilon\frac{D\bar{v}}{D\bar{t}} = -\mathrm{Re}\varepsilon P\frac{\partial \bar{p}}{\partial \bar{y}} + \varepsilon^3\frac{\partial}{\partial \bar{x}}\left(\bar{\mu}\frac{\partial \bar{v}}{\partial \bar{x}}\right) + \varepsilon\frac{\partial}{\partial \bar{x}}\left(\bar{\mu}\frac{\partial \bar{u}}{\partial \bar{y}}\right) + \varepsilon\frac{\partial}{\partial \bar{y}}\left(2\bar{\mu}\frac{\partial \bar{v}}{\partial \bar{y}}\right), \tag{1.3.5c}$$

$$\mathrm{Pe}\frac{D\bar{\theta}}{D\bar{t}} = \varepsilon^2\frac{\partial^2\bar{\theta}}{\partial \bar{x}^2} + \frac{\partial^2\bar{\theta}}{\partial \bar{y}^2} + \bar{\Phi}, \tag{1.3.5d}$$

$$\bar{\Phi} = 2\mathrm{Br}\left|\varepsilon^2\left(\frac{\partial \bar{u}}{\partial \bar{x}}\right)^2 + \frac{1}{2}\left(\frac{\partial \bar{u}}{\partial \bar{y}}\right)^2 + \varepsilon^2\frac{\partial \bar{u}}{\partial \bar{y}}\frac{\partial \bar{v}}{\partial \bar{x}} + \frac{1}{2}\varepsilon^4\left(\frac{\partial \bar{v}}{\partial \bar{x}}\right)^2 + \varepsilon^2\left(\frac{\partial \bar{v}}{\partial \bar{y}}\right)^2\right|^{\frac{n-1}{2}} *$$

$$\left\{\varepsilon^2\left(\frac{\partial \bar{u}}{\partial \bar{x}}\right)^2 + \frac{1}{2}\left(\frac{\partial \bar{u}}{\partial \bar{y}}\right)^2 + \varepsilon^2\frac{\partial \bar{u}}{\partial \bar{y}}\frac{\partial \bar{v}}{\partial \bar{x}} + \frac{1}{2}\varepsilon^4\left(\frac{\partial \bar{v}}{\partial \bar{x}}\right)^2 + \varepsilon^2\left(\frac{\partial \bar{v}}{\partial \bar{y}}\right)^2\right\}, \tag{1.3.5e}$$

$$\text{on } \bar{y} = +1\text{:}\quad \bar{u} = 0,\quad \bar{v} = V(\bar{x}),\quad \bar{\theta} = 0, \tag{1.3.5f}$$

$$\text{on } \bar{y} = -1\text{:}\quad \bar{u} = 0,\quad \bar{v} = (-1+E)V(\bar{x}),\quad \bar{\theta} = 1. \tag{1.3.5g}$$

The Reynolds and Péclet numbers share the same sign, but this sign is reversed when the flow changes from injection through the walls to suction through the walls of the channel.

In order to balance the effects of pressure and viscosity, we now set $P = \left(\varepsilon^2\mathrm{Re}\right)^{-1}$. If we now introduce a stream function

$$\psi(x_1, x_2) = V_0 V_U L\bar{\psi}(\bar{x}, \bar{y}) \quad \text{where} \quad (\bar{u}, \bar{v}) = \left(\frac{\partial \bar{\psi}}{\partial \bar{y}}, -\frac{\partial \bar{\psi}}{\partial \bar{x}}\right) \tag{1.3.6}$$

then the continuity equation is automatically satisfied, and the system becomes,

$$\mathrm{Re}\frac{D}{D\bar{t}}\left(\frac{\partial\bar{\psi}}{\partial\bar{y}}\right) = -\frac{\partial\bar{p}}{\partial\bar{x}} + \varepsilon^2\frac{\partial}{\partial\bar{x}}\left(2\bar{\mu}\frac{\partial^2\bar{\psi}}{\partial\bar{x}\partial\bar{y}}\right) + \frac{\partial}{\partial\bar{y}}\left(\bar{\mu}\frac{\partial^2\bar{\psi}}{\partial\bar{y}^2}\right) - \varepsilon^2\frac{\partial}{\partial\bar{y}}\left(\bar{\mu}\frac{\partial^2\bar{\psi}}{\partial\bar{x}^2}\right), \tag{1.3.7a}$$

$$-\mathrm{Re}\varepsilon\frac{D}{D\bar{t}}\left(\frac{\partial\bar{\psi}}{\partial\bar{x}}\right) = -\frac{1}{\varepsilon}\frac{\partial\bar{p}}{\partial\bar{y}} - \varepsilon^3\frac{\partial}{\partial\bar{x}}\left(\bar{\mu}\frac{\partial^2\bar{\psi}}{\partial\bar{x}^2}\right) + \varepsilon\frac{\partial}{\partial\bar{x}}\left(\bar{\mu}\frac{\partial^2\bar{\psi}}{\partial\bar{y}^2}\right) - \varepsilon\frac{\partial}{\partial\bar{y}}\left(2\bar{\mu}\frac{\partial^2\bar{\psi}}{\partial\bar{y}\partial\bar{x}}\right), \tag{1.3.7b}$$

$$\mathrm{Pe}\frac{D\bar{\theta}}{D\bar{t}} = \varepsilon^2\frac{\partial^2\bar{\theta}}{\partial\bar{x}^2} + \frac{\partial^2\bar{\theta}}{\partial\bar{y}^2} + \bar{\Phi}, \tag{1.3.7c}$$

$$\bar{\Phi} = 2\mathrm{Br}\left|\varepsilon^2\left(\frac{\partial^2\bar{\psi}}{\partial\bar{x}\partial\bar{y}}\right)^2 + \frac{1}{2}\left(\frac{\partial^2\bar{\psi}}{\partial\bar{y}^2}\right)^2 - \varepsilon^2\frac{\partial^2\bar{\psi}}{\partial\bar{y}^2}\frac{\partial^2\bar{\psi}}{\partial\bar{x}^2} + \frac{1}{2}\varepsilon^4\left(\frac{\partial^2\bar{\psi}}{\partial\bar{x}^2}\right)^2 + \varepsilon^2\left(\frac{\partial^2\bar{\psi}}{\partial\bar{y}\partial\bar{x}}\right)^2\right|^{\frac{n-1}{2}} *$$

$$\left\{\varepsilon^2\left(\frac{\partial^2\bar{\psi}}{\partial\bar{x}\partial\bar{y}}\right)^2 + \frac{1}{2}\left(\frac{\partial^2\bar{\psi}}{\partial\bar{y}^2}\right)^2 - \varepsilon^2\frac{\partial^2\bar{\psi}}{\partial\bar{y}^2}\frac{\partial^2\bar{\psi}}{\partial\bar{x}^2} + \frac{1}{2}\varepsilon^4\left(\frac{\partial^2\bar{\psi}}{\partial\bar{x}^2}\right)^2 + \varepsilon^2\left(\frac{\partial^2\bar{\psi}}{\partial\bar{y}\partial\bar{x}}\right)^2\right\}^{\frac{n-1}{2}}, \tag{1.3.7d}$$

$$\text{on } \bar{y} = +1\text{:}\quad \frac{\partial\bar{\psi}}{\partial\bar{y}} = 0, \quad -\frac{\partial\bar{\psi}}{\partial\bar{x}} = V(\bar{x}), \quad \bar{\theta} = 0, \tag{1.3.7e}$$

$$\text{on } \bar{y} = -1\text{:}\quad \frac{\partial\bar{\psi}}{\partial\bar{y}} = 0, \quad -\frac{\partial\bar{\psi}}{\partial\bar{x}} = (-1+E)V(\bar{x}), \quad \bar{\theta} = 1. \tag{1.3.7f}$$

Now, by multiplying the $\bar{y}$-momentum equation up by ε, and dropping the overbar notation we obtain the nondimensional governing equations

$$\mathrm{Re}\frac{D}{Dt}\left(\frac{\partial\psi}{\partial y}\right) = -\frac{\partial p}{\partial x} + \varepsilon^2\frac{\partial}{\partial x}\left(2\mu\frac{\partial^2\psi}{\partial x\partial y}\right) + \frac{\partial}{\partial y}\left(\mu\frac{\partial^2\psi}{\partial y^2}\right) - \varepsilon^2\frac{\partial}{\partial y}\left(\mu\frac{\partial^2\psi}{\partial x^2}\right), \tag{1.3.8a}$$

$$-\mathrm{Re}\varepsilon^2\frac{D}{Dt}\left(\frac{\partial\psi}{\partial x}\right) = -\frac{\partial p}{\partial y} - \varepsilon^4\frac{\partial}{\partial x}\left(\mu\frac{\partial^2\psi}{\partial x^2}\right) + \varepsilon^2\frac{\partial}{\partial x}\left(\mu\frac{\partial^2\psi}{\partial y^2}\right) - \varepsilon^2\frac{\partial}{\partial y}\left(2\mu\frac{\partial^2\psi}{\partial y\partial x}\right), \tag{1.3.8b}$$

$$\mathrm{Pe}\frac{D\theta}{Dt} = \varepsilon^2\frac{\partial^2\theta}{\partial x^2} + \frac{\partial^2\theta}{\partial y^2} + \Phi, \tag{1.3.8c}$$

$$\Phi = 2\mathrm{Br}\left|\varepsilon^2\left(\frac{\partial^2\psi}{\partial x\partial y}\right)^2 + \frac{1}{2}\left(\frac{\partial^2\psi}{\partial y^2}\right)^2 - \varepsilon^2\frac{\partial^2\psi}{\partial y^2}\frac{\partial^2\psi}{\partial x^2} + \frac{1}{2}\varepsilon^4\left(\frac{\partial^2\psi}{\partial x^2}\right)^2 + \varepsilon^2\left(\frac{\partial^2\psi}{\partial y\partial x}\right)^2\right|^{\frac{n-1}{2}} *$$

$$\left\{\varepsilon^2\left(\frac{\partial^2\psi}{\partial x\partial y}\right)^2 + \frac{1}{2}\left(\frac{\partial^2\psi}{\partial y^2}\right)^2 - \varepsilon^2\frac{\partial^2\psi}{\partial y^2}\frac{\partial^2\psi}{\partial x^2} + \frac{1}{2}\varepsilon^4\left(\frac{\partial^2\psi}{\partial x^2}\right)^2 + \varepsilon^2\left(\frac{\partial^2\psi}{\partial y\partial x}\right)^2\right\}^{\frac{n-1}{2}}, \tag{1.3.8d}$$

$$\text{on } y = +1\text{:}\quad \frac{\partial\psi}{\partial y} = 0, \quad -\frac{\partial\psi}{\partial x} = V(x), \quad \theta = 0, \tag{1.3.8e}$$

$$\text{on } y = -1\text{:}\quad \frac{\partial\psi}{\partial y} = 0, \quad -\frac{\partial\psi}{\partial x} = (-1+E)V(x), \quad \theta = 1. \tag{1.3.8f}$$

One characteristic scale that has not been defined is L, the distance from the origin to the end of the channel along the x_1 axis. This quantity is in some sense arbitrary, as

it can be defined in terms of the other parameters of the problem in hand. In the case of a solely thermally varying viscosity, we wish to only consider the flow of fluid in the region where the effects of inertia and conduction are balanced. In order to do this, we limit the region of interest to distances along the channel length that are smaller than the typical thermal conduction length; thus we define

$$L = \mathrm{Pe}\, h \ \ (\mathrm{Pe} \gg 1). \tag{1.3.9}$$

However, in the case of the viscosity depending solely upon the rate-of-shear, this previous definition is not useful as we would not consider any temperature equation associated with the flow. In this case we would define L in terms of the aspect ratio of the channel, and then consider the limiting case of an increasingly small aspect ratio

$$\varepsilon = h/L, \ \varepsilon \ll 1. \tag{1.3.10}$$

Therefore, in the case where we can have both temperature and rate-of-shear variation within the viscosity function, we must take L large enough such that the channel aspect ratio is sufficiently small and also large enough that the region of interest still encloses the region of inertia-conduction balance

$$L \gg \max\{h/\varepsilon,\, h\mathrm{Pe}\}\,. \tag{1.3.11}$$

As we are not considering the effects of viscous dissipation of heat we may take $\mathrm{Br} \ll 1$ uniformly across the channel. Taking the curl of the momentum equations gives

$$\begin{aligned}
&\mathrm{Re}\left(\frac{\partial^3\psi}{\partial t\partial y^2} + \frac{\partial\psi}{\partial y}\frac{\partial^3\psi}{\partial x\partial y^2} - \frac{\partial\psi}{\partial x}\frac{\partial^3\psi}{\partial y^3}\right) - \mathrm{Re}\,\varepsilon^2\left(-\frac{\partial^3\psi}{\partial t\partial x^2} - \frac{\partial\psi}{\partial y}\frac{\partial^3\psi}{\partial x^3} + \frac{\partial\psi}{\partial x}\frac{\partial^3\psi}{\partial y\partial x^2}\right)\\
&= \frac{\partial^2}{\partial y^2}\left(\mu\frac{\partial^2\psi}{\partial y^2}\right) + 2\varepsilon^2\frac{\partial^2}{\partial y\partial x}\left(2\mu\frac{\partial^2\psi}{\partial x\partial y}\right) - \varepsilon^2\frac{\partial^2}{\partial y^2}\left(\mu\frac{\partial^2\psi}{\partial x^2}\right) - \varepsilon^2\frac{\partial^2}{\partial x^2}\left(\mu\frac{\partial^2\psi}{\partial y^2}\right)\\
&+ \varepsilon^4\frac{\partial^2}{\partial x^2}\left(\mu\frac{\partial^2\psi}{\partial x^2}\right),
\end{aligned} \tag{1.3.12a}$$

$$\mathrm{Pe}\frac{D\theta}{Dt} = \frac{\partial^2\theta}{\partial y^2} + \varepsilon^2\frac{\partial^2\theta}{\partial x^2}, \tag{1.3.12b}$$

$$\text{on } y = +1\text{:} \quad \frac{\partial\psi}{\partial y} = 0, \quad -\frac{\partial\psi}{\partial x} = V(x), \quad \theta = 0, \tag{1.3.12c}$$

$$\text{on } y = -1\text{:} \quad \frac{\partial\psi}{\partial y} = 0, \quad -\frac{\partial\psi}{\partial x} = (-1+E)V(x), \quad \theta = 1. \tag{1.3.12d}$$

Finally, we obtain the leading order unsteady problem

$$\mathrm{Re}\left(\frac{\partial^3\psi}{\partial t\partial y^2}+\frac{\partial\psi}{\partial y}\frac{\partial^3\psi}{\partial x\partial y^2}-\frac{\partial\psi}{\partial x}\frac{\partial^3\psi}{\partial y^3}\right)=\frac{\partial^2}{\partial y^2}\left(\mu\frac{\partial^2\psi}{\partial y^2}\right), \tag{1.3.13a}$$

$$\mathrm{Pe}\left(\frac{\partial\theta}{\partial t}+\frac{\partial\psi}{\partial y}\frac{\partial\theta}{\partial x}-\frac{\partial\psi}{\partial x}\frac{\partial\theta}{\partial y}\right)=\frac{\partial^2\theta}{\partial y^2}, \tag{1.3.13b}$$

$$\mu=M(\theta)\left|\frac{\partial^2\psi}{\partial y^2}\right|^{n-1}, \tag{1.3.13c}$$

$$\text{on } y=+1\text{:}\quad \frac{\partial\psi}{\partial y}=0,\quad -\frac{\partial\psi}{\partial x}=V(x),\quad \theta=0, \tag{1.3.13d}$$

$$\text{on } y=-1\text{:}\quad \frac{\partial\psi}{\partial y}=0,\quad -\frac{\partial\psi}{\partial x}=(-1+E)V(x),\quad \theta=1. \tag{1.3.13e}$$

In most cases we will consider the steady states of this system, but in the case of temporal stability the unsteady system will be needed.

When the exponent $n=1$ and $E=0$, we obtain the two porous-walled Newtonian fluid flow problems

$$\mathrm{Re}\left(\frac{\partial^3\psi}{\partial t\partial y^2}+\frac{\partial\psi}{\partial y}\frac{\partial^3\psi}{\partial x\partial y^2}-\frac{\partial\psi}{\partial x}\frac{\partial^3\psi}{\partial y^3}\right)=\frac{\partial^2}{\partial y^2}\left(\mu\frac{\partial^2\psi}{\partial y^2}\right), \tag{1.3.14a}$$

$$\mathrm{Pe}\left(\frac{\partial\theta}{\partial t}+\frac{\partial\psi}{\partial y}\frac{\partial\theta}{\partial x}-\frac{\partial\psi}{\partial x}\frac{\partial\theta}{\partial y}\right)=\frac{\partial^2\theta}{\partial y^2}, \tag{1.3.14b}$$

$$\mu=M(\theta)\ \text{(exponential or algebraic form as appropriate)}, \tag{1.3.14c}$$

$$\text{on } y=+1\text{:}\quad \frac{\partial\psi}{\partial y}=0,\quad -\frac{\partial\psi}{\partial x}=V(x),\quad \theta=0, \tag{1.3.14d}$$

$$\text{on } y=-1\text{:}\quad \frac{\partial\psi}{\partial y}=0,\quad -\frac{\partial\psi}{\partial x}=-V(x),\quad \theta=1, \tag{1.3.14e}$$

and if there is no temperature variation of viscosity, so $\mu\equiv 1$, this further reduces to

$$\mathrm{Re}\left(\frac{\partial^3\psi}{\partial t\partial y^2}+\frac{\partial\psi}{\partial y}\frac{\partial^3\psi}{\partial x\partial y^2}-\frac{\partial\psi}{\partial x}\frac{\partial^3\psi}{\partial y^3}\right)=\frac{\partial^4\psi}{\partial y^4}, \tag{1.3.15a}$$

$$\mathrm{Pe}\left(\frac{\partial\theta}{\partial t}+\frac{\partial\psi}{\partial y}\frac{\partial\theta}{\partial x}-\frac{\partial\psi}{\partial x}\frac{\partial\theta}{\partial y}\right)=\frac{\partial^2\theta}{\partial y^2}, \tag{1.3.15b}$$

$$\text{on } y=+1\text{:}\quad \frac{\partial\psi}{\partial y}=0,\quad -\frac{\partial\psi}{\partial x}=V(x),\quad \theta=0, \tag{1.3.15c}$$

$$\text{on } y=-1\text{:}\quad \frac{\partial\psi}{\partial y}=0,\quad -\frac{\partial\psi}{\partial x}=-V(x),\quad \theta=1. \tag{1.3.15d}$$

We shall mainly focus on the one walled ($E=1$) problems but having the problems posed in a general manner allows some progress to be made on the two walled problem with equal wall flow conditions ($E=0$) and on the intermediate problem with unequal

wall flow conditions ($0 < E < 1$). The effects of the various non-Newtonian influences will be considered separately; either the power-law fluid model is used and then the temperature equation is not coupled to the flow problem and so is not considered further, or the temperature-dependent viscosity model is used and both equations are needed.

The main techniques used in this work are the calculation of similarity solutions of separable form, the numerical solution of associated boundary and initial value ode problems arising from using the similarity solutions in the governing pdes and subsequent asymptotic analyses exploiting small or large parameters that are present. The structure of the thesis is as follows: Chapter 1 introduces the non-Newtonian problem and sets out its general formulation; Chapter 2 contains a literature review of work that has been conducted on the Newtonian $E \in [0, 1]$ and non-isothermal $E = 0$ problems by previous researchers; Chapter 3 covers preliminary work on the power-law fluid problem, in particular containing a similarity solution of separable form, small Re asymptotic analysis and formulation of the temporal and spatial stability problems for the power-law fluid; Chapter 4 contains numerical results for the $E = 1$ power-law problem, bifurcation diagrams and asymptotic analysis for the small Re and large $\mathrm{Re} < 0$ injection problems and a statement of the spatial stability problem in this specific case; Chapter 5 covers the nonisothermal $E = 1$ temperature dependent viscosity problem and contains an asymptotic analysis of the $\mathrm{Re} < 0$, $\mathrm{Pe} < 0$ regime for the temperature sensitivity parameter $\beta = \mathcal{O}(1)$, statement of the temporal and spatial stability problems, numerical results and discussion for the base flow for a range of Pe and β and numerical results and discussion for a limited range of Pe and β for the temporal stability; Chapter 6 contains initial numerical results for the isothermal $E = 0$ power-law fluid problem, comprising of a bifurcation diagram and selected solution plots for a range of power-law exponents; Chapter 7 contains the conclusions and directions for further work; Appendix A details the calculations required to show that a particular case of a boundary value problem from Section 4.1.3 has appropriate boundary conditions; Appendix B contains asymptotic analysis for the nonisothermal $E = 1$ temperature dependent viscosity problem for $\mathrm{Re} < 0$, $\mathrm{Pe} < 0$ for $\beta \gg 1$ and parallels the corresponding section §5.2 in Chapter 5.

Chapter 2

Previous work

In this chapter we wish to present a brief overview of work that has been done on the problems under consideration. This has been broken down into two sections: one on the isothermal problem and one on the nonisothermal problem. As the majority of work has been on the isothermal problem this section is itself divided into two subsections: firstly the two porous walled problem with symmetric solutions and secondly the two porous walled problem with asymmetric solutions and the one porous walled problem.

2.1 Isothermal problems

2.1.1 Two porous walled problem with symmetric solutions

Various asymptotic results have been deduced or proven for the two porous walled problem with solutions that are symmetrical about the channel centreline. The original work by Berman [Ber53] produced a first order perturbation solution for the small $\mathrm{Re} > 0$ suction limit. Sellars [Sel55] obtained an expression for the high $\mathrm{Re} > 0$ suction limit. This was subsequently extended by Terrill [Ter64] and further work by Robinson [Rob76] described the three different symmetric suction solution types (I, II, III) that are possible in this limit. Authors define these solution types differently but we shall use the descriptions given by Zaturska et al. [ZDB88]: type I solutions exist for all values of Re whereas types II and III only exist beyond a critical positive value of the Reynolds number, given as $\mathrm{Re} = 12.165$. The type I and II solutions differ by exponentially small terms in the limit $\mathrm{Re} \to \infty$, first shown by Robinson [Rob76]. Figure 2.1.1 gives a schematic of the type I, II, and III symmetric suction solutions, showing their general form in the upper half of the channel. Terrill's subsequent paper [Ter65] addresses the large injection solution and he corrects an earlier attempt by Yuan [Yua56], which does not predict the correct behaviour of the third derivative of

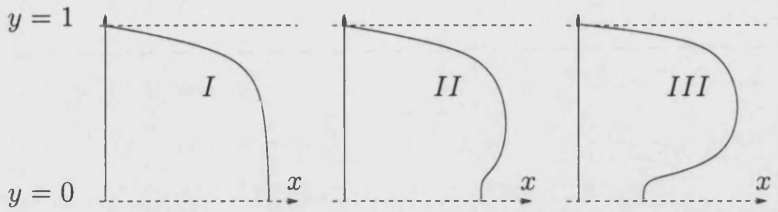

Figure 2.1.1. A schematic of the Type I, II and III symmetric suction solution profiles for the Berman problem. Each of the profiles corresponds to the first derivative of the solution function $f(y)$ and depicts the horizontal component of the fluid velocity for flow from left to right, situated where $x < 0$. As the Reynolds number increases, the type I profile flattens out in the channel centre and steepens at the walls, while the type II profile approaches the type I behaviour as the Reynolds number continues to increase. The Type III profile behaves differently in that, while the profile steepens at the wall, the local minimum at the channel centre becomes negative as the Reynolds number increases.

the solution across the channel centreline, by constructing an outer solution and an inner solution near the channel centreline.

In 1984 Durlofsky and Brady [DB84] showed that any injection solution is spatially stable, that the type I $\mathrm{Re} > 0$ suction solutions are spatially stable but the types II and III solutions for $\mathrm{Re} > 0$ are spatially unstable.

Two papers by Lu, MacGillivray and Hastings [LMH92, HLM92] proved some of the numerically known properties of the solutions of the boundary value problem. It was proved that there is at least one solution for all values of Re, and for sufficiently large $\mathrm{Re} > 0$ there are three solutions, confirming the work in Robinson's 1976 paper [Rob76]. For the injection solution, it was proved that the behaviour of the solution, away from the channel walls, was sinusoidal and as $\mathrm{Re} \to -\infty$, the leading order behaviour was linear. The concave down and increasing non-concave suction solutions have a vanishing second derivative as $\mathrm{Re} \to \infty$ and also have a linear leading order behaviour. As $\mathrm{Re} \to \infty$ these solutions have two distinct regions: an inviscid inner region and a viscous boundary layer near the wall. The three different solution types (I,II,III) correspond to the four cases detailed in [LMH92] in the following way: the concave down solution for $\mathrm{Re} < 0$ and $\mathrm{Re} > 0$ corresponds to the type I injection and suction solutions; the increasing non-concave solution for sufficiently large $\mathrm{Re} > 0$ corresponds to the type II solution; the solution with a single zero in the half-channel interior for large enough $\mathrm{Re} > 0$ corresponds to the type III solution.

The type III solutions for $\mathrm{Re} > 0$ were also studied by MacGillivray and Lu in [ML94] and two rigorous results were proved for the internal zero of these solutions, namely that the internal zeros move toward the wall as $\mathrm{Re} \to \infty$ and that the minimum of the first derivative of the solution tends to $-\infty$ as $\mathrm{Re} \to \infty$. The asymptotic

description of the solution to the boundary value problem was of an inviscid outer region, a viscous boundary layer near the wall and a novel transition layer in which transcendentally small terms were included.

The paper of Cox and A.C. King in 1997 [CK97] established the first detailed asymptotic description of the type III suction flows via the transformation of the boundary value problem derived from a similarity solution of two porous walled problem into an initial value problem (using a method described by Terrill in [Ter64]). The four region asymptotic behaviour of the solution to this initial value problem, up to and including the second zero of the first derivative of the solution, allowed Cox and King to reconstruct the flow and perform comparisons with other numerical solutions to the original boundary value problem. Ferro and Gnavi [FG00] show that the type I solutions are spatially stable for a range of Reynolds numbers, but asymmetric perturbations to the symmetric solutions are able to cause instability.

Numerical solutions and analysis of the symmetric problems have been produced by various authors in the course of their work mentioned above. Zaturska, Drazin and Banks [ZDB88] used numerical results for the symmetric problem to perform temporal stability analysis of the asymmetric problem, and also calculated a phase plane for the unsteady type I solution. MacGillivray and Lu [ML94] compare their asymptotic results to a numerical solution of the original boundary value problem and also to the numerics in [ZDB88] and note that their transition layer yields better results. The asymptotic work in [CK97] on the initial value problem is compared to direct numerical solution of the boundary value problem to show the accuracy of their asymptotic results; they also disagree with some of the details of the numerical results produced within [ZDB88]. A full two-dimensional calculation is compared to the behaviour of the similarity solutions of type I in order to examine the spatial stability predictions of their work.

Variations to the two porous walled problem in §1 are also investigated by researchers. Durlofsky and Brady [DB84] consider solutions in an axisymmetric tube geometry and show that the injection solutions are spatially stable and the suction solutions are spatially stable as long as there is no flow reversal within the tube. They also consider the basic two porous walled channel problem with accelerating (or decelerating) walls and conclude that both the injection and suction solutions are spatially unstable as there are always regions of flow reversal within the channel. Cox [Cox91a] considers the accelerating wall problem in the channel by recasting it as an initial value problem. Cox then proves that the number of solutions to the initial value problem that have a zero of the first derivative is at most two. From these solutions the flow behaviour within the channel can be recovered, and he is able to identify solutions

analogous to types $I - III$.

2.1.2 Two porous walled problem with asymmetric solutions and the one porous walled problem

The two porous walled problem with asymmetric solutions only received attention once the 1998 paper by Zaturska et al. [ZDB88] demonstrated the existence of asymmetric solutions in the suction case. Asymptotic descriptions of the flow behaviour for suction solutions of type I_a, I_a' and III_a, III_a' were obtained: type I_a consists of an inviscid sinusoidal core and viscous boundary layers at the walls; type III_a consists of an inviscid core, viscous boundary layers at the walls and a viscous shear layer about the mid-line of the channel. Zaturska et al. found the asymmetric solutions numerically by perturbing the symmetric solutions with antisymmetric eigenfunctions. They established that temporally stable asymmetric solutions exist for a limited range of Reynolds numbers.

In 1991 Cox produced two papers [Cox91b, Cox91a] considering variations of the original two porous walled and one porous walled problems. For the problem of injection through the upper wall and an impermeable lower wall, Cox [Cox91a] found that in the limit $\mathrm{Re} \to -\infty$ there are two flow regions: an inviscid outer region and a viscous boundary layer near the impermeable wall, in which the solution is the Falkner-Skan[1] profile with $m = 1$. In this situation there is only one steady solution and it is temporally stable. For the two porous walled problem and large $\mathrm{Re} > 0$ suction flow with different amounts of suction at each wall, he noted that there was a three region behaviour, with an inviscid core and viscous boundary layers at each wall. In this case the general conclusion to be drawn is that, for large enough $\mathrm{Re} > 0$, the solutions are spatially unstable. The type I_a solution is temporally unstable for a range of Re values. Considering the situation of suction at the upper wall only, in the steady problem there are two cases: for small $\mathrm{Re} > 0$ there are three solution branches, one temporally stable and two temporally unstable; for large enough $\mathrm{Re} > 0$ flow reversal occurs and so there is a loss of temporal stability as perturbations can be carried in both directions within the channel. For the unsteady suction problem, the only stable solution for large $\mathrm{Re} > 0$ occurred as part of a limit cycle. This limit cycle has two parts: an inward part (according to the behaviour of the limit cycle on the phase plane [Cox91b, fig.9 p.15]), which has an inviscid solution structure away from the channel

[1]The Falkner-Skan problem (this description being a paraphrase of the description given by Batchelor [Bat01, page 316]) describes the boundary layer flow of a fluid adjacent to a solid boundary, aligned with the x-axis, where the far field fluid horizontal velocity is given by $u = Cx^m$ with $C > 0$ and m constants. A solution of the boundary layer equations may be found of the form $\psi = (\nu U x)^{1/2} f(\eta)$, $\eta = (U/\nu x)^{1/2} y$ and the boundary layer system is found to be $mf'^2 - (1/2)(m+1)ff'' = m + f'''$. The case $m = 1$ corresponds to the flow of fluid toward a stagnation point at a wall.

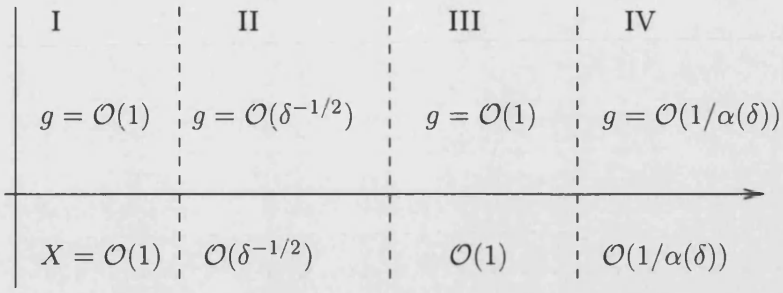

Figure 2.1.2. Schematic of the single porous walled solution structure in the initial value problem in [CK97], where $\alpha(\delta) = \log\left[4\log\delta^{-1} + 6\log\left(4\log\delta^{-1}\right)^{1/2}\right]^{1/2}$ and δ is the difference between the initial guess for the second derivative of $g(X)$ and a critical value below which no solution occurs.

walls, the amplitude of which is exponentially decreasing; the outward part also has an inviscid core away from the walls but it is rapidly growing and is moderated by the viscous solution near the matching point with the viscous boundary layer. Cox mentions that the growing inviscid solution appears to be an intermediate asymptotic. The temporal stability analysis was performed by using a shooting method to solve the two-point boundary value problem and the corresponding eigenvalue problem.

For the one porous wall problems Cox [Cox91a] transforms the boundary value problem into an initial value problem and proves that the number of solutions with a zero of their first derivative is either two or none, and then compares numerical solutions with the known injection and suction solution asymptotics in this case. He also considers the problem with just one accelerating wall (no suction or injection) and the theoretical results follow through without much amendment. In 1997 Cox and A.C. King [CK97] produced a four region asymptotic description of the solution to the initial value problem obtained after transforming the one porous walled channel boundary value problem. The fluid flow field is recovered from the numerical solution of the initial value problem combined with the asymptotics and covers both the injection and suction flows. A schematic of the four region structure is given in Figure 2.1.2, which is not given in [CK97].

Ferro and Gnavi [FG00] extend the spatial stability results of the similarity solutions to the two porous walled suction problem. They report that the type I_a solution is spatially stable if there is no flow reversal within the channel whereas the type III_a solutions are spatially unstable for any Re > 0 as there is always a region of flow reversal within the channel. Numerical experiments suggested that these types III_a solutions were unstable to both symmetric and antisymmetric perturbations. They concluded that there is a small range of Re > 0 within which the possible similarity

solutions are spatially stable; the smaller end of the range of Reynolds numbers permits symmetric spatially stable solutions and the higher end permits asymmetric spatially stable similarity solutions.

A paper by J.R. King and Cox [KC01] considers the steady and unsteady solutions of the one porous walled problem and the authors are interested in the large Re limits of the problem. As we are only looking at the steady problem the discussion will be limited to that case. In contrast to the previous work on the one porous walled problem the authors obtain results directly from the boundary value problem formulation and not via Terrill's [Ter64] transformation to an initial value problem. They summarise the three known asymptotic limits of small Re, large negative Re corresponding to injection driven flow and large positive Re, corresponding to suction driven flow. The small Re solution is a regular perturbation series and the large injection solution is a singular perturbation series solution comprising of an inviscid outer region away from the lower wall and a viscous boundary layer near the lower wall, as reported by Cox in [Cox91b] and [Cox91a]. The final case of large positive Re consists of a four region solution; there is an interior region around the nearest internal zero of the solution function to the upper wall, a boundary layer adjacent to the upper wall, an outer inviscid region in the main body of the channel and a boundary layer adjacent to the lower wall. There are exponentially small terms involved in the boundary layer at the upper wall which asymptotically match with terms in the interior layer, and these terms have an influence upon the scalings of the interior layer which are then determined by matching the solution in that layer to that in the outer, inviscid, region. The authors' novel use of an optimal truncation method upon the diverging series solutions allows an accurate approximation to be calculated in the case where inverse powers of $\log(1/\mathrm{Re})$ occur.

The 2004 paper by Cox and J.R. King [CK04] considers the large Reynolds number asymptotics of the two-walled porous channel problem in both the $E = 0$ and $0 < E < 1$ cases, obtaining asymptotic descriptions of the asymmetric type I_1 and III_1 solutions for $E = 0$, an improved asymptotic description of the symmetric type III solution for $E = 0$, and large Reynolds number asymptotic descriptions for the type I_1 and III_1 solutions of the $0 < E < 1$ problem (two walled problem with unequal suction rates). They use matched asymptotic expansions with exponentially small terms at interior layers and boundary layers together with multiple regions within the channel width to produce the high suction asymptotic solutions. These are constructed in two ways: either an "exact" method is used where matching of solutions is attempted between the outer and inner solutions in the usual manner, or an "ad-hoc" method is used where the outer solution boundary conditions are replaced with conditions applied at the interior zero(s) of the solutions. The "ad-hoc" method is seen to yield better

numerical estimates of the outer solution structure than the usual "exact" method, with the authors noting that the improved numerical accuracy has come at the cost of a fully systematic approach to the asymptotic analysis. The analysis is guided by a detailed examination of the particular boundary layer problems that arise in the course of matching and are recorded in a companion paper, [CK05].

The companion paper by J.R. King and Cox, [CK05], considers the boundary layer flows driven by the injection or suction of a viscous fluid at a porous channel wall. Multiple solutions are reported for high enough rates of suction and these solutions have different forms; one solution corresponds to the previously found monotone solution (which connects to the injection solution branch) and the other two solution forms show regions of flow reversal near to the porous channel wall. The solutions with flow reversal are not connected to the main branch of solutions. One solution exhibits reversed flow regions above a critical suction rate and the other solution has reversed flow only up to a critical flow rate. The three different solution branches are examined in the limit of large suction (and injection where it is valid) and the reversed flow solutions involve the matching of exponentially small terms. Numerical simulations are also performed in order to assess the quality of the asymptotic analysis. The reported multiple solutions are important in the asymptotic description of the various high suction rate solutions of the Berman problem and are used in [CK04] accordingly. The authors then relate their solutions to the known solutions for the flow of a viscous fluid within the boundary layer of an impermeable walled channel whose walls are accelerating and also to the three dimensional suction flow boundary layer solutions, where the number of coexisting solutions is found to be greater than that of the analogous two-dimensional problem.

2.2 Nonisothermal problem

The only work on the injection or suction of fluid within a channel with porous walls and involving temperature is [FG02]. Figure 2.2.1 shows a bifurcation diagram reproducing Figure 2 in [FG02] for the flow of a Newtonian fluid in an isothermal two porous walled channel upon which the different base solution branches are presented.

2.2.1 Ferro and Gnavi, 2002

Ferro and Gnavi [FG02] consider the effects of viscosity gradients upon the stability of Berman flows in the two porous walled problem. They take, for simplicity, an exponential viscosity function $\mu(T) = \exp(-\gamma T)$. If $\gamma > 0$ then the viscosity decreases as the temperature increases (typical for most liquids) but if $\gamma < 0$ then the viscosity increases as the temperature increases (an example of this behaviour is that of dry

air at atmospheric pressure at temperatures above $0°C$ [Bat01, Appendix 1]). The exponential form of viscosity is a good fit for the behaviour of water in the range $10 - 100°C$.

Asymptotics are presented for the low thermal conductivity limit of $|\mathrm{Pe}| \gg 1$ in the cases of $I_1(\gamma), I_3(\gamma)$ without flow reversal. The solution types are labelled analogously to those of the isothermal case: types I_1, I_2 and I_3 correspond to different sections of the type I solution branch for nonzero γ. In the case of large suction the solution structure comprises an isothermal layer and either one or two temperature boundary layer(s), depending upon the behaviour of the flow function. Ferro and Gnavi comment that the temperature in the isothermal layer cannot be found using standard perturbation theory and they resort to a variational approach to obtain its value. For the injection scenario there are two outer layers near the walls of the channel and an inner thermal boundary layer near the stagnation line. In the limit of low thermal conductivity two fluids of different constant viscosities are injected into the channel and the temperature jump within the channel occurs across the stagnation line. An analytical description of the branches of the bifurcation diagram close to the first bifurcation point is produced.

Ferro and Gnavi then reproduce the bifurcation results of previous authors in the isothermal case to provide a contrast to their bifurcation results. There are solution branches analogous to those in the $\gamma = 0$ problems; in particular there is only one branch of solutions that exist for all Re with $\gamma \neq 0$, $I_1(\gamma)$. They introduce the effective Reynolds number, which can only be calculated after the flow problem has been solved, which is the Reynolds number divided by the mean viscosity in the channel. It is useful for distinguishing the artefacts caused by the viscosity gradients from those which occur due to the value of the mean viscosity in the channel. They found that for the steady state solutions, for a fixed value of the effective Reynolds number, the stagnation line for $\gamma > 0$ ($\gamma < 0$) is displaced toward the wall of lower (higher) temperature, i.e. where the viscosity is lowest.

Next the temporal stability of the $\gamma \neq 0$ steady state solutions is examined. For $\gamma \neq 0$ the (Re, γ) plane is divided into four regions, in which different types of temporally stable solution can be found. For fixed γ, these four types are: a single temporally stable solution; two temporally stable solutions; one temporally stable solution and one temporally stable periodic solution; and two temporally stable periodic solutions. This division of the plane is not equal and there is a bias toward one sign of γ. Reinterpreting these results in terms of the effective Reynolds number removes any bias and reintroduces symmetry into the (Re, γ) plane. The displacement of the flow field toward regions of lower viscosity accentuates the instability of the asymmetric solution whereas if it enhances the symmetry of the flow field the stability of the corresponding

solution is improved. In the case of the unsteady problem, the authors note that the stronger the dependence of the viscosity upon the temperature, the more marked the increase of the critical Reynolds number corresponding to a Höpf bifurcation bringing periodic solutions.

The spatial stability of solutions is then considered. The authors note that only temporally and spatially stable solutions are observable in practice. Their results are that solutions of type I_1 and I_3 are spatially stable if there is no flow reversal in the channel and that all other solution types are spatially unstable; this result is the same as that found in the constant viscosity spatial stability analysis. Thus, for the injection problem the solutions are spatially stable for any $\mathrm{Re} < 0$ while the suction solutions are only spatially stable up to a certain critical value of the Reynolds number, dependent upon γ. The quantitative behaviour of the solutions in the presence of thermal gradients is similar to that of the temporal stability case, but the regions in which the stable solutions are to be found are much smaller and the critical Reynolds number is again reduced.

The authors finally conclude that most of the solutions of the temperature-dependent viscosity problem are temporally and/or spatially unstable. The thermal effects reduce the values of critical Reynolds numbers, and also enhance the stability or instability of the solutions, depending upon whether the shifting of the solution toward regions of lower viscosity enhances the symmetry or asymmetry of the flow field.

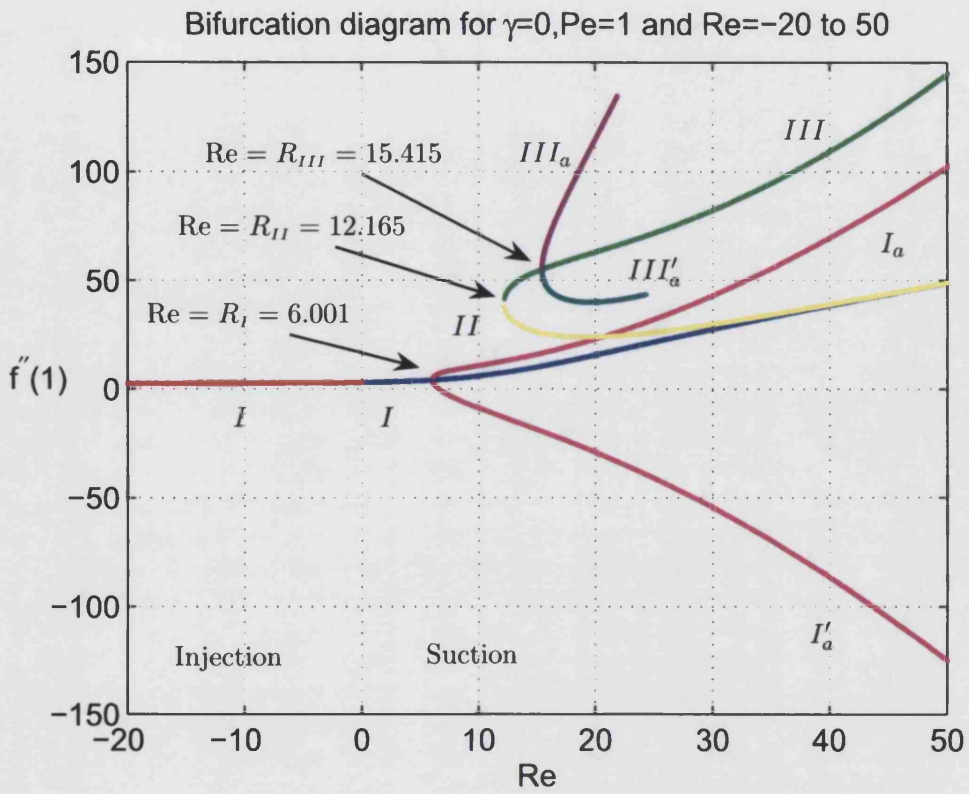

Figure 2.2.1. Bifurcation diagram for the constant viscosity problem with suction or injection in [FG02]. The flow profile along the channel is proportional to $-f(y)$ and $f''(1)$ is proportional to the viscous stress at the upper channel wall.

Chapter 3

Isothermal power law fluid problem - preliminaries

In this chapter we start by seeking a similarity solution of separable form for the power-law fluid flow problem in the general two porous walled geometry as a basis for further work in subsequent chapters. We then construct a small Reynolds number expansion of the flow function coming from the similarity solution and finally pose the temporal and spatial stability problems for the two porous walled isothermal flow.

3.1 Similarity solutions

Introducing the following rescalings

$$x = \alpha X,\ y = \beta Y,\ \psi(x,y) = \gamma S(X,Y) \qquad (\alpha,\beta,\gamma \in \mathbb{R}) \tag{3.1.1}$$

into the governing steady isothermal system

$$\mathrm{Re}\left(\frac{\partial\psi}{\partial y}\frac{\partial^3\psi}{\partial x\partial y^2} - \frac{\partial\psi}{\partial x}\frac{\partial^3\psi}{\partial y^3}\right) = \frac{\partial^2}{\partial y^2}\left(\left|\frac{\partial^2\psi}{\partial y^2}\right|^{n-1}\frac{\partial^2\psi}{\partial y^2}\right), \tag{3.1.2}$$

$$\text{on } y=+1\text{:}\quad \frac{\partial\psi}{\partial y} = 0, \quad -\frac{\partial\psi}{\partial x} = V(x), \tag{3.1.3}$$

$$\text{on } y=-1\text{:}\quad \frac{\partial\psi}{\partial y} = 0, \quad -\frac{\partial\psi}{\partial x} = (-1+E)V(x), \tag{3.1.4}$$

we obtain from the governing equation that the following relation must hold

$$\alpha\gamma^{-1}|\gamma|^{n-1} = \beta|\beta^2|^{n-1}, \tag{3.1.5}$$

for invariance. If we assume that $\alpha, \beta, \gamma > 0$ and that $\gamma = \alpha^\lambda$ for some choice of λ, then we have that

$$\alpha^m = \beta \quad \text{where } m = \frac{1 + (n-2)\lambda}{2n-1}. \tag{3.1.6}$$

This gives

$$\psi(x,y) = \alpha^\lambda S(x/\alpha, y/\beta) = x^\lambda S(1, y/\beta) = x^\lambda f(\eta), \text{ where } \eta = yx^{-m}. \tag{3.1.7}$$

The governing partial differential equation for $\psi(x,y)$ is transformed into the principal differential equation for $f(\eta)$,

$$\mathrm{Re}\big((\lambda - 2m) f' f'' - \lambda f f'''\big) = \big(|f''|^{n-1} f''\big)'', \quad \text{where } ' = \frac{\mathrm{d}}{\mathrm{d}\eta}, \tag{3.1.8}$$

while the boundary conditions become

$$\text{on } \eta x^m = +1\text{: } x^{\lambda-m} f'(\eta) = 0, \ -\lambda x^{\lambda-1} f(\eta) + m x^{\lambda-1} \eta f'(\eta) = V(x), \tag{3.1.9}$$

$$\text{on } \eta x^m = -1\text{: } x^{\lambda-m} f'(\eta) = 0, \ -\lambda x^{\lambda-1} f(\eta) + m x^{\lambda-1} \eta f'(\eta) = (-1+E) V(x). \tag{3.1.10}$$

Now as the boundaries of the η domain are to remain independent of x under the similarity transformation, we must have that $m = 0$, and so $\eta = y$. In summary we have that

$$\psi(x,y) = x^\lambda f(y), \quad \lambda = \frac{1}{2-n}, \quad V(x) = -\lambda x^{\lambda-1}, \tag{3.1.11}$$

and $f(y)$ satisfies the principal differential equation

$$\lambda \mathrm{Re}\left(f' f'' - f f'''\right) = \left(f'' |f''|^{n-1}\right)'', \tag{3.1.12}$$

and the boundary conditions

$$\text{on } y = +1\text{: } \quad f' = 0, \quad f = 1, \tag{3.1.13}$$

$$\text{on } y = -1\text{: } \quad f' = 0, \quad f = -1 + E. \tag{3.1.14}$$

The boundary conditions $f(1) = 1$, $f(-1) = -1 + E$ arise as we are only considering normal wall velocities that are similarity solutions of separable form. We then find that we must consider two cases in order to proceed further: uniform injection/suction or variable injection/suction. Before investigating these two cases we should see if there are more general separable similarity solution forms that could be applied.

3.1.1 Alternative similarity solution forms

Since, in (3.1.11), we required $m = 0$ to preserve the boundary conditions (3.1.9) and (3.1.10), we now choose to seek a more general form of separable solution, namely

$$\psi(x,y) = -g(x)f(y). \tag{3.1.15}$$

Substituting this into the steady isothermal system yields,

$$\mathrm{Re}gg'\left(f'f'' - ff'''\right) = g\left|g\right|^{n-1}\left(-nf^{(\mathrm{iv})}\left|f''\right|^{n-1} - n(n-1)f''\left(f'''\right)^2\left|f''\right|^{n-3}\right), \tag{3.1.16}$$

$$\text{on } y = +1: \quad -gf' = 0, \quad g'f = V(x), \tag{3.1.17}$$

$$\text{on } y = -1: \quad -gf' = 0, \quad g'f = (-1+E)V(x), \tag{3.1.18}$$

where $'$ means the derivative with respect to the argument of the relevant function.

For (3.1.16) to be separable, we require

$$\frac{gg'}{g\left|g\right|^{n-1}} = \frac{-nf^{(\mathrm{iv})}\left|f''\right|^{n-1} - n(n-1)f''\left(f'''\right)^2\left|f''\right|^{n-3}}{\mathrm{Re}\left(f'f'' - ff'''\right)} = r \tag{3.1.19}$$

to hold, where r is the separation constant. This means that we have to satisfy

$$gg' = rg\left|g\right|^{n-1}, \quad V(x) = g', \quad g(0) = 0 \quad \text{(flow symmetry condition)}, \tag{3.1.20}$$

leaving the modified equation for $f(y)$,

$$r\mathrm{Re}\left(f'f'' - ff'''\right) = -nf^{(\mathrm{iv})}\left|f''\right|^{n-1} - n(n-1)f''\left(f'''\right)^2\left|f''\right|^{n-3}, \tag{3.1.21}$$

$$\text{on } y = +1: \quad f' = 0, \quad f = 1, \tag{3.1.22}$$

$$\text{on } y = -1: \quad f' = 0, \quad f = -1 + E, \tag{3.1.23}$$

which in general has to be considered numerically.

We assume that $g(x)$ is not identically zero otherwise it would yield a trivial form for $\psi(x,y)$. The relevant form of the suction or injection profile corresponding to a particular solution $g(x)$ is determined by the requirement that $g'(x) = V(x)$, coming from considering the boundary conditions upon the walls.

Cancelling a factor of $g(x)$, we are left with a Bernoulli-type equation for $g(x)$, with

solutions

$$g(x) = \begin{cases} (c + r(2-n)x)^{\frac{1}{2-n}}, & g(x) > 0 \text{ and } n \neq 2 \Rightarrow V(x) = r\,(c + r(2-n)x)^{\frac{n-1}{2-n}} \\ A\exp(rx), & n = 2 \Rightarrow V(x) = r\exp(rx) \\ -(c - r(2-n)x)^{\frac{1}{2-n}}, & g(x) < 0 \text{ and } n \neq 2 \Rightarrow V(x) = -r\,(c - r(2-n)x)^{\frac{n-1}{2-n}} \end{cases} \tag{3.1.24}$$

subject to conditions upon x, r, c, A and n.

We want to have suction or injection throughout the whole length of the channel and as such we must consider the solution branches that are nonzero for all x. We also want to impose the symmetry condition $\psi(0,y) = \psi_{xx}(0,y) = 0$, an assumption that was implicitly made in Berman's paper [Ber53].

When $n \neq 2$ if we impose the condition $g(0) = 0$ then we find that $c = 0$. Rewriting the function as

$$g(x) = \operatorname{sgn}(x)\,(r(2-n)|x|)^{\frac{1}{2-n}} = \begin{cases} (r(2-n)x)^{\frac{1}{2-n}}, & x > 0,\ n \neq 2 \\ -(r(2-n)(-x))^{\frac{1}{2-n}}, & x < 0,\ n \neq 2 \end{cases} \tag{3.1.25}$$

allows the determination of the separation constant $r = a^{2-n}/(2-n)$ for some constant a. The simplest choice is to take $a = 1$, i.e. that any extra arbitrary constant in the definition of ψ can be absorbed into the f-problem by redefining the Reynolds number; in this case the separation constant is $r = 1/(2-n) = \lambda$. We can then simplify the form of $g(x)$ to

$$g(x) = \operatorname{sgn}(x)|x|^{\frac{1}{2-n}},\ n \neq 2, \tag{3.1.26}$$

and have thus extended $g(x)$ to have an odd symmetry about $x = 0$. In this case we then have that the injection or suction function $V(x)$ is given by

$$V(x) = \frac{1}{2-n}|x|^{\frac{n-1}{2-n}},\quad n \neq 2. \tag{3.1.27}$$

In the case $n = 2$ the governing equation becomes

$$r\mathrm{Re}gg'\left(f'f'' - ff'''\right) = g\,|g|\left(-2f^{(\mathrm{iv})}\,|f''| - 2f''\left(f'''\right)^2|f''|^{-1}\right), \tag{3.1.28}$$

with the solution for $g(x)$ in this case being

$$g(x) = \pm B\exp(\pm rx),\ B > 0,\ r \in \mathbb{R}. \tag{3.1.29}$$

However, we cannot impose the symmetry conditions upon g without forcing it to be identically zero, and so in this case the centreline has been, in effect, pushed off to plus

or minus infinity. Solutions of this form are dissimilar to those in the $n \neq 2$ case due to the lack of symmetry. Fluid injection occurs when $g' < 0$, which is the situation when the minus signs are taken in the above form of $g(x)$ and in this case the separation constant r must remain negative; in contrast, suction occurs when $g' > 0$ which is the result of taking the positive signs and in this situation r must remain positive.

3.1.2 Uniform injection or suction case

If the injection or suction is constant throughout the channel length (so that $V(x) = 1$) we must either have that the separation constant $r = 0$ or that $\lambda = 1$. As $r = 0$ gives a trivial form for $g(x)$ this is not possible, and so we must have $\lambda = 1$ but then any possible similarity solution only holds if $n = 1$ i.e. if the fluid is Newtonian.

In the case of a power-law viscosity function, we conclude that there is no similarity solution of separable form considered that is valid across the entire channel for the case of uniform injection or suction problem. We are then left to consider whether a similarity solution of separable form is relevant over a reduced part of the domain, e.g. where the solution structure may contain boundary layer phenomena (where $\mathrm{Re} \gg 1$). This is considered in later sections.

3.1.3 Variable injection or suction case

In contrast to the previous subsection, if we allow the form of the suction or injection function to be determined whilst finding a separable similarity solution, we may be able to find other valid solutions with variable suction or injection along the channel length. These solutions are exactly those described in section 3.1.1.

3.2 Preliminary asymptotic analysis

3.2.1 Small Re limit

To consider the $\mathrm{Re} \to 0$ limit, let us pose the regular expansion of $f(y)$ in $\varepsilon = r\mathrm{Re} = \mathrm{Re}/(2-n)$ (assuming $r = \mathcal{O}(1)$), namely

$$f(y) = f_0(y) + \varepsilon f_1(y) + \varepsilon^2 f_2(y) + \cdots . \tag{3.2.1}$$

Integrating the governing ordinary differential equation once gives,

$$\varepsilon\left(f'^2 - ff''\right) = \left(-f''\left|f''\right|^{n-1}\right)' + \beta, \tag{3.2.2}$$

$$\text{on } y = +1: \quad f' = 0, \quad f = 1, \tag{3.2.3}$$

$$\text{on } y = -1: \quad f' = 0, \quad f = -1 + E, \tag{3.2.4}$$

and substituting the regular expansion for $f(y)$ into the system (3.2.2)–(3.2.4), expanding the integration constant in powers of ε,

$$\beta = \beta_0 + \varepsilon\beta_1 + \varepsilon^2\beta_2 + \cdots \tag{3.2.5}$$

and approximating the modulus using (3.3.1) gives the following series of problems at each order:

$$\mathcal{O}(1): \quad 0 = -\left(|f_0''|^{n-1}f_0''\right)' + \beta_0, \tag{3.2.6}$$

$$\text{on } y = +1: \quad f_0' = 0, \quad f_0 = 1, \tag{3.2.7}$$

$$\text{on } y = -1: \quad f_0' = 0, \quad f_0 = -1 + E, \tag{3.2.8}$$

$$\mathcal{O}(\varepsilon): \quad f_0'^2 - f_0 f_0'' = -\left(n|f_0''|^{n-1}f_1''\right)' + \beta_1, \tag{3.2.9}$$

$$\text{on } y = +1: \quad f_1' = 0, \quad f_1 = 0, \tag{3.2.10}$$

$$\text{on } y = -1: \quad f_1' = 0, \quad f_1 = 0. \tag{3.2.11}$$

For the $\mathcal{O}(1)$ problem (3.2.6)–(3.2.8), an exact solution can be found in the general case where the wall flow rates are not necessarily equal. First consider the situation where $f_0'' > 0$: numerical evidence suggests this is near the lower wall. Denoting the solution in this region by f_{0+}, we intend to solve the ode

$$\left(f_{0+}''\right)^{n\prime} = \beta_0, \tag{3.2.12}$$

$$\text{on } y = -1: \quad f_{0+} = -1 + E, \quad f_{0+}' = 0. \tag{3.2.13}$$

This has solution

$$f_{0+}(y) = \frac{(\beta_0 y + c_0)^{2+\frac{1}{n}}}{\beta_0^2\left(2+\frac{1}{n}\right)\left(1+\frac{1}{n}\right)} + c_1 y + c_2 \tag{3.2.14}$$

where c_0, c_1, c_2 are constants of integration. It is clear that $f_{0+}'' \searrow 0_+$ as $y \to y^* = -\frac{c_0}{\beta_0}$. Applying the two boundary conditions allows the determination of c_1 and c_2 in terms

of the remaining quantities β_0, c_0 and E, giving

$$c_1 = -\frac{(c_0-\beta_0)^{1+\frac{1}{n}}}{\beta_0\left(1+\frac{1}{n}\right)}, \tag{3.2.15}$$

$$c_2 = -1+E-\frac{(c_0-\beta_0)^{1+\frac{1}{n}}}{\beta_0\left(1+\frac{1}{n}\right)}\left[1+\frac{c_0-\beta_0}{\beta_0\left(2+\frac{1}{n}\right)}\right]. \tag{3.2.16}$$

If we now consider the region where $f_0'' < 0$, which is near the upper wall, we have to solve the following ode

$$\left(-f_{0-}''\right)^{n\,\prime} = -\beta_0, \tag{3.2.17}$$

$$\text{on } y=+1: \quad f_{0-}=1, \quad f_{0-}'=0. \tag{3.2.18}$$

This has solution

$$f_{0-}(y) = \frac{-\left(d_0-\beta_0 y\right)^{2+\frac{1}{n}}}{\beta_0^2\left(2+\frac{1}{n}\right)\left(1+\frac{1}{n}\right)} + d_1 y + d_2. \tag{3.2.19}$$

We can see that $f_{0-}'' \searrow 0_-$ as $y \to y^* = \frac{d_0}{\beta_0}$. If we apply the two boundary conditions we obtain the following values for the integration constants d_1 and d_2,

$$d_1 = -\frac{(d_0-\beta_0)^{1+\frac{1}{n}}}{\beta_0\left(1+\frac{1}{n}\right)}, \tag{3.2.20}$$

$$d_2 = 1+\frac{(d_0-\beta_0)^{1+\frac{1}{n}}}{\beta_0\left(1+\frac{1}{n}\right)}\left[1+\frac{d_0-\beta_0}{\beta_0\left(2+\frac{1}{n}\right)}\right]. \tag{3.2.21}$$

Now in order to proceed to the general solution of the problem, we must first have that f_0 and f_0' are continuous about $y = y^*$; this needs the two descriptions of y^* to coincide, and so we have that $d_0 = -c_0$. Imposing continuity of $f_0'(y^*)$ needs $d_1 = c_1$, and this implies $d_0 = c_0 = 0$, which in turn implies $y^* = 0$. Now imposing the continuity of $f_0(y^*)$ requires $d_2 = c_2$, and this yields

$$\beta_0 = -\left(1-\frac{E}{2}\right)^n\left(2+\frac{1}{n}\right)^n. \tag{3.2.22}$$

In summary we have that the leading order solution is

$$f_0(y) = \begin{cases} f_{0+}(y) = \frac{\left(1-\frac{1}{2}E\right)}{\left(1+\frac{1}{n}\right)}(-y)^{2+\frac{1}{n}} + \frac{\left(1-\frac{1}{2}E\right)\left(2+\frac{1}{n}\right)}{\left(1+\frac{1}{n}\right)}y + \frac{1}{2}E, & y\in[-1,0], \\ f_{0-}(y) = -\frac{\left(1-\frac{1}{2}E\right)}{\left(1+\frac{1}{n}\right)}y^{2+\frac{1}{n}} + \frac{\left(1-\frac{1}{2}E\right)\left(2+\frac{1}{n}\right)}{\left(1+\frac{1}{n}\right)}y + \frac{1}{2}E, & y\in[0,1], \end{cases} \tag{3.2.23}$$

equivalently stated as

$$f_0(y) = \begin{cases} f_{0+}(y) = \frac{(2-E)(n+1)}{2n}(-y)^{2+1/n} + \frac{(2-E)(2n+1)}{2(n+1)}y + \frac{E}{2}, & y \in [-1,0], \\ f_{0-}(y) = -\frac{(2-E)(n+1)}{2n}y^{2+1/n} + \frac{(2-E)(2n+1)}{2(n+1)}y + \frac{E}{2}, & y \in [0,1]. \end{cases} \tag{3.2.24}$$

Turning to the $\mathcal{O}(\varepsilon)$ problem (3.2.9)–(3.2.11), we again must split the problem into two parts, coinciding with the regions of positive and negative values of $f_0''(y)$.

In the region where $f_{0+}(y)$ is valid, $y \in [-1,0]$, we can substitute the general (i.e. not $E = 0$ specific) leading order solution into the $\mathcal{O}(\varepsilon)$ equation (3.2.9) and find an expression for $f_{1+}(y)$, namely

$$\begin{aligned} f_{1+}(y) &= R_0 + R_1(-y) + R_2(-y)^{1+1/n} + R_3(-y)^{2+1/n} \\ &+R_4(-y)^{2+2/n} + R_5(-y)^{3+2/n} + R_6(-y)^{4+3/n}, \quad y \in [-1,0], \end{aligned} \tag{3.2.25}$$

where R_0–R_6 are constants; the values of R_0, R_1, R_2 and R_3 are to be determined while the values of R_4, R_5 and R_6 are known as they come from the forcing zeroth-order terms in (3.2.9).

We can immediately use the two boundary conditions at $y = -1$ to give two equations relating the R_i coefficients

$$f_{1+}(-1) = 0: \quad R_0 + R_1 + R_2 + R_3 + R_4 + R_5 + R_6 = 0, \tag{3.2.26}$$

$$\begin{aligned} \frac{\mathrm{d}f_{1+}}{\mathrm{d}y}(-1) = 0: \quad & -R_1 - (1+1/n)R_2 - (2+1/n)R_3 - (2+2/n)R_4 \\ & - (3+2/n)R_5 - (4+3/n)R_6 = 0. \end{aligned} \tag{3.2.27}$$

The corresponding function $f_{1-}(y)$ valid on $y \in [0,1]$ is

$$\begin{aligned} f_{1-}(y) &= C_0 + C_1 y + C_2 y^{1+1/n} + C_3 y^{2+1/n} \\ &+C_4 y^{2+2/n} + C_5 y^{3+2/n} + C_6 y^{4+3/n}, \quad y \in [0,1], \end{aligned} \tag{3.2.28}$$

where C_0–C_6 are constants; the values of C_0 up to C_3 are to be determined whereas the values of C_4, C_5 and C_6 are known. Applying the two boundary conditions at $y = 1$ gives two equations for the coefficients C_i

$$f_{1-}(1) = 0: \quad C_0 + C_1 + C_2 + C_3 + C_4 + C_5 + C_6 = 0, \tag{3.2.29}$$

$$\begin{aligned} \frac{\mathrm{d}f_{1-}}{\mathrm{d}y}(1) = 0: \quad & C_1 + (1+1/n)C_2 + (2+1/n)C_3 + (2+2/n)C_4 \\ & + (3+2/n)C_5 + (4+3/n)C_6 = 0. \end{aligned} \tag{3.2.30}$$

It remains to specify four more conditions in order to determine the values of the constants; these conditions are that $f_1(y)$ and $f_1'(y)$ should be continuous at $y = 0$ and that the quantities $f_1''(y)|f_0''(y)|^{n-1}$ and $(f_1''(y)|f_0''(y)|^{n-1})'$ should also be continuous at $y = 0$, the latter two conditions corresponding to the continuity of shear and normal stresses across $y = 0$ respectively. Altogether these specify that

$$C_0 = R_0, \quad C_1 = -R_1, \quad C_2 = R_2, \quad C_3 = -R_3. \tag{3.2.31}$$

Solving the four remaining simultaneous equations for the unknown coefficients gives the values of all the unknowns in terms of C_4, C_5 and C_6

$$C_0 = C_4 = -\frac{(2n)^n(2n+1)^{2-n}(2-E)^{2-n}E}{16(n+1)^2(n+2)}, \tag{3.2.32a}$$

$$C_1 = C_5 + 2C_6 = \frac{(2n)^n(2n+1)^{2-n}(2-E)^{3-n}(8n^2-3n-9)}{48(n+1)^3(3n+2)(4n+3)}, \tag{3.2.32b}$$

$$C_2 = -2C_4 = \frac{(2n)^n(2n+1)^{2-n}(2-E)^{2-n}E}{8(n+1)^2(n+2)}, \tag{3.2.32c}$$

$$C_3 = -2C_5 - 3C_6 = -\frac{(2n)^n(2n+1)^{2-n}(2-E)^{3-n}(3n^2-n-3)}{8(n+1)^3(3n+2)(4n+3)}, \tag{3.2.32d}$$

$$C_4 = -\frac{(2n)^n(2n+1)^{2-n}(2-E)^{2-n}E}{16(n+1)^2(n+2)}, \tag{3.2.32e}$$

$$C_5 = \frac{(n-1)(2n)^n(2n+1)^{2-n}(2-E)^{3-n}}{16(n+1)^3(3n+2)}, \tag{3.2.32f}$$

$$C_6 = -\frac{(2n)^{n+2}(2n+1)^{2-n}(2-E)^{3-n}}{96(n+1)^3(3n+2)(4n+3)}, \tag{3.2.32g}$$

$$R_0 = C_0,\ R_1 = -C_1,\ R_2 = C_2,\ R_3 = -C_3,\ R_4 = C_4,\ R_5 = -C_5,\ R_6 = -C_6. \tag{3.2.32h}$$

We can state the value of β_1 as

$$\beta_1 = \frac{9(2n+1)^2(2-E)^2}{4(3n+2)(4n+3)}. \tag{3.2.33}$$

The first order perturbation term $f_1(y)$ is therefore found to be

$$f_1(y) = \begin{cases} f_{1+}(y) \text{ given in (3.2.25)}, & y \in [-1,0], \\ f_{1-}(y) \text{ given in (3.2.28)}, & y \in [0,1], \end{cases} \tag{3.2.34}$$

where the coefficients C_i and R_i are given in (3.2.32a)–(3.2.32h).

3.3 Linear stability analysis

We wish to perform a numerical linear stability analysis of the power-law viscosity fluid flow in order to establish whether flows are temporally or spatially stable or not. In practice, it is only stable flows that are observable, as the perturbations have not destroyed the base flow to which they were applied. In each case the essence of the method is to take a specified flow field and add an infinitesimal perturbation, either in space or in time, and to see what happens next. If the perturbation decreases to zero, then the base or specified flow is said to be stable to that infinitesimal perturbation; if the perturbation increases without bound and overshadows the base flow, the base flow is said to be unstable to that particular infinitesimal perturbation.

The analysis of stability is based upon reducing the perturbed problem to an eigenvalue problem by linearisation of the perturbed problem about the base flow and approximating the perturbed flow in an appropriate manner. For temporal stability a normal mode representation is used, while for the spatial stability the perturbation takes the form of a power of the space-dimension dependence of the base flow. In doing either of these, an unknown scalar is introduced to the problem, which takes the role of an eigenvalue.

3.3.1 Spatial stability

The steady version of the system (1.3.13a)–(1.3.13e), for the case $n \neq 2$, describes the base flow to which perturbations are applied. We add a spatially-dependent perturbation function $\epsilon H(x,y)$, where $\epsilon \ll 1$, to the base flow described by the stream function, giving $\psi(x,y) = -G(x)F(y) + \epsilon H(x,y)$. Substituting this into the steady system produces

$$\begin{aligned}
&\mathrm{Re}\left\{\left(-GF' + \epsilon H_y\right)\left(-G'F'' + \epsilon H_{xyy}\right) - \left(-G'F + \epsilon H_x\right)\left(-GF''' + \epsilon H_{yyy}\right)\right\} \\
&\qquad = \left(\left|-GF'' + \epsilon H_{yy}\right|^{n-1}\left(-GF'' + \epsilon H_{yy}\right)\right)_{yy}, \\
&\text{on } y = +1: \quad -GF' + \epsilon H_y = 0, \;\; G'F - \epsilon H_x = V(x), \\
&\text{on } y = -1: \quad -GF' + \epsilon H_y = 0, \;\; G'F - \epsilon H_x = (-1+E)V(x),
\end{aligned}$$

where $'$ denotes differentiation with respect to the argument and subscripts refer to partial differentiation. This must now be simplified by expanding the modulus term.

For generic terms $a \neq 0$, b and c one would obtain

$$\begin{aligned}\left|a+\epsilon b+\epsilon^2 c+\cdots\right|^k &= |a|^k \left|1+\epsilon b/a+\epsilon^2 c/a+\cdots\right|^k \\ &= |a|^k + \epsilon k a b\,|a|^{k-2} + \\ &\epsilon^2\left(\frac{k}{2}(2ac+b^2)+\frac{k}{2}(k-2)a^2b^2\right)|a|^{k-2}+\cdots . \end{aligned} \tag{3.3.1}$$

Using this expansion, and neglecting terms of quadratic or greater order in ϵ, produces the following problems at each order

$$\begin{aligned}
&\mathcal{O}(1) \quad \mathrm{Re}GG'\left(F'F''-FF'''\right) = G\,|G|^{n-1}\left(-F''\,|F''|^{n-1}\right)'', \\
&\qquad \text{on } y=+1\text{:}\quad GF'=0,\ G'F=V(x), \\
&\qquad \text{on } y=-1\text{:}\quad GF'=0,\ G'F=(-1+E)V(x), \\
&\mathcal{O}(\epsilon) \quad \mathrm{Re}\left(-GF'H_{xyy}-G'F''H_y+GF'''H_x+G'FH_{yyy}\right) = n\left(H_{yy}\left|-GF''\right|^{n-1}\right)_{yy}, \\
&\qquad \text{on } y=+1\text{:}\quad H_y=0,\ H_x=0, \\
&\qquad \text{on } y=-1\text{:}\quad H_y=0,\ H_x=0.
\end{aligned}$$

The $\mathcal{O}(1)$ terms reproduce the base flow and they can be recast as two separate ordinary differential equations (via the method of separation of variables) in order to determine similarity solutions of the base flow, leading to equations (3.1.20) and (3.1.21)–(3.1.23). However, to progress further with the perturbation function and so the $\mathcal{O}(\epsilon)$ problem, let us seek perturbations of almost the same similarity form as the leading order terms, the only difference being that the spatial functional dependence along the channel length is raised to an unknown power. Thus, we seek solutions of the form

$$\psi(x,y) = -G(x)F(y)+\epsilon G^m(x)\hat{H}(y),\ \ m\in\mathbb{R},$$

and in doing so are restricting the question of stability to that of perturbations of powers of similarity solutions of separable form. This therefore leaves the question of the spatial stability of a solution with respect to perturbations of a more general form to be considered elsewhere. Recalling that we sought nontrivial $G(x)$ satisfying (3.1.20), the governing equation for the $\mathcal{O}(\epsilon)$ problem is

$$mr\mathrm{Re}\left(F'\hat{H}''-F'''\hat{H}\right)+r\mathrm{Re}\left(F''\hat{H}'-F\hat{H}'''\right) = -n\left(\hat{H}''\,|F''|^{n-1}\right)''.$$

If we define a scaled Reynolds number

$$\hat{R} = \frac{r\mathrm{Re}}{n} = \frac{\mathrm{Re}}{n(2-n)} \tag{3.3.2}$$

then we can restate the $\mathcal{O}(\epsilon)$ problem as

$$m\hat{R}\left(F'\hat{H}'' - F'''\hat{H}\right) + \hat{R}\left(F''\hat{H}' - F\hat{H}'''\right) = -\left(\hat{H}''\left|F''\right|^{n-1}\right)''.$$

It now remains to apply appropriate boundary conditions to the perturbation function. The boundary conditions at the channel walls are solely $\mathcal{O}(1)$ conditions and so the correct spatial perturbation boundary conditions are homogeneous. Thus, the eigenvalue problem for determination of the spatial stability of a given base flow F can be stated as

$$m\hat{R}\left(F'''\hat{H} - F'\hat{H}''\right) + \hat{R}\left(F\hat{H}''' - F''\hat{H}'\right) = \left(\hat{H}''\left|F''\right|^{n-1}\right)'', \tag{3.3.3}$$

$$\text{on } y = +1: \quad \hat{H}' = 0, \quad \hat{H} = 0, \tag{3.3.4}$$

$$\text{on } y = -1: \quad \hat{H}' = 0, \quad \hat{H} = 0. \tag{3.3.5}$$

Where nontrivial functions $\hat{H}$ satisfying (3.3.3)–(3.3.5) exist they are called eigenfunctions and the corresponding values of m are called eigenvalues. The stability of solutions is determined by the eigenvalues, and their interpretation is summarised in Table 3.1. This has been constructed by considering the general behaviour of the x^λ term multiplying the y-dependent function $\hat{H}$, and the behaviour described there should be compared with numerical computation of the eigenvalues and corresponding eigenfunctions. For example, for large values of x, the suction problem has fluid entering the channel from large x positions. If the product $(m-1)\lambda > 0$, then the perturbation term may not be smaller than the base flow and in this case the disturbances would overshadow the base flow behaviour, destroying the similarity solution downstream of the channel end. Thus, the suction problem is unstable to perturbations when $(m-1)\lambda > 0$; this produces the entries for both $\lambda > 0$, $m > 1$ and $\lambda < 0$, $m < 1$ when $x \gg 1$. Then it does not matter whether the flow is stable or not for $x \ll 1$, as the similarity form has already been destroyed by the perturbations and so the solution form that has been assumed is no longer valid. In the case of fluid injection the perturbation at $x \ll 1$ must remain small for the injection flow to be stable; the product $(m-1)\lambda < 0$ must be satisfied for $x^{m\lambda} < x$ as $x \ll 1$. If the flow is unstable for $x \ll 1$ then the corresponding downstream flow for $x \gg 1$ is not necessarily going to be of the assumed similarity form.

		$x \ll 1$		$x \gg 1$	
		$\lambda < 0$ $(n > 2)$	$\lambda > 0$ $(0 < n < 2)$	$\lambda < 0$ $(n > 2)$	$\lambda > 0$ $(0 < n < 2)$
Inj.	$m < 1$	stable	unstable	unstable	unstable
	$m > 1$	unstable	stable	unstable	unstable
Suc.	$m < 1$	-	unstable	unstable	stable
	$m > 1$	unstable	-	stable	unstable

Table 3.1. Summary of the predictions of spatial stability of similarity solutions for values of the eigenvalue m, parameter $\lambda = 1/(2-n)$ and for large or small x. An entry of "–" in the suction cases indicates that the upstream position is unstable and so no prediction can be made about stability of the location in question in the case of suction.

In the case $n = 1$ (Newtonian fluid flow) the stability problem reduces to

$$m\mathrm{Re}\left(F'''\hat{H} - F'\hat{H}''\right) + \mathrm{Re}\left(F\hat{H}''' - F''\hat{H}'\right) = \hat{H}^{(\mathrm{iv})}, \tag{3.3.6}$$

$$\text{on } y = +1: \quad \hat{H}' = 0, \quad \hat{H} = 0, \tag{3.3.7}$$

$$\text{on } y = -1: \quad \hat{H}' = 0, \quad \hat{H} = 0. \tag{3.3.8}$$

3.3.2 Temporal stability

In order to consider the temporal stability of the fluid flow we must start with the system (1.3.13a)–(1.3.13e) (for the case $n \neq 2$). Before adding perturbations to the base flow, it is worthwhile recording, for future reference, a similarity solution for the unsteady problem. Substituting the variables

$$x = \alpha\bar{x}, \; y = \beta\bar{y}, \; \psi = \gamma\bar{\psi}, \; t = \delta\bar{t} \quad (\alpha, \beta, \gamma, \delta \in \mathbb{R} > 0)$$

into the unsteady partial differential equation yields the following relations between the four quantities

$$\frac{\gamma}{\beta^2\delta} = \frac{\gamma^2}{\alpha\beta^3} = \frac{\gamma^n}{\beta^{2n+2}}.$$

First, noting that as the y-domain of the channel is fixed, we must have $\beta = 1$. Then we find that

$$\gamma = \alpha^{\frac{1}{2-n}}, \; \delta = \alpha^{\frac{1-n}{2-n}},$$

and so the form of similarity solution for the unsteady problem is

$$\bar{\psi}(\bar{x}, \bar{y}, \bar{t}) = x^{\frac{1}{2-n}}\psi(1, y, tx^{\frac{n-1}{2-n}}) = x^{\frac{1}{2-n}}f(y, \tau), \quad \tau = tx^{\frac{n-1}{2-n}}. \tag{3.3.9}$$

Returning to the question of temporal stability, we now add a time-dependent perturbation function to the steady base flow stream function. Substituting

$$\psi(x,y,t) = -G(x)F(y) + \epsilon H(x,y,t), \quad \epsilon \ll 1,$$

into the unsteady system produces

$$\begin{aligned}
&\mathrm{Re}\left(\epsilon H_{yyt} + \left(-GF' + \epsilon H_y\right)\left(-G'F'' + \epsilon H_{xyy}\right)\right.\\
&\qquad \left. - \left(-G'F + \epsilon H_x\right)\left(-GF''' + \epsilon H_{yyy}\right)\right)\\
&= \left(|-GF'' + \epsilon H_{yy}|^{n-1}\left(-GF'' + \epsilon H_{yy}\right)\right)_{yy}.
\end{aligned}$$

Using the expansion for the modulus given in equation (3.3.1), we obtain the following leading order and first order perturbation problems,

$$\begin{aligned}
\mathcal{O}(1)\quad & \mathrm{Re}GG'\left(F'F'' - FF'''\right) = -G|G|^{n-1}\left(F''|F''|^{n-1}\right)'',\\
& \text{on } y=+1\text{:}\quad GF' = 0,\ G'F = V(x),\\
& \text{on } y=-1\text{:}\quad GF' = 0,\ G'F = (-1+E)V(x),\\
\mathcal{O}(\epsilon)\quad & \mathrm{Re}\left(H_{yyt} - G'\left(F''H_y - FH_{yyy}\right) - G\left(F'H_{xyy} - F'''H_x\right)\right)\\
& \qquad = n|G|^{n-1}\left(|F''|^{n-1}H_{yy}\right)_{yy},\\
& \text{on } y=+1\text{:}\quad H_y = 0,\ H_x = 0,\\
& \text{on } y=-1\text{:}\quad H_y = 0,\ H_x = 0.
\end{aligned}$$

The $\mathcal{O}(1)$ statement reproduces the steady base flow problem (3.1.16)–(3.1.18) and so we can use the fact that the functions $F(y)$, $G(x)$ satisfy separate ordinary differential equations; in particular, if we use (3.1.20) in the first order perturbation problem we can replace $r|G|^{n-1}$ with G'. If we now require $H(x,y,t)$ to be of the form

$$H(x,y,t) = \exp(st)\bar{H}(x,y)$$

then we may obtain, after cancelling common factors, the following bidimensional eigenvalue problem,

$$r\mathrm{Re}\left(s\frac{\bar{H}_{yy}}{G'} + \frac{G}{G'}\left(F'''\bar{H}_x - F'\bar{H}_{xyy}\right) + F\bar{H}_{yyy} - F''\bar{H}_y\right) = n\left(|F''|^{n-1}\bar{H}_{yy}\right)_{yy}, \tag{3.3.10}$$

$$\text{on } y=+1\text{:}\quad \bar{H}_y = 0,\ \bar{H}_x = 0, \tag{3.3.11}$$

$$\text{on } y=-1\text{:}\quad \bar{H}_y = 0,\ \bar{H}_x = 0. \tag{3.3.12}$$

In order to obtain one dimensional eigenvalue problems we must use a different form for the perturbation term rather than just expanding in normal modes, as this fails to work here. It is found that we need a non-uniform time scale dependent upon the function $G'(x)$[1]. Returning to the $\mathcal{O}(\epsilon)$ problem above, setting

$$H(x,y,t) = -G(x)f(y,\tau), \quad \tau = G'(x)t, \tag{3.3.13}$$

produces the partial differential equation for $f(y,\tau)$,

$$\begin{aligned} r\mathrm{Re}\left(-f_{yy\tau} - Ff_{yyy} + F''f_y + F'\left(f_{yy} + (n-1)\tau f_{yy\tau}\right)\right. \\ \left. -F'''\left(f + (n-1)\tau f_\tau\right)\right) = -n\left(|F''|^{n-1}f_{yy}\right)_{yy}, \end{aligned} \tag{3.3.14}$$

where we have used the fact that

$$\frac{GG''}{G'} = (n-1)G'.$$

If we wish to obtain an ordinary differential equation boundary value problem, we must split the function $f(y,\tau)$ into separate y- and τ-dependent functions. Then we must approximate the τ-dependence for large and small τ. Thus the total perturbed stream function becomes

$$\psi(x,y,t) = G(x)\left(-F(y) + \epsilon f(y,\tau)\right) = G(x)\left(-F(y) + \epsilon f_0(y)T(\tau)\right), \tag{3.3.15}$$

and we now wish to approximate $T(\tau)$ in the limits of large and small τ.

For $\tau \ll 1$ the partial differential equation (3.3.14) becomes

$$r\mathrm{Re}\left(-f_{0_{yy}}T_\tau - Ff_{0_{yyy}}T + F''f_{0_y}T + F'f_{0_{yy}}T + F'''f_0T\right) = -n\left(|F''|^{n-1}f_{0_{yy}}T\right)_{yy}.$$

If we assume that

$$T(\tau) = \exp(s\tau), \quad \text{for } \tau \ll 1, s \in \mathbb{R},$$

then upon simplification we are left with the following eigenvalue problem for $f_0(y)$, where s is the unknown eigenvalue and the base flow F has already been determined,

$$n\left(|F''|^{n-1}f_0''\right)'' + r\mathrm{Re}\left(F'f_0'' + F''f_0' - F'''f_0 - Ff_0'''\right) = sr\mathrm{Re}f_0'', \tag{3.3.16}$$

$$\text{on } y = +1: \quad f_0' = 0, \ f_0 = 0, \tag{3.3.17}$$

$$\text{on } y = -1: \quad f_0' = 0, \ f_0 = 0. \tag{3.3.18}$$

[1]This is reminiscent of the similarity solution form described in equation (3.3.9)

For $\tau \gg 1$, we approximate $T(\tau)$ by

$$T(\tau) = \tau^s, \quad \text{for } \tau \gg 1,\ s \in \mathbb{R},$$

and then substitute this into the partial differential equation (3.3.14). Using the fact that $\tau \gg 1$, the partial differential equation is simplified to become the following eigenvalue problem

$$\begin{aligned} &n\left(|F''|^{n-1}f_0''\right)'' + r\mathrm{Re}\left(F''f_0' + F'f_0'' - F'''f_0 - Ff_0'''\right) \\ &= s\mathrm{Re}r(n-1)\left(F'''f_0 - F'f_0''\right), \qquad (3.3.19) \\ &\text{on } y = +1: \quad f_0' = 0,\ (1+(n-1)s)f_0 = 0, \qquad (3.3.20) \\ &\text{on } y = -1: \quad f_0' = 0,\ (1+(n-1)s)f_0 = 0, \qquad (3.3.21) \end{aligned}$$

where s is the unknown eigenvalue and the base flow F has already been found. This particular form of perturbation, arising from the need to split the variables for the perturbation in a different manner from that for normal modes, has been used in the analysis of the spatial and temporal stability of Jeffery-Hamel flows[2] by McAlpine and Drazin [MD98].

The case where $\tau \gg 1$ is able to give information about the stability properties at different positions along the channel, i.e. for $\tau \gg 1$ we can have

- $G' \gg 1,\ t = \mathcal{O}(1)$: stability information for large x-positions at small and order one times, as $G' \sim x^\lambda$;
- $G' \ll 1,\ t = \mathcal{O}(1)$: stability information for small times near the channel origin ;
- $G' = \mathcal{O}(1),\ t \gg 1$: stability information for large times for order one x-positions within the channel.

3.4 Regularisation for power-law viscosity numerical work

In order to perform numerical studies upon the ordinary differential equation for $f(y)$ we must use a regularised version of the problem. This is because the function $|f''(y)|$ is not analytic, and this causes numerical routines to have problems converging upon a correct solution. The regularisation modifies the problem so that the resulting function $(f''^2+\delta^2)^{1/2}$ is analytic and the value $\delta > 0$ is user provided. The parameter δ is chosen

[2] A Jeffery-Hamel flow is, in polar coordinates (r,θ), the two-dimensional flow of incompressible viscous fluid between stationary impermeable planes located at $\theta = \pm\alpha$, driven by a steady source or sink of fluid of strength Q at $r = 0$ where the planes intersect.

to be small, and the idea is that, as it is reduced, the solutions obtained for successive δ-values should become better and better approximations to the solution of the original problem, where the nonanalytic terms appear.

Using the regularisation

$$|f''| \to \mathcal{A} = \left(f''^2 + \delta^2\right)^{\frac{1}{2}} \tag{3.4.1}$$

the nondimensional power-law part of the viscosity term μ becomes

$$\mu \to \left(f''^2 + \delta^2\right)^{\frac{n-1}{2}} = \mathcal{A}^{n-1} \tag{3.4.2}$$

and the ordinary differential equation that is to be solved is now

$$r\mathrm{Re}\left(f'f'' - ff'''\right) = -f^{(\mathrm{iv})}\left(nf''^2 + \delta^2\right)\mathcal{A}^{n-3} - (n-1)f''f'''^2\left(nf''^2 + 3\delta^2\right)\mathcal{A}^{n-5} \tag{3.4.3}$$

$$\text{on } y = +1: \quad f' = 0, \ f = 1, \tag{3.4.4}$$

$$\text{on } y = -1: \quad f' = 0, \ f = -1 + E, \tag{3.4.5}$$

where r is the aforementioned separation constant.

3.4.1 Regularised spatial stability problem

In order to perform numerical solutions of the spatial stability problem, we again will need to regularise the problem formulation in the same manner as that for the base flow problem considered above in §3.4. Performing the regularisation the spatial stability problem is then restated in a form that can be further manipulated, if needed, for numerical work, as follows

$$\begin{aligned} &mr\mathrm{Re}\left(F'''H - F'H''\right) + r\mathrm{Re}\left(FH''' - F''H'\right) \\ &= nH^{(\mathrm{iv})}\mathcal{A}^{n-1} + 2n(n-1)\mathcal{A}^{n-3}F''F'''H''' \\ &+ n(n-1)(n-3)H''\left(F''\right)^2\left(F'''\right)^2\mathcal{A}^{n-5} + n(n-1)H''\left(F'''^2 + F''F^{(\mathrm{iv})}\right)\mathcal{A}^{n-3} \end{aligned} \tag{3.4.6}$$

$$\text{on } y = +1: \quad H' = 0, \quad H = 0, \tag{3.4.7}$$

$$\text{on } y = -1: \quad H' = 0, \quad H = 0, \tag{3.4.8}$$

where r is the separation constant arising from the base flow problem, F is proportional to the transverse fluid velocity component in the base problem, m is the unknown eigen-

value and H is the unknown eigenfunction. This problem must be supplemented by one more condition in order to determine the eigenfunctions, which acts as a normalisation condition. In this case we take

$$H''(-1) = 1. \tag{3.4.9}$$

In the case $n = 1$, the regularised spatial stability problem reduces to

$$mr\mathrm{Re}\left(F'''H - F'H''\right) + \mathrm{Re}\left(FH''' - F''H'\right) = H^{(\mathrm{iv})}, \tag{3.4.10}$$

$$\text{on } y = +1: \quad H' = 0, \quad H = 0, \tag{3.4.11}$$

$$\text{on } y = -1: \quad H' = 0, \quad H = 0, \tag{3.4.12}$$

which agrees with the analytical formulation of the problem given earlier in (3.3.6)–(3.3.8), and in previous work by [ZDB88] and [DB84].

3.4.2 Regularised temporal stability problem

Again, a regularisation of the modulus term is required in order to perform numerical work on the temporal stability eigenproblem. However, in this case there will be two different regularised problems, corresponding to the two τ limits appearing in the temporal stability problem's formulation.

For the first, $\tau \ll 1$ limit, the regularised eigenproblem for the eigenfunction $f_0(y)$ and eigenvalue s is

$$\begin{aligned} sr\mathrm{Re}f_0'' &= n\mathcal{A}^{n-1}f_0^{(\mathrm{iv})} + 2n(n-1)F''F'''f_0'''\mathcal{A}^{n-3} + n(n-1)f_0''\left(F'''^2 + F''F^{(\mathrm{iv})}\right)\mathcal{A}^{n-3} \\ &+ n(n-1)(n-3)f_0''F''^2F'''^2\mathcal{A}^{n-5} + r\mathrm{Re}\left(F'f_0'' + F''f_0' - F'''f_0 - Ff_0'''\right) \end{aligned} \tag{3.4.13}$$

$$\text{on } y = +1: \quad f_0' = 0, \ f_0 = 0, \tag{3.4.14}$$

$$\text{on } y = -1: \quad f_0' = 0, \ f_0 = 0, \tag{3.4.15}$$

and the eigenfunction normalisation condition is

$$f_0''(-1) = 1. \tag{3.4.16}$$

For the limit $\tau \gg 1$, the regularised temporal stability problem for the eigenfunction

$f_0(y)$ and eigenvalue s becomes

$$\begin{aligned} &sr(n-1)\mathrm{Re}\left(F'''f_0 - F'f_0''\right) = n\mathcal{A}^{n-1}f_0^{(\mathrm{iv})} \\ &+ 2n(n-1)f_0'''F''F''''\mathcal{A}^{n-3} + n(n-1)f_0''\left(F''''^2 + F''F^{(\mathrm{iv})}\right)\mathcal{A}^{n-3} \\ &+ n(n-1)(n-3)f_0''F''^2F''''^2\mathcal{A}^{n-5} \\ &+ r\mathrm{Re}\left(F'f_0'' + F''f_0' - F''''f_0 - Ff_0'''\right), \end{aligned} \tag{3.4.17}$$

$$\text{on } y = +1: \quad f_0' = 0,\ (1+(n-1)s)f_0 = 0, \tag{3.4.18}$$

$$\text{on } y = -1: \quad f_0' = 0,\ (1+(n-1)s)f_0 = 0, \tag{3.4.19}$$

and the eigenfunction normalisation condition is

$$f_0''(-1) = 1. \tag{3.4.20}$$

In the specific case of $n = 1$ where the temporal stability of Newtonian fluid flow is being considered, the temporal stability problem reduces to

$$s\mathrm{Re}f_0'' = f_0^{(\mathrm{iv})} + \mathrm{Re}\left(F'f_0'' + F''f_0' - Ff_0''' - F''''f_0\right), \tag{3.4.21}$$

$$\text{on } y = +1: \quad f_0' = 0,\ f_0 = 0, \tag{3.4.22}$$

$$\text{on } y = -1: \quad f_0' = 0,\ f_0 = 0, \tag{3.4.23}$$

together with the eigenfunction normalisation condition,

$$f_0''(-1) = 1, \tag{3.4.24}$$

which also agrees with the analytical formulation (3.3.16)–(3.3.18).

3.4.3 Summary

In this chapter we have found a similarity solution for the flow of a power-law fluid in a channel driven by fluid injection or suction through the porous channel walls. We have then used this solution as a basis for a small Re expansion of the solution, for linear spatial and temporal stability problems and then presented the equivalent regularised problems for flow and stability calculations. In subsequent chapters we restrict attention to the power-law fluid with exponent $n \in (0, 2)$. Flowing materials modelled by power-law fluid viscosity models are more commonly found with their power-law exponents in this range than for $n > 2$. We shall further restrict attention of the fluid flow to that within a one porous walled channel, corresponding to the problem selection parameter $E = 1$.

Chapter 4

Isothermal power law fluid problem - one porous walled channel

4.1 Numerical results for base flows

4.1.1 Type I solution bifurcation results

In this section we produce bifurcation diagrams for the various power law flows considered and a selection of assorted profiles. In each bifurcation plot the variable plotted on horizontal axis is $\hat{R}$ (defined in equation (3.3.2)), but the quantity plotted on the vertical axis depends upon the wall being considered. If the upper wall is considered then the quantity plotted on the vertical axis is $-f''(1)$ (or its logarithm depending upon the scales of the surrounding data). The quantity $-f''(1)$ is plotted rather than $f''(1)$ as the latter is generally negative. The importance of the second derivative of $f(y)$ is that it is related to the viscous shear stress and so $f''(1)$ is proportional to the viscous stress at the upper wall[1].

The regularised system (3.4.3)–(3.4.5) has been solved for each set of data plotted with the value of the regularisation parameter $\delta = 0.01$ unless otherwise stated.

[1]The upper wall stress per unit area is given by $\tau_w = \mu\psi_{yy}(x,1)$ with units Pa and has the dimensionless form $\tau_w = -K\left|V_0V_UL/2h^2\right|^{n-1}(V_0V_UL/h^2)x^{1/(2-n)}\left|x^{1/(2-n)}\right|^{n-1}f''(1)\left|f''(1)\right|^{n-1}$ using the similarity form $\psi = -x^{1/(2-n)}f(y)$.

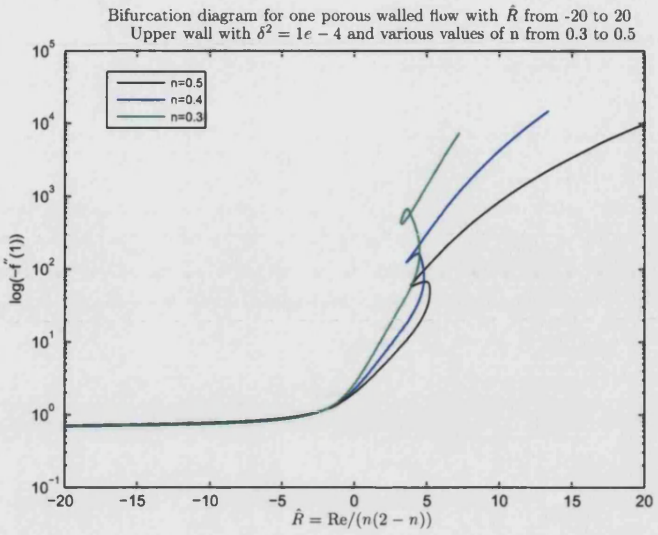

Figure 4.1.1. Bifurcation diagram for upper-wall data for various $0.3 \leq n \leq 0.5$

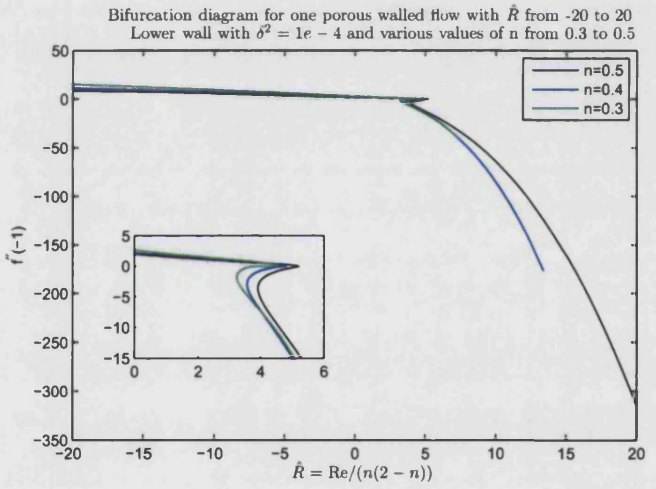

Figure 4.1.2. Bifurcation diagram for lower-wall data for various $0.3 \leq n \leq 0.5$

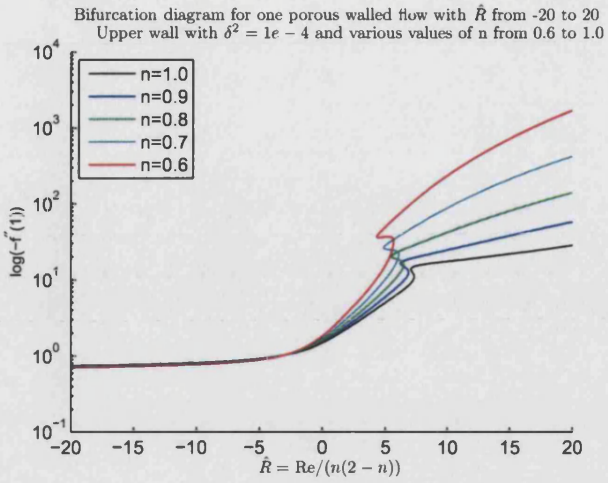

Figure 4.1.3. Bifurcation diagram for upper-wall data for various $0.6 \leq n \leq 1$

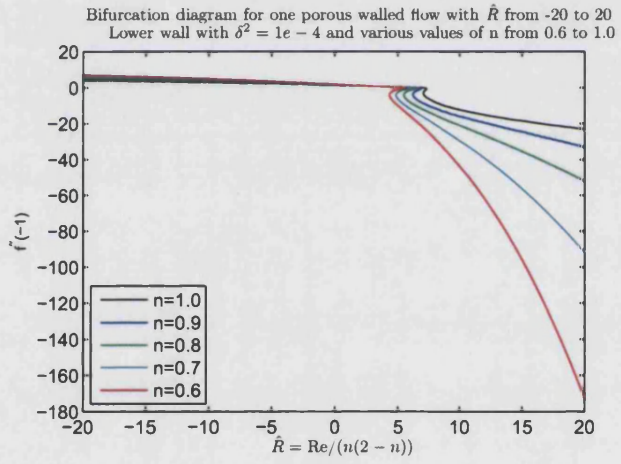

Figure 4.1.4. Bifurcation diagram for lower-wall data for various $0.6 \leq n \leq 1$

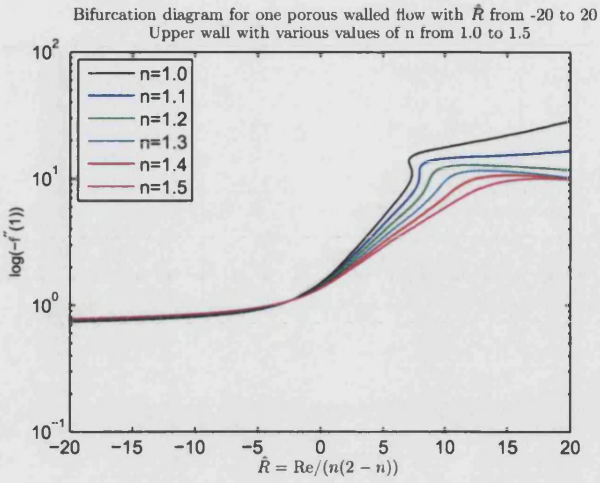

Figure 4.1.5. Bifurcation diagram for upper-wall data for various $1 \leq n \leq 1.5$

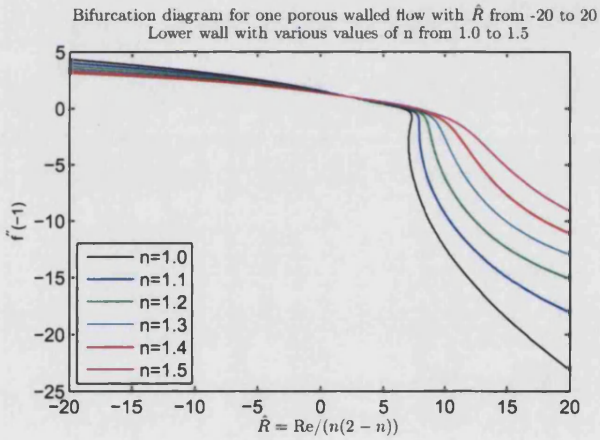

Figure 4.1.6. Bifurcation diagram for lower-wall data for various $1 \leq n \leq 1.5$

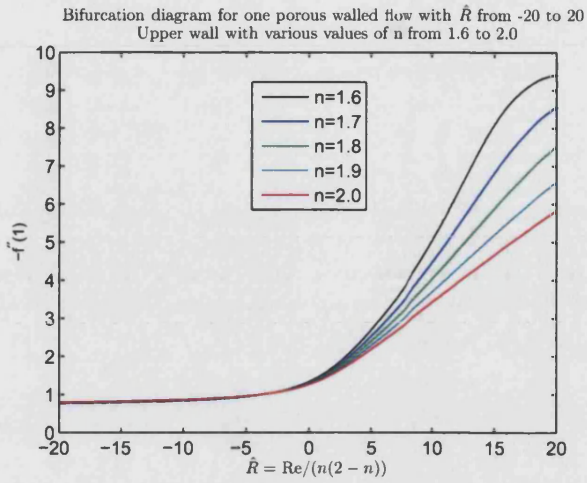

Figure 4.1.7. Bifurcation diagram for upper-wall data for various $1.6 \leq n \leq 2$. Note the change of scale for the vertical axis.

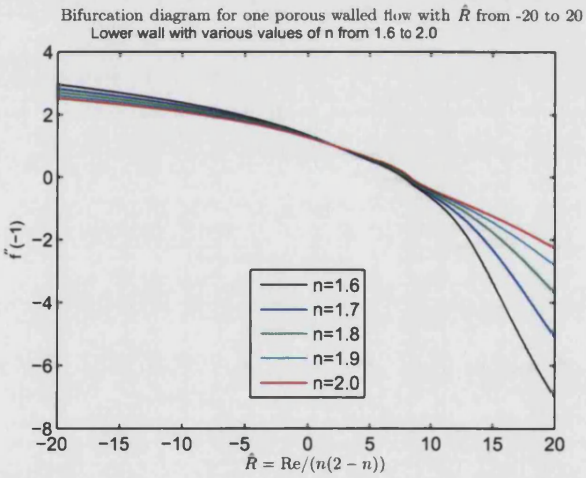

Figure 4.1.8. Bifurcation diagram for lower-wall data for various $1.6 \leq n \leq 2$

A selection of solutions for fixed values of the flow index n are now given. The two most extreme values of the scaled Reynolds number $\hat{R} = \mathrm{Re}/(n(2-n))$ are for the cases of high injection and suction rates; the intermediate values that are chosen depend on whether the fluid is shear-thinning or shear-thickening. If it is shear-thinning $(0 < n < 1)$ then the intermediate points are where there are turning points on the bifurcation curve. If it is shear-thickening $(1 < n < 2)$ then an intermediate point is chosen where the lower wall stress vanishes and then a second point is chosen if there is a turning point on the curve.

The quantities plotted are $f(y)$ and the first three derivatives of $f(y)$. The values for $f(y)$ and $f'(y)$ are proportional to the vertical and horizontal components of velocity respectively. The quantity $f''(y)$ is related to the fluid vorticity by $\nabla \wedge \psi = \omega \boldsymbol{k} = x f'' \boldsymbol{k}$ and so $f'''(y)$ is proportional to the gradient of the vorticity in the y direction.

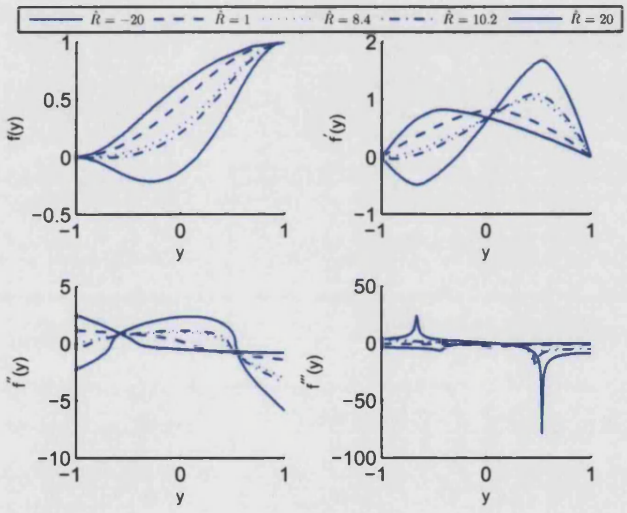

Figure 4.1.9. Flow function $f(y)$ and its first three derivatives for selected values of Re with $n = 2$. The quantity $\hat{R}$ is not used as the governing equation for $f(y)$ does not admit the same scalings for its solution and as such the separation constant in its derivation is arbitrary, and has been taken to have the value of 1 in the case of suction and -1 for injection.

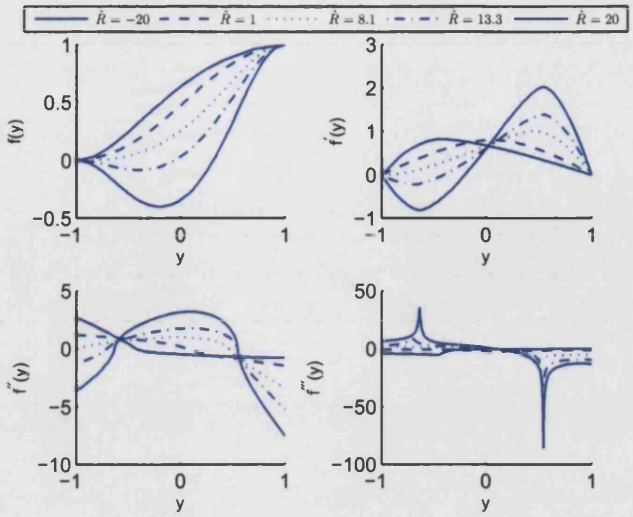

Figure 4.1.10. Flow function $f(y)$ and its first three derivatives for selected values of $\hat{R}$ with $n = 1.8$.

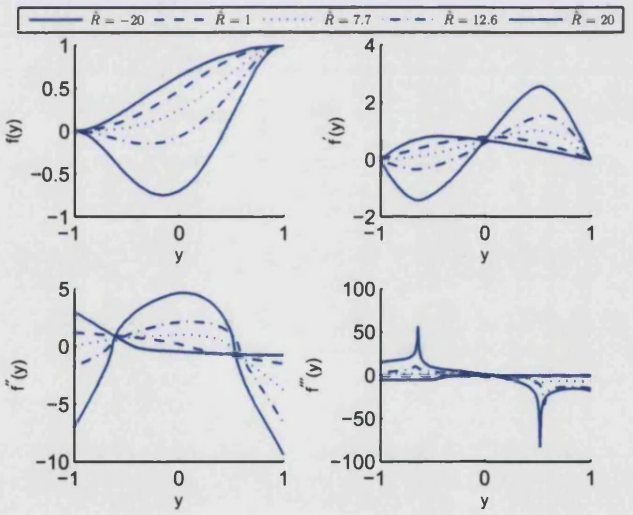

Figure 4.1.11. Flow function $f(y)$ and its first three derivatives for selected values of $\hat{R}$ with $n = 1.6$.

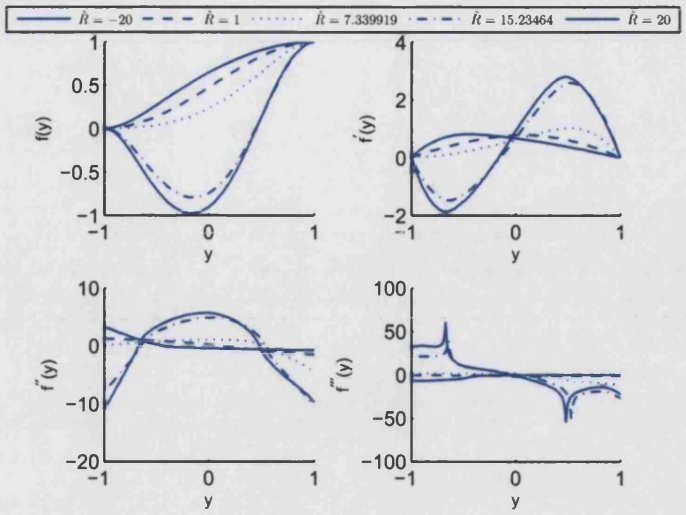

Figure 4.1.12. Flow function $f(y)$ and its first three derivatives for selected values of $\hat{R}$ with $n = 1.4$.

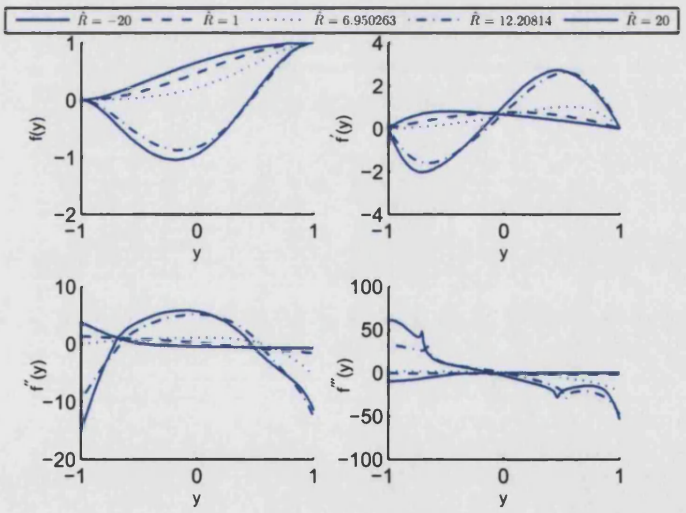

Figure 4.1.13. Flow function $f(y)$ and its first three derivatives for selected values of $\hat{R}$ with $n = 1.2$.

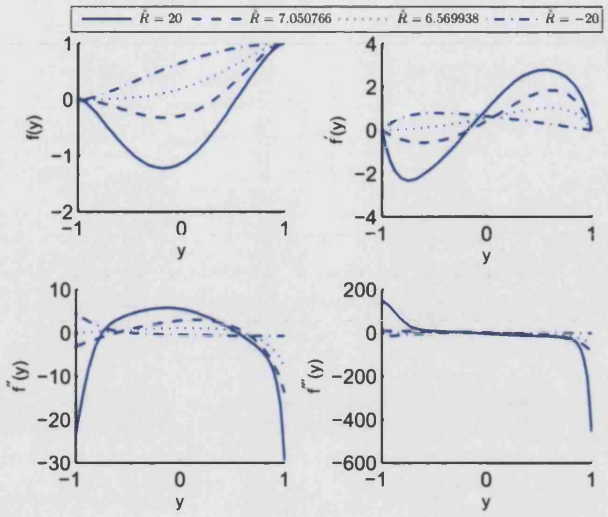

Figure 4.1.14. Flow function $f(y)$ and its first three derivatives for selected values of $\hat{R}$ with $n = 1$.

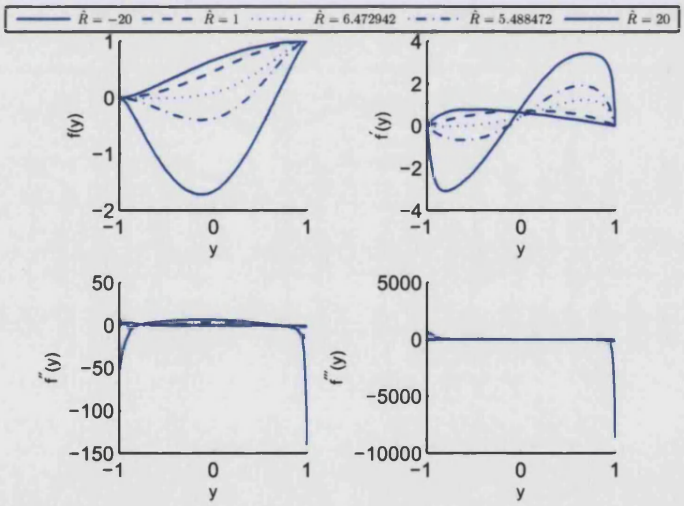

Figure 4.1.15. Flow function $f(y)$ and its first three derivatives for selected values of $\hat{R}$ with $n = 0.8$.

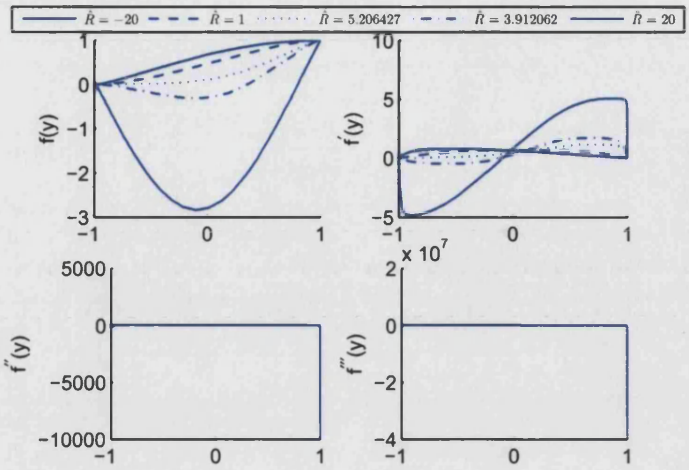

Figure 4.1.16. Flow function $f(y)$ and its first three derivatives for selected values of $\hat{R}$ with $n = 0.5$.

Figures 4.1.1–4.1.8 show the upper and lower wall bifurcation diagrams for the one porous walled channel flow of a power-law fluid for a range of values of exponent n. The main feature of the upper wall diagrams for shear-thinning fluids ($n < 1$) as compared to the Newtonian fluid ($n = 1$) is that the region of hysteresis remains for suction flow and occurs for lower values of $\hat{R}$ as n decreases, whereas the wall stress is increasing as n decreases and the hysteresis region rotates anticlockwise as n decreases. For small enough values of n (stronger shear-thinning fluids) there is a looped region of hysteresis. The corresponding lower wall plots for shear-thinning fluid show that the lower wall stresses for suction flow also increase as n decreases; the hysteresis region becoming flatter in height and covering a greater range of $\hat{R}$ as n decreases. For the injection flow, the upper and lower wall behaviours remain similar as n decreases and are not dissimilar to the Newtonian fluid where $n = 1$.

The solutions for $n = 0.8$ and $n = 0.5$ (Figures 4.1.15 and 4.1.16 respectively) show that injection flow is very similar to that of a Newtonian fluid (Figure 4.1.14). For small values of suction, up to the first turning point on the region of hysteresis, the profiles for $n = 0.8$ and $n = 0.5$ are similar. The final profile for $\hat{R} = 20$ does show differences between the two flows. For $n = 0.5$ the minimum of $f(y)$ is less than that for $n = 0.8$ and the boundary layers in $f'(y)$ for $n = 0.5$ are thinner than those for $n = 0.8$, with a resulting increase in the gradients of $f'(y)$ as these layers are encountered adjacent to the walls. The values of $f''(\pm 1)$ and $f'''(\pm 1)$ are much greater for $n = 0.5$ as compared with $n = 0.8$ and so the wall shear stresses are accordingly greater for smaller n.

As n increases above 1 the bifurcation diagrams for the shear-thickening fluid (Fig-

ures 4.1.5–4.1.8) change in character. The region of hysteresis is lost and the upper wall suction curves flatten out as n increases from $n = 1.1$ to $n = 1.9$, with the maximum value of $-f''(1)$ decreasing as n increases. The lower wall suction curves display a similar trend in that, as n increases, the hysteresis region is lost and the minimum value of $f''(-1)$ reduces towards zero as n increases. An artefact of the hysteresis region remains on the lower wall curves for $n > 1.5$ and near the zero of $f''(-1)$ the curvature of these curves changes sign as n increases. The injection regions for each n are all similar and only the lower wall bifurcation diagrams help to distinguish the curves; the upper wall stress increases as n increases, for a fixed value of $\hat{R}$, and the lower-wall stress decreases as n increases.

The solutions for shear-thickening fluids (Figures 4.1.13–4.1.10) have qualitative similarities. As n increases, the minimum value of the suction $f(y)$ profiles reduces from below -1 when $n = 1.2$ to above -0.5 when $n = 1.8$. The profiles for $f'(y)$ are all sinusoidal for $n > 1$ suction flow, indicating a region of reversed flow where $f'(y) < 0$, and the behaviour of $f'(y)$ around its maxima becomes more peaked as n increases. As the fluid becomes more shear-thickening the wall values of $f''(\pm 1)$ change their relative ordering, from $f''(-1) < f''(1)$ when $n = 1.2$ to $f''(-1) > f''(1)$ when $n = 1.8$. The profiles of $f''(y)$ for injection flow all show that there is an area of non-zero f'' near the lower wall and then $f'' \approx 0$ for the majority of the remaining channel width. The interior zero of $f''(y)$ closest to the upper wall is located on a region with an increasingly steep negative gradient as n increases above 1 and this can be seen in the sizes of the spikes of $f'''(y)$ as n increases.

For $n = 2$ the values of $\hat{R}$ are the same as for Re as the separation constant coming from the separation of variables similarity solution is now arbitrary as compared to the $n \neq 2$ case (where it was determined as $r = 1/(2 - n)$). The trends described for the shear thickening power-law fluid above are still shown for the $n = 2$ bifurcation digram (Figures 4.1.7 and 4.1.8) and for the solution plotted in Figure 4.1.9.

4.1.2 Type I analysis and asymptotics

Small Re asymptotics

The small Reynolds number asymptotics derived in §3.2.1 can be specialised to the isothermal one porous walled channel setting by letting $E = 1$. In this case the first

two terms of the expansion for $f(y)$ are

$$f(y) = f_0(y) + \varepsilon f_1(y) \quad \left(\text{where } \varepsilon = \frac{\mathrm{Re}}{2-n}\right)$$
$$= \begin{cases} f_{0+}(y) + \varepsilon f_{1+}(y), & y \in [-1,0], \\ f_{0-}(y) + \varepsilon f_{1-}(y), & y \in [0,1], \end{cases}$$

where

$$f_{0+}(y) = \frac{n+1}{2n}(-y)^{2+1/n} + \frac{2n+1}{2(n+1)}y + \frac{1}{2},$$
$$f_{0-}(y) = -\frac{n+1}{2n}y^{2+1/n} + \frac{2n+1}{2(n+1)}y + \frac{1}{2},$$
$$\begin{aligned} f_{1+}(y) = &-\frac{(2n)^n(2n+1)^{2-n}}{16(n+1)^2(n+2)} - \frac{(2n)^n(2n+1)^{2-n}(8n^2-3n-9)}{48(n+1)^3(3n+2)(4n+3)}(-y) \\ &+ \frac{(2n)^n(2n+1)^{2-n}}{8(n+1)^2(n+2)}(-y)^{1+1/n} + \frac{(2n)^n(2n+1)^{2-n}(3n^2-n-3)}{8(n+1)^3(3n+2)(4n+3)}(-y)^{2+1/n} \\ &- \frac{(2n)^n(2n+1)^{2-n}}{16(n+1)^2(n+2)}(-y)^{2+2/n} - \frac{(n-1)(2n)^n(2n+1)^{2-n}}{16(n+1)^3(3n+2)}(-y)^{3+2/n} \\ &+ \frac{(2n)^{n+2}(2n+1)^{2-n}}{96(n+1)^3(3n+2)(4n+3)}(-y)^{4+3/n}, \end{aligned}$$
$$\begin{aligned} f_{1-}(y) = &-\frac{(2n)^n(2n+1)^{2-n}}{16(n+1)^2(n+2)} + \frac{(2n)^n(2n+1)^{2-n}(8n^2-3n-9)}{48(n+1)^3(3n+2)(4n+3)}y \\ &+ \frac{(2n)^n(2n+1)^{2-n}}{8(n+1)^2(n+2)}y^{1+1/n} - \frac{(2n)^n(2n+1)^{2-n}(3n^2-n-3)}{8(n+1)^3(3n+2)(4n+3)}y^{2+1/n} \\ &- \frac{(2n)^n(2n+1)^{2-n}}{16(n+1)^2(n+2)}y^{2+2/n} + \frac{(n-1)(2n)^n(2n+1)^{2-n}}{16(n+1)^3(3n+2)}y^{3+2/n} \\ &- \frac{(2n)^{n+2}(2n+1)^{2-n}}{96(n+1)^3(3n+2)(4n+3)}y^{4+3/n}. \end{aligned}$$

In particular this predicts the value of $f''(1)$ for small ε to be

$$f''(1) = -\frac{2n+1}{2n} - \varepsilon\frac{(5n^2+8n+6)(2n)^{n-2}(2n+1)^{2-n}}{(n+2)(3n+2)(4n+3)} + \mathcal{O}\left(\varepsilon^2\right), \tag{4.1.1}$$

which, when $n = 1$, agrees with the known Newtonian prediction [Ter64]

$$f''(1)\big|_{n=1} = -\frac{3}{2} - \frac{19}{70}\mathrm{Re} + \mathcal{O}\left(\mathrm{Re}^2\right).$$

The leading order small Re expression and its first three derivatives are plotted in Figures 4.1.17 and 4.1.18 for values of n between 0 and 2. The leading order expressions

are used as an initial guess for the numerical simulations by using the continuity in $\hat{R}$ of the solution for small $\hat{R}$.

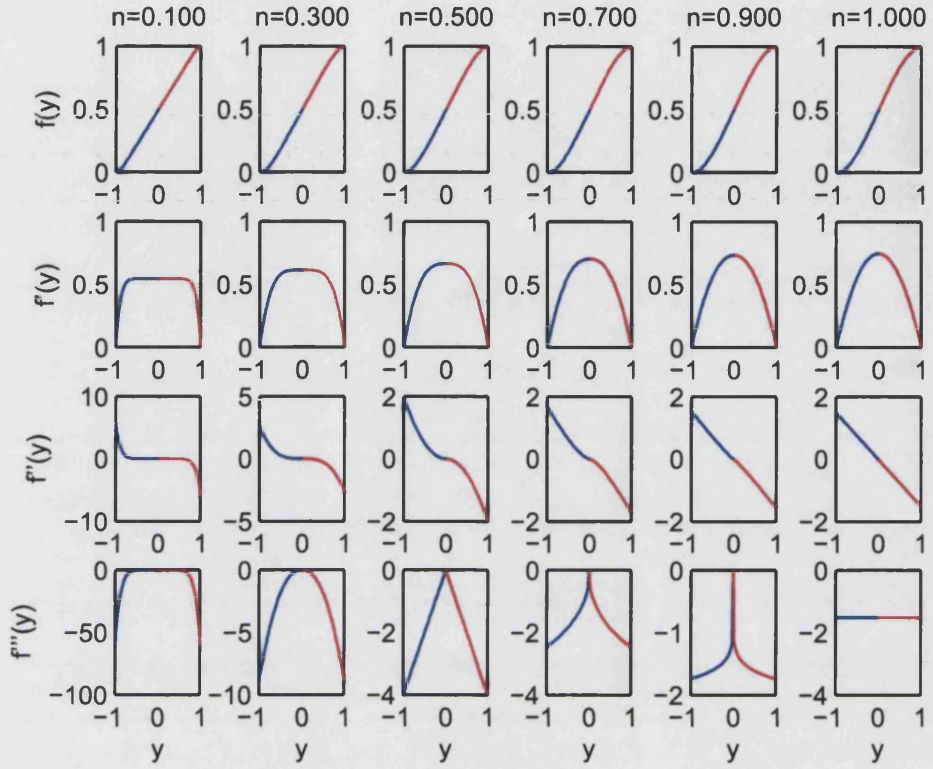

Figure 4.1.17. Algebraic small Reynolds number profiles for the one walled flow problem - here $0 < n \leq 1$. The profiles are presented in a tabular layout, with n increasing from left to right and the number of derivatives of $f(y)$ taken increasing from top to bottom.

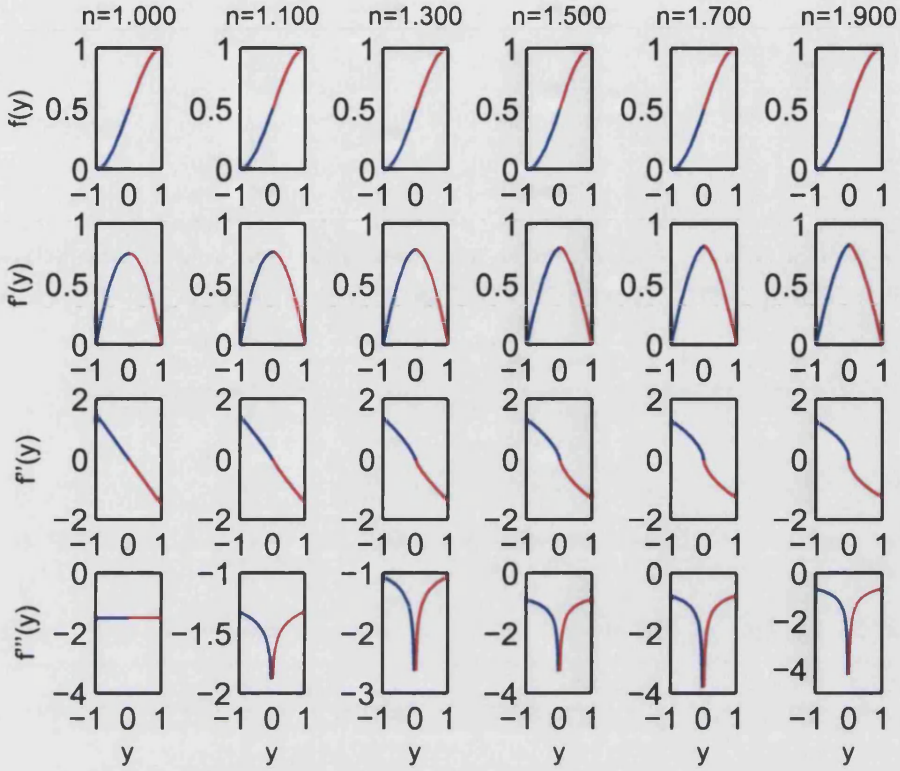

Figure 4.1.18. Algebraic small Reynolds number profiles for the one walled flow problem - here $1 \leq n \leq 2$. The profiles are presented in a tabular layout, with n increasing from left to right and the number of derivatives of $f(y)$ taken increasing from top to bottom.

4.1.3 Large $\mathrm{Re} \to -\infty$ asymptotics

We wish to consider the large injection behaviour of the power-law fluid in the one porous walled channel, governed by the following ordinary differential equation

$$\left(-f''\left|f''\right|^{n-1}\right)'' = \frac{\mathrm{Re}}{2-n}\left(f'f'' - ff'''\right), \tag{4.1.2}$$

$$\text{on } y = +1: \quad f = 1, \quad f' = 0, \tag{4.1.3}$$

$$\text{on } y = -1: \quad f = 0, \quad f' = 0. \tag{4.1.4}$$

If we define $\varepsilon = -\frac{2-n}{\mathrm{Re}}$ as the small perturbation parameter, we can see that there will be an outer inviscid flow region and an inner viscous boundary layer near the

impermeable lower wall. For the outer problem we expand $f(y)$ in regular powers of ε,

$$f(y) = f_0(y) + \varepsilon f_1(y) + \mathcal{O}\left(\varepsilon^2\right), \tag{4.1.5}$$

and solve at each order in turn. The problem for $f_0(y)$ is

$$f_0' f_0'' - f_0 f_0''' = 0, \tag{4.1.6}$$
$$\text{on } y = +1: \quad f_0 = 1, \quad f_0' = 0, \tag{4.1.7}$$
$$\text{on } y = -1: \quad f_0 = 0, \tag{4.1.8}$$

and has solution

$$f_0(y) = \cos\left(\frac{\pi(y-1)}{4}\right). \tag{4.1.9}$$

The problem for $f_1(y)$ is

$$f_1' f_0'' + f_0' f_1'' - f_0 f_1''' - f_1 f_0''' = 0, \tag{4.1.10}$$
$$\text{on } y = +1: \quad f_1 = 0, \quad f_1' = 0, \tag{4.1.11}$$

and has solution

$$f_1(y) = C(y-1)\sin\left(\frac{\pi(y-1)}{4}\right), \tag{4.1.12}$$

where the constant C is to be determined by matching to the solution in the inner region.

To consider the inner region adjacent to the lower wall, we rescale the problem with the scalings

$$y = -1 + \varepsilon^{\frac{1}{1+n}} Y, \quad f(y) = \varepsilon^{\frac{1}{1+n}} F(Y) \tag{4.1.13}$$

to obtain the inner problem

$$-\left(F''\left|F''\right|^{n-1}\right)'' + F'F'' - FF''' = 0, \tag{4.1.14}$$
$$\text{on } Y = 0: \quad F = 0, \quad F' = 0, \tag{4.1.15}$$
$$\text{as } Y \to \infty: \quad F \sim \frac{\pi}{4} Y, \tag{4.1.16}$$

where the far field behaviour has been chosen to ensure matching to the outer flow region. Again we expand the solution $F(Y)$ in regular powers of ε,

$$F(Y) = F_0(Y) + \varepsilon F_1(Y) + \mathcal{O}\left(\varepsilon^2\right),$$

and obtain the leading order inner problem

$$-\left(F_0''\left|F_0''\right|^{n-1}\right)'' + F_0'F_0'' - F_0F_0''' = 0, \tag{4.1.17}$$

$$\text{on } Y = 0: \quad F_0 = 0, \quad F_0' = 0, \tag{4.1.18}$$

$$\text{as } Y \to \infty: \quad F_0 \sim \frac{\pi}{4}Y + Y_0, \tag{4.1.19}$$

where the constant Y_0 is determinable from the numerical solution of the inner problem and the coefficient C in the first correction term in the outer region is now determined to have the value $C = Y_0/2$ by matching. We can first ask if this problem is well specified. In Appendix A we detail the calculations required to show that the $n = 1$ case is well specified, the calculations required in the non-Newtonian case are almost the same as seen below.

Near the lower wall we first express $F_0(Y)$ as a Taylor expansion about $Y = 0$,

$$F_0(Y) = \frac{1}{2}AY^2 + \frac{1}{6}BY^3 + \cdots, \tag{4.1.20}$$

and define $F_0(Y) = F_0^{\mathrm{e}}(Y) + \hat{\delta}\hat{F}(Y)$ where $F_0^{\mathrm{e}}(Y) = \frac{1}{2}AY^2 + \frac{1}{6}BY^3$ and $\hat{\delta} \ll 1$. Substituting this in to the leading order inner problem, retaining the terms of $\mathcal{O}\left(\hat{\delta}\right)$ and keeping the first term in the expansion of the modulus term gives an ode for the eigenmodes,

$$-n\hat{F}^{(\mathrm{iv})}\left|A\right|^{n-1} + A\hat{F}' + AY\hat{F}'' - \frac{1}{2}AY^2\hat{F}''' - B\hat{F} = 0. \tag{4.1.21}$$

Taking $\hat{F}(Y) = Y^q$ with $q = 0, 1, 2, 3$ gives four possible eigenmodes. However, the boundary conditions at $Y = 0$ eliminate $q = 0$ and $q = 1$, meaning that there are only two degrees of freedom left if A and B are not specified. The $q = 2$ and $q = 3$ modes are consistent with the boundary conditions imposed at the lower wall, and so a total of two boundary conditions have been imposed so far.

Turning to the far field behaviour, if we now set $F_0(Y) = F_0^{\mathrm{e}}(Y) + \hat{\delta}\hat{F}(Y)$ where $F_0^{\mathrm{e}}(Y) = \frac{\pi}{4}Y + Y_0$, substituting into the governing equation gives an ode for the potential eigenmodes by retaining the lowest order terms on each sides of the equation,

$$\left(\frac{\pi}{4}\hat{F}'' - \frac{\pi}{4}Y\hat{F}'''\right) = \left(n\hat{F}^{(\mathrm{iv})}\left|\hat{F}''\right|^{n-1} + n(n-1)\hat{F}''\left(\hat{F}'''\right)^2\left|\hat{F}''\right|^{n-3}\right). \tag{4.1.22}$$

Upon substituting $\hat{F} \sim AY^q$ with $Y > 0$ and A, q unknown we find that

$$\frac{\pi}{4}Aq(q-1)(3-q)Y^{q-2} = A\,|A|^{n-1}\,q(q-1)(q-2)(q-3+n)\,|q(q-1)|^{n-1}\,Y^{n(q-2)-2} \tag{4.1.23}$$

and the modes $q = 0, 1, 3$ are potential eigenmodes; equating the exponents of Y gives the fourth potential eigenmode with

$$q = -\frac{2n}{1-n}. \tag{4.1.24}$$

This fourth mode predicts decay in the far field when $0 < n < 1$, but if $n > 1$ decay does not occur and in that case it is not consistent with the requirement that $\hat{\delta}\hat{F} \ll F_0^e$ as $Y \to \infty$. When $0 < n < 1$ we find that the constant A is positive and has the value

$$A = \left(\frac{4(2n)^n(n+1)^n}{\pi(3-n)(1-n)^{1-2n}}\right)^{\frac{1}{1-n}}. \qquad (0 < n < 1) \tag{4.1.25}$$

Thus two boundary conditions have been imposed in this case: imposing linear behaviour in the far field eliminates the $q = 3$ and $q = 1$ modes. With the two conditions imposed at the lower wall a total of four conditions have now been imposed and so the problem for $0 < n < 1$ has the correct number of boundary conditions and is well specified. In light of this, the eigenmode for $q = 0$, the constant behaviour, is fixed by the problem already and so should be able to be determined by a numerical solution of the problem.

When $n = 1$ the calculations in Appendix A show that the decaying eigenmode is of an exponential form, $Y^{-4}\exp\left(-\pi Y^2/8\right)$, and the other three modes are the algebraic modes with exponents $q = 0, 1$ and 3 as seen above for $0 < n < 1$ and $n > 1$.

However, for $n > 1$ we see that there must be a point, Y^* say, at which $F_0''(Y^*)$ becomes zero. We are therefore dealing with a free boundary problem to determine this point. If we pose the free boundary value problem as

$$\left(F_0''\,|F_0''|^{n-1}\right)'' = F_0'F_0'' - F_0F_0''', \tag{4.1.26}$$

$$\text{on } Y = 0: \quad F_0 = 0, \quad F_0' = 0, \tag{4.1.27}$$

$$\text{on } Y = Y^*: \quad F_0' = \frac{\pi}{4}, \quad F_0'' = 0, \tag{4.1.28}$$

where the position Y^* is unknown, we are interested in the local behaviour of F_0 about Y^*. For $Y > Y^*$ we have that $F_0 = \frac{\pi}{4}Y + Y_0$. If we consider $F_0(Y)$ of the form

$$F_0(Y) = A_0 - \frac{\pi}{4}(Y^* - Y) + B_0\,(Y^* - Y)^\gamma, \tag{4.1.29}$$

where $Y < Y^*$ and A_0, B_0 are constants to be determined, substitution into the bvp and balancing the highest derivative with the most significant term from $F_0' F_0''$, we find that

$$F_0(Y) \sim A_0 - \frac{\pi}{4}(Y^* - Y) + B_0 (Y^* - Y)^{\frac{2n-1}{n-1}}, \tag{4.1.30}$$

where the constants A_0 and B_0 are related by

$${B_0}^{n-1} = A_0 \frac{(n-1)^{2n-1}}{(2n-1)^{n-1} n^n}. \tag{4.1.31}$$

By continuity of $F_0(Y)$ at $Y = Y^*$ we have the identity

$$A_0 = \frac{\pi}{4} Y^* + Y_0. \tag{4.1.32}$$

By integrating the fourth order two-point bvp (4.1.17)–(4.1.19) once and evaluating the constant of integration by using the far field behaviour, we can then solve the third order two-point bvp obtained for $0 < n < 2$ numerically using Matlab and produce estimates for the constant A_0 as it varies with n. The profile for the solution, its first and second derivative and the far field behaviour are shown in Figures 4.1.19 and 4.1.20, and the numerical values are recorded in Table 4.1. However for values of n above 1.5 it is increasingly difficult to obtain an estimate for Y_0 and so it is better to consider solving the free boundary problem for $n > 1$ separately.

n	Y_0	A	q	Y^*	$Y_0^{\text{estimated}}$
0.1	-0.30109	0.37188	0.22222	-	-
0.2	-0.45963	0.36744	0.50000	-	-
0.3	-0.54714	0.37662	0.85714	-	-
0.4	-0.59573	0.38904	1.33333	-	-
0.5	-0.62265	0.38907	2.00000	-	-
0.6	-0.63729	0.34493	3.00000	-	-
0.7	-0.64479	0.21157	4.66667	-	-
0.8	-0.64807	0.03574	8.00000	-	-
0.9	-0.64878	4.29678E-6	18.00000	-	-
1.0	-0.64790	-	-	-	-
1.1	-0.64603	-	-	-	-
1.2	-0.64353	-	-	-	-
1.3	-0.64066	-	-	-	-
1.4	-0.63757	-	-	-	-
1.5	-0.63437	-	-	2.72925	-0.52299
1.6	-	-	-	2.42048	-0.51455
1.7	-	-	-	2.20711	-0.50665
1.8	-	-	-	2.05286	-0.49927
1.9	-	-	-	1.93647	-0.49234

Table 4.1. This table shows the values of the constant Y_0 obtained by solving the boundary layer problem (4.1.17)–(4.1.19) for $0 < n < 1.5$ when $\text{Re} \to -\infty$. The values of the exponent q and the coefficient A of the decaying term in the far field behaviour for $0 < n < 1$ are found by substitution in (4.1.24) and (4.1.24) .The values of Y^* are calculated from the solution to the free boundary problem (4.1.34)–(4.1.36) and the value of $Y_0^{\text{estimated}}$ is calculated using (4.1.32). The values given from the free boundary problem calculations used the value $\delta = 1e-3$ for the lower end of the z domain and $dsq = 1e-4$ for the numerical regularisation parameter. Changing the small z position from $1e-3$ to $1e-4$ changes the Y^* results in the first or second decimal place and the $Y_0^{\text{estimated}}$ results in the fifth decimal place, and changing the regularisation parameter from $1e-4$ to $1e-5$ changes the Y^* and $Y_0^{\text{estimated}}$ results in the fifth decimal place. Results for $1.1 \leq n < 1.5$ were not successfully obtained.

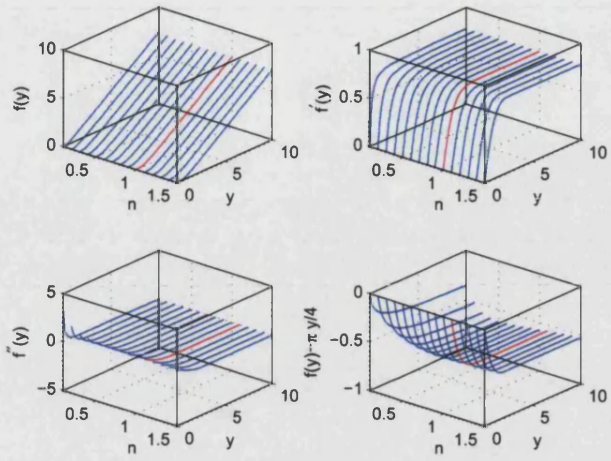

Figure 4.1.19. Profiles and asymptotic behaviour for lower wall region for $0 < n < 1.5$. The data for $n = 1$ is highlighted in red for comparison with the remainder of the plots.

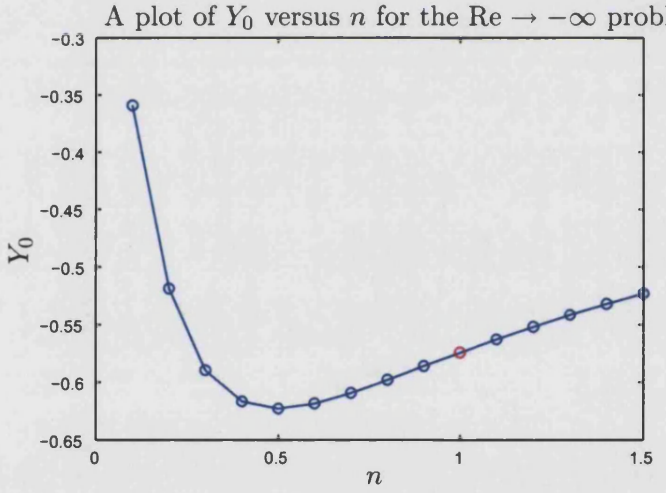

Figure 4.1.20. A plot of the constant Y_0 against n for values $0 < n < 1.5$ as estimated from the numerical solution of the system (4.1.17)–(4.1.19). The data for $n = 1$ is highlighted in red for comparison with the remainder of the values obtained for the constant Y_0.

In order to solve the free boundary value problem for $n > 1$ numerically it is simpler to transform the problem to a fixed domain and then use a shooting method. The scalings

$$F_0(Y) = Y^* G(Z), \quad Z = \frac{Y^* - Y}{Y^*} \tag{4.1.33}$$

place the problem on the fixed domain $Z \in [0,1]$, but now the domain is traversed from $Z = 0$ ($Y = Y^*$) to $Z = 1$ ($Y = 0$), giving

$$\left(G'' \left|G''\right|^{n-1}\right)' = -(Y^*)^{1+n}\left((G')^2 - GG'' - \left(\frac{\pi}{4}\right)^2\right) \tag{4.1.34}$$

$$\text{on } Z = 0\text{:} \quad G' = -\frac{\pi}{4}, \quad G'' = 0, \tag{4.1.35}$$

$$\text{on } Z = 1\text{:} \quad G = 0, \quad G' = 0. \tag{4.1.36}$$

We use the local behaviour near $Y = Y^*_-$ to form an equivalent behaviour for suitably small $Z = \delta \ll 1$, (δ=1e-3 has been used for numerical calculations)

$$G(Z) \sim \frac{A_0}{Y^*} - \frac{\pi}{4}Z + B_0\,(Y^*)^{\frac{n}{n-1}}\,Z^{\frac{2n-1}{n-1}}, \tag{4.1.37}$$

and then solve the $G(Z)$ problem on the fixed domain $Z \in [\delta, 1]$, shooting to obtain values for Y^* and A_0 for each $1 < n < 2$.

4.1.4 Type I stability problem

The eigenproblem for spatial stability is given by the following system,

$$\left(\hat{H}'' \left|F''\right|^{n-1}\right)'' = m\hat{R}\left(F''''\hat{H} - F'\hat{H}''\right) + \hat{R}\left(F\hat{H}'''' - F''\hat{H}'\right), \tag{4.1.38}$$

$$\text{on } y = +1\text{:} \quad \hat{H}' = 0, \quad \hat{H} = 0, \tag{4.1.39}$$

$$\text{on } y = -1\text{:} \quad \hat{H}' = 0, \quad \hat{H} = 0, \tag{4.1.40}$$

where $\hat{R} = \mathrm{Re}/(n(2-n))$ is the rescaled Reynolds number, $F(y)$ is the unperturbed flow function, $\hat{H}(y)$ is the spatial perturbation and m is the eigenvalue corresponding to the spatial perturbation.

This system is coupled with the base flow system for $F(y)$ and so an extended

system is to be solved numerically,

$$\hat{R}\left(FF''' - F'F''\right) = \left(F''\left|F''\right|^{n-1}\right)'', \tag{4.1.41}$$

$$m\hat{R}\left(F'''\hat{H} - F'\hat{H}''\right) + \hat{R}\left(F\hat{H}''' - F''\hat{H}'\right) = \left(\hat{H}''\left|F''\right|^{n-1}\right)'', \tag{4.1.42}$$

$$\text{on } y = +1: \quad F' = 0, \quad F = 1, \quad H = 0, \quad H' = 0, \tag{4.1.43}$$

$$\text{on } y = -1: \quad F' = 0, \quad F = 0, \quad H = 0, \quad H' = 0, \tag{4.1.44}$$

together with the normalisation condition $H''(-1) = 1$. We regularise the modulus terms by replacing them with $\left(F''^2 + \delta^2\right)^{(n-1)/2}$ and then, performing the differentiations, the final system to be solved is

$$\hat{R}\left(FF''' - F'F''\right) = F^{(iv)}\left(nF''^2 + \delta^2\right)A^{n-3}$$
$$+ (n-1)F''\left(F'''\right)^2\left(nF''^2 + 3\delta^2\right)A^{n-5}, \tag{4.1.45}$$

$$m\hat{R}\left(F'''\hat{H} - F'\hat{H}''\right) + \hat{R}\left(F\hat{H}''' - F''\hat{H}'\right) = \hat{H}^{(iv)}A^{n-1} + 2(n-1)\hat{H}'''F''F'''A^{n-3}$$
$$+ (n-1)\hat{H}''\left(F'''^2 + F''F^{(iv)}\right)A^{n-3} + (n-1)(n-3)\hat{H}''F''^2F'''^2A^{n-5}, \tag{4.1.46}$$

$$A = \left(F''^2 + \delta^2\right)^{\frac{1}{2}}$$

$$\text{on } y = +1: \quad F' = 0, \quad F = 1, \quad H = 0, \quad H' = 0, \tag{4.1.47}$$

$$\text{on } y = -1: \quad F' = 0, \quad F = 0, \quad H = 0, \quad H' = 0, \quad H'' = 1. \tag{4.1.48}$$

In the limit $\delta \to 0$ this system reduces to the equivalent system involving modulus signs.

Spatial stability system for small Re

Starting from the base stability eigenproblem (4.1.38)-(4.1.40) we can pose expansions in powers of $\hat{R}$ for $\hat{H}(y)$ and the eigenvalue m,

$$\hat{H}(y) = H_0(y) + \hat{R}H_1(y) + \mathcal{O}\left(\hat{R}^2\right), \quad m = \hat{R}^{-1}m_{-1} + m_0 + \hat{R}m_1 + \mathcal{O}\left(\hat{R}^2\right), \tag{4.1.49}$$

where the inverse power of $\hat{R}$ in m is motivated by the need to retain the eigenvalue in the limit of the eigenproblem as $\hat{R} \to 0$. Now for small $\mathrm{Re}/(2-n) \equiv n\hat{R}$ we can express $F(y)$ as

$$F(y) = f_0(y) + n\hat{R}f_1(y) + \mathcal{O}\left(\left(n\hat{R}\right)^2\right). \tag{4.1.50}$$

The expressions previously derived for this small Re case for $F(y)$ in § 3.2.1 with $E = 1$ suggest that we will need to split the eigenfunction $\hat{H}(y)$ into two parts in a similar manner, namely

$$H_0(y) = \begin{cases} H_{0n}(y), & 0 \le y \le 1, \\ H_{0p}(y), & -1 \le y \le 0, \end{cases} \tag{4.1.51}$$

where the subscripts n, p correspond to the similarly denoted regions for $f_0(y)$.

Substituting into the governing equation we can write down the leading order eigenproblem for the eigenfunction $H_0(y)$ and eigenvalue m_{-1}

$$H_{0n}^{(\mathrm{iv})} = -2\left(\frac{n-1}{n}\right) y^{-1} H_{0n}''' - \left(\frac{(n-1)(n-2)}{n^2} y^{-2} + m_{-1}\left(\frac{2n+1}{2n}\right)^{2-n} \frac{n}{n+1}\left(1 - y^{\frac{2}{n}}\right)\right) H_{0n}'' - m_{-1}\left(\frac{2n+1}{2n}\right)^{2-n} \frac{1}{n} y^{\frac{2}{n}-2} H_{0n}, \tag{4.1.52}$$

$$H_{0p}^{(\mathrm{iv})} = 2\left(\frac{n-1}{n}\right) (-y)^{-1} H_{0p}''' + \left(\frac{(n-1)(n-2)}{n^2} (-y)^{-2} - m_{-1}\left(\frac{2n+1}{2n}\right)^{2-n} \frac{n}{n+1}\left(1 - (-y)^{\frac{2}{n}}\right)\right) H_{0p}'' - m_{-1}\left(\frac{2n+1}{2n}\right)^{2-n} \frac{1}{n} (-y)^{\frac{2}{n}-2} H_{0p}, \tag{4.1.53}$$

$$\text{on } y = +1: \quad H_{0n} = 0, \quad H_{0n}' = 0, \tag{4.1.54}$$

$$\text{on } y = -1: \quad H_{0p} = 0, \quad H_{0p}' = 0, \tag{4.1.55}$$

together with continuity of H_0 and H_0' across $y = 0$. This may be used to provide an initial guess for the eigenvalue and eigenfunction in order to facilitate numerical eigenvalue calculations.

In the case $n = 1$ this reduces to

$$H_{0n}^{(\mathrm{iv})} = -m_{-1}\frac{3}{2}\left(\frac{1}{2}\left(1 - y^2\right) H_{0n}'' + H_{0n}\right), \tag{4.1.56}$$

$$H_{0p}^{(\mathrm{iv})} = -m_{-1}\frac{3}{2}\left(\frac{1}{2}\left(1 - y^2\right) H_{0p}'' + H_{0p}\right), \tag{4.1.57}$$

$$\text{on } y = +1: \quad H_{0n} = 0, \quad H_{0n}' = 0, \tag{4.1.58}$$

$$\text{on } y = -1: \quad H_{0p} = 0, \quad H_{0p}' = 0, \tag{4.1.59}$$

together with continuity of H_0 and H_0' across $y = 0$. It appears that there is not a closed form solution to this bvp and so a numerical approach is needed even for this case.

Chapter 5

Nonisothermal temperature dependent viscosity problem - one porous walled channel

5.1 One porous walled nonisothermal problem summary

We wish to consider the steady nonisothermal one porous walled channel flow problem for a fluid with a temperature dependent viscosity. Starting with the general unsteady formulation of the temperature and stress dependent fluid problem in the two walled geometry as described in § 1.3 by equations (1.3.13a)–(1.3.13e), we can discard the time derivatives as we are interested in the steady state solutions of the problem and then set $E = 1$ to obtain the one porous walled geometry. In order to simplify the problem further we then take $n = 1$, and so are considering a Newtonian viscous fluid with a temperature dependent modification to its viscosity. This gives the following nondimensional system of equations to be solved for the unknown temperature distribution $\theta(x, y)$ and stream function $\psi(x, y)$

$$\mathrm{Re}\left(\frac{\partial\psi}{\partial y}\frac{\partial^3\psi}{\partial x\partial y^2} - \frac{\partial\psi}{\partial x}\frac{\partial^3\psi}{\partial y^3}\right) = \frac{\partial^2}{\partial y^2}\left(\mu\frac{\partial^2\psi}{\partial y^2}\right), \tag{5.1.1a}$$

$$\mathrm{Pe}\left(\frac{\partial\psi}{\partial y}\frac{\partial\theta}{\partial x} - \frac{\partial\psi}{\partial x}\frac{\partial\theta}{\partial y}\right) = \frac{\partial^2\theta}{\partial y^2}, \tag{5.1.1b}$$

$$\mu = M(\theta), \tag{5.1.1c}$$

$$\text{on } y = +1: \quad \frac{\partial\psi}{\partial y} = 0, \quad -\frac{\partial\psi}{\partial x} = 1, \quad \theta = 0, \tag{5.1.1d}$$

$$\text{on } y = -1: \quad \frac{\partial\psi}{\partial y} = 0, \quad \frac{\partial\psi}{\partial x} = 0, \quad \theta = 1, \tag{5.1.1e}$$

and we recall that the nondimensional groups Re and Pe share the same sign.

We restrict the temperature-viscosity relation to an exponential form $\mu = \exp(-\beta\theta(y))$. This form is used by Ockendon and Ockendon [OO77] in the related problem of the entry region Poiseuille flow in a channel with walls that are nonisothermal and a temperature dependent viscosity. They are concerned with the flow behaviour in the high β limit. This chapter is concerned with $\beta = \mathcal{O}(1)$ behaviour. Appendix B considers the large β limit of the problem currently under consideration for both exponential and algebraic viscosity functional forms in the regimes $\mathrm{Re} = \mathcal{O}(1)$ with $\mathrm{Pe} \gg 1$ and $\mathrm{Re} \ll 1$ with $\mathrm{Pe} \gg 1$, and for the algebraic viscosity form in the regimes $\mathrm{Re} \gg 1$ with $\mathrm{Pe} \gg 1$, where the three resulting cases $\mathrm{Pr} \ll 1$, $\mathrm{Pr} = \mathcal{O}(1)$ and $\mathrm{Pr} \gg 1$ are considered.

If we now look for a similarity solution to the steady problem we find that it must have the form

$$\psi(x,y) = -xf(y), \quad \theta(x,y) = g(y), \tag{5.1.2}$$

and that we are now solving the coupled system

$$\mathrm{Re}\left(f'f'' - ff'''\right) = -\left(\exp(-\beta g(y))f''\right)'', \tag{5.1.3a}$$

$$\mathrm{Pe}fg' = g'', \tag{5.1.3b}$$

$$\text{on } y = +1: \quad f' = 0, \quad f = 1, \quad g = 0, \tag{5.1.3c}$$

$$\text{on } y = -1: \quad f' = 0, \quad f = 0, \quad g = 1, \tag{5.1.3d}$$

where $'$ denotes $\frac{\mathrm{d}\cdot}{\mathrm{d}y}$.

5.1.1 Solutions in particular parameter cases

One observation is that we can integrate the temperature equation (5.1.3b), giving

$$g(y) = \frac{\int_{-1}^{y} \exp\left(\mathrm{Pe}\int_{-1}^{s} f(r)\mathrm{d}r\right)\mathrm{d}s}{\int_{-1}^{1} \exp\left(\mathrm{Pe}\int_{-1}^{s} f(r)\mathrm{d}r\right)\mathrm{d}s} \qquad \text{where } y \in [-1,1], \tag{5.1.4}$$

and substituting this into (5.1.3a) gives an integro-differential equation for $f(y)$.

We can also record some simple solutions for special choices of the nondimensional parameters Re and Pe. In the case of $\mathrm{Pe} = 0$, we can solve the equation for $g(y)$ exactly, giving $g(y) = \frac{1}{2}(1-y)$, and then we have the following problem for $f(y)$,

$$\mathrm{Re}\left(f'f'' - ff'''\right) = -\left(\exp\left(-\frac{\beta}{2}(1-y)\right)f''\right)'', \tag{5.1.5}$$

together with the remaining boundary conditions for $f(y)$.

If $\mathrm{Re} = 0$ we find that

$$f(y) = \frac{\int_{-1}^{y}(y-t)(t-a)\exp(\beta g(t))\,\mathrm{d}t}{\int_{-1}^{1}(1-t)(t-a)\exp(\beta g(t))\,\mathrm{d}t}, \tag{5.1.6}$$

where the constant a is defined to be

$$a = \frac{\int_{-1}^{1} s\exp(\beta g(s))\,\mathrm{d}s}{\int_{-1}^{1}\exp(\beta g(s))\,\mathrm{d}s}. \tag{5.1.7}$$

5.2 Asymptotic analysis

We now wish to consider the behaviour of the fluid flow and temperature functions in the case of fluid injection through the upper wall whilst the lower wall is heated. We initially consider the case of rapid injection of fluid, $\mathrm{Re} < 0$ large, with comparable thermal convection and conduction length scales, where $\mathrm{Pe} < 0$ is of order one, in which case the viscous boundary layer adjacent to the lower wall is the dominant flow feature. We then increase the size of Pe. The case where both of the nondimensional groups are large can be split into three sub-cases, firstly where Pe is smaller than Re, then where they are comparable and finally where Pe exceeds Re; these cases describe the transition from the dominant boundary layer being initially viscous to eventually thermal. The final case is where Pe is large and Re is of order one and the thermal boundary layer is the main feature of the flow.

For the large Pe limits considered in this chapter we have assumed that $\beta = \mathcal{O}(1)$. In the limit of large β the behaviour described here changes and the thermal boundary layers for $\beta = \mathcal{O}(1)$ split into sublayers when the viscosity function is of exponential form. This behaviour is described in Appendix B for the cases $\mathrm{Pe} \gg 1$ with $\mathrm{Re} \ll 1$ (section B.1.1) and $\mathrm{Re} = \mathcal{O}(1)$ (section B.1.2) for the exponential viscosity model, and for $\mathrm{Pe} \gg 1$ with $\mathrm{Re} \ll 1$ (section B.1.1), $\mathrm{Re} = \mathcal{O}(1)$ (section B.1.2) and $\mathrm{Re} \gg 1$ (subsections contained within B.1.3) with an algebraic viscosity model.

5.2.1 Large injection $\mathrm{Re} \to -\infty$ with $\mathrm{Pe} = \mathcal{O}(1)$

Starting with the system (5.1.3a)–(5.1.3d) where $\mathrm{Pe} = \mathcal{O}(1)$ and $\mathrm{Re} \to -\infty$, we have an outer region where we neglect the small perturbed term in the flow equation. In this region we suppose that

$$f(y) = f_0(y) + (-\mathrm{Re})^{-1/2} f_1(y) + \mathcal{O}\left(-\mathrm{Re}^{-1}\right), \tag{5.2.1}$$

$$g(y) = g_0(y) + (-\mathrm{Re})^{-1/2} g_1(y) + \mathcal{O}\left(-\mathrm{Re}^{-1}\right), \tag{5.2.2}$$

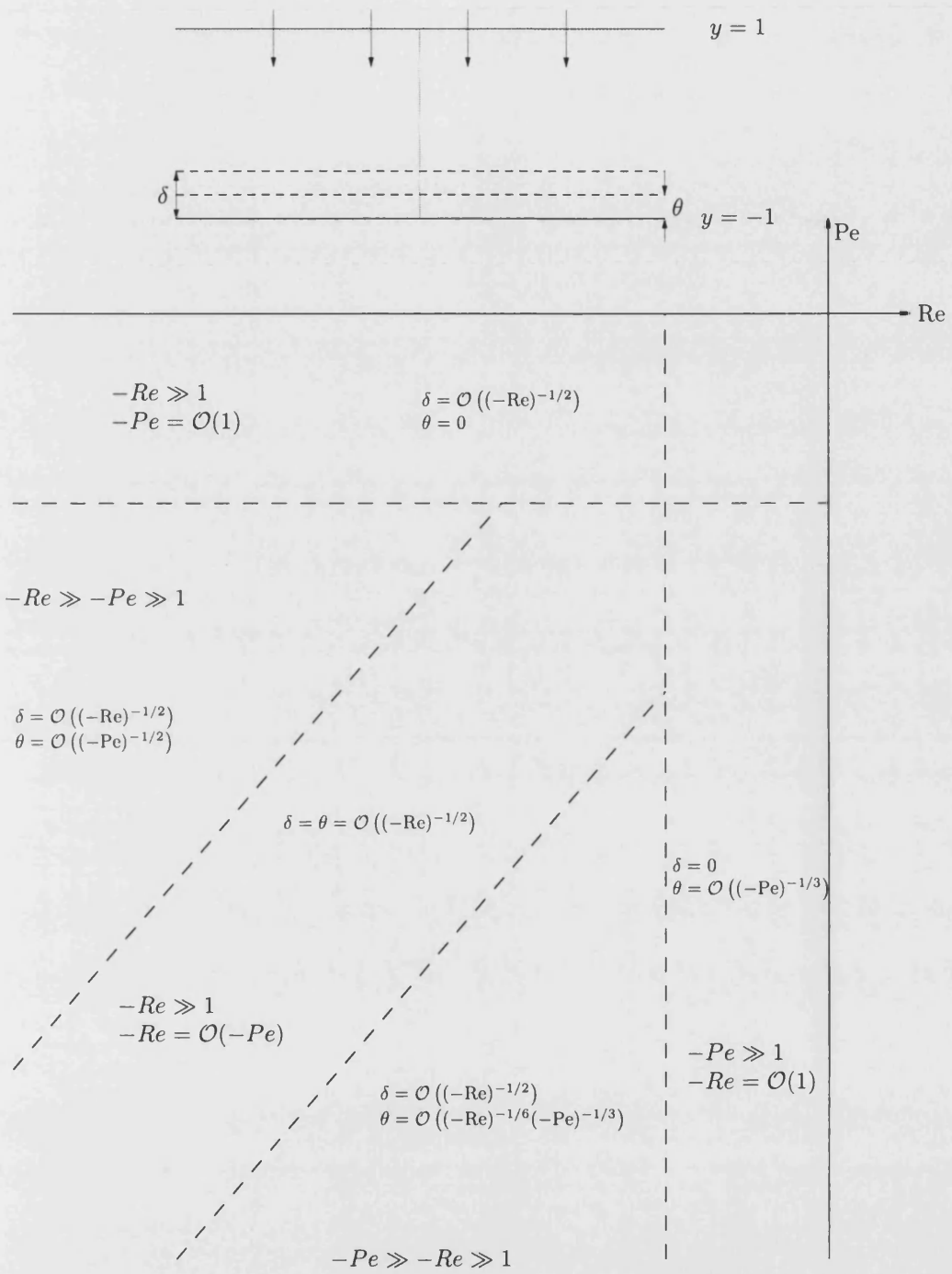

Figure 5.2.1. A graphical summary of the different behaviours associated with the various limits considered for the one walled nonisothermal problem. The extent of the viscous and thermal boundary layers are denoted by δ and θ respectively.

where the scaling has been suggested by that of the boundary layer. We then wish to solve the following reduced problem at leading order

$$0 = f_0' f_0'' - f_0 f_0''', \tag{5.2.3}$$

$$\frac{1}{\mathrm{Pe}} g_0'' = f_0 g_0', \tag{5.2.4}$$

$$\text{on } y = +1: \quad f_0' = 0, \quad f_0 = 1, \quad g_0 = 0, \tag{5.2.5}$$

$$\text{on } y = -1: \quad f_0 = 0, \quad g_0 = 1. \tag{5.2.6}$$

As the order of the f_0 equation has been reduced by one it is only possible to satisfy three of the four f boundary conditions from the full problem. The leading order outer solution is found to be

$$f_0(y) = \cos\left(\frac{\pi}{4}(1-y)\right), \quad g_0(y) = \frac{1}{A_0}\int_y^1 I_0(s)\mathrm{d}s, \tag{5.2.7}$$

where

$$I_0(y) = \exp\left(-\frac{4\mathrm{Pe}}{\pi}\sin\left(\frac{\pi}{4}(1-y)\right)\right), \quad A_0 = \int_{-1}^1 I_0(s)\mathrm{d}s. \tag{5.2.8}$$

A boundary layer at the lower wall is needed and the appropriate scalings are motivated by the desire to reinstate the highest derivative in the f equation and for the far field behaviour leaving the boundary layer to match to that of the outer region. These requirements yield

$$f = (-\mathrm{Re})^{-1/2} F(Y), \quad y = (-\mathrm{Re})^{-1/2} Y, \quad g(y) = G(Y), \tag{5.2.9}$$

with the boundary layer system

$$\left(\mu(\beta G)F''\right)'' = F'F'' - FF''', \tag{5.2.10}$$

$$G'' = -\frac{\mathrm{Pe}}{\mathrm{Re}} FG', \tag{5.2.11}$$

$$\text{on } Y = 0: \quad F = 0, \quad F' = 0, \quad G = 1, \tag{5.2.12}$$

$$\text{as } Y \to \infty: \quad F \sim \frac{\pi}{4} Y, \quad G \to 0. \tag{5.2.13}$$

Now as $\mathcal{O}\left((-\mathrm{Re})^{-1}\right) \ll \mathcal{O}\left((-\mathrm{Re})^{-1/2}\right)$ we expand the boundary layer functions as a

series in powers of $(-\mathrm{Re})^{-1/2}$,

$$F(Y) = F_0(Y) + (-\mathrm{Re})^{-1/2} F_1(Y) + \cdots, \tag{5.2.14}$$

$$G(Y) = G_0(Y) + (-\mathrm{Re})^{-1/2} G_1(Y) + \cdots, \tag{5.2.15}$$

and so the leading order boundary layer problem is

$$\left(\mu(\beta G_0) F_0''\right)'' = F_0' F_0'' - F_0 F_0''', \tag{5.2.16}$$

$$G_0'' = 0, \tag{5.2.17}$$

$$\text{on } Y = 0: \quad F_0 = 0, \quad F_0' = 0, \quad G_0 = 1, \tag{5.2.18}$$

$$\text{as } Y \to \infty: \quad F_0 \sim \frac{\pi}{4} Y, \quad G_0 \to 0. \tag{5.2.19}$$

In this region the temperature problem has already been satisfied and so we are only interested in the F_0 problem,

$$\left(\mu(\beta G_0) F_0''\right)'' = F_0' F_0'' - F_0 F_0''', \tag{5.2.20}$$

$$\text{on } Y = 0: \quad F_0 = 0, \quad F_0' = 0, \tag{5.2.21}$$

$$\text{as } Y \to \infty: \quad F_0 \sim \frac{\pi}{4} Y - Y_0. \tag{5.2.22}$$

where $\mu_0 = \mu(\beta G_0)$ is a known constant and Y_0 is a constant that is to be found as part of a numerical solution. The governing equation is fourth order and so requires four boundary conditions. Two boundary conditions have been applied at the lower wall and two boundary conditions are imposed by the linear behaviour in the far-field. The constant solution can in principle be determined from a numerical solution to the problem. It is possible to rescale the problem to remove the constant μ_0 via

$$Y = \left(\frac{4\mu_0}{\pi}\right)^{1/2} z, \quad F = \left(\frac{\pi\mu_0}{4}\right)^{1/2} \rho, \quad Y_0 = \left(\frac{\pi\mu_0}{4}\right)^{1/2} z_0; \tag{5.2.23}$$

integrating once and using the far-field behaviour yields the Falkner-Skan equation [Bat01, page 316]

$$\rho''' = \rho'^2 - \rho\rho'' - 1, \tag{5.2.24}$$

$$\text{on } z = 0: \quad \rho = 0 \quad \rho' = 0, \tag{5.2.25}$$

$$\text{as } z \to \infty: \quad \rho' \sim 1. \tag{5.2.26}$$

The constant z_0 can be determined numerically by fitting a linear function to the far field behaviour of $\rho(z)$; z_0 is then the z-intercept of that function. A Matlab program

was written to solve the Falkner-Skan problem as an initial-value problem; it did this by minimising the square of the difference between the first derivative of the solution and unity at the end of a truncated domain. This was run for increasing domain lengths and the computed values for z_0 and $\rho''(0)$ were found to be

$$z_0 = 0.647900, \quad \rho''(0) = 1.232588 \quad \text{(to 6 d.p.)}. \tag{5.2.27}$$

The first correction terms for the outer region are now found by solving

$$0 = f_0' f_1'' + f_1' f_0'' - f_0 f_1''' - f_1 f_0''', \tag{5.2.28}$$

$$\frac{1}{\mathrm{Pe}} g_1'' = f_0 g_1' + f_1 g_0', \tag{5.2.29}$$

$$\text{on } y = 1: \quad f_1 = 0, \quad f_1' = 0, \quad g_1 = 0. \tag{5.2.30}$$

$$\text{as } y \to -1: \quad f_1 \text{ matches to } F, \quad g_1 \to 0. \tag{5.2.31}$$

The function $f_1(y)$ is found to be

$$f_1(y) = A(1-y)\sin\left(\frac{\pi}{4}(1-y)\right), \quad A = -\frac{1}{2}\left(\frac{\pi\mu_0}{4}\right)^{1/2} z_0, \tag{5.2.32}$$

where the coefficient A is found by matching to the behaviour of the leading order boundary layer solution. The solution for $g_1(y)$ can then be found, giving

$$g_1(y) = \mathrm{Pe}\frac{4}{\pi}\left(\frac{\mu_0}{\pi}\right)^{1/2}\frac{z_0}{A_0}\left(\frac{A_1}{A_0}\int_y^1 I_0(s)\mathrm{d}s - \int_y^1 I_0(s)I_1(s)\mathrm{d}s\right), \tag{5.2.33}$$

$$I_1(y) = \frac{\pi}{4}(1-y)\cos\left(\frac{\pi}{4}(1-y)\right) - \sin\left(\frac{\pi}{4}(1-y)\right), \tag{5.2.34}$$

where the constant A_1 is defined to be

$$A_1 = \int_{-1}^1 I_1(s)\mathrm{d}s. \tag{5.2.35}$$

5.2.2 Large injection $\mathrm{Re} \to -\infty$ with $\mathrm{Pe} \to -\infty$

The regime $1 \ll -\mathrm{Pe} \ll -\mathrm{Re}$

In this case we expect to have an outer region, a thermal boundary layer adjacent to the lower wall and a viscous boundary layer contained within the thermal boundary layer. Starting from the system (5.1.3a)–(5.1.3d), in the outer region we neglect the terms multiplied by the small quantities 1/Re and 1/Pe and expand the unknown functions as

$$f(y) = f_0(y) + o(1), \quad g(y) = g_0(y) + o(1), \tag{5.2.36}$$

giving the following system to be solved at leading order,

$$0 = f_0' f_0'' - f_0 f_0''', \tag{5.2.37}$$

$$0 = f_0 g_0', \tag{5.2.38}$$

$$\text{on } y = 1: \quad f_0 = 1, \quad f_0' = 0, \quad g_0 = 0, \tag{5.2.39}$$

$$\text{on } y = -1: \quad f_0 = 0. \tag{5.2.40}$$

The equation for g_0 suggests that the correct solution is that $g_0 = 0$ in this region and we then find that

$$f_0(y) = \cos\left(\frac{\pi}{4}(1-y)\right), \quad g_0(y) = 0. \tag{5.2.41}$$

In order to consider the solution near the lower wall, we need the near-wall behaviour of the leading order outer solution $f_0(y)$,

$$f_0(y = -1 + \delta Y) \approx \frac{\pi}{4}\delta Y \quad (\delta \ll 1, Y = \mathcal{O}(1)). \tag{5.2.42}$$

We next consider the thermal boundary layer near the lower wall. To recover the highest derivative in the temperature equation, we rescale the independent and dependent variables in the following manner,

$$y = -1 + (-\mathrm{Pe})^{-1/2} Y, \quad f = (-\mathrm{Pe})^{-1/2} F, \quad g = G \tag{5.2.43}$$

where we have used the small y behaviour of the outer solution for f_0 to achieve matching behaviour as we move from the thermal boundary layer into the outer region. The thermal boundary layer equations are

$$-\frac{\mathrm{Pe}}{\mathrm{Re}}\left(\mu(\beta G)F''\right)'' = F'F'' - FF''', \tag{5.2.44}$$

$$G'' = -FG', \tag{5.2.45}$$

$$\text{on } Y = 0: \quad F = 0, \quad F' = 0, \quad G = 1, \tag{5.2.46}$$

$$\text{as } Y \to \infty: \quad F \sim \frac{\pi}{4}Y, \quad G \to 0. \tag{5.2.47}$$

As $\frac{\mathrm{Pe}}{\mathrm{Re}} \ll 1$ we choose to expand the thermal boundary layer solution as

$$F(Y) = F_0(Y) + (-\mathrm{Pe})^{-1/2} F_1(Y) + \cdots, \tag{5.2.48}$$

$$G(Y) = G_0(Y) + (-\mathrm{Pe})^{-1/2} G_1(Y) + \cdots, \tag{5.2.49}$$

and then to lowest order we are solving

$$0 = F_0' F_0'' - F_0 F_0''', \tag{5.2.50}$$

$$G_0'' = -F_0 G_0', \tag{5.2.51}$$

$$\text{on } Y = 0: \quad F_0 = 0, \quad F_0' = 0, \quad G_0 = 1, \tag{5.2.52}$$

$$\text{as } Y \to \infty: \quad F_0 \sim \frac{\pi}{4} Y, \quad G_0 \to 0. \tag{5.2.53}$$

The far field behaviour for F_0 is sufficient to satisfy the differential equation for F_0 but not all of the boundary conditions, but this can be corrected in a smaller viscous boundary layer nearer to the wall. The leading order solutions in this thermal layer are

$$F_0(Y) = \frac{\pi}{4} Y, \tag{5.2.54}$$

$$G_0(Y) = \operatorname{erfc}\left(\sqrt{\frac{\pi}{8}} Y\right). \tag{5.2.55}$$

We finally wish to consider an inner-inner region near the lower wall where the viscous effects become significant. The rescalings used to examine this region are

$$Y = \left(\frac{\mathrm{Pe}}{\mathrm{Re}}\right)^{1/2} \hat{Y}, \quad F = \left(\frac{\mathrm{Pe}}{\mathrm{Re}}\right)^{1/2} \hat{F}, \quad G = \hat{G}, \tag{5.2.56}$$

which were motivated by the need to recover the viscous term in the $\hat{F}(\hat{Y})$ equation and matching the far-field behaviour of $\hat{F}$ to that in the $Y = \mathcal{O}(1)$ region. We obtain the viscous boundary layer system

$$-\left(\mu(\beta\hat{G})\hat{F}''\right)'' = \hat{F}'\hat{F}'' - \hat{F}\hat{F}''', \tag{5.2.57}$$

$$\hat{G}'' = -\frac{\mathrm{Pe}}{\mathrm{Re}} \hat{F}\hat{G}', \tag{5.2.58}$$

$$\text{on } \hat{Y} = 0: \quad \hat{F} = 0, \quad \hat{F}' = 0, \quad \hat{G} = 1, \tag{5.2.59}$$

$$\text{as } \hat{Y} \to \infty: \quad \hat{F} \sim \frac{\pi}{4} \hat{Y}, \ \hat{G}(\hat{Y}) \text{ matches to } G(Y) \text{ when } Y = \mathcal{O}(1). \tag{5.2.60}$$

In this viscous boundary layer region $\hat{G} = 1 - o(1)$ and so the $\hat{G}$ equation is satisfied and the viscosity term $\mu(\beta\hat{G})$ is constant. If we expand the functions in this region as

$$\hat{F}(\hat{Y}) = \bar{F}_0(\hat{Y}) + \left(\frac{\mathrm{Pe}}{\mathrm{Re}}\right)^{1/2} \bar{F}_1(\hat{Y}) + \cdots, \tag{5.2.61}$$

$$\hat{G}(\hat{Y}) = \bar{G}_0(\hat{Y}) + \left(\frac{\mathrm{Pe}}{\mathrm{Re}}\right)^{1/2} \bar{G}_1(\hat{Y}) + \cdots, \tag{5.2.62}$$

then to leading order we are solving

$$-\mu(\beta)\bar{F}_0^{(\mathrm{iv})} = \bar{F}_0'\bar{F}_0'' - \bar{F}_0\bar{F}_0''', \tag{5.2.63}$$

$$\text{on } \hat{Y} = 0: \quad \bar{F}_0 = 0, \quad \bar{F}_0' = 0, \tag{5.2.64}$$

$$\text{as } \hat{Y} \to \infty: \quad \bar{F}_0 \sim \frac{\pi}{4}\hat{Y} - \bar{Y}_0, \tag{5.2.65}$$

where again the constant term in the far field behaviour comes from analysing the degrees of freedom of the existing far-field conditions (see Appendix A).

We can rescale this problem to make the coefficient of the highest derivative unity by the scalings

$$\hat{Y} = \left(\frac{4\mu(\beta)}{\pi}\right)^{1/2} z, \quad \bar{F}_0 = \left(\frac{\mu(\beta)\pi}{4}\right)^{1/2} \bar{\rho}, \quad \bar{Y}_0 = \left(\frac{\mu(\beta)\pi}{4}\right)^{1/2} z_0 \tag{5.2.66}$$

giving the following system

$$\bar{\rho}^{(\mathrm{iv})} = \bar{\rho}'''\bar{\rho} - \bar{\rho}'\bar{\rho}'', \tag{5.2.67}$$

$$\text{on } z = 0: \quad \bar{\rho} = 0, \quad \bar{\rho}' = 0, \tag{5.2.68}$$

$$\text{as } z \to \infty: \quad \bar{\rho} \sim z - z_0. \tag{5.2.69}$$

Integrating the system up once produces

$$\bar{\rho}''' = \bar{\rho}''\bar{\rho} - \bar{\rho}'^2 + 1, \tag{5.2.70}$$

$$\text{on } z = 0: \quad \bar{\rho} = 0, \quad \bar{\rho}' = 0, \tag{5.2.71}$$

$$\text{as } z \to \infty: \quad \bar{\rho}' \sim 1. \tag{5.2.72}$$

This is not the same as the Falkner-Skan system (5.2.24)–(5.2.26); making the change

of variables $P(\eta) = \bar{\rho}(-z)$ we find that $P(\eta)$ satisfies

$$-P''' = P''P - P'^2 + 1 \quad \Leftrightarrow \quad P''' = P'^2 - PP'' - 1 \tag{5.2.73}$$

$$\text{on } \eta = 0: \quad P = 0, \quad P' = 0, \tag{5.2.74}$$

$$\text{as } \eta \to -\infty: \quad P' \sim -1, \tag{5.2.75}$$

and further analysis is required to determine the solution properties in this case.

If we now return to the thermal boundary layer region we find that the far-field constant $\bar{Y}_0$ produces an extra term in the expression for $F(Y)$, and we can find the complete expansion for $F(Y)$ in integer powers of Pe^{-1} by matching to the outer sinusoidal behaviour, giving

$$F(Y) = \sum_{n=0}^{\infty} \left(\frac{\pi Y}{4}\right)^{2n+1} \frac{(\mathrm{Pe})^{-n}}{(2n+1)!} - \left(\frac{\mathrm{Pe}}{\mathrm{Re}}\right)^{1/2} \left(\frac{\pi\mu(\beta)}{4}\right)^{1/2} z_0 + \mathcal{O}\left(\frac{(-\mathrm{Pe})^{1/2}}{-\mathrm{Re}}\right), \tag{5.2.76}$$

$$G(Y) = \operatorname{erfc}\left(\sqrt{\frac{\pi}{8}}Y\right) + \mathcal{O}\left(\left(\frac{\mathrm{Pe}}{\mathrm{Re}}\right)^{1/2}\right). \tag{5.2.77}$$

The $\mathcal{O}\left(\left(\frac{\mathrm{Pe}}{\mathrm{Re}}\right)^{1/2}\right)$ term in $F(Y)$ can be matched to the first order correction term in the outer region; if the outer solutions are expanded as

$$f(y) = f_0(y) + \left(\frac{1}{\mathrm{Re}}\right)^{1/2} f_1(y) + \cdots, \tag{5.2.78}$$

$$g(y) = g_0(y) + \left(\frac{1}{\mathrm{Re}}\right)^{1/2} g_1(y) + \cdots, \tag{5.2.79}$$

then the first order corrections terms satisfy

$$0 = f_0' f_1'' + f_0'' f_1' - f_0 f_1''' - f_1 f_0''', \tag{5.2.80}$$

$$0 = f_0 g_1' + f_1 g_0', \tag{5.2.81}$$

$$\text{on } y = 1: \quad f_1 = 0, \quad f_1' = 0, \quad g_1 = 0. \tag{5.2.82}$$

We find that

$$f_1(y) = C\,(y-1)\sin\left(\frac{\pi}{4}(1-y)\right), \quad g_1(y) = 0, \tag{5.2.83}$$

where the constant C has the value

$$C = \frac{1}{2}\left(\frac{\pi\mu(\beta)}{4}\right)^{1/2} z_0, \tag{5.2.84}$$

which has been determined by matching to the solution in the inner thermal region. We then have that the outer solution is

$$f(y) = \cos\left(\frac{\pi}{4}(1-y)\right) - \left(\frac{\mathrm{Pe}}{\mathrm{Re}}\right)^{1/2} \frac{1}{2}\left(\frac{\pi\mu(\beta)}{4}\right)^{1/2} z_0(1-y)\sin\left(\frac{\pi}{4}(1-y)\right) + \mathcal{O}\left((-\mathrm{Re})^{-1}\right), \tag{5.2.85}$$

$$g(y) = 0. \tag{5.2.86}$$

The regime $1 \ll -\mathrm{Pe} = \mathcal{O}(-\mathrm{Re})$

Starting with the system (5.1.3a)–(5.1.3d) we again have an outer region in which the highest derivatives in both differential equations are neglected. In this region we suppose that

$$f(y) = f_0(y) + o(1), \quad g(y) = g_0(y) + o(1), \tag{5.2.87}$$

and that we are solving the system

$$0 = f_0' f_0'' - f_0 f_0''', \tag{5.2.88}$$

$$0 = f_0 g_0', \tag{5.2.89}$$

$$\text{on } y = 1: \quad f_0 = 1, \quad f_0' = 0, \quad g_0 = 0, \tag{5.2.90}$$

$$\text{on } y = -1: \quad f_0 = 0. \tag{5.2.91}$$

We may only impose three conditions upon the solution $f_0(y)$ and one upon $g_0(y)$, and we have the leading order outer solutions

$$f_0(y) = \cos\left(\frac{\pi}{4}(1-y)\right), \quad g_0(y) = 0. \tag{5.2.92}$$

In the boundary layer region adjacent to the lower wall we wish to recover the viscous and thermal effects that have been neglected in the outer region. As $\mathrm{Pe} = \mathcal{O}(\mathrm{Re})$ we will have to recover both of the highest derivatives simultaneously. The required scalings are

$$y = -1 + (-\mathrm{Re})^{-1/2} Y, \quad f = (-\mathrm{Re})^{-1/2} F, \quad g = G, \tag{5.2.93}$$

motivated by recovering the highest derivatives and matching to the lower-wall be-

haviour of the solution in the outer region, giving the boundary layer system

$$\left(\mu(\beta G)F''\right)'' = F'F'' - FF''', \tag{5.2.94}$$

$$G'' = -kFG', \tag{5.2.95}$$

$$\text{on } Y = 0: \quad F = 0, \quad F' = 0, \quad G = 1, \tag{5.2.96}$$

$$\text{as } Y \to \infty: \quad F \sim \frac{\pi}{4}Y, \quad G \to 0, \tag{5.2.97}$$

where $k = \mathrm{Pe}/\mathrm{Re} = \mathcal{O}(1)$.

If we now expand the functions $F(Y)$, $G(Y)$ as

$$F(Y) = F_0(Y) + (-\mathrm{Re})^{-1/2}F_1(Y) + \cdots, \tag{5.2.98}$$

$$G(Y) = G_0(Y) + (-\mathrm{Re})^{-1/2}G_1(Y) + \cdots \tag{5.2.99}$$

and expand the viscosity function as

$$\mu(\beta G(Y)) = \exp(-\beta G_0)(1 - \beta(-\mathrm{Re})^{-1/2}G_1 + \cdots), \tag{5.2.100}$$

we obtain the leading order boundary layer system,

$$\left(\mu(\beta G_0)F_0''\right)'' = F_0'F_0'' - F_0F_0''', \tag{5.2.101}$$

$$G_0'' = -kF_0G_0', \tag{5.2.102}$$

$$\text{on } Y = 0: \quad F_0 = 0, \quad F_0' = 0, \quad G_0 = 1, \tag{5.2.103}$$

$$\text{as } Y \to \infty: \quad F_0 \sim \frac{\pi}{4}Y - Y_0, \quad G_0 = 0. \tag{5.2.104}$$

where, as already noted, Y_0 is not the same constant as in the $-\mathrm{Re} \gg 1$, $-\mathrm{Pe} = \mathcal{O}(1)$ boundary layer case as the viscosity is still significant throughout this inner region. The above coupled system encompasses the viscous and thermal effects that are encountered within the boundary layer in this particular double limit of $-\mathrm{Pe} \to \infty$, $-\mathrm{Re} \to \infty$, and the solution for $G_0(Y)$ may be written as

$$G_0(Y) = \frac{\int_Y^\infty \exp\left(-k\int_0^s F_0(r)\mathrm{d}r\right)\mathrm{d}s}{\int_0^\infty \exp\left(-k\int_0^s F_0(r)\mathrm{d}r\right)\mathrm{d}s}, \tag{5.2.105}$$

$$= 1 - \frac{\int_0^Y \exp\left(-k\int_0^s F_0(r)\mathrm{d}r\right)\mathrm{d}s}{\int_0^\infty \exp\left(-k\int_0^s F_0(r)\mathrm{d}r\right)\mathrm{d}s}. \tag{5.2.106}$$

As $Y \to \infty$, the far field behaviour of $G_0(Y)$ is

$$G_0(Y) \sim -\frac{4A_0}{k\pi Y}\exp\left(-\frac{k\pi}{8}Y^2\right) \quad \text{for some } A_0 \in \mathbb{R}, \tag{5.2.107}$$

and so G_0 satisfies the asymptotic relationship

$$G_0' \sim -\frac{k\pi}{4} Y G_0 \quad \text{as } Y \to \infty. \tag{5.2.108}$$

Returning to the outer region away from the lower wall, we may expand the solutions there in powers of $(-\mathrm{Re})^{-1/2}$,

$$f(y) = f_0(y) + (-\mathrm{Re})^{-1/2} f_1(y) + \cdots, \tag{5.2.109}$$

$$g(y) = g_0(y) + (-\mathrm{Re})^{-1/2} g_1(y) + \cdots, \tag{5.2.110}$$

and find that the first correction terms obey the following governing equations,

$$0 = f_0' f_1'' + f_1' f_0'' - f_0 f_1''' - f_1 f_0''', \tag{5.2.111}$$

$$0 = f_0 g_1' + f_1 g_0', \tag{5.2.112}$$

$$\text{on } y = 1: \quad f_1 = 0, \quad f_1' = 0, \quad g_1 = 0, \tag{5.2.113}$$

$$\text{on } y = -1: \quad f_1 = 0. \tag{5.2.114}$$

The first order correction terms for the outer solutions are

$$f_1(y) = C(y-1)\sin\left(\frac{\pi}{4}(1-y)\right), \quad g_1 = 0, \tag{5.2.115}$$

and the value of the constant C is found by matching to the leading order inner solution, giving

$$C = -\frac{Y_0}{2}, \tag{5.2.116}$$

where the value of the constant Y_0 is not necessarily the same as that of the analogous constant in the Falkner-Skan equations (5.2.24)–(5.2.26). The outer solution to first order is

$$f(y) = \cos\left(\frac{\pi}{4}(1-y)\right) - (-\mathrm{Re})^{-1/2}\frac{1}{2} Y_0 (1-y)\sin\left(\frac{\pi}{4}(1-y)\right) + \mathcal{O}\left(-\mathrm{Re}^{-1}\right), \tag{5.2.117}$$

$$g(y) = 0. \tag{5.2.118}$$

The regime $1 \ll -\mathrm{Re} \ll -\mathrm{Pe}$

Starting with (5.1.3a)–(5.1.3d) we have an outer region in which the highest derivatives multiplied by small terms are neglected. In this region we suppose that

$$f(y) = f_0(y) + o(1), \quad g(y) = g_0(y) + o(1), \tag{5.2.119}$$

and that we are solving the system

$$0 = f_0' f_0'' - f_0 f_0''', \tag{5.2.120}$$

$$0 = f_0 g_0', \tag{5.2.121}$$

$$\text{on } y = 1: \quad f_0 = 1, \quad f_0' = 0, \quad g_0 = 0, \tag{5.2.122}$$

$$\text{on } y = -1: \quad f_0 = 0. \tag{5.2.123}$$

We may only impose three conditions upon the solution $f_0(y)$ and one upon $g_0(y)$, and we have the leading order outer solutions

$$f_0(y) = \cos\left(\frac{\pi}{4}(1-y)\right), \quad g_0(y) = 0. \tag{5.2.124}$$

We next consider the inner region near the lower wall in which the viscous effects are significant, but the thermal effects are expected to still be negligible. Using the scalings

$$y = -1 + (-\mathrm{Re})^{-1/2} Y, \quad f = (-\mathrm{Re})^{-1/2} F, \quad g = G, \tag{5.2.125}$$

motivated by recovering the viscous effects and matching to the behaviour of $f(y)$ in the outer region, we find that the appropriate inner region equations are

$$\left(\mu(\beta G) F''\right)'' = F' F'' - F F''', \tag{5.2.126}$$

$$-\frac{\mathrm{Re}}{\mathrm{Pe}} G'' = F G'. \tag{5.2.127}$$

However, as the ratio $\mathrm{Re}/\mathrm{Pe} \ll 1$, we obtain that $G = 0$ to leading order as we expect F to be nontrivial. If we expand the solution in this region as

$$F(Y) = F_0(Y) + o(1), \quad G(Y) = G_0(Y) + o(1), \tag{5.2.128}$$

then to leading order we are solving the temperature independent system,

$$F_0^{(\mathrm{iv})} = F_0' F_0'' - F_0 F_0''', \tag{5.2.129}$$

$$\text{on } Y = 0: \quad F_0 = 0, \quad F_0' = 0, \tag{5.2.130}$$

$$\text{as } Y \to \infty: \quad F_0 \sim \frac{\pi}{4} Y - Y_0. \tag{5.2.131}$$

This can be transformed into the Falkner-Skan problem (5.2.24)–(5.2.26) by integrating once and using the scalings

$$Y = \left(\frac{\pi}{4}\right)^{-1/2} z, \quad F = \left(\frac{\pi}{4}\right)^{1/2} \rho, \quad Y_0 = \left(\frac{\pi}{4}\right)^{-1/2} z_0. \tag{5.2.132}$$

In order to facilitate the matching of the subsequent thermal boundary layer solution with the solution in the viscous boundary layer, we define the constant A_0 by

$$A_0 = F_0'''(0) = \left(\frac{\pi}{4}\right)^{3/2} \rho''(0). \tag{5.2.133}$$

We must now consider the temperature variation which occurs in a thermal boundary layer which is contained within the viscous boundary layer and is situated closer to the lower wall. In this case, as we have already solved the problem for $F(Y)$ we must use its small Y behaviour as the appropriate matching constraint; together with recovering the highest derivative in the temperature equation we find that the appropriate scalings are

$$Y = \left(\frac{\mathrm{Re}}{\mathrm{Pe}}\right)^{1/3} \bar{Y}, \quad F = \left(\frac{\mathrm{Re}}{\mathrm{Pe}}\right)^{2/3} \bar{F}, \quad G = \bar{G}, \tag{5.2.134}$$

yielding the thermal boundary layer system

$$\left(\mu(\beta\bar{G})\bar{F}''\right)'' = \frac{\mathrm{Re}}{\mathrm{Pe}} \left(\bar{F}'\bar{F}'' - \bar{F}\bar{F}'''\right), \tag{5.2.135}$$

$$\bar{G}'' = -\bar{F}\bar{G}', \tag{5.2.136}$$

$$\text{on } \bar{Y} = 0: \quad \bar{F} = 0, \quad \bar{F}' = 0, \quad \bar{G} = 1, \tag{5.2.137}$$

$$\text{as } \bar{Y} \to \infty: \quad \bar{F} \sim \frac{1}{2} A_0 \bar{Y}^2, \quad \bar{G} \to 0. \tag{5.2.138}$$

To lowest order, if we expand the solutions as

$$\bar{F}(\bar{Y}) = \bar{F}_0(\bar{Y}) + \mathcal{O}\left(\frac{\mathrm{Re}}{\mathrm{Pe}}\right), \quad \bar{G}(\bar{Y}) = \bar{G}_0(\bar{Y}) + \mathcal{O}\left(\frac{\mathrm{Re}}{\mathrm{Pe}}\right), \tag{5.2.139}$$

we obtain the leading order thermal boundary problem

$$\left(\mu(\beta\bar{G}_0)\bar{F}_0''\right)'' = 0, \tag{5.2.140}$$

$$\bar{G}_0'' = -\bar{F}_0\bar{G}_0', \tag{5.2.141}$$

$$\text{on } \bar{Y} = 0: \quad \bar{F}_0 = 0, \quad \bar{F}_0' = 0, \quad \bar{G}_0 = 1, \tag{5.2.142}$$

$$\text{as } \bar{Y} \to \infty: \quad \bar{F}_0 \sim \frac{1}{2} A_0 \bar{Y}^2, \quad \bar{G}_0 \to 0. \tag{5.2.143}$$

The leading order solutions may be expressed as the coupled integrals

$$\bar{G}_0 = \frac{\int_{\bar{Y}}^{\infty} \exp\left(-\int_0^s \bar{F}_0(r)\mathrm{d}r\right)\mathrm{d}s}{\int_0^{\infty} \exp\left(-\int_0^s \bar{F}_0(r)\mathrm{d}r\right)\mathrm{d}s}, \tag{5.2.144}$$

$$= 1 - \frac{\int_0^{\bar{Y}} \exp\left(-\int_0^s \bar{F}_0(r)\mathrm{d}r\right)\mathrm{d}s}{\int_0^{\infty} \exp\left(-\int_0^s \bar{F}_0(r)\mathrm{d}r\right)\mathrm{d}s}, \tag{5.2.145}$$

$$\bar{F}_0 = A_0 \int_0^{\bar{Y}} \frac{\bar{Y} - s}{\mu(\beta \bar{G}_0(s))}\mathrm{d}s, \tag{5.2.146}$$

where the coefficient A_0 in the expression for $\bar{F}_0(\bar{Y})$ is found by matching to the small Y behaviour in the viscous boundary layer.

5.2.3 Injection with $-\mathrm{Re} = \mathcal{O}(1)$ and $\mathrm{Pe} \to -\infty$

Again starting with the system (5.1.3a)–(5.1.3d) where $\mathrm{Re} = \mathcal{O}(1)$ and $\mathrm{Pe} \to -\infty$, we have an outer region where we neglect the small perturbed term in the temperature equation, and then an inner region where the temperature effects are significant.

In the outer region we suppose that

$$f(y) = f_0(y) + o(1), \quad g(y) = g_0(y) + o(1), \tag{5.2.147}$$

and that we are solving the system

$$-\frac{1}{\mathrm{Re}}\left(\mu(\beta g_0) f_0''\right)'' = f_0' f_0'' - f_0 f_0''', \tag{5.2.148}$$

$$0 = f_0 g_0', \tag{5.2.149}$$

$$\text{on } y = 1: \quad f_0 = 1, \quad f_0' = 0, \quad g_0 = 0, \tag{5.2.150}$$

$$\text{on } y = -1: \quad f_0 = 0, \quad f_0' = 0. \tag{5.2.151}$$

We may only impose one boundary condition upon g_0 as the highest derivative has been lost. In this case it makes $g_0 = 0$ and so the viscosity term is now unity, and we are thus solving a temperature independent flow problem in the outer region. As $f_0(y)$ approaches the lower wall it has the approximate behaviour

$$f_0(y) = \frac{1}{2} f_0''(-1)(-1+y)^2 \quad \text{as } y \to -1. \tag{5.2.152}$$

In order to recover the highest derivative in the temperature equation we must rescale the system and investigate the resulting thermal boundary layer. The correct

scalings are found to be

$$y = -1 + (-\mathrm{Pe})^{-1/3} Y, \quad f = (-\mathrm{Pe})^{-2/3} F, \quad g = G, \tag{5.2.153}$$

and the thermal boundary layer system becomes

$$\left(\mu(\beta G) F''\right)'' = \frac{\mathrm{Re}}{\mathrm{Pe}} \left(F' F'' - F F'''\right), \tag{5.2.154}$$

$$G'' = -F G', \tag{5.2.155}$$

$$\text{on } Y = 0: \quad F = 0, \quad F' = 0, \quad G = 1, \tag{5.2.156}$$

$$\text{as } Y \to \infty: \quad F \sim \frac{1}{2} f_0''(-1) Y^2, \quad G \to 0. \tag{5.2.157}$$

If we now expand the solution in the thermal layer as

$$F(Y) = F_0(Y) + o(1), \tag{5.2.158}$$

$$G(Y) = G_0(Y) + o(1), \tag{5.2.159}$$

then the leading order thermal boundary layer problem is

$$\left(\mu(\beta G_0) F_0''\right)'' = 0, \tag{5.2.160}$$

$$G_0'' = -F_0 G_0', \tag{5.2.161}$$

$$\text{on } Y = 0: \quad F_0 = 0, \quad F_0' = 0, \quad G_0 = 1, \tag{5.2.162}$$

$$\text{as } Y \to \infty: \quad F_0 \sim \frac{1}{2} f_0''(-1) Y^2, \quad G_0 \to 0. \tag{5.2.163}$$

The solution to this system may be expressed as the coupled integrals

$$F_0(Y) = f_0''(-1) \int_0^Y \frac{Y - s}{\mu(\beta G_0(s))} \mathrm{d}s, \tag{5.2.164}$$

$$G_0(Y) = \frac{\int_Y^\infty \exp\left(-\int_0^s F_0(r) \mathrm{d}r\right) \mathrm{d}s}{\int_0^\infty \exp\left(-\int_0^s F_0(r) \mathrm{d}r\right) \mathrm{d}s}. \tag{5.2.165}$$

5.3 Stability analysis

5.3.1 Temporal stability problem

Starting with the unsteady governing equations in the form

$$\frac{\partial f''}{\partial t} = \frac{1}{\mathrm{Re}}\left(\exp(-\beta g)f''\right)'' + \left(f'f'' - ff'''\right), \tag{5.3.1a}$$

$$\frac{\partial g}{\partial t} = \frac{1}{\mathrm{Pe}}g'' - fg', \tag{5.3.1b}$$

$$\text{on } y = +1\text{:} \quad f' = 0, \quad f = 1, \quad g = 0, \tag{5.3.1c}$$

$$\text{on } y = -1\text{:} \quad f' = 0, \quad f = 0, \quad g = 1, \tag{5.3.1d}$$

we add a temporal perturbation to the functions $f(y)$ and $g(y)$ via

$$f = f_0(y) + \delta\exp(st)F(y), \quad g = g_0(y) + \delta\exp(st)G(y), \quad \delta \ll 1,\ s \in \mathbb{R}, \tag{5.3.2}$$

and substitute these perturbed forms into the unsteady equations. After expressing the resulting exponential term involving the perturbation $\delta G(y)$ via its power series form, we can then consider the problems at each order. At $\mathcal{O}(1)$ we recover the steady governing equations for $f_0(y)$ and $g_0(y)$,

$$0 = \frac{1}{\mathrm{Re}}\left(\exp(-\beta g_0)f_0''\right)'' + \left(f_0'f_0'' - f_0f_0'''\right), \tag{5.3.3a}$$

$$0 = \frac{1}{\mathrm{Pe}}g_0'' - f_0g_0', \tag{5.3.3b}$$

$$\text{on } y = +1\text{:} \quad f_0' = 0, \quad f_0 = 1, \quad g_0 = 0, \tag{5.3.3c}$$

$$\text{on } y = -1\text{:} \quad f_0' = 0, \quad f_0 = 0, \quad g_0 = 1, \tag{5.3.3d}$$

while at $\mathcal{O}(\delta)$ we obtain the ode system governing temporal stability,

$$sF'' = \frac{1}{\mathrm{Re}}\left(\exp(-\beta g_0)(F'' - \beta f_0''G)\right)'' + f_0'F'' + f_0''F' - f_0F'''' - f_0'''F, \tag{5.3.4a}$$

$$sG = \frac{1}{\mathrm{Pe}}G'' - f_0G' - Fg_0', \tag{5.3.4b}$$

$$\text{on } y = +1\text{:} \quad F' = 0, \quad F = 0, \quad G = 0, \tag{5.3.4c}$$

$$\text{on } y = -1\text{:} \quad F' = 0, \quad F = 0, \quad G = 0. \tag{5.3.4d}$$

We can estimate the values of the first few eigenvalues of the temporal stability system in the $\beta = 0$ and small Re or Pe cases, with a view to using these as appropriate initial guesses for the numerical solution of the $\beta \neq 0$ stability problems via continuation in β from zero to an appropriate value.

When $\beta = 0$, the stability equations are

$$sF'' = \frac{1}{\mathrm{Re}}F'''' + f_0'F'' + f_0''F' - f_0F''' - f_0'''F, \tag{5.3.5}$$

$$sG = \frac{1}{\mathrm{Pe}}G'' - f_0G' - Fg_0'. \tag{5.3.6}$$

If we now consider the case where $\mathrm{Pe} = 0$ and Re is small, expanding the eigenfunctions and eigenvalue as

$$F(y) = F_0(y) + \mathrm{Re}F_1(y) + \cdots, \quad G(y) = G_0(y) + \mathrm{Re}G_1(y) + \cdots,$$
$$s\mathrm{Re} = -s_0 + \mathrm{Re}s_1 + \cdots, \tag{5.3.7}$$

and collecting the lowest order terms from each equation gives

$$F(y): \quad -s_0F_0'' = F_0^{(iv)}, \tag{5.3.8}$$

$$G(y): \quad 0 = G_0'', \tag{5.3.9}$$

and hence we obtain $G_0 = 0$.

The eigenfunctions $F_0(y)$ can be divided into two different sets, according to whether the eigenfunctions are even or odd functions. In both cases the fourth order ode is solved with four homogeneous conditions and a normalisation condition of $F_0''(-1) = 1$. Similar modes to the modes recorded below have previously been found in the context of the isothermal $E = 0$ problem considered by Zaturska et.al. [ZDB88]. For the even solutions, we find that

$$F_0(y) = F_{0k}^e(y) = \frac{1}{s_{0k}^e}\left(1 - \frac{\cos\left(\sqrt{s_{0k}^e}y\right)}{\cos\left(\sqrt{s_{0k}^e}\right)}\right), \quad s_0 = s_{0k}^e = (k\pi)^2,\ k \in \mathbb{N}, \tag{5.3.10}$$

and the first three eigenvalues are -9.87, -39.48 and -88.83 approximately. For the odd solutions,

$$F_0(y) = F_{0k}^o(y) = \frac{1}{s_{0k}^o}\left(\frac{\sin\left(\sqrt{s_{0k}^o}y\right)}{\sin\left(\sqrt{s_{0k}^o}\right)} - y\right), \quad s_0 = s_{0k}^o,\ k \in \mathbb{N}, \tag{5.3.11}$$

where $\sqrt{s_{0k}^o}$ is a positive root of the equation $\tan(\sqrt{s_{0k}^o}) = \sqrt{s_{0k}^o}$. The first three such eigenvalues are -20.19, -59.68 and -118.9 approximately. We can see that the eigenvalues for the even and odd modes interlace in this case. It remains to be seen whether this property is preserved as we move away from $\beta = 0$; for $\beta = 0$ the interlacing of the eigenvalues remains until the real parts coalesce.

For $\beta = 0$ and $F(y) = 0$ it is only necessary to expand $G(y)$ and s in terms of Pe,

$$G(y) = G_0(y) + \mathrm{Pe}G_1(y) + \cdots, \quad \mathrm{Pe}s = -s_0 + \mathrm{Pe}s_1 + \cdots, \tag{5.3.12}$$

and at lowest order we obtain the ode eigenvalue problem

$$G_0'' + s_0 G_0 = 0, \quad G_0(-1) = G_0(1) = 0, \quad G_0'(-1) = 1, \tag{5.3.13}$$

with the latter condition being a normalisation condition. We can again split the eigenfunctions into those that are even eigenfunctions and those that are odd, and we find that the even eigenfunctions are

$$G_0(y) = G_{0k}^e(y) = \frac{\cos\left(\sqrt{s_{0k}^e}y\right)}{\sqrt{s_{0k}^e}\sin\left(\sqrt{s_{0k}^e}\right)}, \quad s_{0k}^e = \left(\frac{(2k-1)}{2}\pi\right)^2, \; k \in \mathbb{N}, \tag{5.3.14}$$

and the odd eigenfunctions are

$$G_0(y) = G_{0k}^o(y) = \frac{\sin\left(\sqrt{s_{0k}^o}y\right)}{\sqrt{s_{0k}^o}\cos\left(\sqrt{s_{0k}^o}\right)}, \quad s_{0k}^o = (k\pi)^2, \; k \in \mathbb{N}. \tag{5.3.15}$$

We can represent these eigenfunctions in a single form via

$$G_{0k}(y) = \frac{\sin\left(\sqrt{s_{0k}}(1+y)\right)}{\sqrt{s_{0k}}}, \quad s_{0k} = \left(\frac{k\pi}{2}\right)^2, \; k \in \mathbb{N}, \tag{5.3.16}$$

where even values of k select the even eigenfunctions and odd values select the odd eigenfunctions.

5.3.2 Spatial stability problem

The steady governing equations involving the stream function $\psi(x,y)$ and temperature function $T(x,y)$ are

$$\mathrm{Re}\left(\psi_y\psi_{xyy} - \psi_x\psi_{yyy}\right) = \left(\exp(-\beta T)\psi_{yy}\right)_{yy}, \tag{5.3.17a}$$

$$\left(\psi_y T_x - \psi_x T_y\right) = \frac{1}{\mathrm{Pe}}T_{yy}, \tag{5.3.17b}$$

$$\text{on } y = +1: \quad \psi_y = 0, \quad -\psi_x = 1, \quad T = 0, \tag{5.3.17c}$$

$$\text{on } y = -1: \quad \psi_y = 0, \quad -\psi_x = 0, \quad T = 1. \tag{5.3.17d}$$

If we add spatial perturbations to both the stream and temperature functions of

the form

$$\psi(x,y) = -xf(y) + \delta\psi_1(x,y), \quad T(x,y) = g_0(y) + \delta T_1(x,y), \quad \delta \ll 1, \tag{5.3.18}$$

and substitute them into the governing equations, we obtain

$$\begin{aligned}&\mathrm{Re}\left((-xf' + \delta\psi_{1y})(-f'' + \delta\psi_{1xyy}) - (-f + \delta\psi_{1x})(-xf''' + \delta\psi_{1yyy})\right) = \\ &\left(\exp(-\beta(g_0 + \delta T_1))(-xf'' + \delta\psi_{1yy})\right)_{yy},\end{aligned} \tag{5.3.19a}$$

$$\left((-xf' + \delta\psi_{1y})(g_0 + \delta T_{1x}) - (-f + \delta\psi_{1x})(g_0' + \delta T_{1y})\right) = \frac{1}{\mathrm{Pe}}\left(g_{0yy} + \delta T_{1yy}\right), \tag{5.3.19b}$$

$$\text{on } y = +1: \quad -xf' + \delta\psi_{1y} = 0, \quad f - \delta\psi_{1x} = 1, \quad g_0 + \delta T_1 = 0, \tag{5.3.19c}$$

$$\text{on } y = -1: \quad -xf' + \delta\psi_{1y} = 0, \quad f - \delta\psi_{1x} = 0, \quad g_0 + \delta T_1 = 1. \tag{5.3.19d}$$

We now approximate the exponential viscosity term by $\exp(-\beta g_0)(1 - \delta\beta T_1)$ and then consider the problems at each order in turn. At leading order we obtain the base problems

$$\mathrm{Re}\left(f'f'' - ff'''\right) = \left(-\exp(-\beta g_0)f''\right)'', \tag{5.3.20a}$$

$$fg_0' = \frac{1}{\mathrm{Pe}}g_0'', \tag{5.3.20b}$$

$$\text{on } y = +1: \quad f = 1, \quad f' = 0, \quad g_0 = 0, \tag{5.3.20c}$$

$$\text{on } y = -1: \quad f = 0, \quad f' = 0, \quad g_0 = 1, \tag{5.3.20d}$$

and at $\mathcal{O}(\delta)$ we have the following pde system,

$$\mathrm{Re}\left(-xf'\psi_{1xyy} - f''\psi_{1y} + xf'''\psi_{1x} + f\psi_{1yyy}\right) = \left(\exp(-\beta g_0)(\psi_{1yy} + \beta x f'' T_1)\right)_{yy}, \tag{5.3.21a}$$

$$-xf'T_{1x} - \psi_{1x}g_0' + fT_{1y} = \frac{1}{\mathrm{Pe}}T_{1yy}, \tag{5.3.21b}$$

accompanied with homogeneous boundary conditions for ψ_1 and T_1. This system admits separable solutions of the form

$$\psi = x^\lambda H(y), \quad T_1 = x^\eta K(y),$$

and setting $\lambda = 1 + \eta$ permits the reduction to the following coupled odes for $H(y)$ and

$K(y)$,

$$\mathrm{Re}\left(fH''' - f''H'\right) + \lambda\mathrm{Re}\left(f'''H - f'H''\right) = \left(\exp(-\beta g_0)(H'' + \beta f''K)\right)'', \quad (5.3.22a)$$

$$fK' + f'K - \lambda(Hg_0' + f'K) = \frac{1}{\mathrm{Pe}}K'', \quad (5.3.22b)$$

$$\text{on } y = +1: \quad H = 0, \quad H' = 0, \quad K = 0, \quad (5.3.22c)$$

$$\text{on } y = -1: \quad H = 0, \quad H' = 0, \quad K = 0. \quad (5.3.22d)$$

5.4 Numerical results

In this section we present numerical solutions to the governing equations computed using various codes written using Matlab and discuss the results.

5.4.1 Flow profiles

The base flow problem has been solved for appropriate combinations of parameters $|\mathrm{Pe}| = 0.1, 1, 5, 10$ and $\beta = -3, -2, -1, 0, 1, 2, 3, 4, 5$, where positive values of Pe correspond to positive Re indicating suction flows and negative Pe correspond to negative Re indicating injection flows. It is necessary to increase the range of Reynolds numbers for the suction cases as the Péclet number increases in order to capture the important features that arise in the bifurcation diagrams.

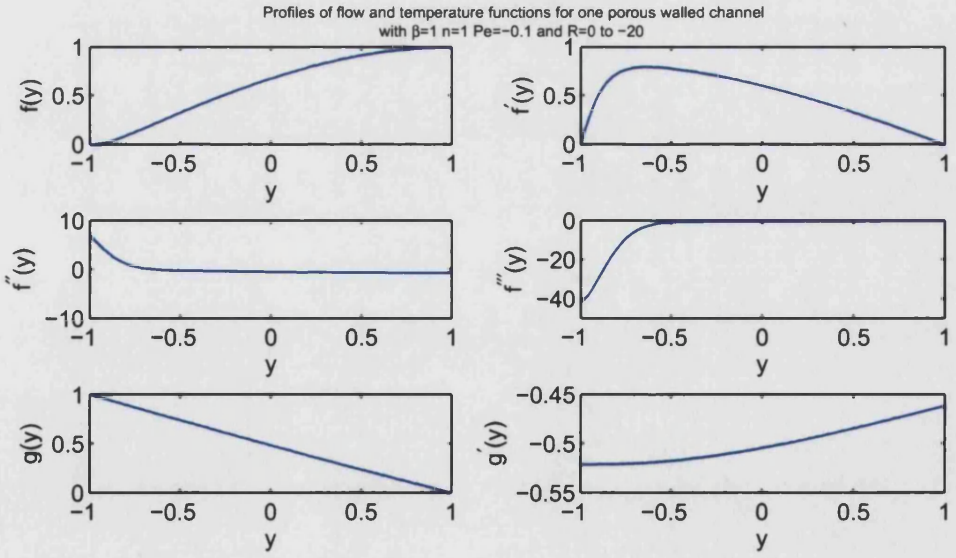

Figure 5.4.1. Solution profiles for the one porous walled nonisothermal channel flow with $\mathrm{Pe} = -0.1$, $\beta = 1$ and $\mathrm{Re} = -20$.

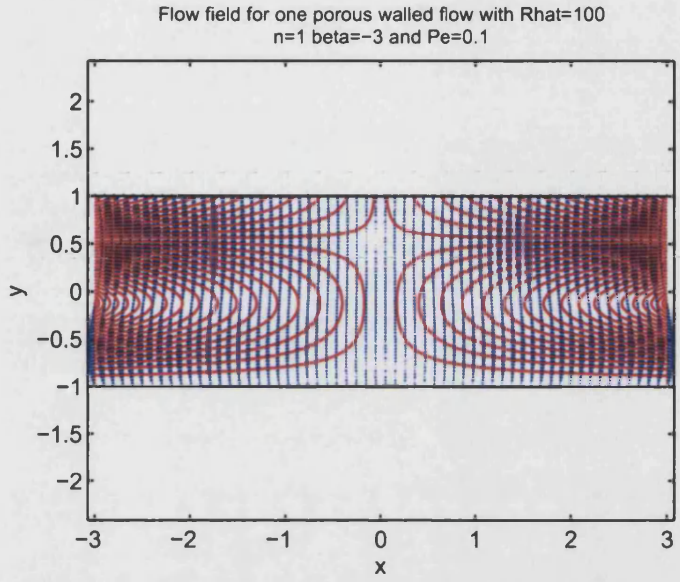

Figure 5.4.2. Flow field for the one porous walled nonisothermal channel flow with $\mathrm{Pe} = 0.1$, $\beta = -3$ and $\mathrm{Re} = 100$.

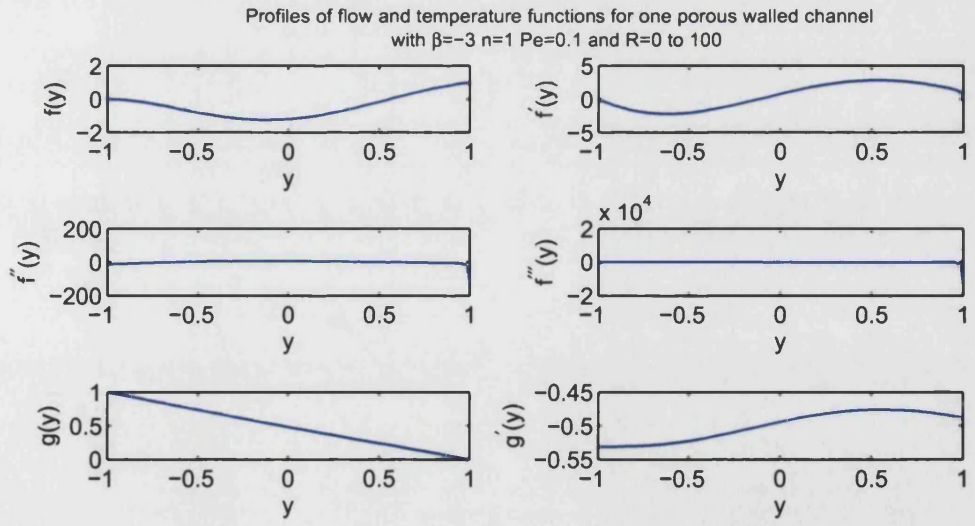

Figure 5.4.3. Solution profiles for the one porous walled nonisothermal channel flow with $\mathrm{Pe} = 0.1$, $\beta = -3$ and $\mathrm{Re} = 100$.

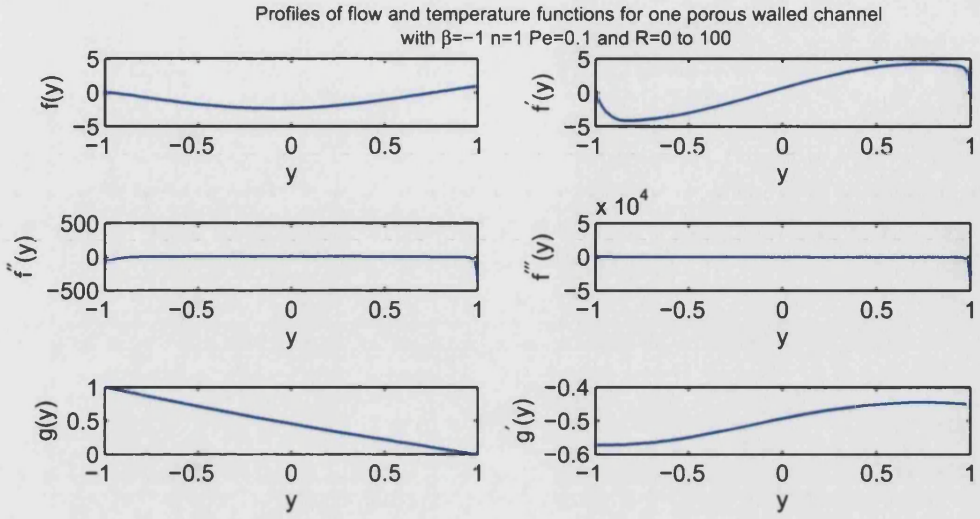

Figure 5.4.4. Solution profiles for the one porous walled nonisothermal channel flow with $\mathrm{Pe} = 0.1$, $\beta = -1$ and $\mathrm{Re} = 100$.

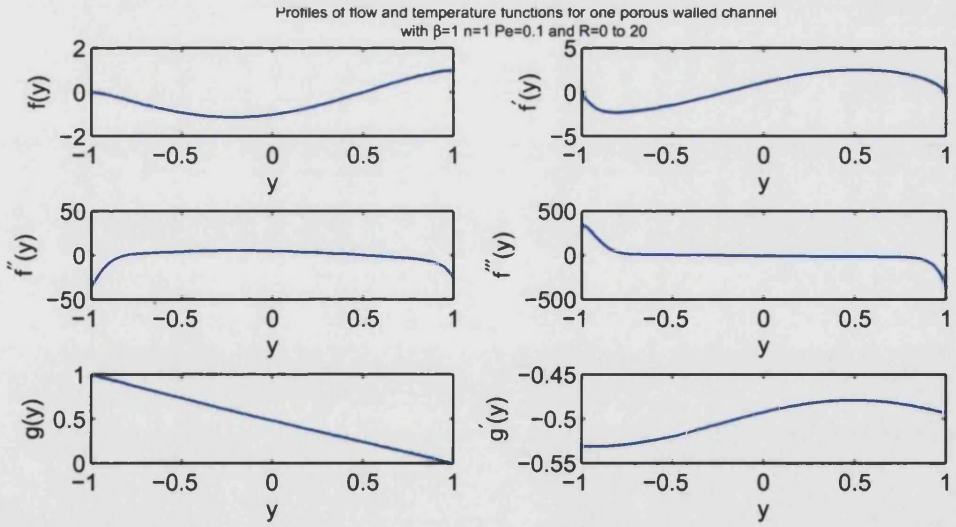

Figure 5.4.5. Solution profiles for the one porous walled nonisothermal channel flow with $\mathrm{Pe} = 0.1$, $\beta = 1$ and $\mathrm{Re} = 20$.

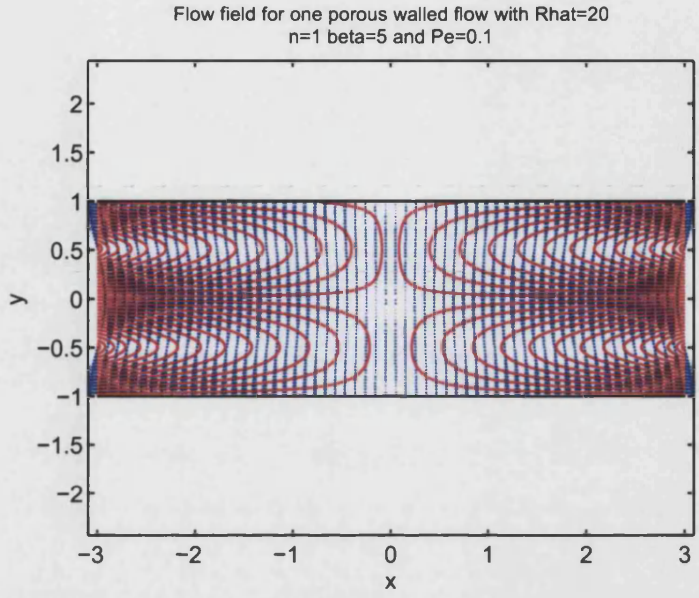

Figure 5.4.6. Flow field for the one porous walled nonisothermal channel flow with Pe = 0.1, $\beta = 5$ and Re = 20.

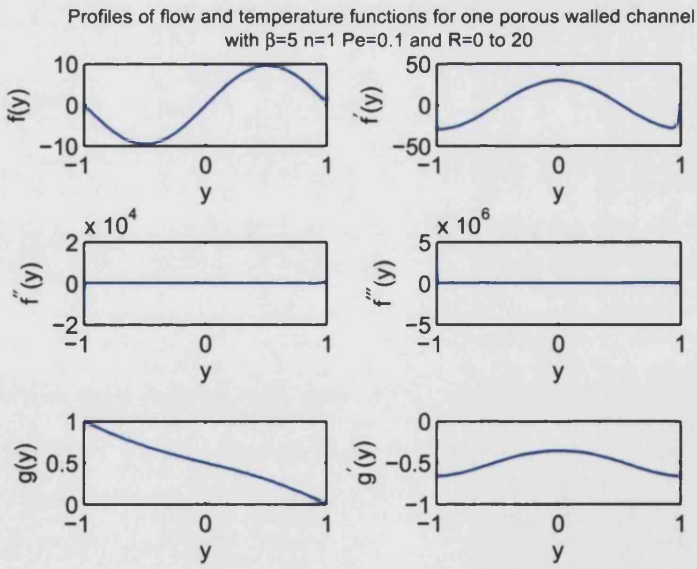

Figure 5.4.7. Solution profiles for the one porous walled nonisothermal channel flow with Pe = 0.1, $\beta = 5$ and Re = 20.

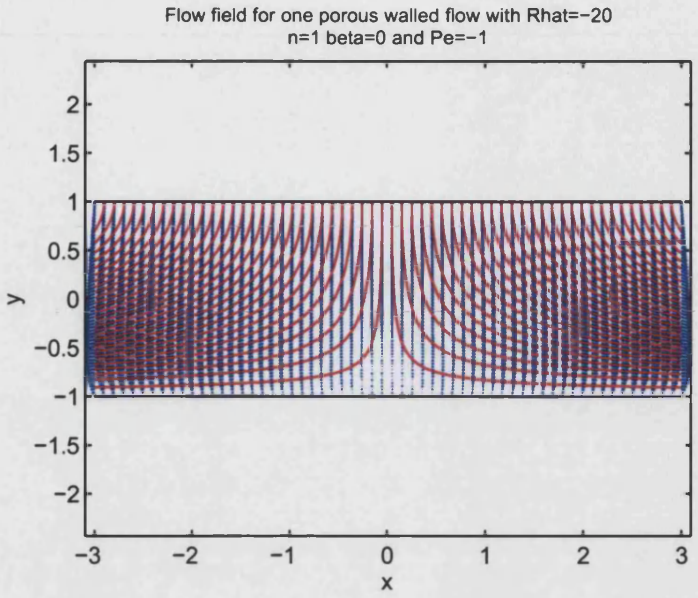

Figure 5.4.8. Flow field for the one porous walled nonisothermal channel flow with $\mathrm{Pe} = -1$, $\beta = 0$ and $\mathrm{Re} = -20$.

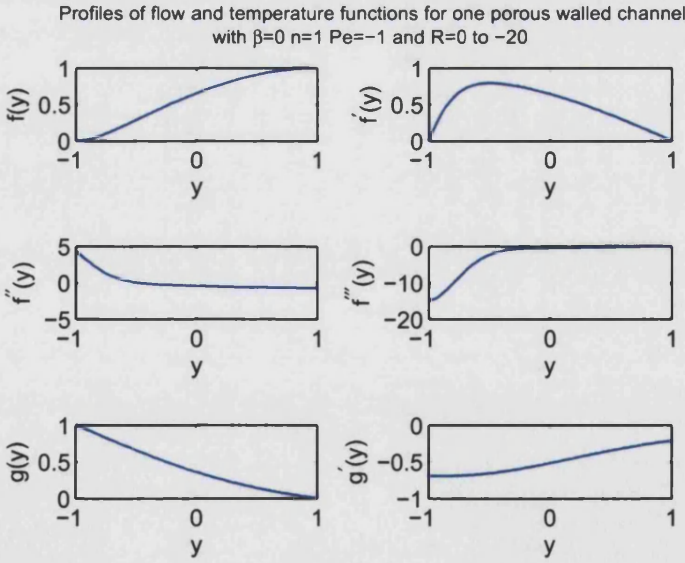

Figure 5.4.9. Solution profiles for the one porous walled nonisothermal channel flow with $\mathrm{Pe} = -1$, $\beta = 0$ and $\mathrm{Re} = -20$.

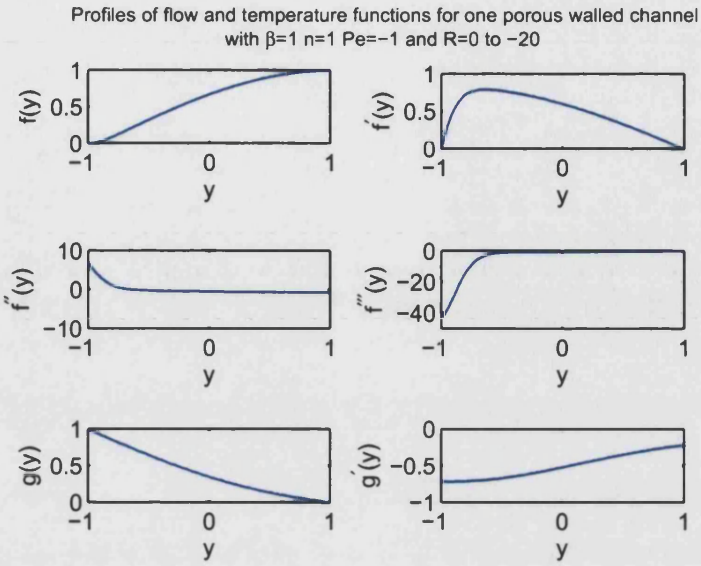

Figure 5.4.10. Solution profiles for the one porous walled nonisothermal channel flow with $\mathrm{Pe} = -1$, $\beta = 1$ and $\mathrm{Re} = -20$.

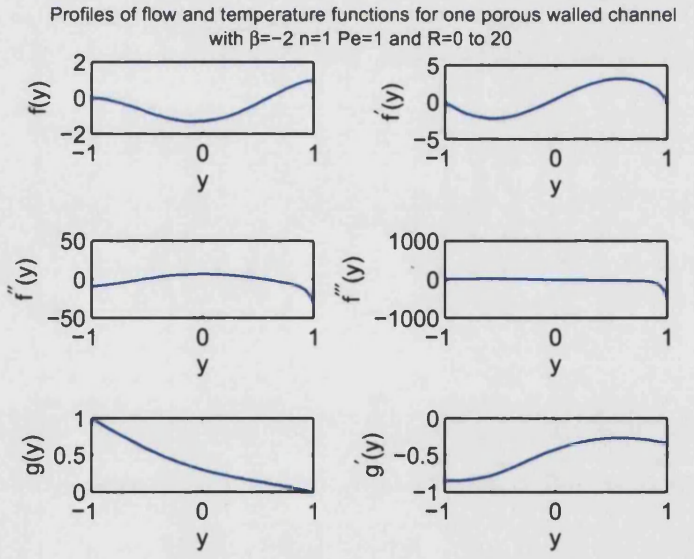

Figure 5.4.11. Solution profiles for the one porous walled nonisothermal channel flow with $\mathrm{Pe} = 1$, $\beta = -2$ and $\mathrm{Re} = 20$.

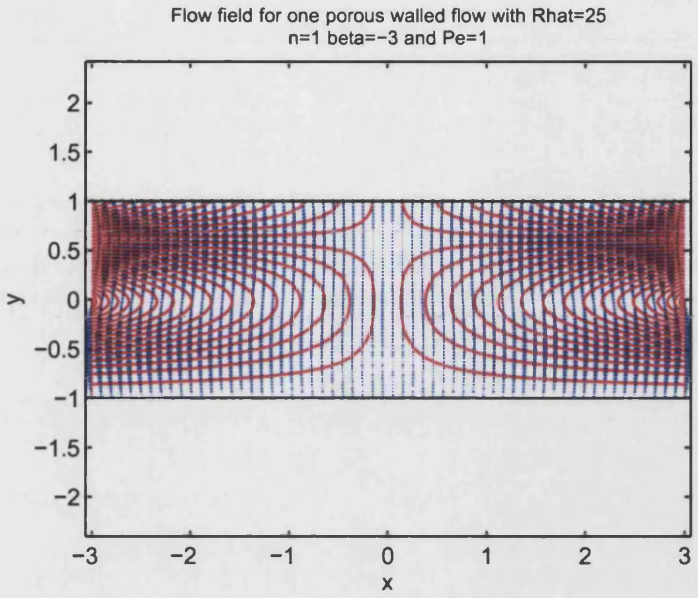

Figure 5.4.12. Flow field for the one porous walled nonisothermal channel flow with Pe = 1, $\beta = -3$ and Re = 25.

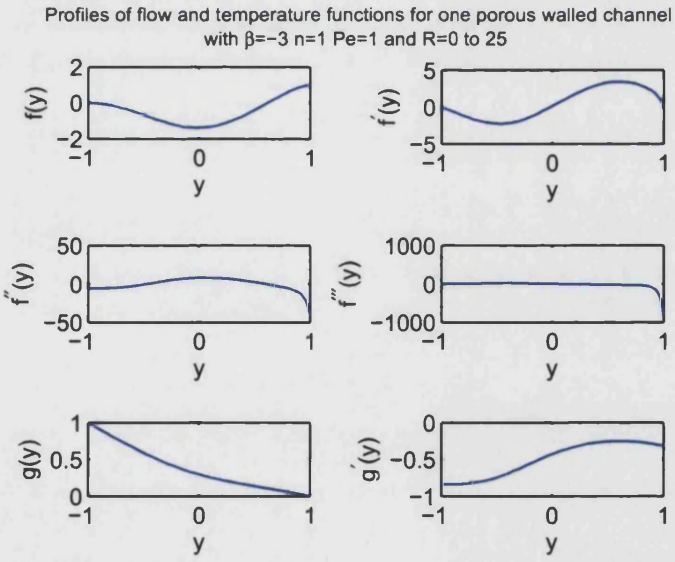

Figure 5.4.13. Solution profiles for the one porous walled nonisothermal channel flow with Pe = 1, $\beta = -3$ and Re = 25.

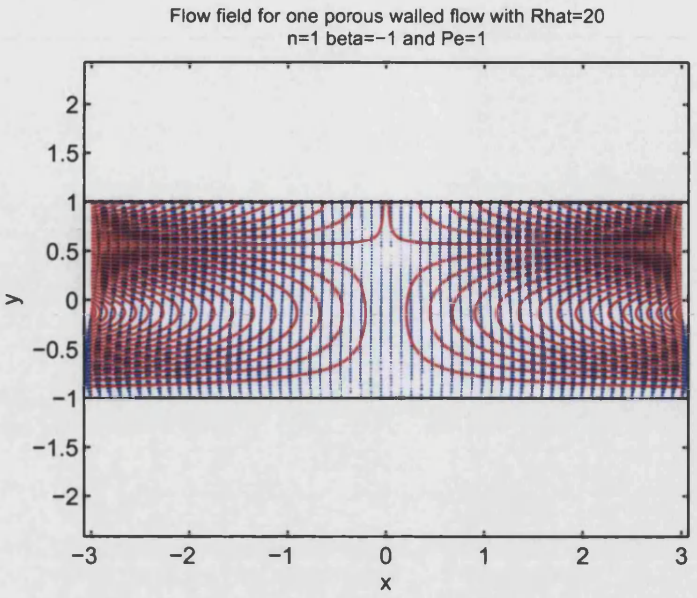

Figure 5.4.14. Flow field for the one porous walled nonisothermal channel flow with Pe = 1, $\beta = -1$ and Re = 20.

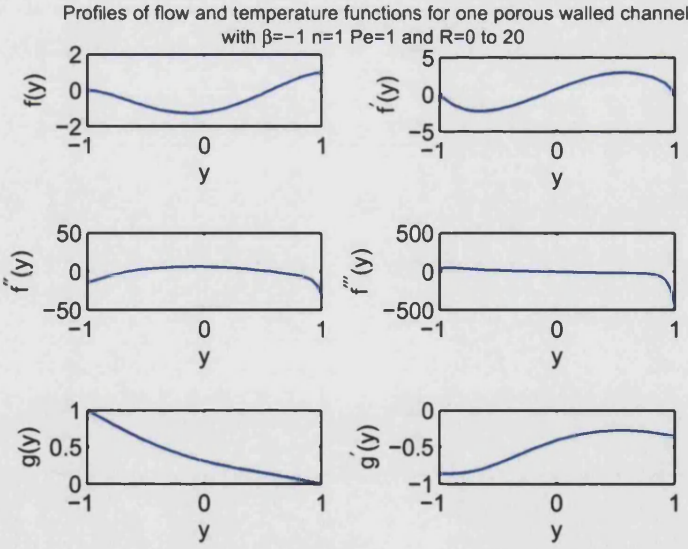

Figure 5.4.15. Solution profiles for the one porous walled nonisothermal channel flow with Pe = 1, $\beta = -1$ and Re = 20.

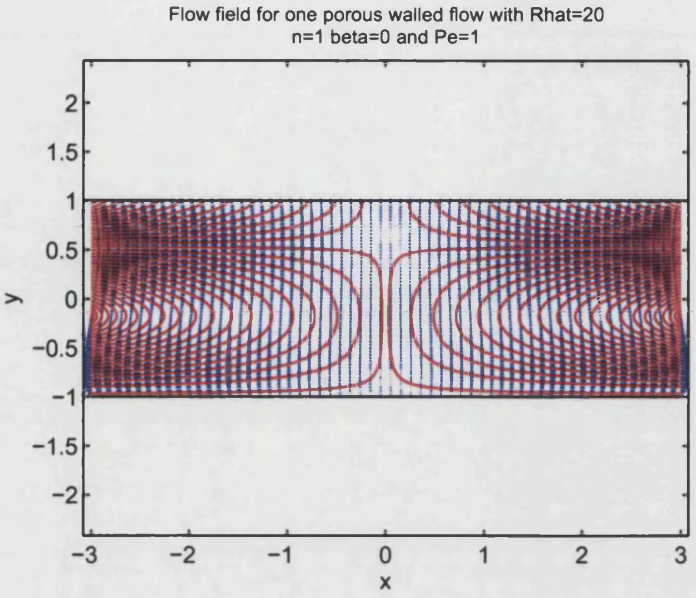

Figure 5.4.16. Flow field for the one porous walled nonisothermal channel flow with Pe = 1, $\beta = 0$ and Re = 20.

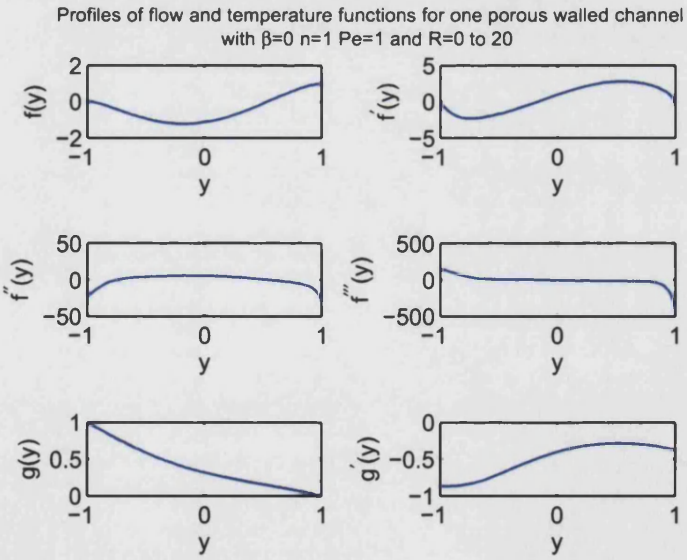

Figure 5.4.17. Solution profiles for the one porous walled nonisothermal channel flow with Pe = 1, $\beta = 0$ and Re = 20.

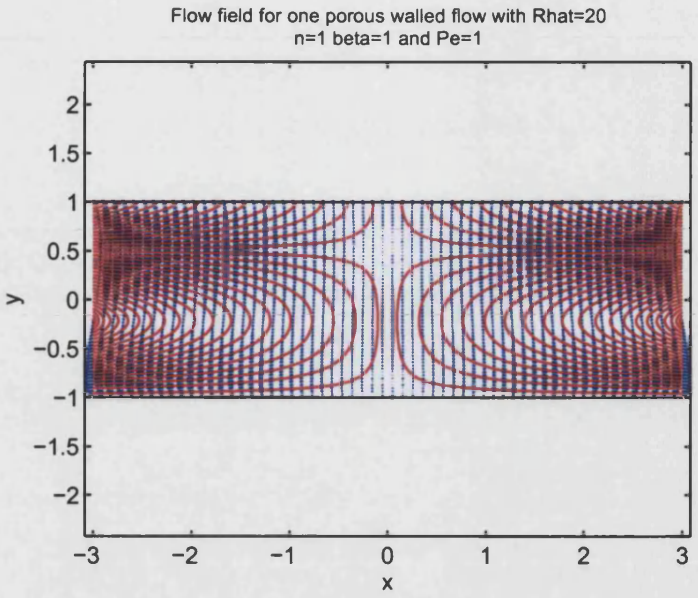

Figure 5.4.18. Flow field for the one porous walled nonisothermal channel flow with Pe = 1, $\beta = 1$ and Re = 20.

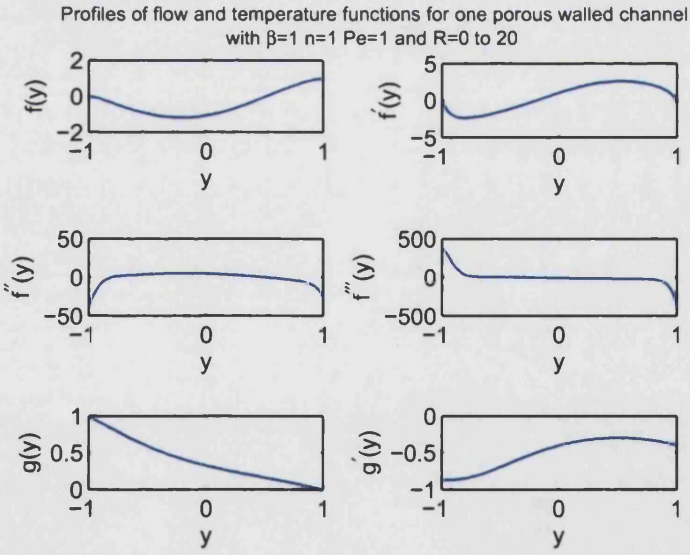

Figure 5.4.19. Solution profiles for the one porous walled nonisothermal channel flow with Pe = 1, $\beta = 1$ and Re = 20.

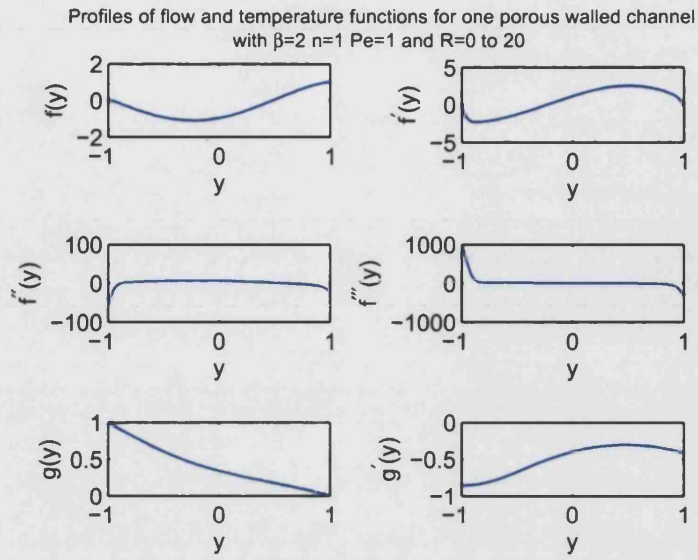

Figure 5.4.20. Solution profiles for the one porous walled nonisothermal channel flow with Pe = 1, $\beta = 2$ and Re = 20.

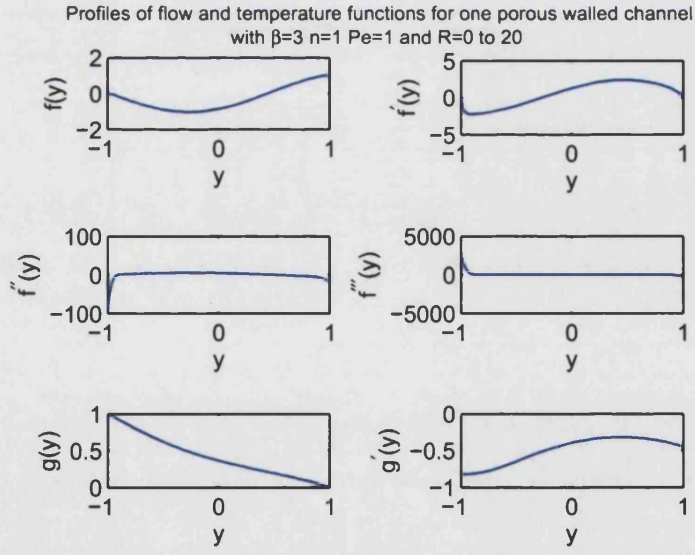

Figure 5.4.21. Solution profiles for the one porous walled nonisothermal channel flow with Pe = 1, $\beta = 3$ and Re = 20.

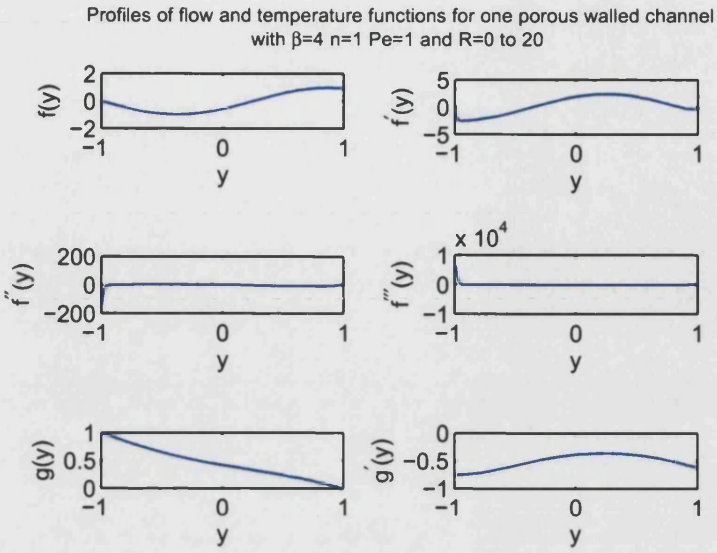

Figure 5.4.22. Solution profiles for the one porous walled nonisothermal channel flow with $\mathrm{Pe} = 1$, $\beta = 4$ and $\mathrm{Re} = 20$.

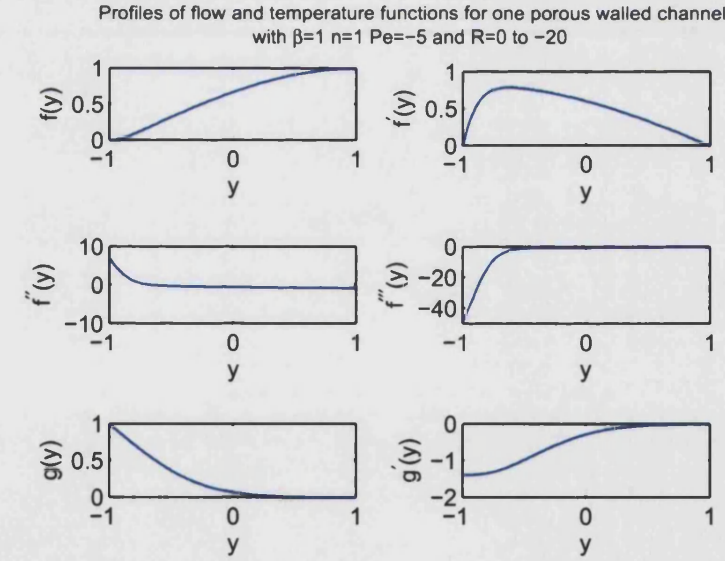

Figure 5.4.23. Solution profiles for the one porous walled nonisothermal channel flow with $\mathrm{Pe} = -5$, $\beta = 1$ and $\mathrm{Re} = -20$.

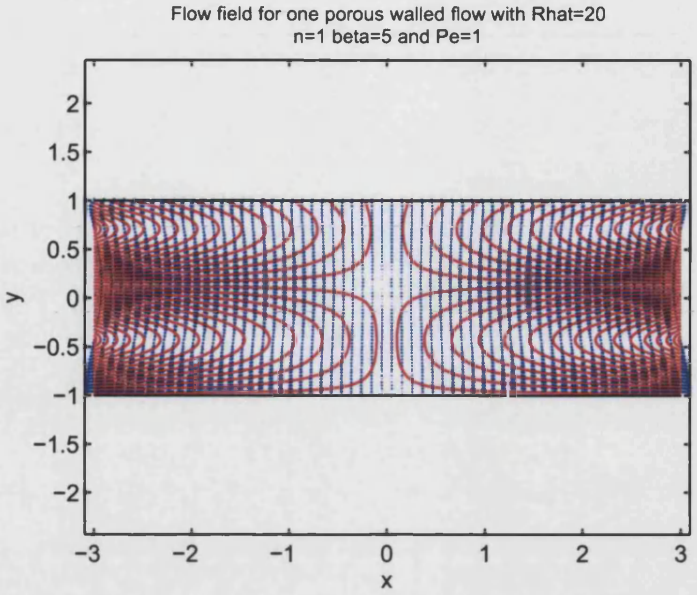

Figure 5.4.24. Flow field for the one porous walled nonisothermal channel flow with Pe = 1, $\beta = 5$ and Re = 20.

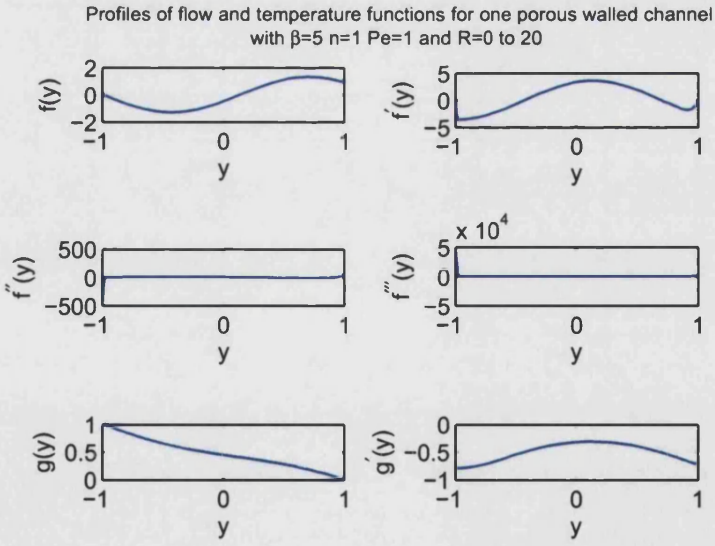

Figure 5.4.25. Solution profiles for the one porous walled nonisothermal channel flow with Pe = 1, $\beta = 5$ and Re = 20.

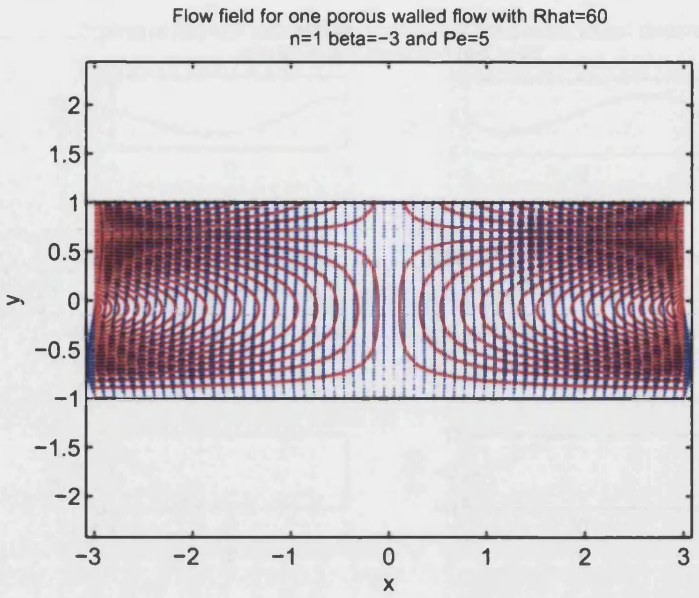

Figure 5.4.26. Flow field for the one porous walled nonisothermal channel flow with Pe = 5, $\beta = -3$ and Re = 60.

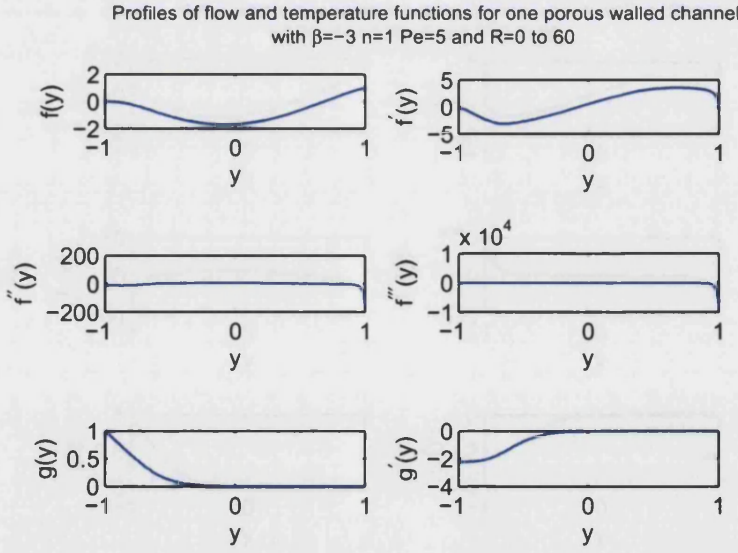

Figure 5.4.27. Solution profiles for the one porous walled nonisothermal channel flow with Pe = 5, $\beta = -3$ and Re = 60.

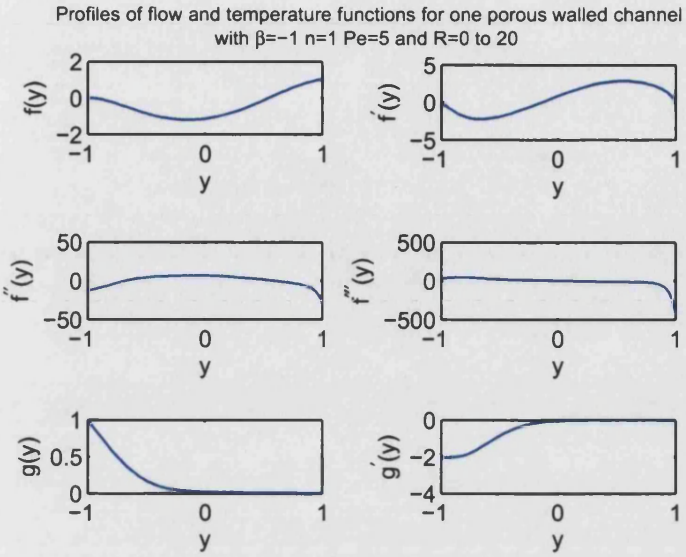

Figure 5.4.28. Solution profiles for the one porous walled nonisothermal channel flow with $\mathrm{Pe} = 5$, $\beta = -1$ and $\mathrm{Re} = 20$.

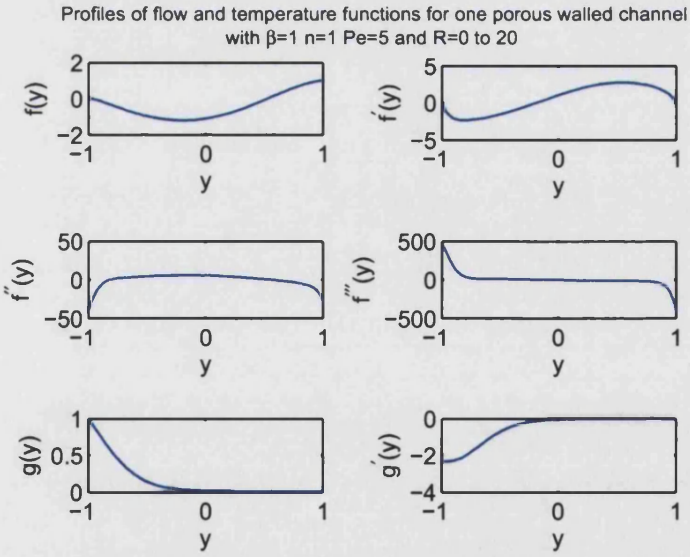

Figure 5.4.29. Solution profiles for the one porous walled nonisothermal channel flow with $\mathrm{Pe} = 5$, $\beta = 1$ and $\mathrm{Re} = 20$.

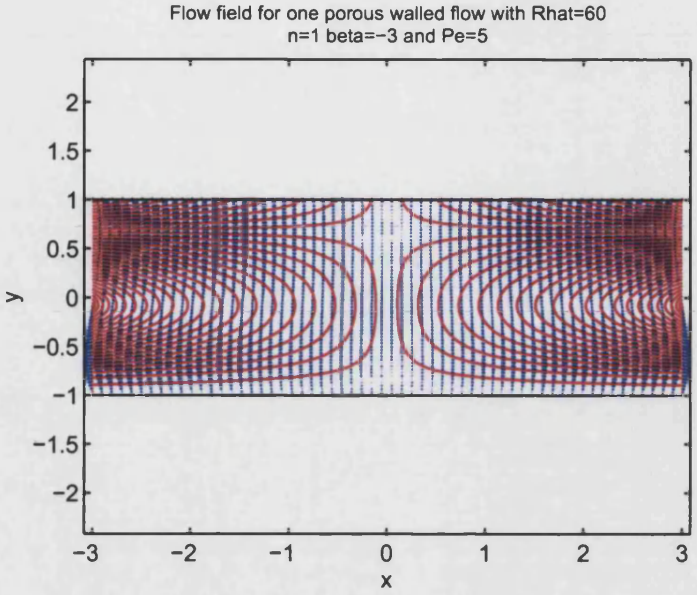

Figure 5.4.30. Flow field for the one porous walled nonisothermal channel flow with Pe = 5, $\beta = 5$ and Re = 20.

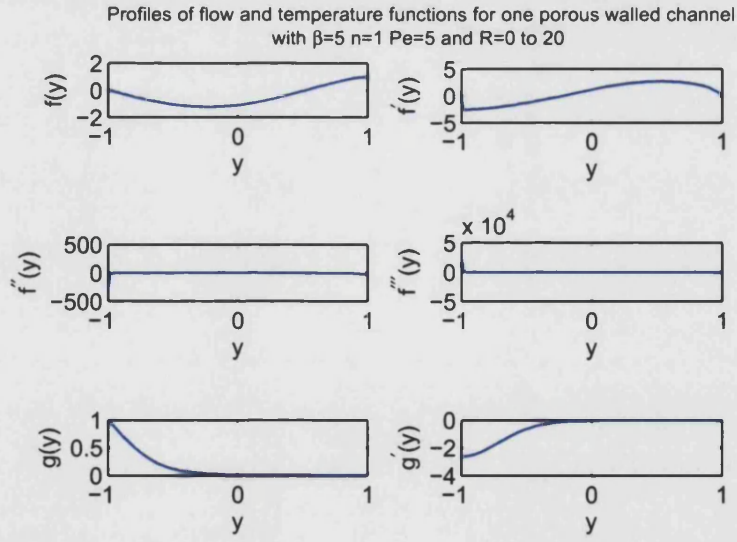

Figure 5.4.31. Solution profiles for the one porous walled nonisothermal channel flow with Pe = 5, $\beta = 5$ and Re = 20.

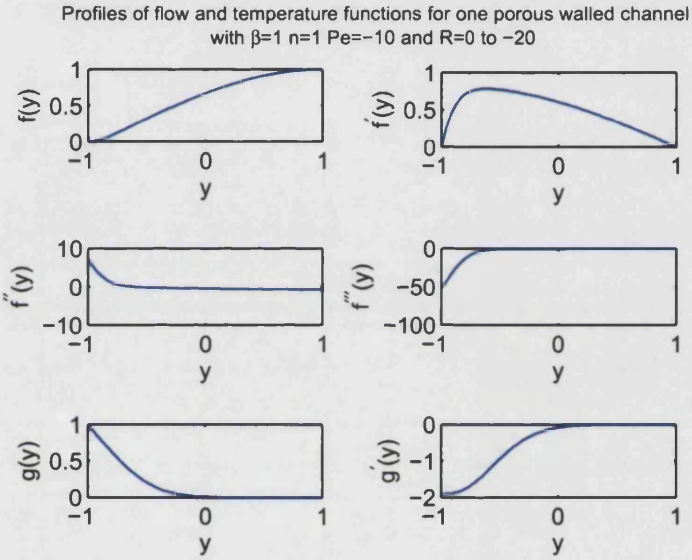

Figure 5.4.32. Solution profiles for the one porous walled nonisothermal channel flow with $\mathrm{Pe} = -10$, $\beta = 1$ and $\mathrm{Re} = -20$.

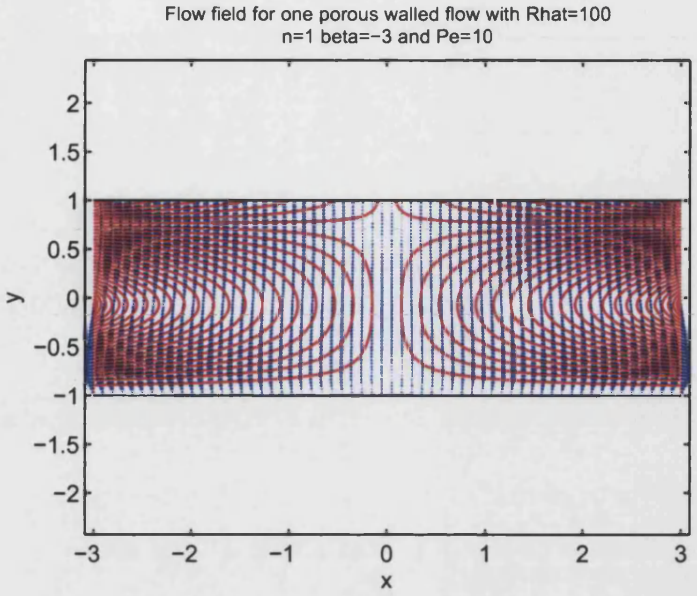

Figure 5.4.33. Flow field for the one porous walled nonisothermal channel flow with Pe = 10, $\beta = -3$ and Re = 100.

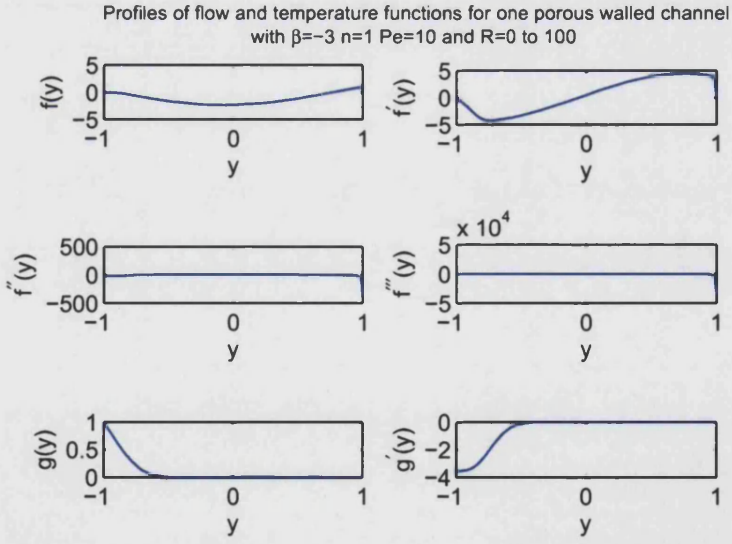

Figure 5.4.34. Solution profiles for the one porous walled nonisothermal channel flow with Pe = 10, $\beta = -3$ and Re = 100.

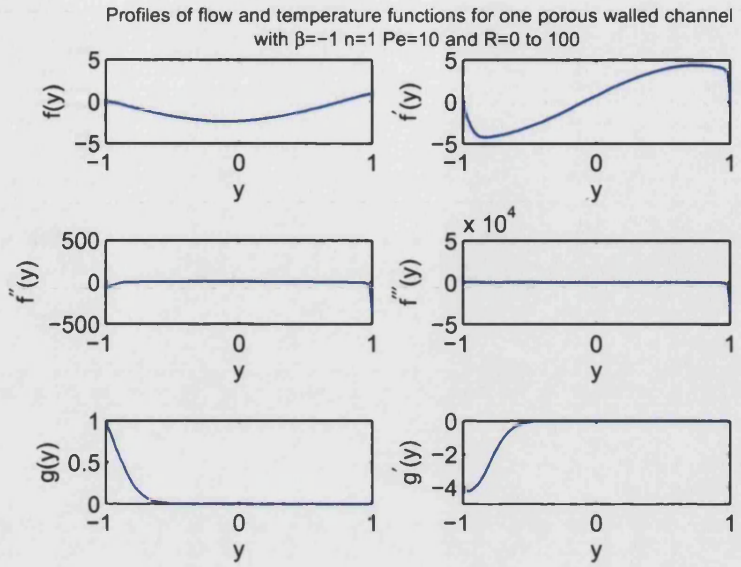

Figure 5.4.35. Solution profiles for the one porous walled nonisothermal channel flow with Pe = 10, $\beta = -1$ and Re = 100.

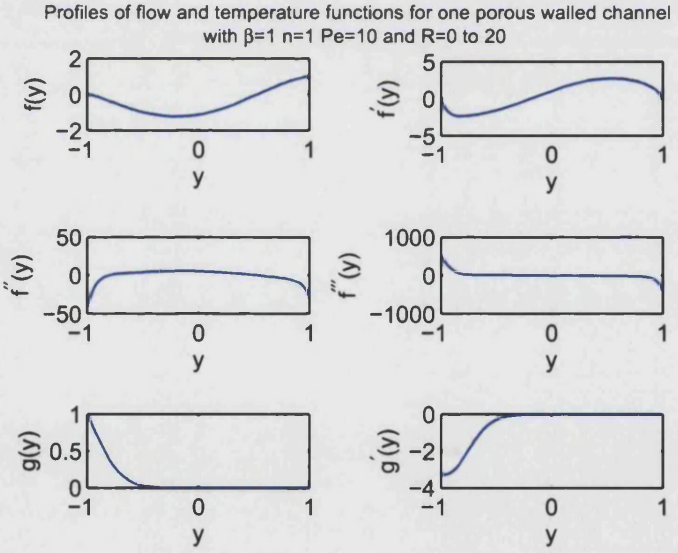

Figure 5.4.36. Solution profiles for the one porous walled nonisothermal channel flow with Pe = 10, $\beta = 1$ and Re = 20.

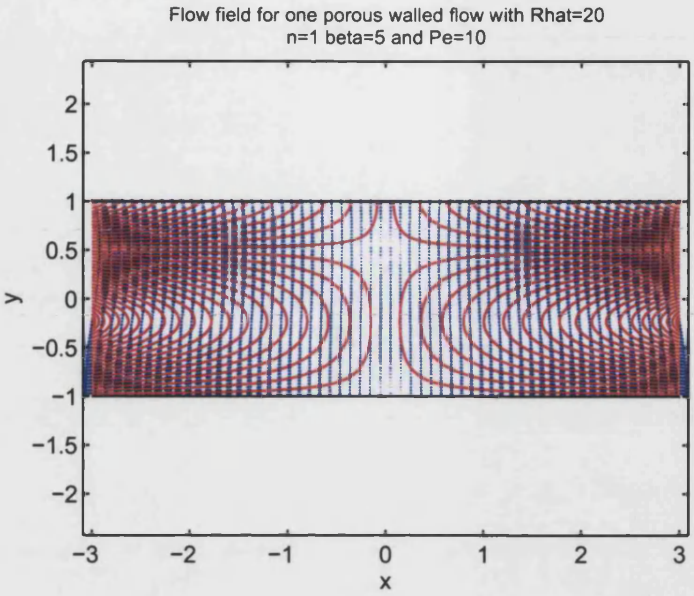

Figure 5.4.37. Flow field for the one porous walled nonisothermal channel flow with Pe = 10, $\beta = 5$ and Re = 20.

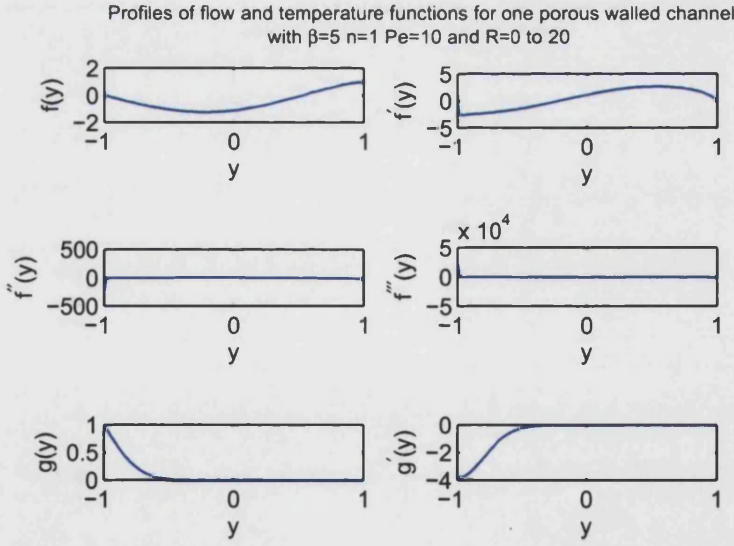

Figure 5.4.38. Solution profiles for the one porous walled nonisothermal channel flow with Pe = 10, $\beta = 5$ and Re = 20.

5.4.2 Discussion of solution profiles

The $\beta = 0$, Pe $= -1$, Re $= -20$ injection solution in Figure 5.4.9 is typical of the injection flow solutions for the range of β and Pe considered. The main features of the profiles are that the solution $f(y)$ is increasing, $f'(y)$ is single signed and splits into two regions, a narrow region of increase away from zero at the lower wall and then a shallower decreasing behaviour away from the local maximum down to zero at the upper wall. The temperature distribution within the channel, $g(y)$, is not far from a linearly decreasing function, with a gradient slightly steeper than the Pe $= 0$ solution of $-1/2$ near the lower wall and decreasing to a slightly shallower gradient than the Pe $= 0$ prediction at the upper wall. The injection solution profiles for the case $\beta = 1$ shown in Figure 5.4.10 show that the effect of changing β upon the flow solution is minimal. The flow field for $\beta = 0$, Figure 5.4.8 shows that the fluid that enters the channel through the upper wall is smoothly transported out of the channel ends and that the maximum horizontal fluid velocity occurs a short distance away from the heated lower channel wall.

Moving on to the suction flow solutions, the $\beta = 0$, Pe $= 1$, Re $= 20$ solution shown in Figure 5.4.17 is one basis against which comparisons with other suction solutions can be made. The main features of this particular solution are that $f(y)$ and $f'(y)$ both take positive and negative values over the channel width for this particular combination of Pe and Re. This corresponds to regions of flow which are flowing in opposite directions to other regions within the channel i.e. recirculation. Where $f(y) < 0$ and $x > 0$ there will be fluid moving in the direction of decreasing x and where $f(y) > 0$ there will be fluid moving in the direction of increasing x; where $f'(y) < 0$ and $x > 0$ fluid will be moving downwards and where $f'(y) > 0$ fluid will be moving upwards in the positive x half of the channel. The temperature $g(y)$ is decreasing throughout the channel width, with a relatively steep gradient near the lower wall, then a region of increasingly shallow gradient as the region of recirculating flow occurs and as the upper wall is approached the gradient becomes increasingly negative. The flow field shown in Figure 5.4.16 illustrates the large proportion of the channel width that is undergoing recirculating flow and the correspondingly thin region adjacent to the upper wall where fluid is successfully being removed from the channel.

As β is increased to 1, Figure 5.4.19 show that the regions of positive and negative $f(y)$ and $f'(y)$ remain and so recirculating flow will again occur. The changes compared to the $\beta = 0$ in Figure 5.4.17 are that the gradients of $f''(y)$ and $f'''(y)$ are larger at the wall than when $\beta = 0$ and that there is now a region of almost constant negative gradient of $g'(y)$ adjacent to the lower wall. The corresponding flow field is shown in Figure 5.4.18 and is similar to that for $\beta = 0$, shown in Figure 5.4.16.

The suction solution profiles in Figures 5.4.20, 5.4.21, 5.4.22 and 5.4.25, for $\beta = 2, 3, 4$ and 5 respectively, show that as β increases the behaviour of $f(y)$ near the upper wall changes from increasing to the wall value as the wall is approached to decreasing from above the wall value as the wall is approached. The corresponding $f'(y)$ profile show steeper gradients at the lower wall as β increases and a change of behaviour at the upper wall, from $f'(y)$ being positive and decreasing for $\beta = 2, 3$ to $f'(y)$ having a second internal zero and the position of this internal zero moving away from the upper wall for $\beta = 4, 5$. The gradients of $f''(y)$ and $f'''(y)$ become steeper at the walls as β increases. The gradient of $g'(y)$ near the lower wall decreases as β increases while the behaviour in the remainder of the channel does not vary with β. The temperature $g(y)$ is nonzero throughout the channel for all β. The corresponding flow field for $\beta = 5$, Figure 5.4.24, shows a large region of recirculation in the lower half of the channel and a region of reversing flow in the upper half of the channel, the streamlines of which making a more acute angle with the upper wall as $|x|$ increases.

As β decreases from zero, the main changes to the solution behaviour are that the region where $f(y) < 0$ is moving away from the lower wall and the minimum of $f(y)$ is moving closer to the centre of the channel as β decreases. The value of $f''(-1)$ is increasing as β decreases and the behaviour of $f''(y)$ near the lower wall changes from increasing then decreasing when $\beta = -1$ to slowly increasing then increasing then decreasing when $\beta = -3$. The temperature $g(y)$ does not change much with β for this value of Pe. Figures 5.4.15, 5.4.11 and 5.4.13 show the solution profiles for $\beta = -1, -2$ and -3 respectively and Figures 5.4.14 and 5.4.12 show the flow fields for the cases $\beta = -1$ and $\beta = -3$, where it can be seen that the stagnation line (the horizontal line through the flow field through which no fluid passes vertically) and the mid-line of the recirculation region have been displaced towards the upper wall as β decreases from $\beta = -1$ in Figure 5.4.14 to $\beta = -3$ in Figure 5.4.12.

When |Pe| is increased to 5, in the case of injection Figure 5.4.23 shows that the main changes from |Pe| = 1 are that the gradients of $f''(y)$ and $f'''(y)$ near the lower wall are steeper and that the temperature function $g(y)$ decreases to zero much more rapidly as we move away from the lower wall, with almost all of the temperature drop occurring before the mid-line of the channel is reached. When $\beta = 1$, Pe $= 5$ in the case of suction flow, Figure 5.4.29 again shows that there will be a region of recirculating flow within the channel as $f(y)$, $f'(y)$ are multisigned. The gradients of $f''(y)$ and $f'''(y)$ are steep near the channel walls and very shallow by comparison in the body of the channel; the width of the boundary layer of $f''(y)$ and $f'''(y)$ at the upper wall is thinner than that at the lower wall. The temperature function $g(y)$ is such that all the significant temperature changes occur in the lower half of the channel and the gradient

$g'(y)$ is always negative, being large initially and increasing to just below zero before the centre of the channel.

When $\beta = 5$, Pe $= 5$ comparison with $\beta = 1$, Pe $= 5$ shows that, in Figure 5.4.31, there is a much thinner and steeper boundary layer for $f'(y)$ adjacent to the lower wall, that the behaviour of $f''(y)$ and $f'''(y)$ near the walls is correspondingly steeper and confined to thinner regions. The temperature function $g(y)$ also changes and now the region of small $g(y)$ extends from the upper wall well into the lower half of the channel. The flow field for the case $\beta = 5$, Pe $= 5$ is shown in Figure 5.4.30 and as compared to $\beta = 5$, Pe $= 1$ in Figure 5.4.24 there is now no region of reversing streamlines in the upper portion of the channel and the recirculating region now extends to cover almost 3/4 of the channel width instead of the entire width for the $\beta = 5$, Pe $= 1$ case.

As β decreases below zero and Pe $= 5$, Figures 5.4.28 and 5.4.27 for $\beta = -1$ and -3 respectively show that the region of recirculation remains and the gradients in $f''(y)$ and $f'''(y)$ near the walls increase in magnitude. The nonzero region of significant change of $g(y)$ is still confined to the lower half of the channel in both cases. The flow field for $\beta = -3$, Pe $= 5$ in Figure 5.4.26 shows that the recirculating region extends to cover over 3/4 of the channel width and that the region of flow near the upper wall must change direction in a very thin region in order to satisfy the no slip condition at the upper wall, as compared to the flow field for $\beta = -3$, Pe $= 1$ in Figure 5.4.12.

When |Pe| is increased again to |Pe| $= 10$, the changes as seen going from |Pe| $= 1$ to |Pe| $= 5$ are present and are increased. For the case of injection flow with Pe $= -10$, Figure 5.4.32 shows almost the same behaviour as for Pe $= -5$ and Pe $= -1$. The gradients of $f''(y)$ and $f'''(y)$ near the lower wall have increased and the temperature changes are again confined to the lower half of the channel, in this case a little more restricted than for the smaller negative values of Pe.

As β increases above zero, Figures 5.4.36 and 5.4.38 for $\beta = 1$ and 5 respectively show that as β increases, the regions of rapid variation of $f'(y)$, $f''(y)$ and $f'''(y)$ become thinner and more pronounced. As β increases, the gradient $g'(y)$ near the lower wall is steeper initially and now the region of significant temperature change is confined to the lowest quarter of the channel width. Figure 5.4.37 shows the flow field for Pe $= 10$, $\beta = 5$ and the stagnation line is located a quarter of the width of the channel away from the upper wall with the remainder of the channel width being occupied by a recirculating flow.

For β below zero, Figures 5.4.35 and 5.4.34 for $\beta = -1$ and -3 respectively show that regions of recirculation will remain and that, in the cases illustrated for Re $= 100$, the flow function and its derivative are very similar. The only difference between the solutions can be seen in the temperature $g(y)$ and its derivative, where for $\beta = -3$

the gradient away from the lower wall is slightly less steep than that for $\beta = -1$. Figure 5.4.33 shows that the recirculation region takes up the majority of the channel width and that the stagnation line has shifted further towards the upper wall than in the case of Pe = 5, however the overall behaviour is similar to the Pe = 5 case for lower Reynolds numbers, as shown in Figure 5.4.26.

Finally, when |Pe| is reduced to |Pe| = 0.1 the main feature of all the solutions is that the entire channel width is needed for the temperature to drop from $g = 1$ at the lower wall to $g = 0$ at the upper wall. For $\beta = 1$, Pe $= -0.1$ injection flow, Figure 5.4.1 shows that the flow solution $f(y)$ is similar to that of the other injection flows, but the temperature solution is almost linearly decreasing with a gradient that is initially just steeper than the Pe = 0 solution of $-1/2$ and then becomes shallower as the upper wall is approached, ending up with a gradient that is less than the Pe = 0 solution of $-1/2$.

The suction solution $\beta = 1$, Pe = 0.1 shown in Figure 5.4.5 predicts recirculating flow in the lower section of the channel and has relatively wide regions of high gradients of $f'(y)$, $f''(y)$ and $f'''(y)$ near the walls. The temperature solution $g(y)$ is again almost linearly decreasing, the gradient of which varies by less than 10% of the Pe = 0 prediction of $-1/2$ over the channel width. However, when β is increased to $\beta = 5$, Pe = 0.1 the flow behaviour shown in Figure 5.4.7 changes from that seen for other values of β and Pe. The solution $f(y)$ now takes on an almost sinusoidal form and has a large amplitude; the boundary layers in $f'(y)$ near the walls are very thin (thinner at the lower wall than at the upper wall) and the form of $f'(y)$ is now that there are two regions of flow directed away from the origin of the channel adjacent to the channel walls and a central region directed towards the channel origin. The values of $f''(y)$ and $f'''(y)$ are very large in thin layers at the channel walls. The temperature solution $g(y)$ is still decreasing over the whole width of the channel but the gradient initially diminishes and subsequently increases as the channel width is traversed. The corresponding flow field, Figure 5.4.6, now shows two almost equally sized regions of reversed flow, one in each half of the channel width; the boundary layers required at each wall in order to satisfy the boundary conditions are not visible in this figure.

As β decreases below zero, Figures 5.4.4 for $\beta = -1$ and 5.4.3 for $\beta = -3$ show that the magnitude of the solution $f(y)$ decreases as β decreases and that the variation in the higher derivatives of $f(y)$, although similar in form, also decreases in magnitude as β decreases. The temperature solution $g(y)$ remains decreasing over the channel width and the gradient varies more for $\beta = -1$ than for $\beta = -3$; indeed for $\beta = -3$ the gradient $g'(y)$ remains constant for a short region next to the lower wall. The flow field for $\beta = -3$, Pe = 0.1 shown in Figure 5.4.2 illustrates the recirculating region of flow taking up the majority of the channel width and it is similar in structure to that for other values of Pe.

5.4.3 Bifurcation diagrams

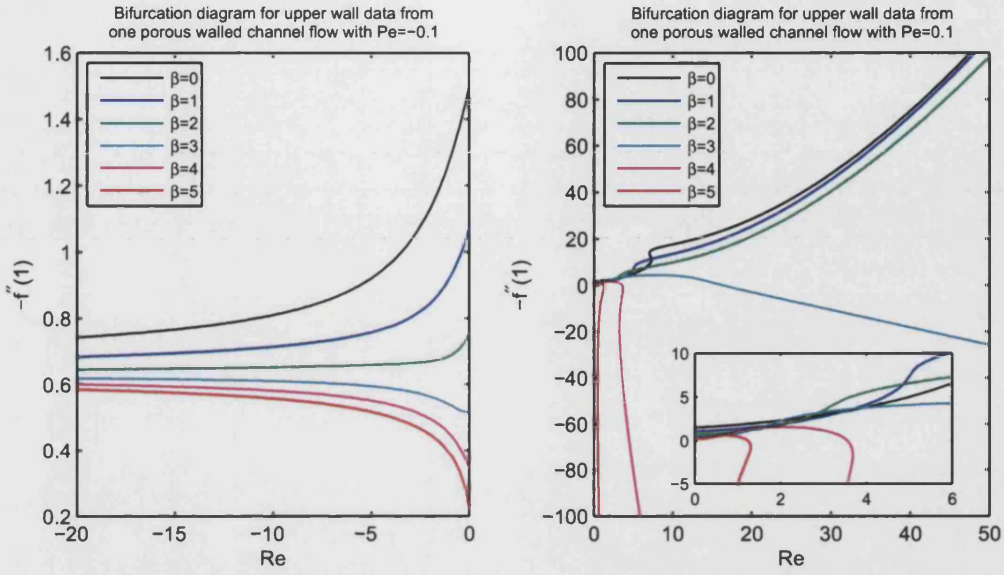

Figure 5.4.39. A pair of bifurcation plots for the one porous walled nonisothermal channel flow for $|\mathrm{Pe}| = 0.1$, $\beta = 0, 1, 2, 3, 4, 5$ with injection and suction, the data coming from the solution at the upper wall.

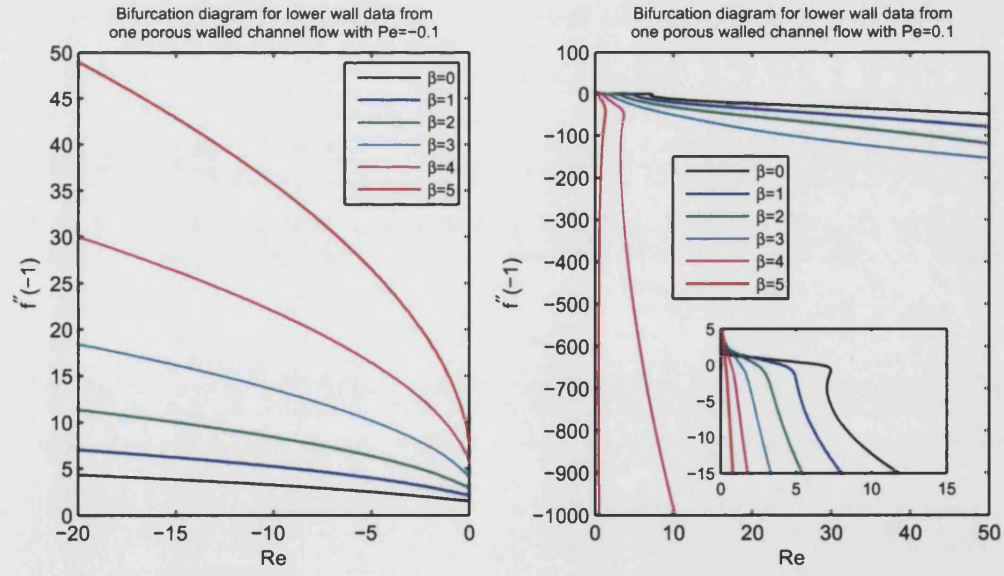

Figure 5.4.40. A pair of bifurcation plots for the one porous walled nonisothermal channel flow for $|\mathrm{Pe}| = 0.1$, $\beta = 0, 1, 2, 3, 4, 5$ with injection and suction, the data coming from the solution at the lower wall.

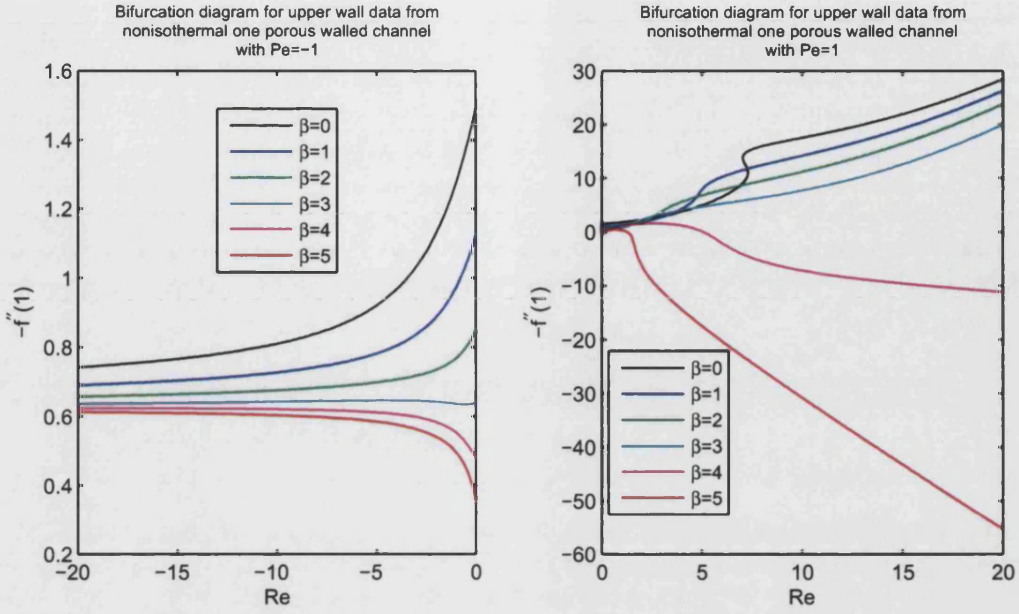

Figure 5.4.41. A pair of bifurcation plots for the one porous walled nonisothermal channel flow for $|\mathrm{Pe}| = 1$, $\beta = 0, 1, 2, 3, 4, 5$ with injection and suction, the data coming from the solution at the upper wall.

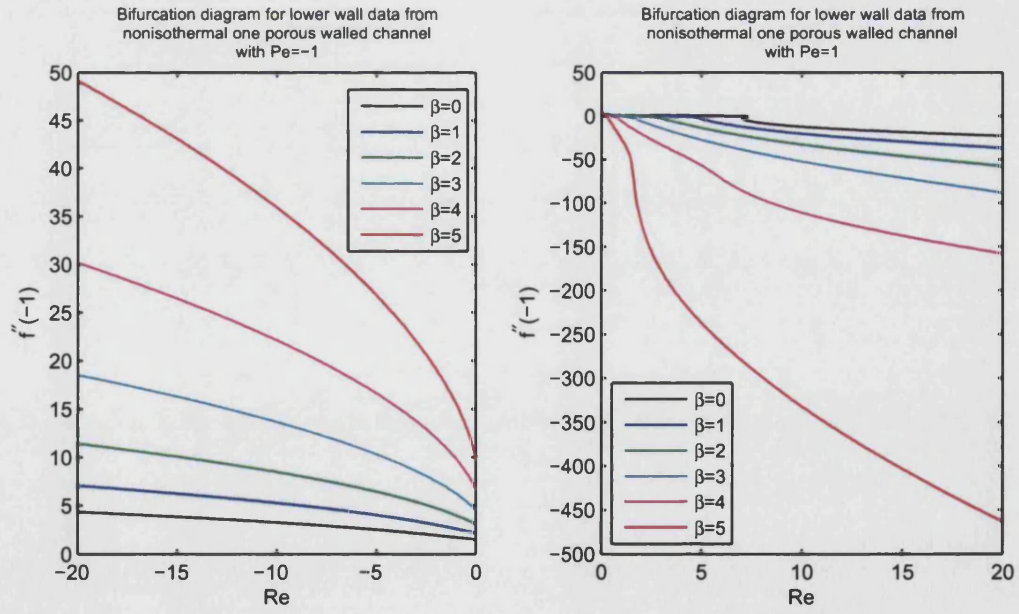

Figure 5.4.42. A pair of bifurcation plots for the one porous walled nonisothermal channel flow for $|\mathrm{Pe}| = 1$, $\beta = 0, 1, 2, 3, 4, 5$ with injection and suction, the data coming from the solution at the lower wall.

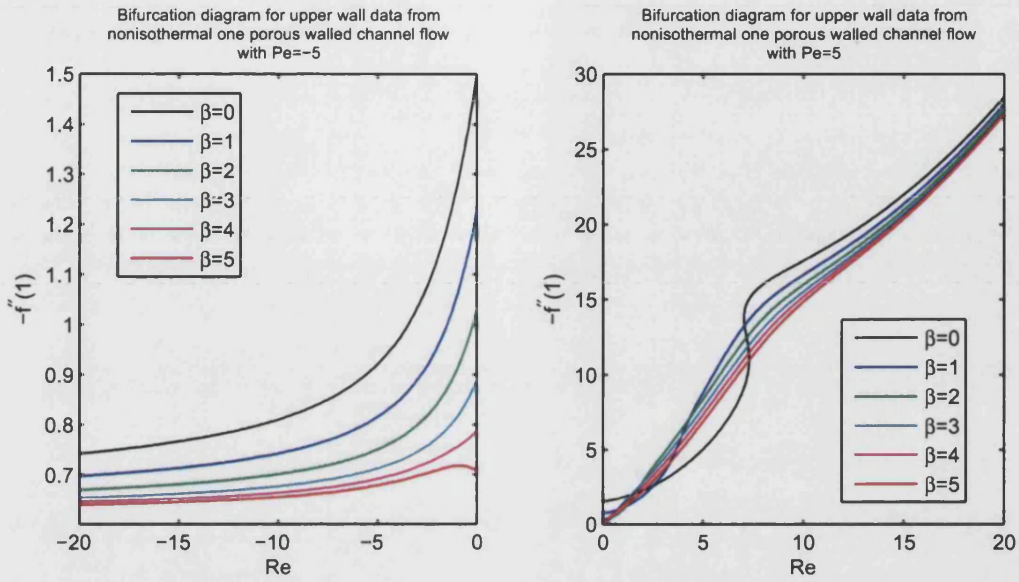

Figure 5.4.43. A pair of bifurcation plots for the one porous walled nonisothermal channel flow for $|\mathrm{Pe}| = 5$, $\beta = 0, 1, 2, 3, 4, 5$ with injection and suction, the data coming from the solution at the upper wall.

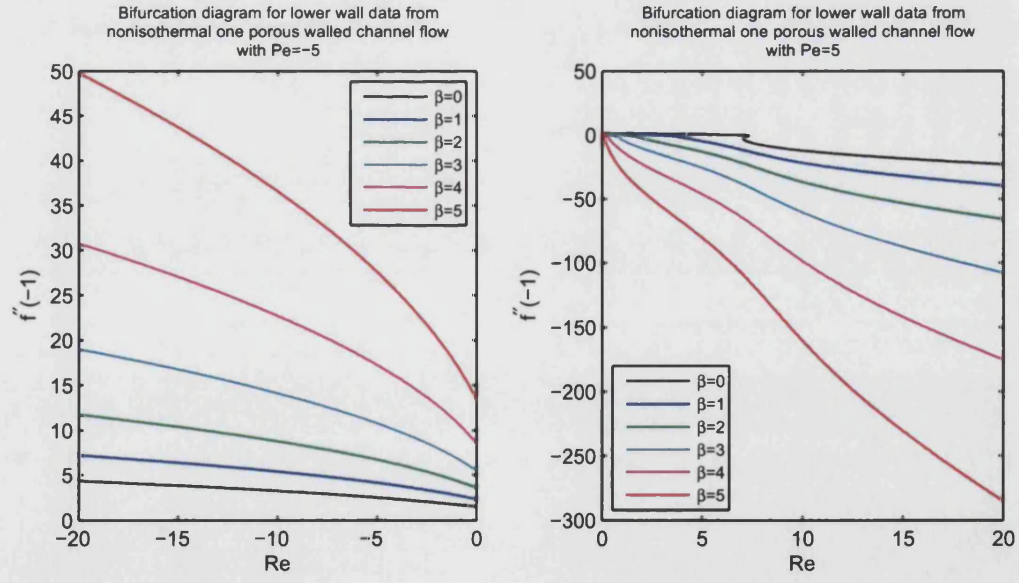

Figure 5.4.44. A pair of bifurcation plots for the one porous walled nonisothermal channel flow for $|\mathrm{Pe}| = 5$, $\beta = 0, 1, 2, 3, 4, 5$ with injection and suction, the data coming from the solution at the lower wall.

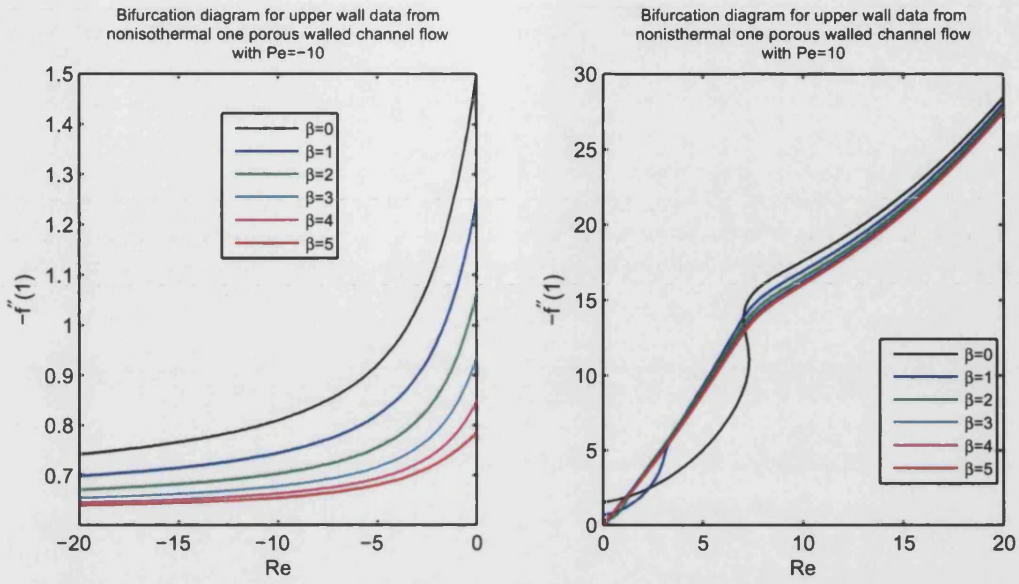

Figure 5.4.45. A pair of bifurcation plots for the one porous walled nonisothermal channel flow for $|\mathrm{Pe}| = 10$, $\beta = 0, 1, 2, 3, 4, 5$ with injection and suction, the data coming from the solution at the upper wall.

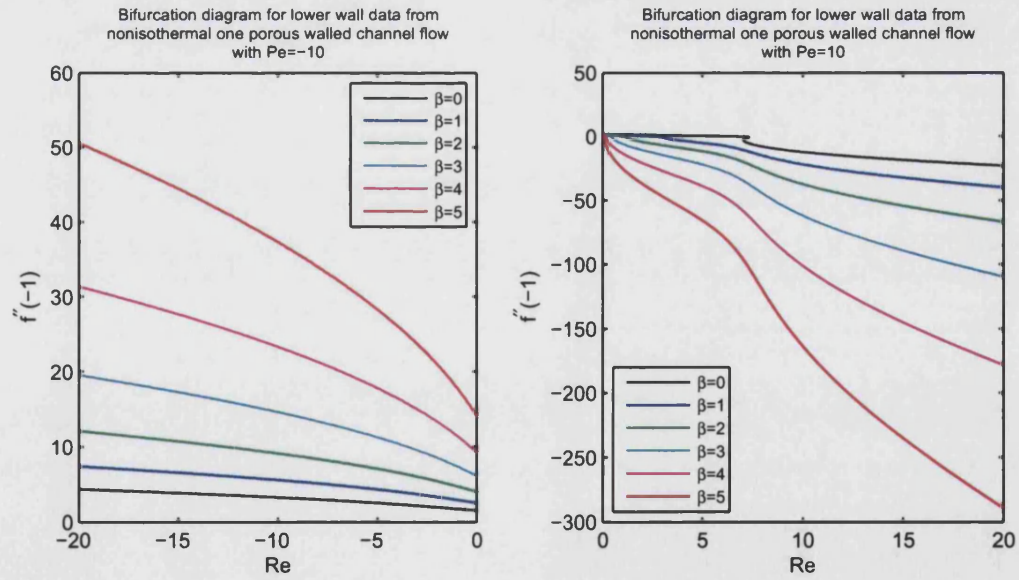

Figure 5.4.46. A pair of bifurcation plots for the one porous walled nonisothermal channel flow for $|\mathrm{Pe}| = 10$, $\beta = 0, 1, 2, 3, 4, 5$ with injection and suction, the data coming from the solution at the lower wall.

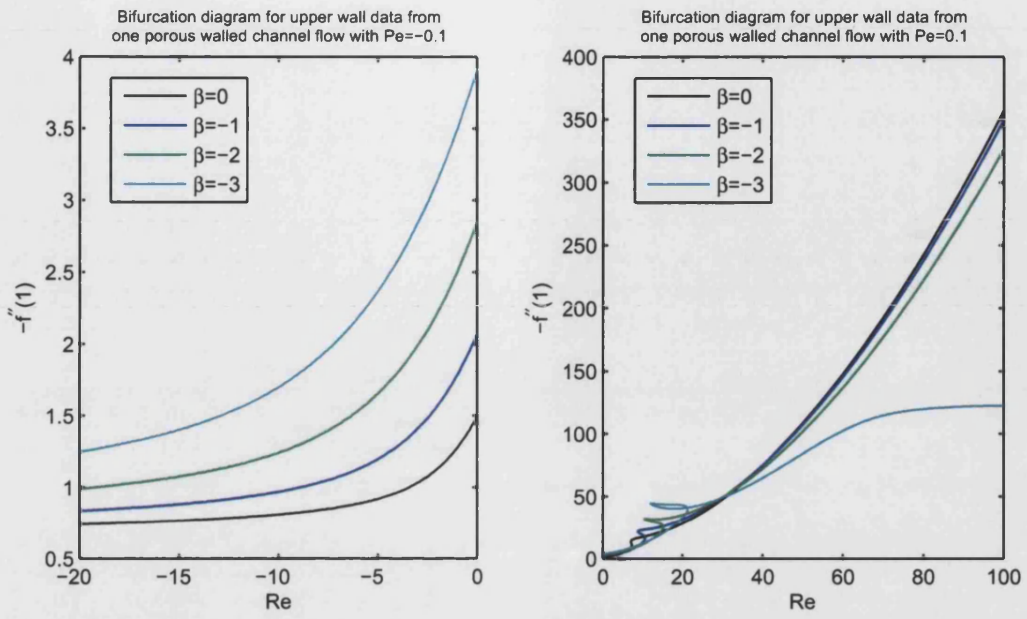

Figure 5.4.47. A pair of bifurcation plots for the one porous walled nonisothermal channel flow for $|\mathrm{Pe}| = 0.1$, $\beta = -3, -2, -1, 0$ with injection and suction, the data coming from the solution at the upper wall.

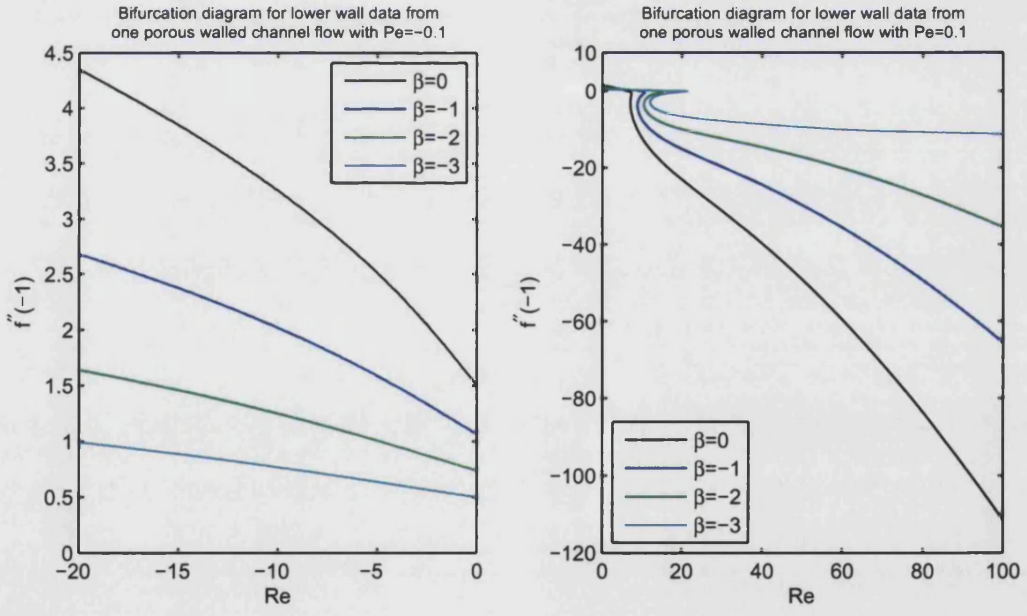

Figure 5.4.48. A pair of bifurcation plots for the one porous walled nonisothermal channel flow for $|\mathrm{Pe}| = 0.1$, $\beta = -3, -2, -1, 0$ with injection and suction, the data coming from the solution at the lower wall.

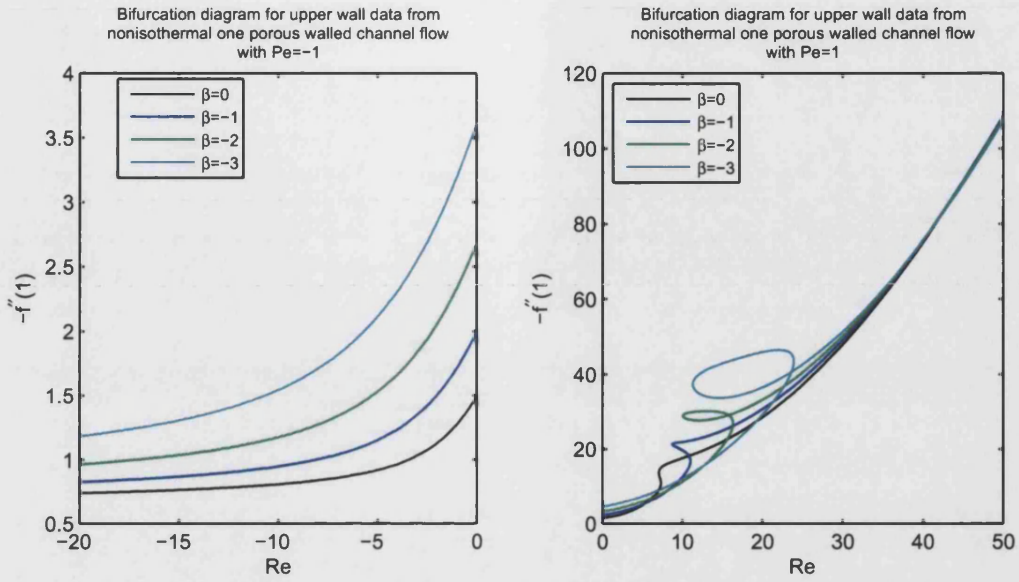

Figure 5.4.49. A pair of bifurcation plots for the one porous walled nonisothermal channel flow for $|\mathrm{Pe}| = 1$, $\beta = -3, -2, -1, 0$ with injection and suction, the data coming from the solution at the upper wall.

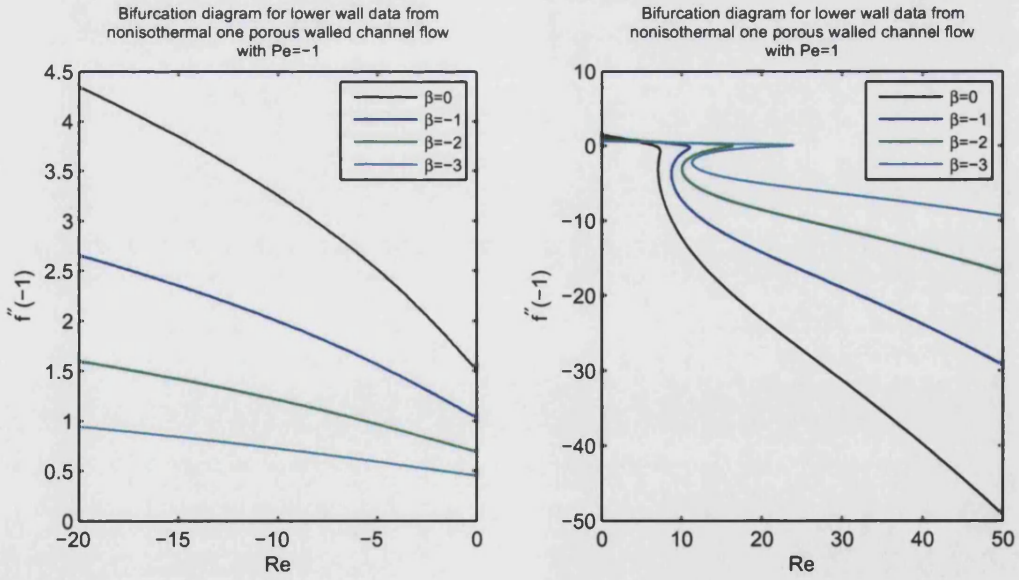

Figure 5.4.50. A pair of bifurcation plots for the one porous walled nonisothermal channel flow for $|\mathrm{Pe}| = 1$, $\beta = -3, -2, -1, 0$ with injection and suction, the data coming from the solution at the lower wall.

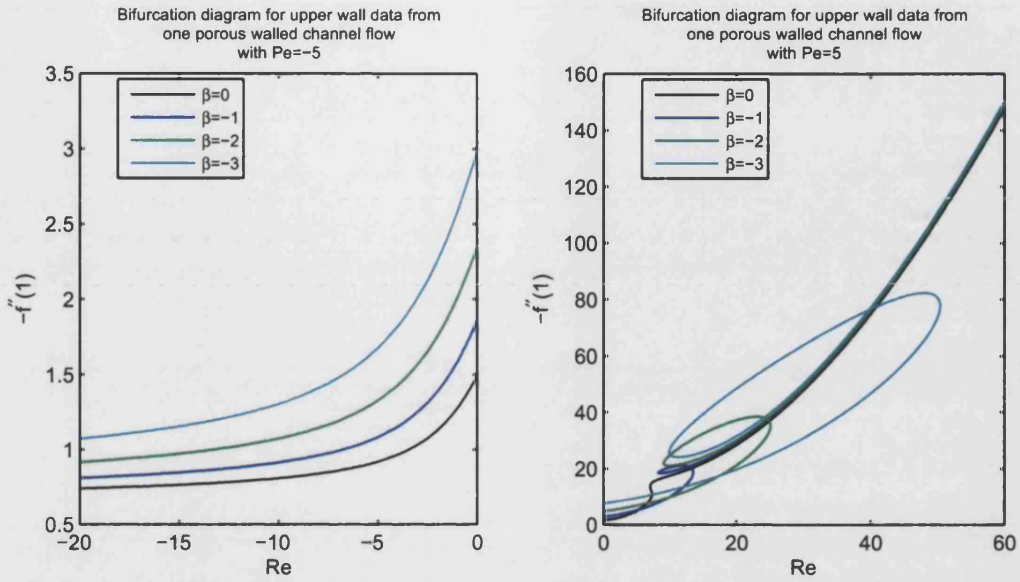

Figure 5.4.51. A pair of bifurcation plots for the one porous walled nonisothermal channel flow for $|\mathrm{Pe}| = 5$, $\beta = -3, -2, -1, 0$ with injection and suction, the data coming from the solution at the upper wall.

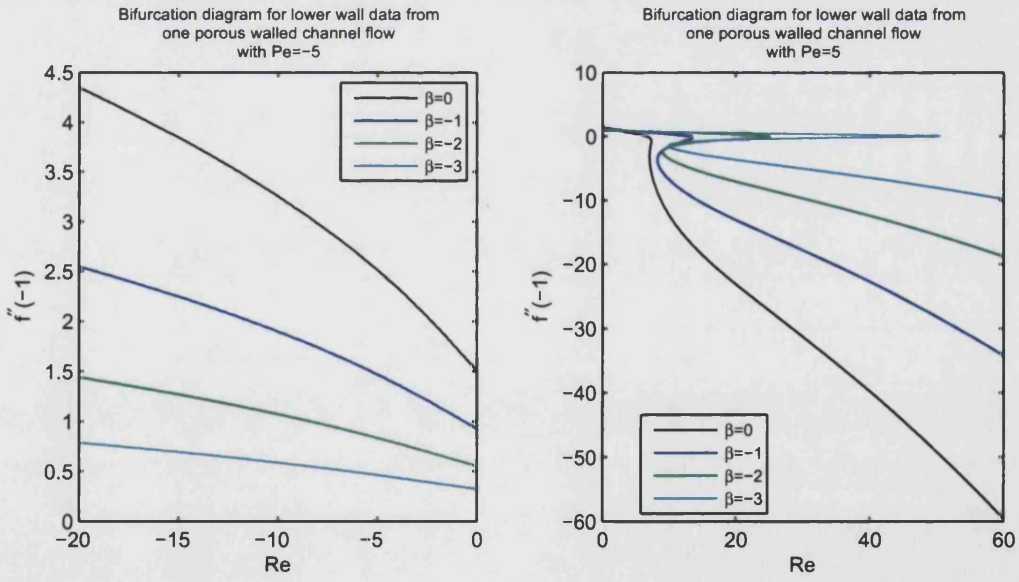

Figure 5.4.52. A pair of bifurcation plots for the one porous walled nonisothermal channel flow for $|\mathrm{Pe}| = 5$, $\beta = -3, -2, -1, 0$ with injection and suction, the data coming from the solution at the lower wall.

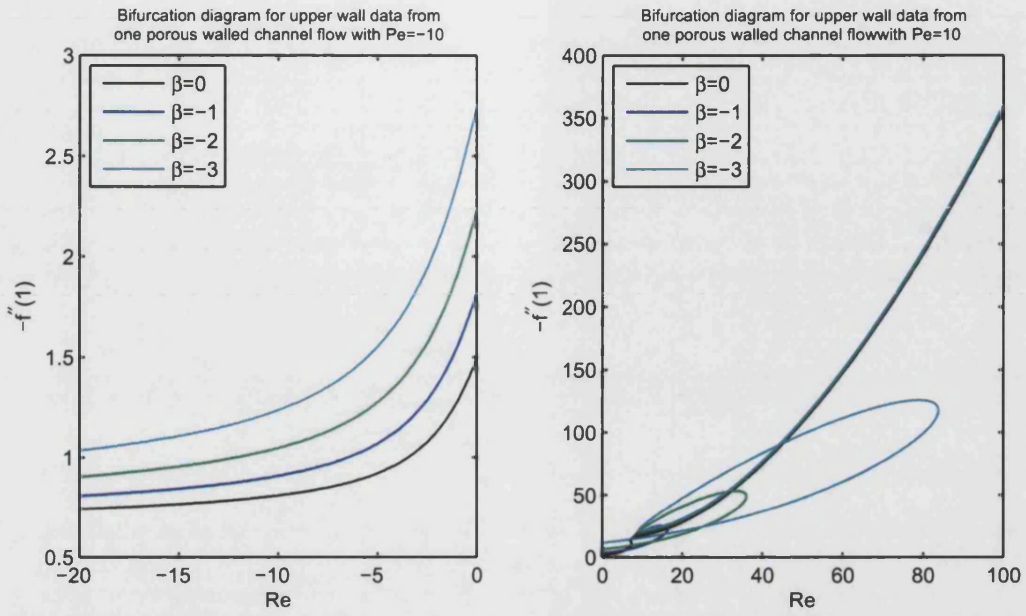

Figure 5.4.53. A pair of bifurcation plots for the one porous walled nonisothermal channel flow for $|\mathrm{Pe}| = 10$, $\beta = -3, -2, -1, 0$ with injection and suction, the data coming from the solution at the upper wall.

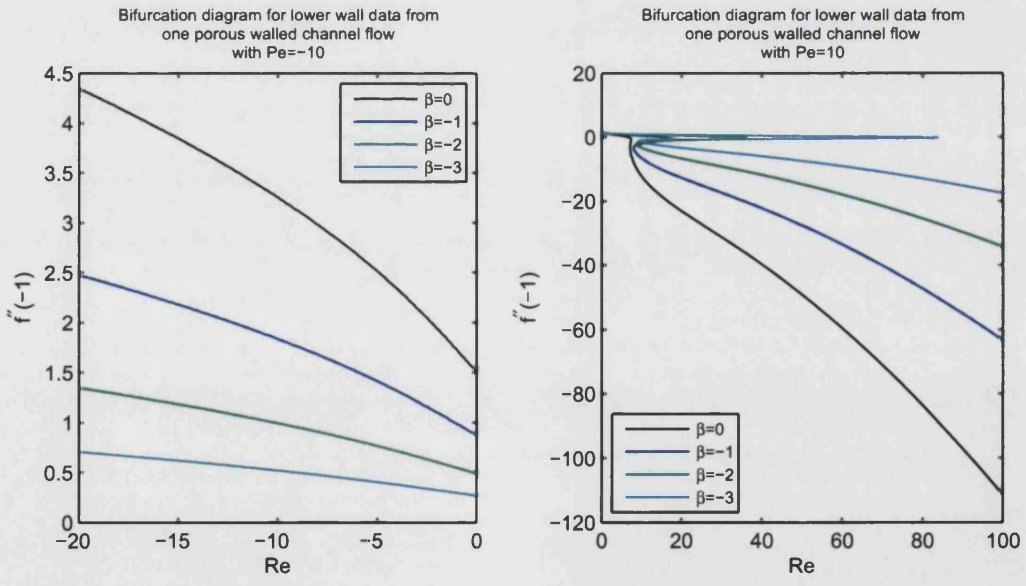

Figure 5.4.54. A pair of bifurcation plots for the one porous walled nonisothermal channel flow for $|\mathrm{Pe}| = 10$, $\beta = -3, -2, -1, 0$ with injection and suction, the data coming from the solution at the lower wall.

5.4.4 Discussion of bifurcation diagrams

We first consider the bifurcation plots in Figures 5.4.39–5.4.46 where Pe > 0 and $\beta \geq 0$. For Figure 5.4.39 in the case of suction (Re, Pe > 0) with Pe $= 0.1$, as β increases from 0 the region of hysteresis on the bifurcation curve disappears, and for $\beta \geq 3$ there is a value of the Reynolds number at which the upper wall stress passes through zero. For $\beta = 4, 5$ there are again regions of hysteresis and both of these curves are strongly decreasing for small Reynolds numbers. At the lower wall, Figure 5.4.40 shows that each bifurcation curve changes sign, at which point there is a reversal of flow near the lower wall, but the Reynolds number at which this flow reversal takes place decreases as β increases. For the simulations corresponding to $\beta = 4, 5$ the lower wall stresses are an order of magnitude larger than those of the other values of β and failure of the numerical method to converge precluded calculations further than Re ≈ 10.

For Pe $= 1$ and $\beta \geq 0$ Figure 5.4.41 shows that increasing β from zero eliminates the region of hysteresis and the large Re behaviour of the bifurcation curves moves downwards to lower values as β increases. For $\beta = 4, 5$ the bifurcation curves pass through zero. The lower wall behaviour in Figure 5.4.42 reflects the upper wall behaviour in that the bifurcation curves for $\beta = 0, 1, 2, 3$ are all similar, only the $\beta = 0$ curve has a region of hysteresis and for $\beta = 4, 5$ the large Re behaviour is much greater in magnitude than that of the lower values of β.

For Pe $= 5$ and $\beta \geq 0$ Figure 5.4.43 shows that increasing β from 0 again eliminates the hysteresis region and bunches the curves closer together. The curvature of the bifurcation curves is also reduced as β increases. As Re increases the curves asymptote to the same behaviour. The lower wall behaviour in Figure 5.4.44 shows that for $\beta > 0$ the hysteresis region has been eliminated and a region of oscillation remains on these curves in the region of the turning point on the $\beta = 0$ curve.

For Pe $= 10$ and $\beta \geq 0$ Figure 5.4.45 shows that once $\beta > 0$ then there is no region of hysteresis and the bifurcation curves are much closer together than in the Pe $= 5$ case. The curves all asymptote to the same behaviour for large Re. On the lower wall, Figure 5.4.46 shows that the behaviour is similar to that for Pe $= 5$; there is a region of oscillation on the $\beta > 1$ curves near the turning point on the $\beta = 0$ curve and the oscillation in this case is larger than that of the Pe $= 5$ case.

For all of the injection flows Re < 0, Pe < 0 with $\beta \geq 0$, shown in the left hand plots of Figures 5.4.39–5.4.46, the large Re < 0 behaviours are similar and the curves approach a constant value for each β. This value does not appear to vary greatly with Pe < 0 for each fixed value of β and the ordering of the curves is such that $\beta = 0$ has the highest values and $\beta = 5$ has the smallest values throughout the Re < 0 range where simulations were performed. As Re approaches zero the behaviour of the curves

does vary. For Pe $= -0.1$ and when $\beta = 3,4,5$ the values of $-f''(1)$ drop below their respective Re $\to -\infty$ values as Re $\to 0_-$, while the $\beta = 0,1,2$ values of $-f''(1)$ increase above their Re $\to -\infty$ values as Re $\to 0_-$. As Pe decreases the behaviour changes slightly so that fewer of the small β curves dip below their large Re $\to -\infty$ values as Re $\to 0-$. For Pe $= -1$, Figure 5.4.41 shows that only the $\beta = 4,5$ curves decrease markedly as Re $\to 0_-$ while the $\beta = 3$ curve is almost constant. For Pe $= -5$ Figure 5.4.43 shows that all of the β curves reach values greater than their Re $\to -\infty$ values as Re $\to 0_-$, with the $\beta = 5$ curve showing a local maximum for small $-$Re. Finally for Pe $= -10$ Figure 5.4.45 shows that all the β curves are increasing as Re $\to 0_-$.

The overall effect of increasing values of β is to eliminate the regions of hysteresis in the suction cases, and as Pe increases above Pe $= 1$ the variation in wall stresses at the upper wall becomes smaller whereas the variation in wall-stress at the lower wall is larger but still qualitatively the same as for Pe $= 1$. For the Pe $= 0.1$ simulations it is found that larger values of $\beta = 4,5$ produce a large change in wall-stress at the upper and lower walls; simulations could only be run for a limited range of Reynolds numbers in comparison to the smaller values of $\beta = 0,1,2,3$. The effect of a highly temperature sensitive viscous fluid may not have been fully captured due to the numerical difficulties involved.

Now we shall consider Figures 5.4.47–5.4.54 where Re > 0 and $\beta \leq 0$. For the right half of Figure 5.4.47 where $\beta \leq 0$ and Re > 0 as Re $\to \infty$ the $\beta = 0,-1,-2$ curves all asymptote to the same behaviour whilst the $\beta = -3$ curve has reached an almost constant value of wall stress about 3 times smaller than the other curves. As β decreases a region of "S-shaped" hysteresis on the $\beta = 0$ curve changes into a "loop-shaped" hysteresis region with the Re extent of the loop increasing as β decreases. On the lower wall, shown in Figure 5.4.48 the "S-shaped" hysteresis region is still visible as β decreases from 0, but it becomes more and more squashed perpendicular to the Re axis and more elongated parallel to the Re axis as β becomes more and more negative, with the point at which the wall stress vanishes moving to smaller values of Re as β decreases.

For Pe $= 1$ and $\beta \leq 0$, the upper wall bifurcation curves shown in Figure 5.4.49 display similar behaviour as β decreases. The "S-shaped" hysteresis region for $\beta = 0$ changes into a cusp for $\beta = -1$ and then into a "loop" as β decreases further. The extent of the hysteresis region along the Re axis increases as β decreases, the initial Reynolds number of the hysteresis region increases as β decreases and the overall size of the hysteresis loop also increases as β decreases. The lower wall behaviour shown in Figure 5.4.50 is qualitatively similar to that for Pe $= 0.1$ and is a more pronounced

version of that figure where the curves have been further elongated in the Re direction and squashed in the perpendicular direction.

As the value of Pe increases to Pe = 5 and $\beta \leq 0$, Figure 5.4.51 shows similar behaviours occurring for the bifurcation curves as for the case of Pe = 1. The $\beta = 0$ "S-shaped" hysteresis region changes into a tight "loop" for $\beta = -1$ and as β decreases further the bifurcation curves show that the "loop" changes into a more "spiral-like" shape. The range of Re where hysteresis occurs increases as β decreases and the vertical extent of the "loops" also increases. The "loops" seem to be aligning in the same direction in the $-f''(1)$–Re plane. The lower wall bifurcation diagram Figure 5.4.52 again shows that the "S-shaped" hysteresis region visible for $\beta = 0$ becomes more and more deformed as β decreases.

When Pe = 10 and $\beta \leq 0$ the same behaviour is shown in Figure 5.4.53; the "S-shaped" hysteresis region for $\beta = 0$ changes into "loops" for $\beta < 0$ and the hysteresis "loops" increase in size as β decreases. The extent of the hysteresis region has increased so much that the numerical simulations must be run up to Re = 100 to ensure that the region has been captured correctly for $\beta = -3$; by this point the other bifurcation curves have all already approached their same behaviour as Re increases past Re = 20. The lower wall behaviour shown in Figure 5.4.54 is a more squashed vertically and stretched horizontally version of the previous lower-wall behaviours for Pe > 0 and $\beta \leq 0$.

For the injection flows with $\beta \leq 0$ as shown in Figures 5.4.48–5.4.54, the behaviour for decreasing values of Pe is similar for each value of β. As β decreases the upper wall stresses are increased over that of the $\beta = 0$ values, and the lower wall stresses as decreased in comparison to the $\beta = 0$ values. The upper wall stresses decrease from a maximum at $\text{Re} = 0_-$ in a manner broadly inversely proportional to $-\text{Re}$ as Re decreases. The lower wall stresses increase as Re decreases from 0 with the gradients for each value of β for fixed Pe decreasing slightly when comparing behaviours across Pe values.

The effect of the negative values of β in the viscosity function, corresponding to cooling of the lower channel wall, is that the regions of hysteresis are enlarged as β decreases and Pe increases in the suction cases. Both the wall-stresses at the lower and upper walls changed quantitatively as β decreased from 0, even if they qualitatively remained similar.

5.5 Temporal stability for an isothermal reference case

In order to numerically solve the temporal stability problem we must solve the steady base flow problem and the unsteady perturbation problem in parallel. It is necessary to split the perturbation term into its real and imaginary parts and, once a particular representation of the system has been chosen, a system of 21 first order ordinary differential equations is to be solved in Matlab[1]. The complete system, before rewriting as a system of first order ordinary differential equations, is

$$\left(\mu(\beta g_0) f_0''\right)'' = \mathrm{Re}\left(f_0 f_0''' - f_0' f_0''\right), \tag{5.5.1a}$$

$$g_0'' = \mathrm{Pe} f_0 g_0', \tag{5.5.1b}$$

$$\begin{aligned}\left(\mu(\beta g_0)(F_R'' - \beta f_0'' G_R)\right)'' &= \mathrm{Re}\left(f_0' F_R'' + f_0'' F_R' - f_0 F_R''' - f_0''' F_R\right) \\ &\quad + \mathrm{Re}\left(a F_R'' - b F_I''\right),\end{aligned} \tag{5.5.1c}$$

$$\begin{aligned}\left(\mu(\beta g_0)(F_I'' - \beta f_0'' G_I)\right)'' &= \mathrm{Re}\left(f_0' F_I'' + f_0'' F_I' - f_0 F_I''' - f_0''' F_I\right) \\ &\quad + \mathrm{Re}\left(b F_R'' + a F_I''\right),\end{aligned} \tag{5.5.1d}$$

$$G_R'' = \mathrm{Pe}\left(f_0 G_R' - F_R g_0'\right) + \mathrm{Pe}\left(a G_R - b G_I\right), \tag{5.5.1e}$$

$$G_I'' = \mathrm{Pe}\left(f_0 G_I' - F_I g_0'\right) + \mathrm{Pe}\left(b G_R + a G_I\right), \tag{5.5.1f}$$

$$\begin{aligned}&\text{on } y = +1\text{:} \quad f_0' = 0, \quad f_0 = 1, \quad g_0 = 0, \\ &\qquad F_R' = 0, \quad F_R = 0, \quad G_R = 0, \\ &\qquad F_I' = 0, \quad F_I = 0, \quad G_I = 0,\end{aligned} \tag{5.5.1g}$$

$$\begin{aligned}&\text{on } y = -1\text{:} \quad f_0' = 0, \quad f_0 = 0, \quad g_0 = 1, \\ &\qquad F_R' = 0, \quad F_R = 0, \quad G_R = 0, \\ &\qquad F_I' = 0, \quad F_I = 0, \quad G_I = 0, \\ &\qquad F_R'' = 1, \quad F_I'' = 0,\end{aligned} \tag{5.5.1h}$$

where $F(y) = F_R(y) + iF_I(y)$, $G(y) = G_R(y) + iG_I(y)$, $s = a + ib$ and a normalisation condition is given by $F''(-1) = 1$.

For comparison purposes it is necessary to solve the isothermal problem with no temperature dependent viscosity first. Taking $\beta = \mathrm{Pe} = 0$, μ is now constant having the value 1 and together with zero temperature boundary conditions the problem simplifies

[1]The 21st equation comes from forming the ode $\mathrm{dRe}/\mathrm{d}y = 0$ and adding an appropriate boundary condition to facilitate numerical stepping along the bifurcation curves.

to just the temporal stability problem for f_0,

$$f_0^{(\mathrm{iv})} = \mathrm{Re}\left(f_0 f_0''' - f_0' f_0''\right), \tag{5.5.2a}$$

$$g_0'' = 0, \tag{5.5.2b}$$

$$F_R^{(\mathrm{iv})} = \mathrm{Re}\left(f_0' F_R'' + f_0'' F_R' - f_0 F_R''' - f_0''' F_R\right) + \mathrm{Re}\left(aF_R'' - bF_I''\right), \tag{5.5.2c}$$

$$F_I^{(\mathrm{iv})} = \mathrm{Re}\left(f_0' F_I'' + f_0'' F_I' - f_0 F_I''' - f_0''' F_I\right) + \mathrm{Re}\left(bF_R'' + aF_I''\right), \tag{5.5.2d}$$

$$G_R'' = 0, \tag{5.5.2e}$$

$$G_I'' = 0, \tag{5.5.2f}$$

$$\begin{aligned}
&\text{on } y = +1: \quad f_0' = 0, \quad f_0 = 1, \quad g_0 = 0, \\
&\qquad\qquad F_R' = 0, \quad F_R = 0, \quad G_R = 0, \\
&\qquad\qquad F_I' = 0, \quad F_I = 0, \quad G_I = 0,
\end{aligned} \tag{5.5.2g}$$

$$\begin{aligned}
&\text{on } y = -1: \quad f_0' = 0, \quad f_0 = 0, \quad g_0 = 0, \\
&\qquad\qquad F_R' = 0, \quad F_R = 0, \quad G_R = 0, \\
&\qquad\qquad F_I' = 0, \quad F_I = 0, \quad G_I = 0, \\
&\qquad\qquad F_R'' = 1, \quad F_I'' = 0.
\end{aligned} \tag{5.5.2h}$$

The first three pairs of eigenvalues for the suction and injection cases are shown in Figures 5.5.1 and 5.5.3, and Figure 5.5.2 shows the region of the suction flow eigenvalue diagram that contains the critical points for the stability of the base flow.

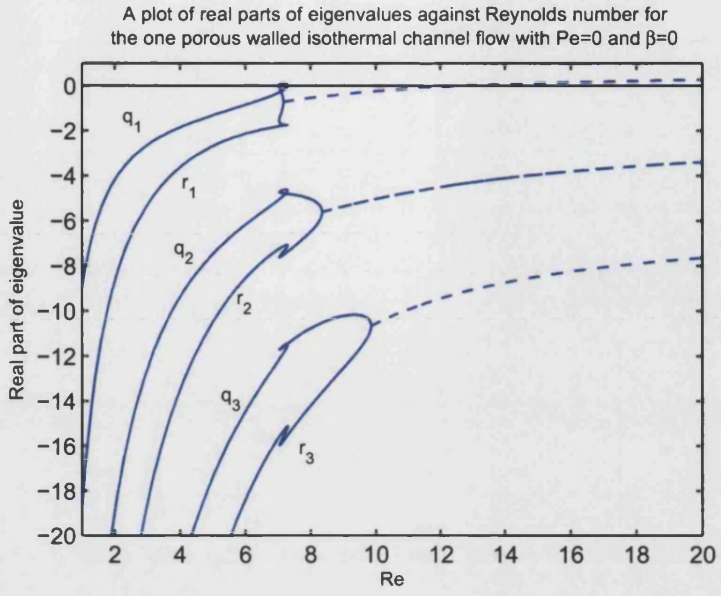

Figure 5.5.1. A plot of the first three pairs of eigenvalues against Reynolds number for the reference case of no temperature dependence of the viscosity and zero boundary conditions for the temperature in the case of one porous walled suction flow.

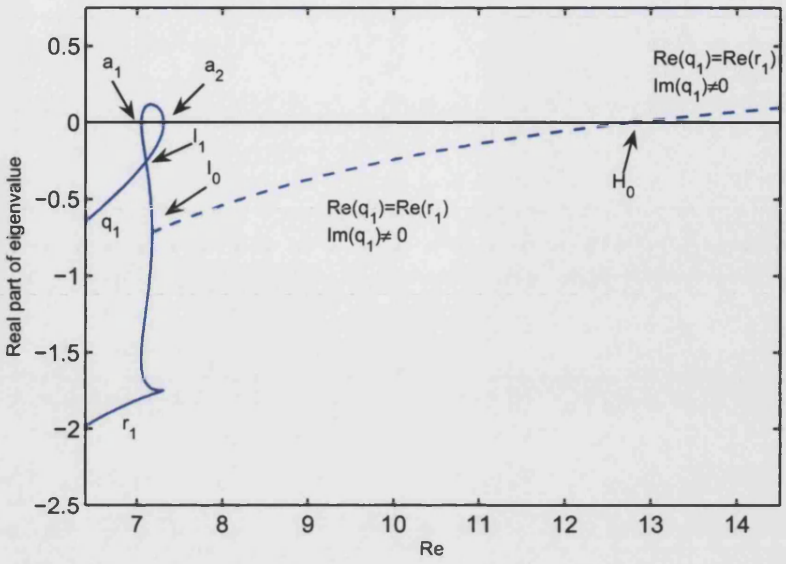

Figure 5.5.2. A plot of the first pair of eigenvalues against Reynolds number for the reference case in Figure 5.5.1 showing labelled points I_0, I_1, a_1, a_2 and H_0 .

The eigenvalue branches q_1 and r_1 in the suction case, as shown in Figure 5.5.1 and in more detail in Figure 5.5.2, are the determining factors for the temporal stability of the base flow $f_0(y)$. For values of the Reynolds number up to the point a_2 at Re = 7.308 (3d.p.) the flow is steady and so is temporally stable as the dominant eigenvalue is real and negative (depicted by a solid line), then the real part of q_1 first becomes positive at this point. Following the q_1 branch around the loop until the point a_1 at Re = 7.051 (3d.p.) the real part of q_1 then becomes negative again, and this loop describes a region of hysteresis in the interval Re $\in (7.051, 7.308)$ (3d.p.) which can be seen on the bifurcation diagram of $-f_0''(1)$ against Re, Figure 5.4.41 ($\beta = 0$ curve). In this region there are three steady solutions, the outer two are temporally stable and the central one is temporally unstable. The branches q_1 and r_1 merge at I_0, at Re = 7.179 (3d.p.), where their real parts coincide, and from this point the complex-conjugate solutions have a non-zero imaginary part (depicted by a dashed line). The corresponding points upon the q_2, r_2 and q_3, r_3 branches are at Re = 8.354 and Re = 9.862 (3d.p.) respectively. When the coalesced q_1, r_1 branches reach H_0 at Re = 12.760 (3d.p.) their real part passes through zero and becomes positive, and this point denotes the loss of temporal stability of the base flow.

In the case of injection, the Reynolds number is negative and so is the time variable, due to the dimensional scalings of time and fluid speed having the same sign. Thus, in the case of injection, if the real part of the eigenvalue is positive then the eigenfunction perturbation to the flow decays and the basic flow is temporally stable. This is what is observed in the simulations, as shown in Figure 5.5.3.

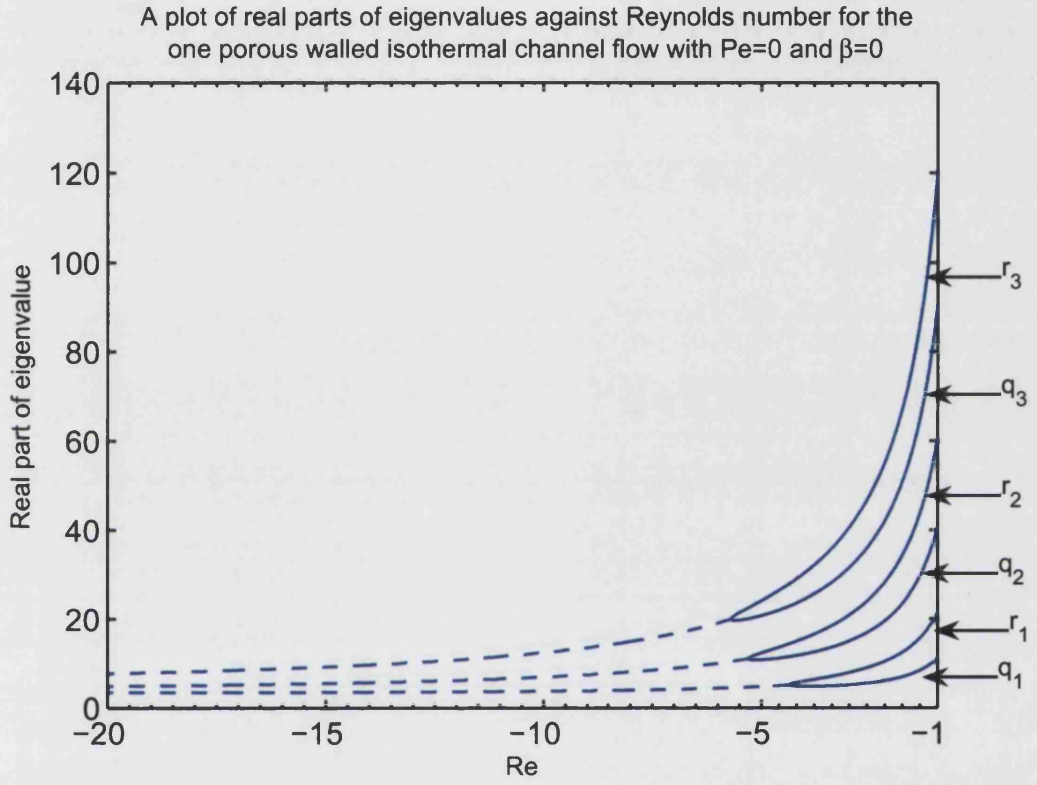

Figure 5.5.3. A plot of the first three pairs of eigenvalues against Reynolds number for the reference case of no temperature dependence of the viscosity and zero boundary conditions for the case of one porous walled injection flow.

5.6 Numerical results for nonisothermal temporal stability calculations

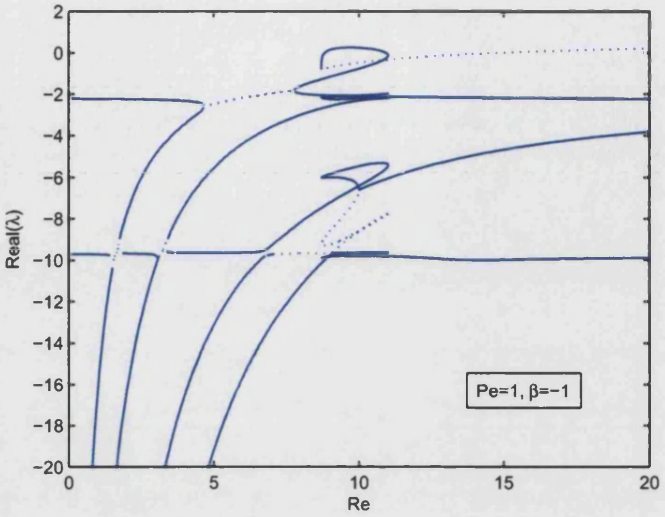

Figure 5.6.1. A plot of eigenvalues against Reynolds number for the nonisothermal Pe $= 1$, $\beta = -1$ suction case in the one porous walled channel system.

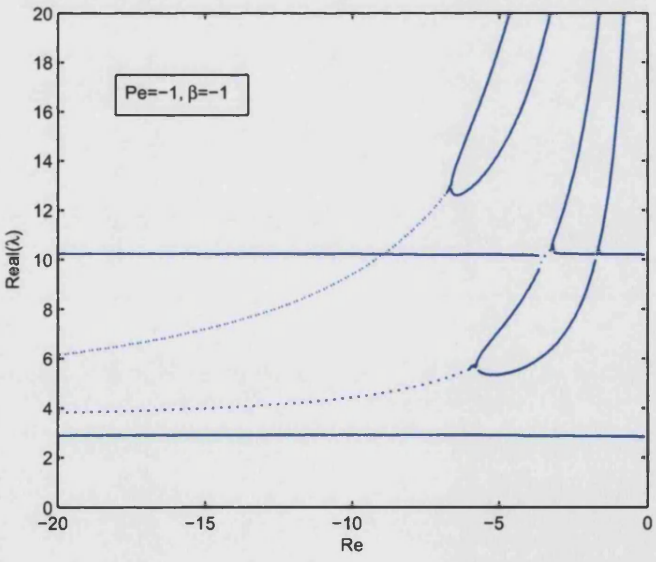

Figure 5.6.2. A plot of eigenvalues against Reynolds number for the nonisothermal Pe $= -1$, $\beta = -1$ injection case for the one porous walled channel system.

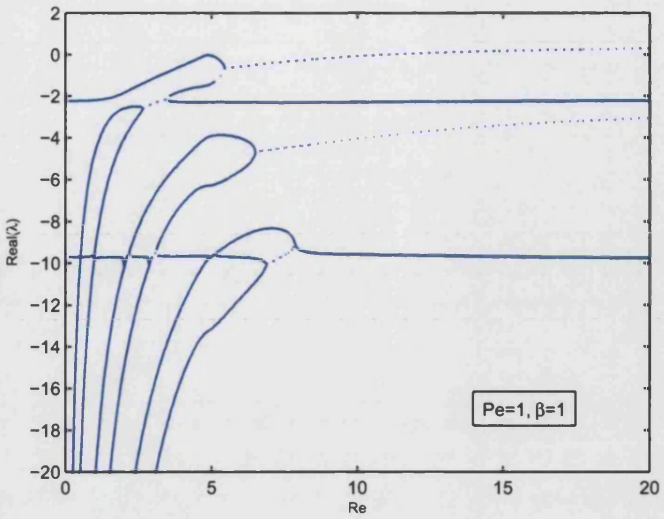

Figure 5.6.3. A plot of eigenvalues against the Reynolds number for the nonisothermal Pe $= 1$, $\beta = 1$ suction case for the one porous walled channel system.

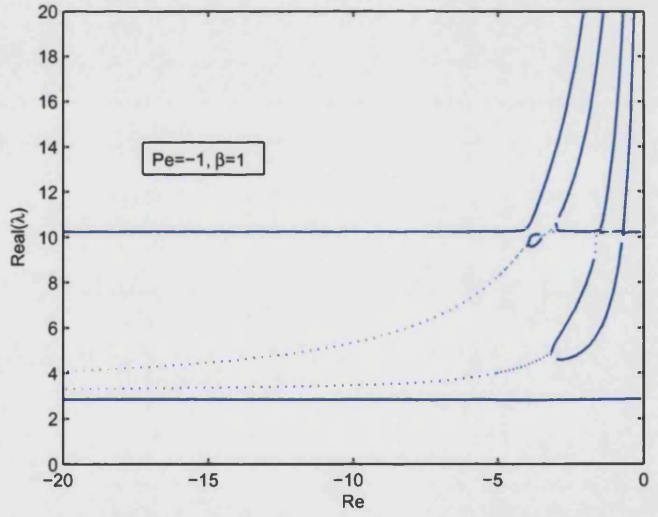

Figure 5.6.4. A plot of eigenvalues against the Reynolds number for the nonisothermal Pe $= -1$, $\beta = 1$ injection case for the one porous walled channel system.

5.6.1 Discussion of the numerical results for nonisothermal temporal stability calculations

Comparing the eigenvalues of the nonisothermal simulations for Pe = 1, $\beta = \pm 1$ (suction) with the corresponding isothermal reference case of Pe = 0, $\beta = 0$ we can immediately see that an extra set of eigenvalues is introduced in the nonisothermal cases. In the $\beta = -1$ case (cooled channel or viscosity increasing with temperature increase) shown in Figure 5.6.1 the looped region of the eigenvalue behaviour is retained, but the shape is more elongated and this is reflected in the greater range of hysteresis: the points a_2 and a_1 now occur at Re = 10.961 (3d.p.) and Re = 8.823 respectively, as opposed to Re = 7.308 and Re = 7.051 in the reference case. There is a region of coalesced eigenvalues between the upper "initially s_1" branch and the "initially q_1" branch prior to the hysteresis region. It also appear that the branch corresponding to r_1 in the reference case does not meet the q_1 or r_1 branches in the range of Reynolds numbers where calculations have been performed. The point at which the eigenvalues on the two uppermost branches then coalesce, I_0, has not been successfully located using both branches in the nonisothermal case, but the numerical evidence suggests that it is located at Re = 8.717 as opposed to Re = 7.719 in the reference case; in both cases this point is located at a higher Reynolds number than the lower end of the hysteresis region. The location of the final critical point H_0, that of the Hopf bifurcation, where a complex conjugate pair of eigenvalues cross the real axis, also shifts to Re = 14.467 in the nonisothermal case from Re = 12.760, and so the region of temporally stable suction solutions is increased to Re $\in (0, 14.467)$

In the $\beta = 1$ case (heated channel or viscosity decreasing with temperature increase) shown in Figure 5.6.3 the looped behaviour of the eigenvalues for suction values of the Reynolds number has been lost. Indeed for $\beta = 1$ there is no region of hysteresis upon the main bifurcation diagram (Figure 5.4.41). The coalescing eigenvalues are no longer the pair s_1 and q_1 but q_1 and r_1 and now the s_1 branch meets the q_1 branch at I_0 where Re = 5.450 as opposed to Re = 7.179 in the reference case. The Hopf bifurcation H_0 now occurs at Re = 11.036 instead of Re = 12.760 in the reference case, and so the region of temporally stable suction solutions has been reduced to Re $\in (0, 11.036)$.

In the injection cases for $\beta = \pm 1$ the qualitative results are similar in that in both cases flows are still temporally stable, with the smallest real part of an eigenvalue being the s_1 eigenvalue in the range of Reynolds numbers calculated. All that differs in the two cases is the relative positions of the crossings of the horizontal s branches with the q and r branches that correspond to those in the isothermal reference case.

Chapter 6

Isothermal power law fluid problem - two porous walled channel

For the two porous walled problem with equal rates of suction or injection through the walls, the parameter $E = 0$, and the base problem under consideration is

$$r\mathrm{Re}\left(f'f'' - ff'''\right) = -\left(nf^{(\mathrm{iv})}\left|f''\right|^{n-1} + n(n-1)f''\left(f'''\right)^2\left|f''\right|^{n-3}\right), \tag{6.0.1}$$

$$\text{on } y = +1: \quad f' = 0, \quad f = 1, \tag{6.0.2}$$

$$\text{on } y = -1: \quad f' = 0, \quad f = -1, \tag{6.0.3}$$

6.1 Numerical results for Type I base flows

6.1.1 Type I solution bifurcation results

In this section we produce a bifurcation diagram for the various power law flows of Type I and a selection of associated flow profiles.

The bifurcation diagram Figure 6.1.1 shows that, as found in the $E = 1$, there is a change of behaviour for the flows of shear-thinning and and shear-thickening fluids in the case of suction. The first observation is that there is a very large range of values for $\log_{10}(-f''(1))$ at the upper wall, ranging from 10^{-2}–10^{-1} for the shear-thickening fluids up to 10^4 for the shear-thinning fluids over the range of Reynolds numbers computed. The injection flows all show similar values for $\log_{10}(-f''(1))$, where the shear-thinning fluids have a higher value of wall-stress as $\mathrm{Re} \to 0$ than the shear-thickening fluids. There appears to be a critical Reynolds number at which the shear-thickening fluids

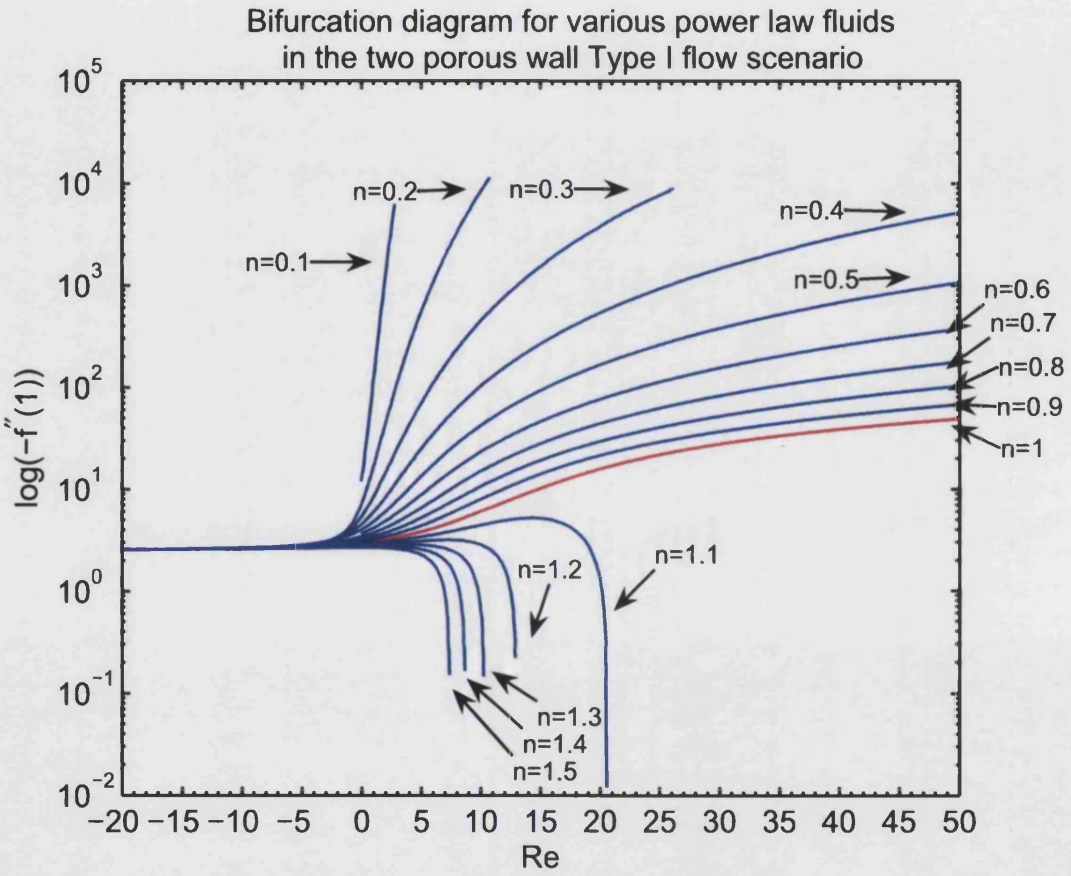

Figure 6.1.1. Solution branches for various values of n for the power law fluid flow in a two-porous-walled channel for the Type I base flow. The value of $\delta = 5e-2$ was chosen for these computations.

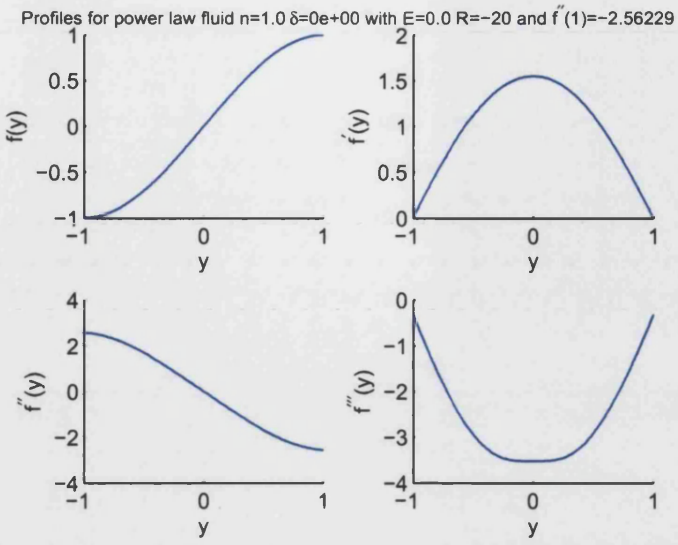

Figure 6.1.2. Typical profile behaviour for all two porous walled injection solution branches with $0 < n < 2$. Here $n = 1$.

have zero wall-stress, ranging from Re $\approx$ 21 for $n = 1.1$ to Re $\approx$ 7 for $n = 1.5$, suggesting that this critical Reynolds number decreases with increasing n. Numerical difficulties have precluded the reliable calculation of $-f''(1)$ for values of $n > 1.5$ or $n < 0.2$ for this problem.

Figures 6.1.3–6.1.8 show the suction flow profiles for power law fluids in a two-porous walled channel with equal suction speeds through each wall. The $n = 1$ cases are shown for comparison: under large injection the function $f(y)$ has a sinusoidal profile and $f'(y)$ has a parabolic profile, proportional to the horizontal flow component. For the large suction flow with $n = 1$, $f(y)$ is almost linear and only deviates from linearity in thin boundary layers adjacent to the walls in order to satisfy the boundary conditions upon the flow. These boundary layers are visible on the $f'(y)$ profile and their influence can be seen on the behaviour of the higher derivatives near the walls. As the value of n is reduced and the fluid becomes shear-thinning, the constant feature across the three representative figures (Figures 6.1.5, 6.1.4 and 6.1.3) is that, although the qualitative features are the same, the gradients of the higher derivatives become much steeper as n decreases. Figure 6.1.5 with $n = 0.8$ has $f''(\pm 1) = \mathcal{O}\left(10^2\right)$ and $f'''(\pm 1) = \mathcal{O}\left(10^4\right)$; when $n = 0.5$ Figure 6.1.4 shows that $f''(\pm 1) = \mathcal{O}\left(10^3\right)$ and $f'''(\pm 1) = \mathcal{O}\left(10^6\right)$. For $n = 0.2$ the results shown in Figure 6.1.3 are for the greatest value of Re that converged, Re = 10.2, and for this value the corresponding derivatives are $f''(\pm 1) = \mathcal{O}\left(10^4\right)$ and

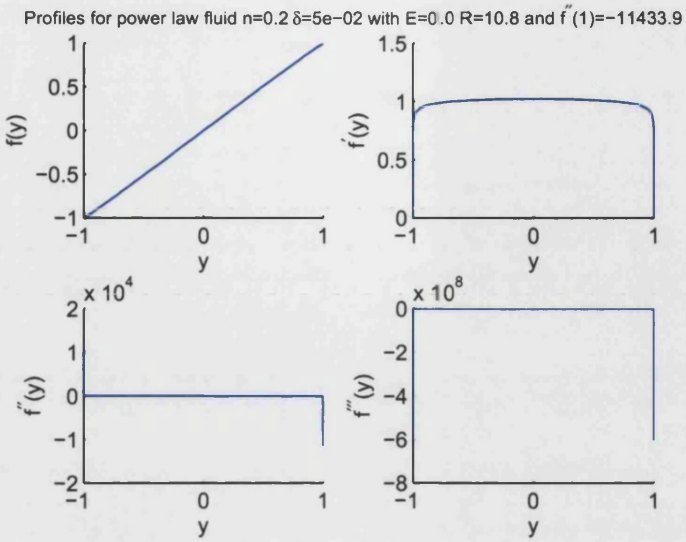

Figure 6.1.3. Profiles for two porous walled suction solution with $n = 0.2$, $\delta = 5e - 2$. Note the reduced value of the Reynolds number, Re = 10.8, at which point the computations failed to converge.

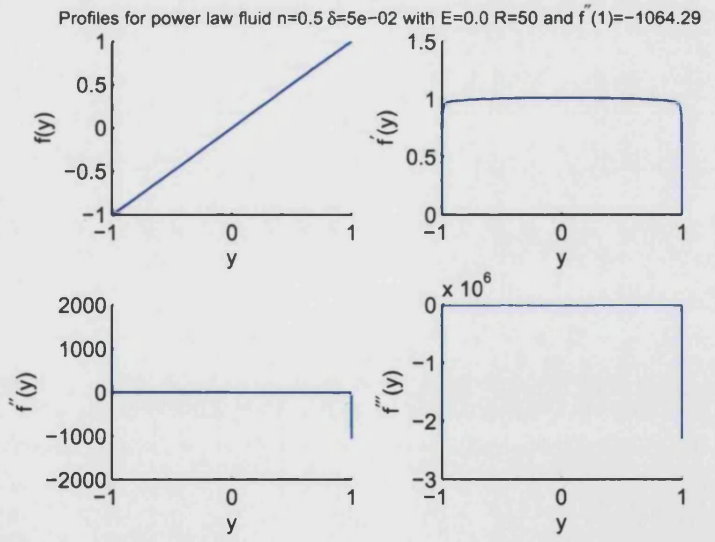

Figure 6.1.4. Profiles for two porous walled suction solution with $n = 0.5$, $\delta = 5e - 2$.

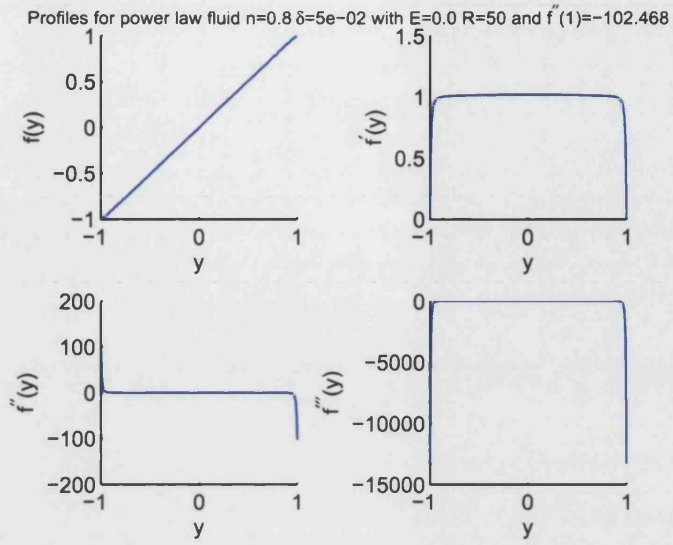

Figure 6.1.5. Profiles for two porous walled suction solution with $n = 0.8$, $\delta = 5e - 2$.

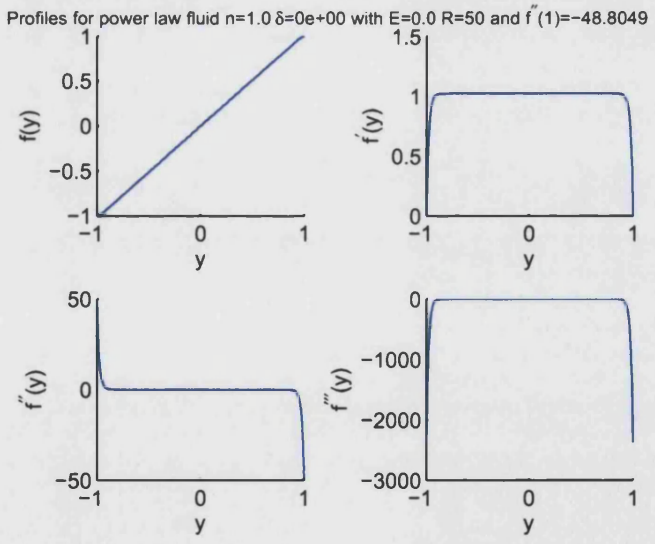

Figure 6.1.6. Profiles for two porous walled suction solution with $n = 1$.

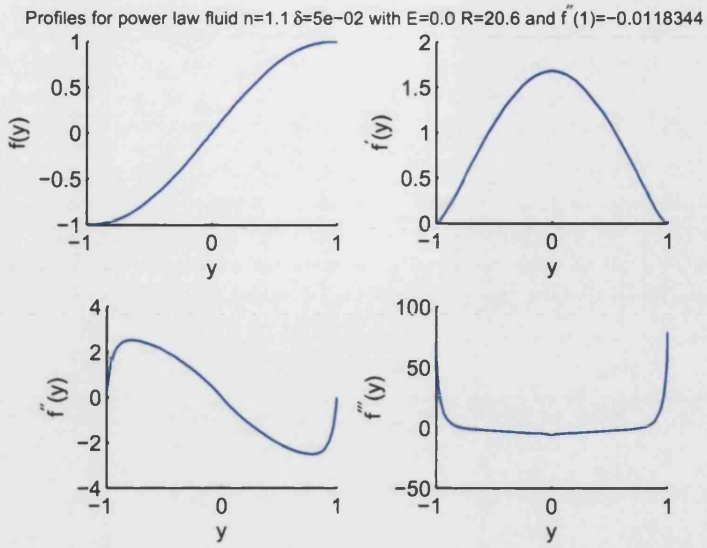

Figure 6.1.7. Profiles for the two porous walled suction solution with $n = 1.1$, $\delta = 5e{-}2$. There is now a maximum value at which the value of $-f''(1)$ remains positive, at approximately $\mathrm{Re} = 20.8$.

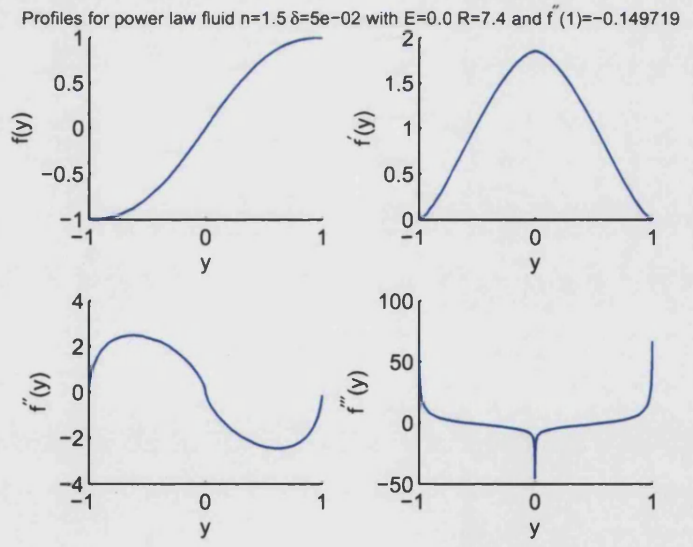

Figure 6.1.8. Profiles for the two porous walled suction solution with $n = 1.5$, $\delta = 5e{-}2$. There is now a maximum value at which the value of $-f''(1)$ remains positive, at approximately $\mathrm{Re} = 7.4$.

$f'''(\pm 1) = \mathcal{O}(10^8)$.

For the shear-thickening suction flows the profiles shown in Figures 6.1.7 and 6.1.8 are for the highest values of Re for which $f''(1) < 0$ holds according to the numerical simulations performed. For $n = 1.1$, the critical Reynolds number is $\mathrm{Re} = 20.8$ and, as shown in Figure 6.1.7, the function $f(y)$ has a sinusoidal profile, $f'(y)$ has a profile that is almost parabolic at the channel centre and flatter than parabolic at the walls and $f''(y)$ is oscillatory with steep gradients at the walls. Looking at the behaviour when $n = 1.5$ in Figure 6.1.8 where the critical Reynolds number has been reduced to $\mathrm{Re} = 7.4$, the main features as identified in Figure 6.1.7 for $n = 1.1$ remain and are accentuated; the $f'(y)$ profile now appears more pointed at the channel centre and even flatter at the walls, the $f''(y)$ profile has a correspondingly steeper gradient at the channel centre (thought not at the walls where it appears flatter than in the $n = 1.1$ case, probably due to the reduced value of the Reynolds number) and the profile of $f'''(y)$ now has a sharp drop at the centre of the channel.

Chapter 7

Conclusions and further work

7.1 Conclusions

This thesis has been concerned with the flow of fluid through a channel with porous walls. In particular it has aimed to extend the basic Newtonian flow problem considered by previous researchers. The two extensions considered are that of introducing a temperature-dependent viscosity and a more general fluid of power-law form and the interest has been in the effects of changing the viscosity. The main thrust of work has been on the one-walled problem as it has received less attention in the literature. The flow problems have been set up for the full two-porous walled problem and then specialisation to the one-porous walled problem has taken place where necessary. For the case of the temperature-dependent viscosity fluid the aim has been to extend the one-porous walled Newtonian fluid work as the two-porous walled case has been considered by Ferro and Gnavi [FG02]. The power-law fluid work has focussed on the one-walled case in the main and initial numerical results have been obtained in the two-walled case.

Summary of power law viscosity fluid results:

Small Re **asymptotics** A small Reynolds number perturbation expansion for the power-law fluid flowing in the two-porous walled geometry has been produced. It encompasses the entire range of the problem selection parameter $E \in [0, 1]$ and can be used as a basis for producing initial conditions for a numerical simulation of the flow over a larger range of Re and where the power law exponent lies in the range $0 \leq n \leq 2$.

Numerical simulations for base flows Numerical simulations of the $E = 0$ two-porous walled channel power-law fluid flow have been performed and

have shown that there is a critical Reynolds number at which the shear-thickening subset of power-law fluids experience a loss of shear-stress at the upper wall under the influence of suction at both walls. Numerical simulations in the $E = 1$ one-porous walled suction case also show this phenomenon.

Large $-\mathrm{Re} \gg 1$ injection asymptotics for $E = 1$ An asymptotic expansion for the one-porous walled large injection flow of power-law fluid has been produced and is analogous to the Newtonian fluid equivalent expression. The free boundary problem determining the width of the nonzero region of f'' within the boundary-layer at the lower wall in this situation has been posed and has been reported to occur in a different geometry, that of the flow of a power-law fluid over a flat plate as investigated by Denier and Dabrowski in [DD04].

Summary of temperature-dependent viscosity fluid results:

Numerical simulations for base flows Numerical simulations of the one-porous walled temperature-dependent-viscosity fluid flows have been carried out for a range of Reynolds numbers corresponding to suction and injection flows, with varying values for the Péclet number and the sensitivity parameter β. In particular it was found that the bifurcation diagrams (Figures 5.4.39-5.4.54) displayed differing behaviours of the wall stress depending upon the values of Pe and β; hysteresis loops occurred for increasingly negative values of β corresponding to cooling the lower wall as compared to the upper wall (or a fluid with viscosity that increases with increasing temperature) whereas the regions of hysteresis were eliminated as the value of $\beta > 0$ increased, corresponding to the heating of the lower wall of the channel relative to the upper wall (or a fluid with viscosity that decreases with increasing temperature).

Numerical simulations for temporal stability Numerical simulations of the temporal stability of the one-porous walled temperature-dependent viscosity were performed for $|\mathrm{Pe}| = 1$, $|\beta| = 1$ and compared to the isothermal flow of a Newtonian fluid. It is found that the range of temporally stable suction solutions is $\mathrm{Re} \in (0, 12.760)$ for $\beta = 0$, increasing to $\mathrm{Re} \in (0, 14.467)$ for $\beta = 1$ and decreasing to $\mathrm{Re} = (0, 11.036)$ for the $\beta = -1$ case.

Asymptotic expressions for $\mathrm{Re} < 0$ Asymptotic descriptions of the injection $\mathrm{Re} < 0$ behaviour for the temperature-dependent viscosity fluid have been produced. These have been derived from the starting point of the similarity

solution derived for the general temperature dependent problem, and the limits of various nondimensional parameters have subsequently been taken. Five different regimes have been considered and cover the changes in behaviour starting from an order one Reynolds number injection flow with a large Péclet number, where the thermal boundary layer is the dominant feature of the flow, through to where the Reynolds and Péclet numbers are comparable, where the thermal and viscous layers are of comparable sizes and which subdivides into three cases according to the relative sizes of Re and Pe, and ending with a large Reynolds number and an order one Péclet number, where the main feature of the flow is the viscous boundary layer. In all these cases the thermal sensitivity parameter $\beta = \mathcal{O}(1)$ and the exponential model has been used for the viscosity dependence. In the limit of $\beta \to \infty$ the analysis in Appendix B shows how the thermal boundary layer will subdivide further according to the particular viscosity model in question. Similar structures have been reported to occur in the related problem of steady laminar flow in a channel driven by a pressure gradient and where the viscosity of the fluid is temperature dependent, where the walls of the channel are suddenly heated after a fixed point along its length [OO77], [Ock79]. The analysis in Appendix B has been derived starting from the partial differential equation system governing the fluid and temperature behaviours and the limits of large $-\mathrm{Re}$ and large β have been taken of that system, in contrast to starting with similarity solution reductions of the system and then considering asymptotic limits.

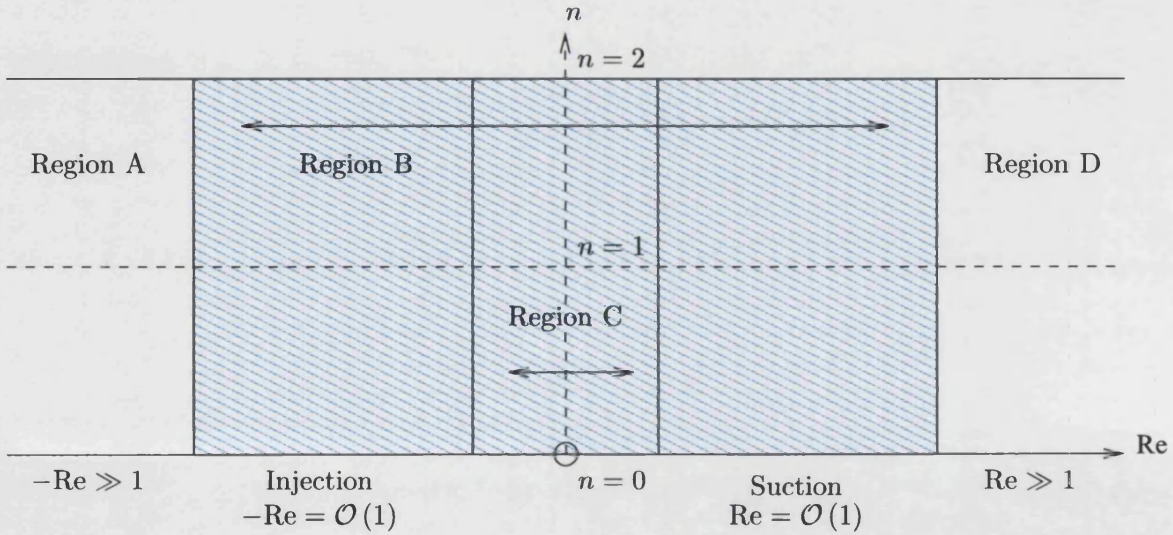

Figure 7.1.1. A graphical summary of the power law fluid results obtained in this work. Region A corresponds to the large injection asymptotic analysis for the one porous walled channel ($E = 1$) in section 4.1.3. The shaded region, Region B, corresponds to where numerical simulations have been run for both the one ($E = 1$) and two ($E = 0$) porous walled geometries in sections 4.1 and 6.1. Region C corresponds to the small Re solution developed in section 3.2.1. Region D has yet to be considered and thus is an area for future work.

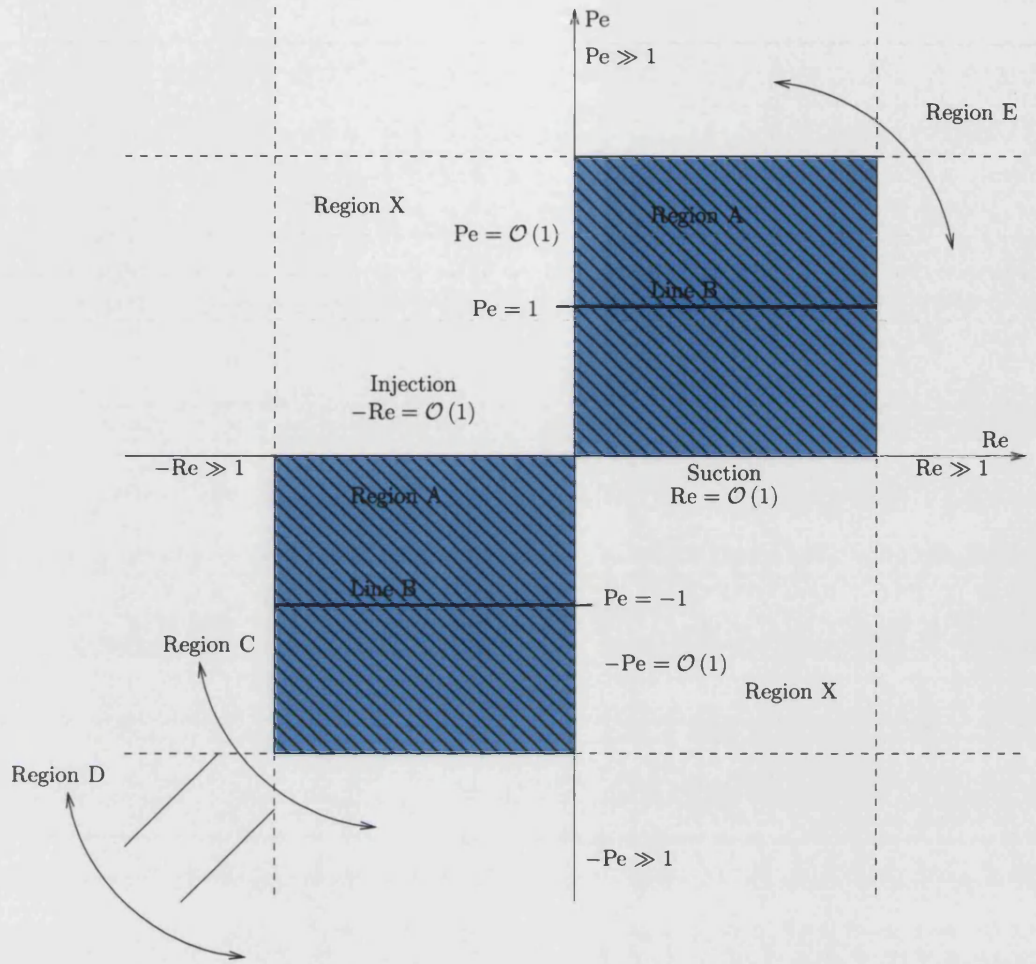

Figure 7.1.2. A graphical summary of the temperature dependent viscosity fluid results obtained in this work for the one porous walled channel. Region A corresponds to the numerical simulations that have been run for $\beta = \mathcal{O}(1)$ under the exponential viscosity model described in sections 5.4-5.4.4. The line B corresponds to the numerical linear temporal stability simulations performed on a subset of the simulations in Region A, and are described in sections 5.6.1-5.6.1. Region C corresponds to the asymptotic analysis performed for the $\mathrm{Re} < 0$, $\mathrm{Pe} < 0$ cases with $\beta = \mathcal{O}(1)$ in section 5.2. Region D corresponds to the large $\beta > 0$ limit of the solutions in Region C and parts of these are discussed in Appendix B for the algebraic and exponential viscosity models. Regions marked X are not valid in the problem under consideration as the nondimensional groups Re and Pe must have the same sign. Region E has yet to be considered and is an area for further work.

7.2 Further work

Further work that could be considered would be to extend the range of temporal stability simulations that have been performed for the temperature-dependent viscosity fluid model, as only an initial set of computations were able to be performed, and to then consider the spatial stability of the flow. The same stability questions could then be asked of the power-law fluid model. In the case of the two-porous walled channel flows, the existence of multiple solutions has been confirmed numerically for the temperature-dependent viscosity model by [FG02] and their stability examined, but the power-law fluid case does not appear to have been investigated. The asymptotic analysis of the large $\mathrm{Re} > 0$ suction flows in both the power-law and temperature-dependent viscosity cases for both the one-porous and two-porous walled channel flows is an area for further work.

The unsteady version of the governing system could also be considered. In this case further numerical experiments would be required to see whether the work presented here has captured the possible steady solutions correctly, and whether time-dependent solutions to the full partial differential equations will tend to other solutions, such as limit cycles. Such numerical simulations would be more challenging, as even in the one porous walled Newtonian case [Cox91b] and [KC01] have found that the periodic solutions for the governing partial differential equation for larger suction Reynolds numbers ($\mathrm{Re} \geq 100$) are very difficult to compute accurately.

Another direction of work could be to increase the thickness of the walls so that they are a porous layer through which flow may occur in addition to flow in the clear portion of the channel. Factors of relative thicknesses of the clear and porous layers and the porosity of the porous layer will now possibly influence the resulting flows; in the Newtonian case work has been done by Deng et.al. [DM05] and was motivated by a part of the process involved in paper-making whereby water is drained from a suspension of fibres settling over a porous layer.

Different fluids or fluid-like materials could also be considered by amending the constitutive equation relating the stresses and shear-rates within the fluid elements, hence amending the viscosity model. The next simplest modifications to the problem would be to consider the Bingham body model and subsequently the Herschel-Bulkley body model. An example of a Bingham material is toothpaste or tomato ketchup, and an example of a Herschel-Bulkley material is minced fish paste [Ste96, 21]. In the Bingham body there is no flow of the fluid if the shear stress is below a critical value called the yield stress in shear T_y; if it exceeds the yield stress then the fluid flows and the deviatoric stress and shear-rate are proportional to each other, the proportionality

function being the viscosity function. In one dimension, the Bingham model equations are

$$\dot{\gamma} = 0, \qquad \text{if } |T| \leq T_y, \tag{7.2.1}$$

$$T - T_y = \mu_p \dot{\gamma}, \qquad \text{if } T > T_y, \tag{7.2.2}$$

where the Bingham model constants are T_y, the yield stress in shear, and μ_p, the plastic viscosity. If the shear-rate $\dot{\gamma} < 0$ then the odd extension of $T - T_y$ is assumed to hold. The one-dimensional Herschel-Bulkley model is given by

$$\dot{\gamma} = 0, \qquad \text{if } |T| \leq T_y, \tag{7.2.3}$$

$$T - T_y = \mu_p |\dot{\gamma}|^{n-1} \dot{\gamma}, \qquad \text{if } T > T_y, \tag{7.2.4}$$

and again if the shear-rate $\dot{\gamma}$ is negative then the odd extension of $T - T_y$ holds. In the three dimensional case, only considering isotropic incompressible materials (and so the Young's modulus of the material is 0.5 in any elastic region of the material) a few preliminary definitions must first be made. If we define the equivalent positive shear rate $\dot{\gamma}_p$ (adding the subscript $\cdot_p$ to distinguish it from the shear rate previously discussed) as

$$\dot{\gamma}_p = 2\sqrt{-\Pi_d} = \sqrt{2 d_{ij} d_{ij}}, \tag{7.2.5}$$

(and so dependence upon $\dot{\gamma}_p$ can be replaced by dependence upon Π_d and vice versa), and define the Von Mises' criterion by which yield is judged to have occurred,

$$\Pi_T = T_y = \frac{1}{3} Y^2 \tag{7.2.6}$$

$$= \frac{1}{2} T_{ij} T_{ij} = \frac{1}{3} Y^2 \quad \text{in Cartesian coordinates,} \tag{7.2.7}$$

where T_y is the yield stress in shear and Y is the yield stress measured in tension, then Herschel-Bulkley material equations can be written as

$$d_{ij} = 0, \qquad \text{if } \Pi_T \leq {T_y}^2, \tag{7.2.8}$$

$$T_{ij} = 2\left(\frac{T_y}{\dot{\gamma}_p} + \mu_p |\dot{\gamma}_p|^{n-1}\right) d_{ij}, \qquad \text{if } T > T_y. \tag{7.2.9}$$

If $n = 1$ then the Bingham model is recovered, if $T_y = 0$ then the power-law fluid model is recovered and if $n = 1$ and $T_y = 0$ then the Newtonian viscous fluid model is recovered.

A similar problem to the one presented here, that of fluid flow within a channel

with accelerating walls, can be considered by simply changing the wall boundary conditions, see [BA81] and [Cox91a] (Cox considers both the two-accelerating walls and one stationary, one accelerating wall problem). The set of solutions for the accelerating or decelerating walls problem is larger than that of the porous walled channel problem [BA81],[Cox91a]. In the purely accelerating walls problem the change of viscosity model to that of a power-law or the inclusion of temperature-dependent viscosity could also present an increased number of solutions as compared to the Newtonian fluid case. There is also an exact solution of the Navier-Stokes system for the hybrid flow of suction and accelerating walls [ZB03] and this is used to numerically investigate the separate problems in order to find further branches of solutions and their stabilities.

Reintroducing the effects of viscous dissipation of heat would also be an interesting problem as it could introduce another mechanism by which the flow could be affected. The viscous dissipation of heat into the fluid would alter the viscosity locally and then could cause unwanted changes in the characteristics of the fluid if they are not controlled, e.g. the physical properties of molten plastics changing under cooling when considered in an injection moulding process.

The related geometry of pipe flow could also be considered for the non-Newtonian fluids and compared to the known Newtonian results. Extensions to the three dimensional porous walled channel and two dimensional pipe or annular flows with porous or accelerating walls could also be considered. Newtonian work has been done by [TBZD91] for the three dimensional channel geometry and the pipe flow problem have been considered by [SW78],[BA81],[DB84] and initially by Berman [Ber58] in the case of an annulus.

Appendix A

Boundary conditions for the Newtonian fluid large injection one porous walled channel problem

In this section we discuss the selection of appropriate boundary conditions for the large Re injection Newtonian one-walled flow problem, which is a special case of that described in section §4.1.3.

The problem of appropriate boundary conditions is encountered in this situation when we consider the flow problem in the boundary layer region $y = \mathcal{O}\left((-\mathrm{Re})^{-1/2}\right)$,

$$\begin{aligned} &F'F'' - FF''' = F^{(\mathrm{iv})}, \qquad (\dagger)\\ &\text{on } Y = 0: \quad F = F' = 0,\\ &\text{as } Y \to \infty: \quad F(Y) \sim \frac{\pi}{4} Y. \end{aligned}$$

It is important to ensure that the correct number of boundary conditions are imposed; in this case we would expect four conditions as this is a fourth order ordinary differential equation. We have to consider how many boundary conditions are actually being applied by the matching condition, as well as how many are imposed at the lower wall boundary.

The lower wall boundary appears to impose two conditions out of a possible four. If we expand $F(Y)$ in a truncated Taylor expansion,

$$F(Y) = \frac{1}{2}AY^2 + \frac{1}{6}BY^3 + \hat{\delta}\hat{F} = F_o + \hat{\delta}\hat{F}, \quad \text{where } \hat{\delta} \ll 1,$$

and substitute this into the governing boundary layer equation, then retaining the $\mathcal{O}\left(\hat{\delta}\right)$ terms we obtain the ordinary differential equation

$$\hat{F}^{(\mathrm{iv})} + \frac{1}{2}AY^2\hat{F}''' - AY\hat{F}'' - A\hat{F}' + B\hat{F} = 0.$$

As this is a fourth order linear ordinary differential equation, we expect there to be four linearly independent solutions, which are eigenmodes. If we now write

$$\hat{F} = 1 + c_1Y + c_2Y^2 + c_3Y^3 + c_4Y^4, \quad c_i \in \mathbb{R}$$

as one possible eigenmode, upon substitution into the $\mathcal{O}\left(\hat{\delta}\right)$ equation we find the following relation between the coefficients at leading order,

$$4!c_4 - Ac_1 + B = 0.$$

If we take

$$\hat{F} = Y + c_2Y^2 + c_3Y^3 + c_4Y^4$$

we find that

$$4!c_4 - A = 0, \text{ as } Y \ll 1.$$

However, taking $\hat{F} \sim Y^2$ or $\hat{F} \sim Y^3$ we find that $0 = 0$ to lowest order, and so no conditions have been imposed upon the coefficients in those cases. Thus in summary we have that there are four potential eigenmodes

$$\hat{F} \sim 1, \quad \hat{F} \sim Y, \quad \hat{F} \sim Y^2, \quad \hat{F} \sim Y^3.$$

The boundary conditions $F_o(0) = 0$, $F_o'(0) = 0$ eliminate the eigenmodes $\hat{F} \sim 1$, $\hat{F} \sim Y$ and so only the third and fourth eigenmodes remain. There are now two degrees of freedom remaining as long as A and B are not specified; exciting the third mode is the same as making small changes to the value of A, and a similar statement holds for the fourth mode and the value of B.

We can now analyse the far field behaviour to see how many boundary conditions are being imposed by the matching condition. If we now substitute

$$F(Y) \sim F_o(Y) + \hat{\delta}\hat{F}(Y)$$

with $F_o(Y) = \pi Y/4$, into the governing equation (†) and again consider the $\mathcal{O}\left(\hat{\delta}\right)$

terms, we obtain the ordinary differential equation

$$\frac{\pi}{4}\hat{F}'' - \frac{\pi}{4}Y\hat{F}''' = \hat{F}'''' \quad \text{as } Y \to \infty.$$

If we now let $\hat{F} \sim Y^q$ then we have that

$$\frac{\pi}{4}q(q-1)Y^{q-2} - \frac{\pi}{4}q(q-1)(q-2)Y^{q-2} = q(q-1)(q-2)(q-3)Y^{q-4}$$

as $Y \to \infty$. We can now see that there are three possible algebraic behaviours, given by $q = 0, 1, 3$, obtained by considering the coefficients of the three terms. However, we still need to find the one remaining behaviour as we are still considering a fourth order linear ordinary differential equation.

As we are seeking a solution to the boundary layer problem that should be matched into the behaviour in the outer region, we should consider an exponentially decaying eigenmode. Taking an eigenmode of the form

$$\hat{F} \sim Y^q \exp\left(-CY^p\right), \quad p > 0,$$

if we differentiate with respect to Y we get

$$\begin{aligned}\hat{F}' &= qY^{q-1}\exp\left(-CY^p\right) - CpY^{q+p-1}\exp\left(-CY^p\right) \\ &\sim -CpY^{q+p-1}\exp\left(-CY^p\right), \quad \text{as } Y \gg 1,\end{aligned}$$

and so substituting this into the differential equation gives, to leading order,

$$\frac{\pi}{4}(-Cp)^2Y^{q+2(p-1)} - \frac{\pi}{4}(-Cp)^3Y^{1+q+3(p-1)} = (-Cp)^4Y^{q+4(p-1)}.$$

The only balance is between the second and third terms, giving $p = 2$, $C = \pi/8$, and leaving q arbitrary to this order. If we then take the next most significant terms obtained by substituting this behaviour into the governing equation, we find that $q = -4$. The fourth eigenmode has now been found to be

$$\hat{F} \sim Y^{-4}\exp\left(-\frac{\pi}{8}Y^2\right).$$

The four possible eigenmodes are

$$\hat{F} \sim Y^3, \quad \hat{F} \sim Y, \quad \hat{F} \sim 1, \quad \hat{F} \sim Y^{-4}\exp\left(-\frac{\pi}{8}Y^2\right).$$

The first mode (cubic) is eliminated as the far field behaviour forces it to have a

zero coefficient. The second mode (linear) is eliminated as the unperturbed far field behaviour fixes its coefficient; changing the value of $\hat{F} \sim AY$ where $A \in \mathbb{R}$ corresponds to changing the prescribed coefficient in the linear far field behaviour, which is not permitted. Thus we have two remaining candidates. The third mode is permissible and corresponds to a constant that is able to be determined by a numerical solution of the boundary layer problem. The fourth mode is exponentially small and decays into the outer region. We have shown that the linear far field behaviour imposes two boundary conditions and so in total all four boundary conditions have been specified and so we conclude that this problem has been well specified.

Appendix B

Nonisothermal temperature dependent viscosity problem - large $-\mathrm{Pe}$ asymptotics for the one porous walled channel problem

The problem under consideration here is that of the temperature-dependent viscosity flow of fluid through a channel with one porous wall, where the sensitivity of the fluid viscosity to temperature is large. The geometry of the channel is shown in Figure B.0.1. In this chapter we obtain approximate solutions directly from the asymptotic expansions of the governing system and so the solutions obtained are not limited to those of similarity solution type. This is in contrast to the work on the $\beta = \mathcal{O}(1)$ problems in Chapter 5 which started with a similarity solution formulation of the problem and then sought asymptotic expansions in different regimes. Another distinction from the work in Chapter 5 is the consideration of an algebraic form for the viscosity function in addition to an exponential form.

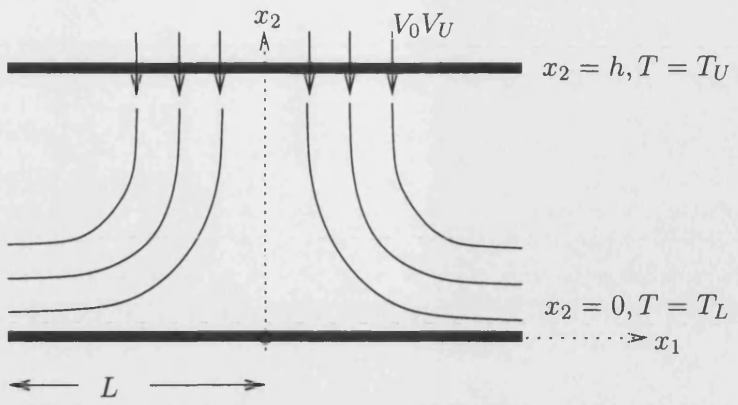

Figure B.0.1. Channel geometry for the one porous walled case.

Starting with the Navier-Stokes equations and energy equation (1.2.14a)–(1.2.14e) and the boundary conditions

$$\text{on } x_2 = h: \quad q_1 = 0, \quad q_2 = -V_0V_U, \tag{B.0.1}$$

$$\text{on } x_2 = 0: \quad q_1 = 0, \quad q_2 = 0, \tag{B.0.2}$$

and noting that $n = 1$, allows the use of the following nondimensionalisations (in the same manner as in § 1.2),

$$x_1 = L\bar{x}, \;\; x_2 = h\bar{y}, \;\; q_1 = \frac{V_0V_UL}{h}\bar{u}, \;\; q_2 = V_0V_U\bar{v}, \;\; t = \frac{h}{V_0V_U}\bar{t},$$
$$\mu = \mu_1\bar{\mu}, \;\; p = \rho V_0^2V_U^2P\bar{p}, \;\; T = T_U + \Delta_T\bar{T},$$

where $\Delta_T = T_U - T_L$ and $\mu_1 = \mu(T = T_U)$. If we now define a stream function $\psi(x, y)$ such that $(u, v) = (\psi_y, -\psi_x)$ and the nondimensional groups

$$\mathrm{Re} = \frac{\rho V_0V_Uh}{\mu_1}, \; \mathrm{Pe} = \frac{\rho cV_0V_Uh}{k}, \; \mathrm{Pr} = \frac{\mathrm{Pe}}{\mathrm{Re}} = \frac{c\mu_1}{k}, \; \mathrm{Br} = \frac{\mu_1V_0^2V_U^2L^2}{k\Delta_Th^2},$$
$$\mathrm{Na} = \frac{V_0^2V_U^2\left|\frac{\mathrm{d}\mu}{\mathrm{d}T}\right|_{T=T_U}}{k}, \; \beta = \frac{\mathrm{Na}}{\mathrm{Br}} = \Delta_T\left|\frac{\frac{\mathrm{d}\mu}{\mathrm{d}T}}{\mu}\right|_{T=T_U}, \; \varepsilon = \frac{h}{L}, \tag{B.0.3}$$

we then obtain the governing partial differential equation system after dropping the

overbars

$$\mathrm{Re}\frac{D}{Dt}\frac{\partial\psi}{\partial y} = -\mathrm{Re}\varepsilon^2 P\frac{\partial p}{\partial x} + \varepsilon^2\frac{\partial}{\partial x}\Big(2\mu\frac{\partial^2\psi}{\partial y\partial x}\Big) + \frac{\partial}{\partial y}\Big(\mu\frac{\partial^2\psi}{\partial y^2}\Big) - \varepsilon^2\frac{\partial}{\partial y}\Big(\mu\frac{\partial^2\psi}{\partial x^2}\Big), \quad \text{(B.0.4a)}$$

$$-\mathrm{Re}\varepsilon\frac{D}{Dt}\frac{\partial\psi}{\partial x} = -\mathrm{Re}\varepsilon P\frac{\partial p}{\partial y} - \varepsilon^3\frac{\partial}{\partial x}\Big(\mu\frac{\partial^2\psi}{\partial x^2}\Big) + \varepsilon\frac{\partial}{\partial x}\Big(\mu\frac{\partial^2\psi}{\partial y^2}\Big) - \varepsilon\frac{\partial}{\partial y}\Big(2\mu\frac{\partial^2\psi}{\partial y\partial x}\Big), \quad \text{(B.0.4b)}$$

$$\mathrm{Pe}\frac{DT}{Dt} = \varepsilon^2\frac{\partial^2 T}{\partial x^2} + \frac{\partial^2 T}{\partial y^2}, \quad \text{(B.0.4c)}$$

$$\text{on } y = 1\text{:} \quad \frac{\partial\psi}{\partial y} = 0, \quad -\frac{\partial\psi}{\partial x} = -1, \quad T = 0, \quad \text{(B.0.4d)}$$

$$\text{on } y = 0\text{:} \quad \frac{\partial\psi}{\partial y} = 0, \quad -\frac{\partial\psi}{\partial x} = 0, \quad T = 1, \quad \text{(B.0.4e)}$$

and we have assumed taken the viscosity function $\mu(T)$ to either have an exponential or algebraic form,

$$\mu = \exp(-\beta T), \text{ or } \mu = (1+\beta T)^{-n}, \quad \text{(B.0.4f)}$$

with $n = 1$ for simplicity, where n is unrelated to the power-law fluid exponent.

(B.0.4g)

We have assumed that $\mathrm{Br} \ll 1$ uniformly across the channel and that $L = \mathrm{Pe}h$, so that we are restricting the region of interest to the horizontal length scale where thermal conduction and inertia are balanced. In this case $\varepsilon = 1/\mathrm{Pe}$.

B.1 $\mathrm{Pe} \gg 1$

We will consider the three cases of $\mathrm{Re} \ll 1$,$\mathrm{Re} = \mathcal{O}(1)$ and $\mathrm{Re} \gg 1$ separately. In the first two cases, the boundary layer structure is seen to be the same as that presented in [OO77] for the problem of Poiseuille flow in a pipe with suddenly heated walls, and so is an application of these boundary layer scalings to a new geometry, even though the equations themselves are not new. In each case $\mathrm{Re} < 0$ and thus we are considering the injection of fluid into the channel through the upper wall.

B.1.1 $\mathrm{Pe} \gg 1, \mathrm{Re} \ll 1$

This regime corresponds to the channel height being much smaller than its length and the inertial effects from the injection of the fluid being less important than the viscous

effects. Choosing $P = \frac{\mathrm{Pe}^2}{\mathrm{Re}}$ in (B.0.4a)–(B.0.4c) then yields the following system at lowest order,

$$\frac{\partial}{\partial y}\left(\mu\frac{\partial^2\psi}{\partial y^2}\right) = \frac{\mathrm{d}p}{\mathrm{d}x}, \tag{B.1.1}$$

$$\frac{\partial\psi}{\partial y}\frac{\partial T}{\partial x} - \frac{\partial\psi}{\partial x}\frac{\partial T}{\partial y} = \frac{1}{\mathrm{Pe}}\frac{\partial^2 T}{\partial y^2}, \tag{B.1.2}$$

together with the boundary conditions

$$\text{on } y = 0: \quad \frac{\partial\psi}{\partial x} = 0, \quad \frac{\partial\psi}{\partial y} = 0, \quad T = 1, \tag{B.1.3}$$

$$\text{on } y = 1: \quad \frac{\partial\psi}{\partial x} = 1, \quad \frac{\partial\psi}{\partial y} = 0, \quad T = 0, \tag{B.1.4}$$

and the symmetry condition

$$\text{at } x = 0: \quad \psi(0,y) = 0, \quad \frac{\partial^2\psi}{\partial x^2}(0,y) = 0. \tag{B.1.5}$$

We may integrate the first equation once with respect to y and seek a similarity solution of the form $T = T(y), \psi = xf(y)$. Assuming $p = p_0 x, c = c_0 x$ we then obtain

$$\mu\frac{\mathrm{d}^2 f}{\mathrm{d}y^2} = p_0 y + c_0, \tag{B.1.6}$$

$$\frac{1}{\mathrm{Pe}}\frac{\mathrm{d}^2 T}{\mathrm{d}y^2} + f\frac{\mathrm{d}T}{\mathrm{d}y} = 0, \tag{B.1.7}$$

subject to the boundary conditions

$$\text{on } y = 0: \quad f = 0, \quad f' = 0, \quad T = 1, \tag{B.1.8}$$

$$\text{on } y = 1: \quad f = 1, \quad f' = 0, \quad T = 0. \tag{B.1.9}$$

In an outer region away from the heated lower wall $T = o(1)$ and so $\mu = 1$. We then find that

$$f = \frac{p_0}{6}y^3 + \frac{c_0}{2}y^2 - \left(\frac{p_0}{2} + c_0\right)y + 1 + \frac{p_0}{3} + \frac{c_0}{2}, \tag{B.1.10}$$

and satisfying the flow boundary conditions requires $c_0 = 6, p_0 = -12$. Thus, in the core flow region, away from the lower heated wall,

$$\psi = xy^2(3 - 2y) + o(1), \quad T = o(1), \quad p = -6x^2. \tag{B.1.11}$$

We now require a thermal boundary layer as we have not been able to satisfy the thermal boundary condition at the lower wall.

We introduce the scalings

$$y = \hat{\alpha} Y, \quad f = \hat{\beta} F, \qquad (Y, F = \mathcal{O}(1))$$

and substituting these into (B.1.1) gives

$$-\frac{\hat{\beta}}{\hat{\alpha}} F \frac{\mathrm{d}T}{\mathrm{d}Y} = \frac{1}{\hat{\alpha}\mathrm{Pe}} \frac{\mathrm{d}^2 T}{\mathrm{d}Y^2}, \tag{B.1.12}$$

with the boundary conditions

$$\text{on } Y = 0: \quad F = \frac{\mathrm{d}F}{\mathrm{d}Y} = 0, \quad T = 1, \tag{B.1.13}$$

$$\text{as } Y \to \infty: \quad T \to 0, \tag{B.1.14}$$

and the solution F must match f when $y = \mathcal{O}(1)$.

If we expand the outer solution f as a Taylor series about $y = 0$ we find that $f \sim \frac{1}{2} f''(0) y^2 = 3y^2$ in this thermal boundary layer. Rewriting this in terms of the boundary layer variables yields $\hat{\alpha}^2 = \hat{\beta}$. The matching condition has given rise to the differential equation

$$\mu \frac{\mathrm{d}^2 F}{\mathrm{d}Y^2} = f''(0) = 6, \tag{B.1.15}$$

and so we require $F \sim 3Y^2$ in $Y = \mathcal{O}(1)$, having used the fact that $T \to 0$ as $Y \to \infty$. Therefore the boundary layer scalings are

$$y = \mathrm{Pe}^{-\frac{1}{3}} Y, \quad f = \mathrm{Pe}^{-\frac{2}{3}} F, \tag{B.1.16}$$

and the boundary layer equations become

$$\mu \frac{\mathrm{d}^2 F}{\mathrm{d}Y^2} = 6, \tag{B.1.17}$$

$$\frac{\mathrm{d}^2 T}{\mathrm{d}Y^2} + F \frac{\mathrm{d}T}{\mathrm{d}Y} = 0, \tag{B.1.18}$$

subject to

$$\text{on } Y = 0: \quad F = \frac{\mathrm{d}F}{\mathrm{d}Y} = 0, \quad T = 1, \tag{B.1.19}$$

$$\text{as } Y \to \infty: \quad T \to 0. \tag{B.1.20}$$

In order to further elucidate the boundary layer structure we must consider the algebraic and exponential functional forms of the viscosity separately.

Algebraic viscosity

As we wish to consider the $\beta \to \infty$ behaviour of the boundary layer, we must rescale the system otherwise the F equation will be inconsistent in this limit. Introducing the scalings

$$Y = \bar{a}\bar{Y}, \quad F = \bar{b}\bar{F}, \qquad (\bar{Y}, \bar{F} = \mathcal{O}(1))$$

into the boundary layer equations (B.1.17–B.1.18) gives

$$\mu \frac{\bar{b}}{\bar{a}^2} \frac{\mathrm{d}^2\bar{F}}{\mathrm{d}\bar{Y}^2} = 6, \tag{B.1.21}$$

$$\frac{1}{\bar{a}^2} \frac{\mathrm{d}^2 T}{\mathrm{d}\bar{Y}^2} + \frac{\bar{b}}{\bar{a}} \bar{F} \frac{\mathrm{d}T}{\mathrm{d}\bar{Y}} = 0. \tag{B.1.22}$$

We need to retain both terms in the temperature equation and must introduce μ_0 in the F equation for it to remain consistent in the $\beta \to \infty$ limit. In this case we obtain the scalings

$$Y = \mu_0^{\frac{1}{3}} \bar{Y}, \quad F = \mu_0^{-\frac{1}{3}} \bar{F} \tag{B.1.23}$$

and the equations become

$$\frac{\mu}{\mu_0} \frac{\mathrm{d}^2\bar{F}}{\mathrm{d}\bar{Y}^2} = 6, \tag{B.1.24}$$

$$\frac{\mathrm{d}^2 T}{\mathrm{d}\bar{Y}^2} + \bar{F} \frac{\mathrm{d}T}{\mathrm{d}\bar{Y}} = 0, \tag{B.1.25}$$

subject to the boundary conditions

$$\text{on } \bar{Y} = 0: \quad \bar{F} = \frac{\mathrm{d}\bar{F}}{\mathrm{d}\bar{Y}} = 0, \quad T = 1, \tag{B.1.26}$$

$$\text{as } \bar{Y} \to \infty: \quad \bar{F} \text{ matches to } f \text{ when } y = \mathcal{O}(1), \quad T \to 0. \tag{B.1.27}$$

As $\beta \to \infty$, the factor on the left hand side of (B.1.24) tends to T^{-n}.
Now, as $\bar{Y} \to \infty$, $T \to 0$ and so $\bar{F}''' = 0$, giving

$$\bar{F} \sim a_1 \bar{Y} \quad \text{as } \bar{Y} \to \infty, \tag{B.1.28}$$

where a_1 is a integration constant. Substituting this into (B.1.25) yields the asymptotic behaviour

$$T \sim \frac{A}{2\bar{Y}} \exp\left\{-\frac{a_1}{2}\bar{Y}^2\right\} \quad \text{as } \bar{Y} \to \infty, \tag{B.1.29}$$

and the value of A is determined from the wall boundary conditions to be $\sqrt{\frac{2a_1}{\pi}}$.

Thus $T = o(1)$ as $\bar{Y} \to \infty$ but the $\bar{F}$ behaviour does not agree with that in the outer region. We need an intermediate layer in which $\bar{F}$ can adjust to the outer behaviour. If we consider (B.1.24) when $T = o(1)$ then we obtain

$$\bar{F} \sim 3\mu_0\bar{Y}^2 + a_1\bar{Y} + a_0. \tag{B.1.30}$$

In the intermediate region we want to have both the quadratic and linear terms being of the same order. If we introduce the scalings

$$\bar{F} = m\hat{F}, \quad \bar{Y} = n\hat{Y}, \qquad (\hat{F}, \hat{Y} = \mathcal{O}(1))$$

into (B.1.24) and (B.1.30) and recall that $T = o(1)$ then we obtain

$$m\hat{F} \sim 3\mu_0 n^2\hat{Y}^2 + a_1 n\hat{Y} + a_0, \tag{B.1.31}$$

$$\frac{1}{\mu_0}\frac{m}{n^2}\frac{\mathrm{d}^2\hat{F}}{\mathrm{d}\hat{Y}^2} = 6. \tag{B.1.32}$$

We must have $n^2\mu_0 = n$ and $\frac{m}{n^2} = \mu_0$ i.e. in this intermediate region the scalings are

$$\bar{F} = \frac{1}{\mu_0}\hat{F}, \quad \bar{Y} = \frac{1}{\mu_0}\hat{Y} \tag{B.1.33}$$

and then in this region

$$T = o(1), \quad \hat{F} \sim 3\hat{Y}^2 + a_1\hat{Y} + \mathcal{O}(\mu_0). \tag{B.1.34}$$

The value of the constant a_1 can be determined numerically. Figure B.1.1 summarises the structure of the boundary layer in this first case.

Exponential viscosity

Starting from (B.1.17–B.1.20) we must again rescale our variables. Using

$$F = l_1F_1, \quad T = 1 - m_1T_1, \quad Y = n_1Y_1, \qquad (F_1, T_1, Y_1 = \mathcal{O}(1))$$

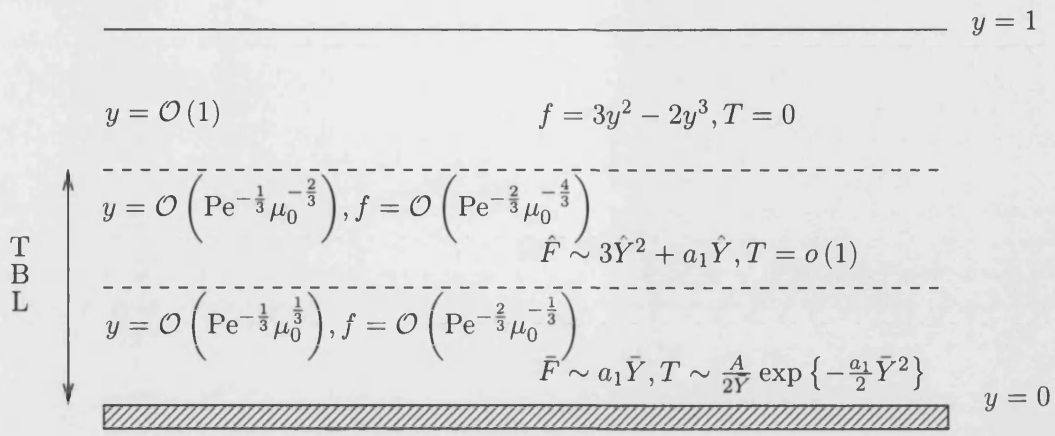

Figure B.1.1. Thermal boundary layer (TBL) structure for Pe $\gg 1$, Re $\ll 1$ in the algebraic viscosity case where $A = \sqrt{\frac{2a_1}{\pi}}$.

we obtain

$$\frac{l_1}{{n_1}^2}\mathrm{e}^{(-\beta+m_1\beta T_1)}\frac{\mathrm{d}^2F_1}{\mathrm{d}{Y_1}^2} = 6, \tag{B.1.35}$$

$$\frac{m_1}{{n_1}^2}\frac{\mathrm{d}^2T_1}{\mathrm{d}{Y_1}^2} + \frac{m_1l_1}{n_1}F_1\frac{\mathrm{d}T_1}{\mathrm{d}Y_1} = 0, \tag{B.1.36}$$

subject to the boundary conditions

$$\text{on } Y_1 = 0: \quad F_1 = \frac{\mathrm{d}F_1}{\mathrm{d}Y_1} = 0, \quad T_1 = 0, \tag{B.1.37}$$

$$\text{as } Y_1 \to \infty: \quad m_1T_1 \to 1, \tag{B.1.38}$$

and that F_1 matches to f when $y = \mathcal{O}(1)$. Now it is clear that $m_1 = \beta^{-1}$ but the choice for the other scales is not yet obvious. So in this region we have

$$\frac{\mathrm{d}^2F_1}{\mathrm{d}{Y_1}^2} = 6\mathrm{e}^{-T_1}, \tag{B.1.39}$$

$$\frac{\mathrm{d}^2T_1}{\mathrm{d}{Y_1}^2} + n_1l_1F_1\frac{\mathrm{d}T_1}{\mathrm{d}Y_1} = 0, \tag{B.1.40}$$

with the corresponding boundary conditions (B.1.37–B.1.38) and the relation

$$l_1 = \frac{{n_1}^2}{\mu_0}. \tag{B.1.41}$$

Now, if we assume that $n_1 l_1 \ll 1$ then

$$T_1 = a_1 Y_1 + a_0 \tag{B.1.42}$$

and then using (B.1.37) together with (B.1.39) gives

$$F_1 = \frac{6}{{a_1}^2} e^{-a_1 Y_1} + \frac{6}{a_1} Y_1 - \frac{6}{{a_1}^2}, \quad T_1 = a_1 Y_1, \tag{B.1.43}$$

in this near wall region.

Now when $T_1 = \mathcal{O}(\beta)$, T will experience $\mathcal{O}(1)$ changes and so we must perform a rescaling. Letting

$$F_1 = l_2 F_2, \quad T_1 = m_2 T_2, \quad Y_1 = n_2 Y_2, \qquad (F_2, T_2, Y_2 = \mathcal{O}(1))$$

we find that we must take $m_2 = \beta$ because of the above argument. Substituting these scalings into (B.1.43) yields $l_2 = m_2 = n_2 = \beta$ and so in this second region

$$\frac{\mathrm{d}^2 F_2}{\mathrm{d}{Y_2}^2} = 0 + \mathcal{O}\left(\beta^2 \exp -a_1 \beta Y_2\right), \tag{B.1.44}$$

$$\frac{\mathrm{d}^2 T_2}{\mathrm{d}{Y_2}^2} + \beta^2 l_1 n_1 F_2 \frac{\mathrm{d}T_2}{\mathrm{d}Y_2} = 0, \tag{B.1.45}$$

with the boundary conditions

$$\text{as } Y_2 \to 0\text{:} \quad F_2 \text{ matches to } F_1, \quad T_2 \to 0, \tag{B.1.46}$$

$$\text{as } Y_2 \to \infty\text{:} \quad F_2 \text{ matches to } f, \quad T_2 \to 1. \tag{B.1.47}$$

Now, as $T_2 = \mathcal{O}(1)$ we must have that $\beta^2 l_1 n_1 = 1$ and together with (B.1.41) we can now determine the scalings in these two regions to be

$$l_1 = \mu_0^{-\frac{1}{3}} \beta^{-\frac{4}{3}}, \quad m_1 = \beta^{-1}, \quad n_1 = \mu_0^{\frac{1}{3}} \beta^{-\frac{2}{3}}, \tag{B.1.48}$$

$$l_2 = m_2 = n_2 = \beta. \tag{B.1.49}$$

Therefore, in this second region, we have that

$$\frac{\mathrm{d}^2 F_2}{\mathrm{d}{Y_2}^2} = 0, \tag{B.1.50}$$

$$\frac{\mathrm{d}^2 T_2}{\mathrm{d}{Y_2}^2} + F_2 \frac{\mathrm{d}T_2}{\mathrm{d}Y_2} = 0, \tag{B.1.51}$$

and solving the F_2 equation subject to the matching condition (B.1.46) gives

$$F_2 = a_3 Y_2 = \frac{6}{a_1} Y_2.$$

Substituting this into the the T_2 equation then gives

$$T_2(Y_2) = A \int_{\infty}^{Y_2} \exp\left\{-\frac{3}{a_1} s^2\right\} \mathrm{d}s + B. \tag{B.1.52}$$

We now need to match the behaviour of T_2 to that of T_1 in the Y_1 region and to that of the core flow.

$$\text{as } Y_2 \to \infty,\ T_2 \to 1: \quad B = 1. \tag{B.1.53}$$

$$\text{as } Y_2 \to 0,\ T_2 \to 0: \quad 1 - A \int_0^{\infty} \exp\left\{-\frac{3}{a_1} s^2\right\} \mathrm{d}s = 0 \Rightarrow A = \sqrt{\frac{12}{a_1 \pi}}. \tag{B.1.54}$$

However, we now need to determine the remaining constant a_1. Let us introduce the coordinate $\tilde{Y}$ in the matching region in the following manner:

$$Y_1 = \beta^{\alpha} \tilde{Y}, \quad Y_2 = \beta^{\alpha - 1} \tilde{Y}, \qquad \left(0 < \alpha < 1,\ \tilde{Y} = \mathcal{O}(1)\right).$$

Then we express T_1 and T_2 in the intermediate variable $\tilde{Y}$ and proceed to determine the value of the constant that will permit asymptotic matching to occur.

$$\begin{aligned}
T_1(Y_1) = T_1(\beta^{\alpha} \tilde{Y}) &= a_1 \beta^{\alpha} \tilde{Y} \\
\beta T_2(Y_2) = \beta T_2(\beta^{\alpha - 1} \tilde{Y}) &= \beta \left\{ 1 - \sqrt{\frac{12}{a_1 \pi}} \int_{\beta^{\alpha-1}\tilde{Y}}^{\infty} \exp\left\{-\frac{3}{a_1} s^2\right\} \mathrm{d}s \right\} \\
&= \beta \left\{ 1 - \sqrt{\frac{12}{a_1 \pi}} \left(\int_0^{\infty} - \int_0^{\beta^{\alpha-1}\tilde{Y}} \exp\left\{-\frac{3}{a_1} s^2\right\} \mathrm{d}s \right) \right\} \\
&= \beta \left\{ 1 - \sqrt{\frac{12}{a_1 \pi}} \sqrt{\frac{a_1}{3}} \left(\int_0^{\infty} - \int_0^{\beta^{\alpha-1}\sqrt{\frac{3}{a_1}}\tilde{Y}} \exp\left(-t^2\right) \mathrm{d}t \right) \right\} \\
&= \beta \left\{ 1 - 1 + \sqrt{\frac{4}{\pi}} \int_0^{\beta^{\alpha-1}\sqrt{\frac{3}{a_1}}\tilde{Y}} \exp\left(-t^2\right) \mathrm{d}t \right\} \\
&= \beta \sqrt{\frac{4}{\pi}} \int_0^{\beta^{\alpha-1}\sqrt{\frac{3}{a_1}}\tilde{Y}} \left(1 - t^2 + \mathcal{O}\left(t^4\right)\right) \mathrm{d}t \\
&= \sqrt{\frac{12}{a_1 \pi}} \beta^{\alpha} \tilde{Y} + \mathcal{O}\left(\beta^{3\alpha - 2}\right).
\end{aligned}$$

For matching to occur we require

$$a_1 = \sqrt{\frac{12}{a_1 \pi}} \quad \therefore a_1 = \left(\frac{12}{\pi}\right)^{\frac{1}{3}} \Rightarrow A = a_1 \tag{B.1.55}$$

We now need a third region to match the behaviour of F_2 to that of the outer flow. In this third region we have that $T = o(1)$. Let

$$F = l_3 F_3, \quad Y = n_3 Y_3, \qquad (F_3, Y_3 = \mathcal{O}(1))$$

and then we may integrate (B.1.17) to obtain

$$F \sim 3Y^2 + a_5 Y + a_6 \quad \Rightarrow l_3 F_3 \sim 3{n_3}^2 {Y_3}^2 + a_5 n_3 Y_3 + a_6. \tag{B.1.56}$$

In the second region

$$F = l_1 l_2 F_2 = \mu_0^{-\frac{1}{3}} \beta^{-\frac{1}{3}} F_2, \quad Y = n_1 n_2 Y_2 = \mu_0^{\frac{1}{3}} \beta^{\frac{1}{3}} Y_2, \tag{B.1.57}$$

and we want to have both the linear and quadratic terms to be of the same order and that $F_3 = \mathcal{O}(1)$. Thus, as

$$\frac{l_3}{l_1 l_2} F_3 \sim 3\left(\frac{n_3}{n_1 n_2}\right)^2 Y_3^2 + \frac{6}{a_1}\frac{n_3}{n_1 n_2} Y_3, \tag{B.1.58}$$

$$\text{and} \quad l_3 = n_3^2, \tag{B.1.59}$$

we find that we must satisfy

$$\frac{n_3}{n_1 n_2} = \frac{n_3^2}{l_1 l_2} \tag{B.1.60}$$

giving

$$l_3 = \mu_0^{-\frac{4}{3}} \beta^{-\frac{4}{3}}, \quad n_3 = \mu_0^{-\frac{2}{3}} \beta^{-\frac{2}{3}}. \tag{B.1.61}$$

The scalings in the third region are

$$F_2 = \frac{1}{\mu_0 \beta} F_3, \quad Y_2 = \frac{1}{\mu_0 \beta} Y_3, \tag{B.1.62}$$

giving

$$F_3 = 3{Y_3}^2 + \frac{6}{a_1} (\mu_0 \beta)^{\frac{2}{3}} Y_3. \tag{B.1.63}$$

Figure B.1.2 summarises the structure of the boundary layer in this first case.

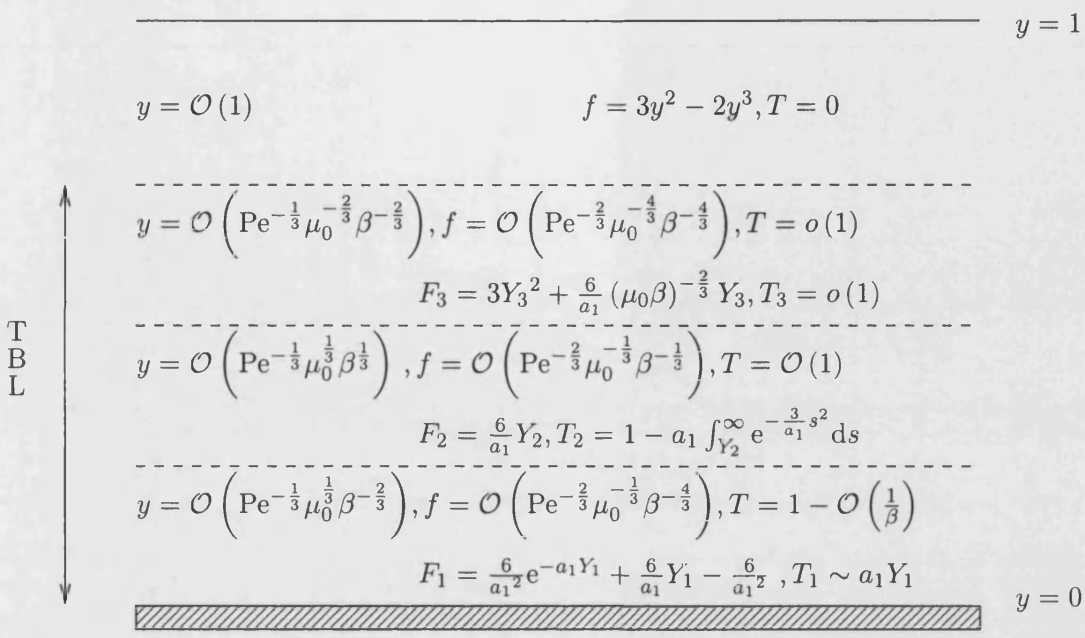

Figure B.1.2. Thermal boundary layer (TBL) structure for Pe $\gg 1$, Re $\ll 1$ in the exponential viscosity case where $a_1 = \left(\frac{12}{\pi}\right)^{\frac{1}{3}}$.

B.1.2 Pe $\gg 1$, Re $= \mathcal{O}(1)$

This combination of Pe and Re corresponds to the situation where the height of the channel is much less than the length, and where the effects of inertia and viscosity are comparable. Starting with (B.0.4a)–(B.0.4c) we choose $P = \mathrm{Pe}^2$ and obtain

$$\frac{\partial\psi}{\partial y}\frac{\partial^2\psi}{\partial x\partial y} - \frac{\partial\psi}{\partial x}\frac{\partial^2\psi}{\partial y^2} = -\frac{\partial p}{\partial x} + \frac{1}{\mathrm{Re}}\frac{\partial}{\partial y}\left(\mu\frac{\partial^2\psi}{\partial y^2}\right), \tag{B.1.64}$$

$$0 = \frac{\partial p}{\partial y}, \tag{B.1.65}$$

$$\frac{\partial\psi}{\partial y}\frac{\partial T}{\partial x} - \frac{\partial\psi}{\partial x}\frac{\partial T}{\partial y} = \frac{1}{\mathrm{Pe}}\frac{\partial^2 T}{\partial y^2}, \tag{B.1.66}$$

subject to

$$\text{on } y = 0: \quad T = 1, \quad \frac{\partial\psi}{\partial y} = 0, \quad \frac{\partial\psi}{\partial x} = 0, \tag{B.1.67}$$

$$\text{on } y = 1: \quad T = 0, \quad \frac{\partial\psi}{\partial y} = 0, \quad \frac{\partial\psi}{\partial x} = 1, \tag{B.1.68}$$

and the symmetry condition

$$\text{at } x = 0: \quad \psi(0,y) = 0, \quad \frac{\partial^2 \psi}{\partial x^2}(0,y) = 0. \tag{B.1.69}$$

The same similarity solution form $\psi = xf(y), T = T(y)$ is used to give

$$\frac{1}{\mathrm{Re}} \frac{\mathrm{d}^2}{\mathrm{d}y^2}\left(\mu \frac{\mathrm{d}^2 f}{\mathrm{d}y^2}\right) = \frac{\mathrm{d}}{\mathrm{d}y}\left(\left(\frac{\mathrm{d}f}{\mathrm{d}y}\right)^2 - f\frac{\mathrm{d}^2 f}{\mathrm{d}y^2}\right), \tag{B.1.70}$$

$$\frac{1}{\mathrm{Pe}} \frac{\mathrm{d}^2 T}{\mathrm{d}y^2} + f\frac{\mathrm{d}T}{\mathrm{d}y} = 0, \tag{B.1.71}$$

subject to

$$\text{on } y = 0: \quad T = 1, \quad f = \frac{\mathrm{d}f}{\mathrm{d}y} = 0, \tag{B.1.72}$$

$$\text{on } y = 1: \quad T = 0, \quad f = 1, \quad \frac{\mathrm{d}f}{\mathrm{d}y} = 0. \tag{B.1.73}$$

We may now consider an outer region in the flow domain where $f \sim f_0 + \mathcal{O}\left(\mathrm{Pe}^{-1}\right)$. In this region $T = 0$ and so $\mu = 1$. Thus f_0 satisfies the Proudman-Johnson equation,

$$\frac{1}{\mathrm{Re}} \frac{\mathrm{d}^4 f_0}{\mathrm{d}y^4} = \frac{\mathrm{d}}{\mathrm{d}y}\left(\left(\frac{\mathrm{d}f_0}{\mathrm{d}y}\right)^2 - f_0\frac{\mathrm{d}^2 f_0}{\mathrm{d}y^2}\right), \tag{B.1.74}$$

with boundary conditions

$$\text{on } y = 0: \quad f_0 = 0, \quad \frac{\mathrm{d}f_0}{\mathrm{d}y} = 0, \tag{B.1.75}$$

$$\text{on } y = 1: \quad f_0 = 1, \quad \frac{\mathrm{d}f_0}{\mathrm{d}y} = 0. \tag{B.1.76}$$

To satisfy the temperature equation we require a thermal boundary layer near $y = 0$. Using the scalings

$$y = \hat{\alpha}Y, \quad f = \hat{\beta}F, \qquad (Y, F = \mathcal{O}(1))$$

we get that

$$\frac{1}{\hat{\alpha}^2}\frac{1}{\mathrm{Pe}}\frac{\mathrm{d}^2 T}{\mathrm{d}Y^2} + \frac{\hat{\beta}}{\hat{\alpha}}F\frac{\mathrm{d}T}{\mathrm{d}Y} = 0 \tag{B.1.77}$$

and therefore we require $\hat{\beta}\hat{\alpha} = \mathrm{Pe}^{-1}$.

Substituting these scalings into the f equation and using the requirement upon $\hat{\alpha}\hat{\beta}$

gives, to lowest order in Pe^{-1},

$$\frac{\hat{\beta}}{\hat{\alpha}^2}\frac{\mathrm{d}^2F}{\mathrm{d}Y^2} = AY + B, \tag{B.1.78}$$

and the boundary conditions have become

$$\text{on } Y = 0: \quad F = 0, \quad \frac{\mathrm{d}F}{\mathrm{d}Y} = 0, \quad T = 1, \tag{B.1.79}$$

$$\text{as } Y \to \infty: \quad T \to 0, \tag{B.1.80}$$

and the solution F must match f_0 when $y = \mathcal{O}(1)$. If we rewrite the Taylor expansion of f_0 about $y = 0$ in the boundary layer variables, we then find that we need $\hat{\beta} = \hat{\alpha}^2$ if we are to match solutions as $Y \to \infty$.

We then find that the boundary layer scalings are

$$y = \mathrm{Pe}^{-\frac{1}{3}}Y, \quad f = \mathrm{Pe}^{-\frac{2}{3}}F, \tag{B.1.81}$$

and the boundary layer equations are, to leading order,

$$\mu\frac{\mathrm{d}^2F}{\mathrm{d}Y^2} = f_0''(0), \qquad \frac{\mathrm{d}^2T}{\mathrm{d}Y^2} + F\frac{\mathrm{d}T}{\mathrm{d}Y} = 0, \tag{B.1.82}$$

$$\text{at } Y = 0: \quad F = \frac{\mathrm{d}F}{\mathrm{d}Y} = 0, \quad T = 1, \tag{B.1.83}$$

$$\text{as } Y \to \infty: \quad F \sim \frac{1}{2}f_0''(0)Y^2, \quad T \to 0. \tag{B.1.84}$$

Algebraic viscosity

We must introduce μ_0 into the F equation in order to have a consistent problem as $\beta \to \infty$. Using the scalings

$$Y = a_1Y_1, \quad F = b_1F_1, \quad T = c_1T_1, \qquad (Y_1, F_1, T_1 = \mathcal{O}(1))$$

in (B.1.82) we find

$$\mu \frac{b_1}{{a_1}^2} \frac{\mathrm{d}^2 F_1}{\mathrm{d}{Y_1}^2} = f_0''(0), \tag{B.1.85}$$

$$\frac{c_1}{{a_1}^2} \frac{\mathrm{d}^2 T_1}{\mathrm{d}{Y_1}^2} + \frac{b_1 c_1}{a_1} F_1 \frac{\mathrm{d}T_1}{\mathrm{d}Y_1} = 0, \tag{B.1.86}$$

$$\text{at } Y_1 = 0: \quad F_1 = 0, \quad \frac{b_1}{a_1} \frac{\mathrm{d}F_1}{\mathrm{d}Y_1} = 0, \quad c_1 T_1 = 1, \tag{B.1.87}$$

$$\text{as } Y_1 \to \infty: \quad b_1 F_1 \sim \frac{1}{2} {a_1}^2 f_0''(0) {Y_1}^2, \quad T_1 \to 0. \tag{B.1.88}$$

We find that the required scalings are

$$Y = \mu_0^{\frac{1}{3}} Y_1, \quad F = \mu_0^{-\frac{1}{3}} F_1, \quad T = T_1, \tag{B.1.89}$$

and so the system to be solved within this region of the boundary layer is

$$\frac{\mu}{\mu_0} \frac{\mathrm{d}^2 F_1}{\mathrm{d}{Y_1}^2} = f_0''(0), \tag{B.1.90}$$

$$\frac{\mathrm{d}^2 T_1}{\mathrm{d}{Y_1}^2} + F_1 \frac{\mathrm{d}T_1}{\mathrm{d}Y_1} = 0, \tag{B.1.91}$$

$$\text{at } Y_1 = 0: \quad F_1 = 0, \quad \frac{\mathrm{d}F_1}{\mathrm{d}Y_1} = 0, \quad T_1 = 1, \tag{B.1.92}$$

$$\text{as } Y_1 \to \infty: \quad T_1 \to 0. \tag{B.1.93}$$

Now, as $Y_1 \to \infty, T_1 \to 0$ and so $\mu \to 1$. Thus

$$\frac{\mathrm{d}^2 F_1}{\mathrm{d}{Y_1}^2} \sim \mu_0 f_0''(0) \Rightarrow F_1 \sim \frac{1}{2} \mu_0 f_0''(0) {Y_1}^2 + d_1 Y_1 + d_2 \tag{B.1.94}$$

and as $\mu_0 \ll 1$ we have

$$\text{as } Y_1 \to \infty: \quad F_1 \sim d_1 Y_1. \tag{B.1.95}$$

Substituting this into (B.1.91) gives the asymptotic behaviour for T_1 as $Y_1 \to \infty$,

$$T_1 \sim \frac{A}{2Y_1} \exp\left(-\frac{d_1}{2} {Y_1}^2\right), \tag{B.1.96}$$

and the value of A, determined from the wall boundary condition, is $\sqrt{\frac{2d_1}{\pi}}$.

The temperature behaviour matches up to that of the core region as $Y_1 \to \infty$ but the flow behaviour does not and so we require an intermediate layer in which the velocity correction may occur. In this intermediate layer $T = T_1 = o(1)$ and so $\mu = 1$.

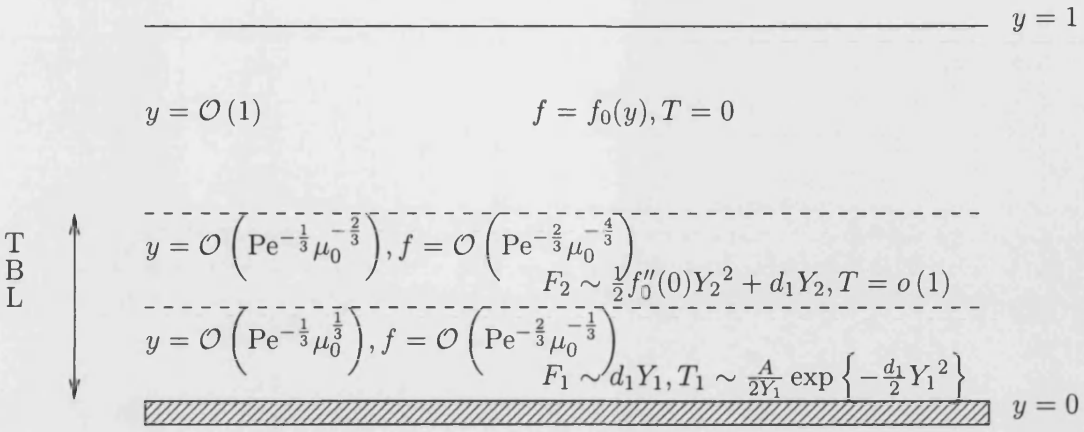

Figure B.1.3. Thermal boundary layer (TBL) structure for Pe $\gg 1$, Re $= \mathcal{O}(1)$ in the algebraic viscosity case where $A = \sqrt{\frac{2d_1}{\pi}}$.

Setting

$$Y_1 = a_2Y_2, \quad F_1 = a_2F_2 \qquad (Y_2, F_2 = \mathcal{O}(1))$$

we wish to have both the quadratic and linear terms coming from the solution of (B.1.90) being of the same order and that

$$\frac{1}{\mu_0}\frac{b_2}{a_2{}^2}\frac{\mathrm{d}^2F_2}{\mathrm{d}Y_2{}^2} = f_0''(0). \tag{B.1.97}$$

Analogous to the Pe $\gg 1$, Re $\ll 1$ case, the required scalings are

$$Y_1 = \frac{1}{\mu_0}Y_2, \quad F_1 = \frac{1}{\mu_0}F_2, \tag{B.1.98}$$

and in this intermediate region

$$F_2 = \frac{1}{2}f_0''(0)Y_2{}^2 + d_3Y_2, \quad T = o(1), \tag{B.1.99}$$

which matches to the core region if $d_3 = d_1$ and d_1 can be determined numerically.

Figure B.1.3 summarises the boundary layer structure in this case.

Exponential viscosity

Starting from (B.1.82–B.1.84) we must again rescale our variables. Using

$$F = l_1F_1, \quad T = 1 - m_1T_1, \quad Y = n_1Y_1, \qquad (F_1, T_1, Y_1 = \mathcal{O}(1))$$

we obtain

$$\frac{l_1}{{n_1}^2}\mathrm{e}^{(-\beta+m_1\beta T_1)}\frac{\mathrm{d}^2F_1}{\mathrm{d}{Y_1}^2} = f_0''(0), \tag{B.1.100}$$

$$\frac{m_1}{{n_1}^2}\frac{\mathrm{d}^2T_1}{\mathrm{d}{Y_1}^2} + \frac{m_1 l_1}{n_1}F_1\frac{\mathrm{d}T_1}{\mathrm{d}Y_1} = 0, \tag{B.1.101}$$

subject to the boundary conditions

$$\text{on } Y_1 = 0: \quad F_1 = \frac{\mathrm{d}F_1}{\mathrm{d}Y_1} = 0, \quad T_1 = 0, \tag{B.1.102}$$

$$\text{as } Y_1 \to \infty: \quad m_1 T_1 \to 1, \tag{B.1.103}$$

and that F_1 matches to f when $y = \mathcal{O}(1)$. Now it is clear that $m_1 = \beta^{-1}$ but the choice for the other scales is not yet obvious. So in this region we have

$$\frac{\mathrm{d}^2F_1}{\mathrm{d}{Y_1}^2} = f_0''(0)\mathrm{e}^{-T_1}, \tag{B.1.104}$$

$$\frac{\mathrm{d}^2T_1}{\mathrm{d}{Y_1}^2} + n_1 l_1 F_1\frac{\mathrm{d}T_1}{\mathrm{d}Y_1} = 0, \tag{B.1.105}$$

with the corresponding boundary conditions (B.1.102–B.1.103) and the relation

$$l_1 = \frac{{n_1}^2}{\mu_0}. \tag{B.1.106}$$

Now, if we assume that $n_1 l_1 \ll 1$ then

$$T_1 = c_1 Y_1 + c_0 \tag{B.1.107}$$

and then using (B.1.102) together with (B.1.104) gives

$$F_1 = \frac{f_0''(0)}{{c_1}^2}\mathrm{e}^{-a_1 Y_1} + \frac{f_0''(0)}{c_1}Y_1 - \frac{f_0''(0)}{{c_1}^2}, \quad T_1 = c_1 Y_1 \tag{B.1.108}$$

in this near wall region.

Now when $T_1 = \mathcal{O}(\beta)$, T will experience $\mathcal{O}(1)$ changes and so we must rescale. Letting

$$F_1 = l_2 F_2, \quad T_1 = m_2 T_2, \quad Y_1 = n_2 Y_2, \qquad (F_2, T_2, Y_2 = \mathcal{O}(1))$$

we find that we need $m_2 = \beta$ so that $T_2 = \mathcal{O}(1)$. Substituting these scalings into

(B.1.108) yields $l_2 = m_2 = n_2 = \beta$ and so in this second region

$$\frac{\mathrm{d}^2 F_2}{\mathrm{d}Y_2{}^2} = 0 + \mathcal{O}\left(\beta^2 \exp -a_1 \beta Y_2\right), \tag{B.1.109}$$

$$\frac{\mathrm{d}^2 T_2}{\mathrm{d}Y_2{}^2} + \beta^2 l_1 n_1 F_2 \frac{\mathrm{d}T_2}{\mathrm{d}Y_2} = 0, \tag{B.1.110}$$

with the boundary conditions

$$\text{as } Y_2 \to 0\text{:} \quad F_2 \text{ matches to } F_1, \quad T_2 \to 0, \tag{B.1.111}$$

$$\text{as } Y_2 \to \infty\text{:} \quad F_2 \text{ matches to } f, \quad T_2 \to 1. \tag{B.1.112}$$

Now, as $T_2 = \mathcal{O}(1)$ we must have that $\beta^2 l_1 n_1 = 1$ and together with (B.1.106) we can now determine the scalings in these two regions to be

$$l_1 = \mu_0^{-\frac{1}{3}} \beta^{-\frac{4}{3}}, \quad m_1 = \beta^{-1}, \quad n_1 = \mu_0^{\frac{1}{3}} \beta^{-\frac{2}{3}}, \tag{B.1.113}$$

$$l_2 = m_2 = n_2 = \beta. \tag{B.1.114}$$

Hence we have that

$$\frac{\mathrm{d}^2 F_2}{\mathrm{d}Y_2{}^2} = 0, \tag{B.1.115}$$

$$\frac{\mathrm{d}^2 T_2}{\mathrm{d}Y_2{}^2} + F_2 \frac{\mathrm{d}T_2}{\mathrm{d}Y_2} = 0. \tag{B.1.116}$$

Solving the F_2 equation subject to the matching condition (B.1.111) gives

$$F_2 = c_4 Y_2 = \frac{f_0''(0)}{c_1} Y_2. \tag{B.1.117}$$

Substituting this into the the T_2 equation then gives

$$T_2(Y_2) = A \int_{\infty}^{Y_2} \exp\left\{-\frac{f_0''(0)}{2c_1} s^2\right\} \mathrm{d}s + c_7. \tag{B.1.118}$$

We now need to match the behaviour of T_2 to that of T_1 in the Y_1 region and to that of the core flow;

$$\text{as } Y_2 \to \infty,\ T_2 \to 1: \quad \Rightarrow c_7 = 1, \tag{B.1.119}$$

$$\text{as } Y_2 \to 0,\ T_2 \to 0: \quad 1 - A \int_0^{\infty} \exp\left\{-\frac{f_0''(0)}{2c_1} s^2\right\} \mathrm{d}s = 0, \Rightarrow A = \sqrt{\frac{2 f_0''(0)}{c_1 \pi}} \tag{B.1.120}$$

However, we now need to determine the remaining constant c_1. Let us introduce the coordinate $\tilde{Y}$ in the matching region in the following manner

$$Y_1 = \beta^{\alpha}\tilde{Y}, \quad Y_2 = \beta^{\alpha-1}\tilde{Y}, \qquad \left(0 < \alpha < 1,\, \tilde{Y} = \mathcal{O}(1)\right). \tag{B.1.121}$$

Expressing T_1 and T_2 in the intermediate variable $\tilde{Y}$ gives

$$\begin{aligned}
T_1(Y_1) = T_1(\beta^{\alpha}\tilde{Y}) &= c_1\beta^{\alpha}\tilde{Y} \\
\beta T_2(Y_2) = \beta T_2(\beta^{\alpha-1}\tilde{Y}) &= \beta\left\{1 - \sqrt{\frac{2f_0''(0)}{c_1\pi}}\int_{\beta^{\alpha-1}\tilde{Y}}^{\infty}\exp\left\{-\frac{f_0''(0)}{2c_1}s^2\right\}\mathrm{d}s\right\} \\
&= \beta\left\{1 - \sqrt{\frac{2f_0''(0)}{c_1\pi}}\left(\int_0^{\infty} - \int_0^{\beta^{\alpha-1}\tilde{Y}}\exp\left\{-\frac{f_0''(0)}{2c_1}s^2\right\}\mathrm{d}s\right)\right\} \\
&= \beta\left\{1 - \sqrt{\frac{4}{\pi}}\left(\int_0^{\infty} - \int_0^{\sqrt{\frac{f_0''(0)}{2c_1}}\beta^{\alpha-1}\tilde{Y}}\exp\left(-t^2\right)\mathrm{d}t\right)\right\} \\
&= \beta\left\{1 - 1 + \sqrt{\frac{4}{\pi}}\int_0^{\sqrt{\frac{f_0''(0)}{2c_1}}\beta^{\alpha-1}\tilde{Y}}\exp\left(-t^2\right)\mathrm{d}t\right\} \\
&= \beta\sqrt{\frac{4}{\pi}}\int_0^{\sqrt{\frac{f_0''(0)}{2c_1}}\beta^{\alpha-1}\tilde{Y}}\left(1 - t^2 + \mathcal{O}\left(t^4\right)\right)\mathrm{d}t \\
&= \sqrt{\frac{2f_0''(0)}{c_1\pi}}\beta^{\alpha}\tilde{Y} + \mathcal{O}\left(\beta^{3\alpha-2}\right).
\end{aligned}$$

For matching to occur we require that

$$c_1 = \sqrt{\frac{2f_0''(0)}{c_1\pi}} \quad \therefore c_1 = \left(\frac{2f_0''(0)}{\pi}\right)^{\frac{1}{3}} \quad \Rightarrow A = c_1 \quad \text{(by (B.1.120))}. \tag{B.1.122}$$

We now need a third region to match the behaviour of F_2 to that of the outer flow. In this third region we have that $T = o(1)$. Let

$$F = l_3F_3, \quad Y = n_3Y_3, \qquad (F_3, Y_3 = \mathcal{O}(1))$$

and then we may integrate (B.1.82) to obtain

$$F \sim \frac{1}{2}f_0''(0)Y^2 + c_8Y + c_9 \quad \Rightarrow l_3F_3 \sim \frac{1}{2}f_0''(0){n_3}^2{Y_3}^2 + c_8n_3Y_3 + c_9. \tag{B.1.123}$$

We want to have the quadratic and linear terms and that $F_3 = \mathcal{O}(1)$ to lowest order. Thus, as

$$\frac{l_3}{l_1 l_2} F_3 \sim \frac{1}{2} f_0''(0) \left(\frac{n_3}{n_1 n_2} \right)^2 Y_3^2 + c_8 \frac{n_3}{n_1 n_2} Y_3 + c_9, \tag{B.1.124}$$

$$\text{and} \quad l_3 = n_3^2, \tag{B.1.125}$$

we find that we must satisfy

$$\frac{n_3}{n_1 n_2} = \frac{n_3^2}{l_1 l_2} \tag{B.1.126}$$

giving

$$l_3 = \mu_0^{-\frac{4}{3}} \beta^{-\frac{4}{3}}, \quad n_3 = \mu_0^{-\frac{2}{3}} \beta^{-\frac{2}{3}}. \tag{B.1.127}$$

The scalings in the third region are

$$F_2 = \frac{l_3}{l_1 l_2} F_3 = \frac{1}{\mu_0 \beta} F_3, \quad Y_2 = \frac{n_3}{n_1 n_2} Y_3 = \frac{1}{\mu_0 \beta} Y_3, \tag{B.1.128}$$

with the constants

$$c_8 = \frac{f_0''(0)}{c_1}, \quad c_9 = 0,$$

and so we have

$$F_3 = \frac{1}{2} f_0''(0) {Y_3}^2 + \frac{f_0''(0)}{c_1} (\mu_0 \beta)^{\frac{2}{3}} Y_3. \tag{B.1.129}$$

Figure B.1.4 summarises the structure of the boundary layer in this case.

B.1.3 $\mathrm{Pe} \gg 1, \mathrm{Re} \gg 1$

This combination of nondimensional groups corresponds to the case where the channel height is much less than its length, and that the inertial effects are more important than the viscous effects. Beginning with the nondimensional governing equations (B.0.4a–B.0.4c) we choose $P = \mathrm{Pe}^2$ and, seeking the same form of similarity solution as in §B.1.2, we obtain the system

$$\frac{1}{\mathrm{Re}} \frac{\mathrm{d}^2}{\mathrm{d}y^2} \left(\mu \frac{\mathrm{d}^2 f}{\mathrm{d}y^2} \right) = \frac{\mathrm{d}}{\mathrm{d}y} \left(\left(\frac{\mathrm{d}f}{\mathrm{d}y} \right)^2 - f \frac{\mathrm{d}^2 f}{\mathrm{d}y^2} \right), \tag{B.1.130}$$

$$\frac{1}{\mathrm{Pe}} \frac{\mathrm{d}^2 T}{\mathrm{d}y^2} + f \frac{\mathrm{d}T}{\mathrm{d}y} = 0, \tag{B.1.131}$$

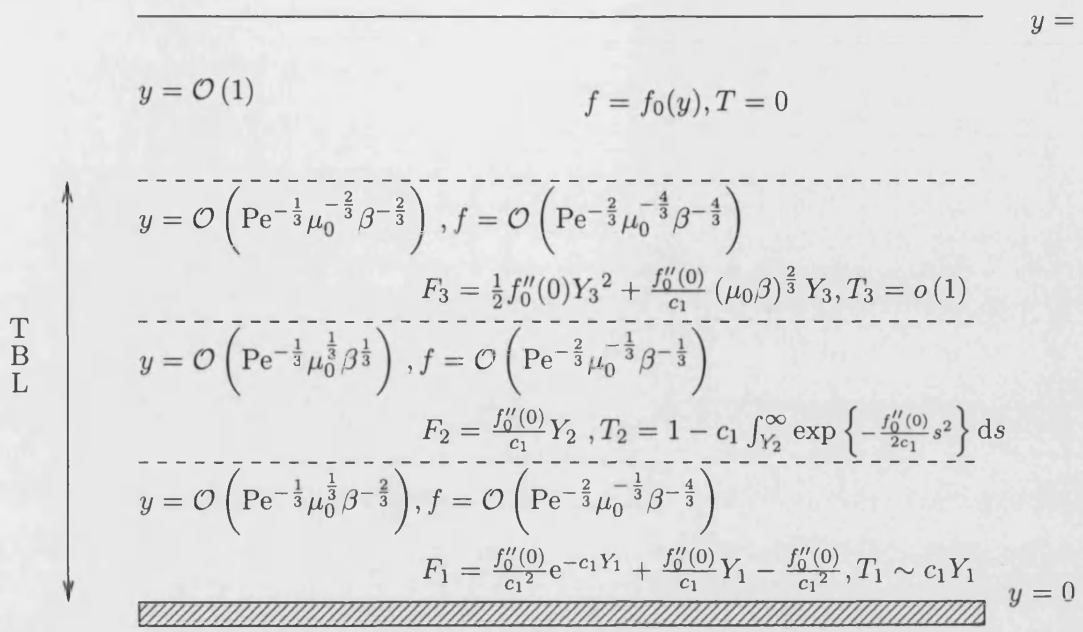

Figure B.1.4. Thermal boundary layer (TBL) structure for $\mathrm{Pe} \gg 1$, $\mathrm{Re} = \mathcal{O}(1)$ in the exponential viscosity case where $c_1 = \left(\frac{2f_0''(0)}{\pi}\right)^{\frac{1}{3}}$.

subject to

$$\text{on } y = 0: \quad T = 1, \quad f = 0, \quad \frac{\mathrm{d}f}{\mathrm{d}y} = 0, \tag{B.1.132}$$

$$\text{on } y = 1: \quad T = 0, \quad f = 1, \quad \frac{\mathrm{d}f}{\mathrm{d}y} = 0. \tag{B.1.133}$$

Let us first consider an outer region in which $f = f_0 + \mathcal{O}\left(\frac{1}{\mathrm{Pe}}\right)$. In this region, $T = 0$, $\mu = 1$ and we have that

$$\frac{\mathrm{d}}{\mathrm{d}y}\left(\left(\frac{\mathrm{d}f_0}{\mathrm{d}y}\right)^2 - f_0\frac{\mathrm{d}^2f_0}{\mathrm{d}y^2}\right) = 0 + \mathcal{O}\left(\frac{1}{\mathrm{Re}}\right), \tag{B.1.134}$$

subject to

$$\text{on } y = 1: \qquad f_0 = 1, \quad \frac{\mathrm{d}f_0}{\mathrm{d}y} = 0. \tag{B.1.135}$$

One solution of this is

$$f_0(y) = \sin\left(\frac{\pi}{2}y\right). \tag{B.1.136}$$

We now require thermal and viscous boundary layers as we have not been able to satisfy the boundary conditions at the lower wall. It is possible that the boundary layer structures depend upon the size of the nondimensional Prandtl number, which is defined by $\mathrm{Pr} = \frac{\mathrm{Pe}}{\mathrm{Re}}$. We must consider three cases ($\mathrm{Pr} \ll 1, \mathrm{Pr} = \mathcal{O}(1), \mathrm{Pr} \gg 1$) and within each of these both forms of viscosity function can be investigated separately.

$\mathrm{Pr} \ll 1$, Algebraic viscosity

Introducing the rescalings

$$f = aF, \quad y = bY, \qquad (F, Y = \mathcal{O}(1))$$

into (B.1.130–B.1.133) yields

$$\frac{a^2}{b^3}\frac{\mathrm{d}}{\mathrm{d}Y}\left(\left(\frac{\mathrm{d}F}{\mathrm{d}Y}\right)^2 - F\frac{\mathrm{d}^2F}{\mathrm{d}Y^2}\right) = \frac{1}{\mathrm{Re}}\frac{a}{b^4}\frac{\mathrm{d}^2}{\mathrm{d}Y^2}\left(\mu\frac{\mathrm{d}^2F}{\mathrm{d}Y^2}\right), \tag{B.1.137}$$

$$\frac{1}{\mathrm{Pe}}\frac{1}{b^2}\frac{\mathrm{d}^2T}{\mathrm{d}Y^2} + \frac{a}{b}F\frac{\mathrm{d}T}{\mathrm{d}Y} = 0, \tag{B.1.138}$$

$$\text{on } Y = 0: \quad T = 1, \quad F = 0, \quad \frac{\mathrm{d}F}{\mathrm{d}Y} = 0, \tag{B.1.139}$$

$$\text{as } Y \to \infty: \quad T \to 0, \quad aF \sim \frac{\pi}{2}bY. \tag{B.1.140}$$

We must have $a = b$ for the asymptotic behaviour of F to be satisfied. Now, as the relative sizes of the nondimensional groups are $1 \gg \frac{1}{\mathrm{Pe}} \gg \frac{1}{\mathrm{Re}}$, we will have a thermal boundary layer and in addition a viscous boundary layer that is contained within the thermal boundary layer.

In the thermal boundary layer we will want to solve the full temperature equation. This forces us to take $a = b = \mathrm{Pe}^{-\frac{1}{2}}$ and so the scalings in this boundary layer are

$$f = \mathrm{Pe}^{-\frac{1}{2}}F, \quad y = \mathrm{Pe}^{-\frac{1}{2}}Y \tag{B.1.141}$$

and so we are solving the system

$$\frac{\mathrm{d}}{\mathrm{d}Y}\left(\left(\frac{\mathrm{d}F}{\mathrm{d}Y}\right)^2 - F\frac{\mathrm{d}^2F}{\mathrm{d}Y^2}\right) = \mathrm{Pr}\frac{\mathrm{d}^2}{\mathrm{d}Y^2}\left(\mu\frac{\mathrm{d}^2F}{\mathrm{d}Y^2}\right), \tag{B.1.142}$$

$$\frac{\mathrm{d}^2T}{\mathrm{d}Y^2} + F\frac{\mathrm{d}T}{\mathrm{d}Y} = 0, \tag{B.1.143}$$

$$\text{on } Y = 0: \quad T = 1, \quad F = 0, \quad \frac{\mathrm{d}F}{\mathrm{d}Y} = 0, \tag{B.1.144}$$

$$\text{as } Y \to \infty: \quad T \to 0, \quad F \sim \frac{\pi}{2}Y. \tag{B.1.145}$$

The F equation is such that the right-hand side is equal to zero to lowest order in Pr. This ordinary differential equation is satisfied by $F = \frac{\pi}{2}Y$ and the boundary conditions for F, except for the derivative condition, are satisfied. We will need a viscous boundary layer to correct the behaviour accordingly.

As we are now taking $F = \frac{\pi}{2}Y$ we only have to satisfy (B.1.143). The temperature dependent viscosity no longer occurs in (B.1.142) and so, to lowest order, (B.1.142) is consistent in the limit $\beta \to \infty$ without having to introduce μ_0. The solution of (B.1.143–B.1.145) is thus given by

$$T = \operatorname{erfc}\left(\frac{\sqrt{\pi}}{2}Y\right). \tag{B.1.146}$$

We now want to satisfy the F conditions at the wall and so must rescale to obtain the correct viscous boundary layer equations. In particular we want to retain the $\mathcal{O}(\mathrm{Pr})$ term. Using the scalings

$$F = a_1 F_1, \quad Y = b_1 Y_1 \qquad (F_1, Y_1 = \mathcal{O}(1))$$

in (B.1.142–B.1.145) we obtain that

$$\frac{\mathrm{d}}{\mathrm{d}Y_1}\left(\left(\frac{\mathrm{d}F_1}{\mathrm{d}Y_1}\right)^2 - F_1\frac{\mathrm{d}^2F_1}{\mathrm{d}{Y_1}^2}\right) = \frac{\mathrm{Pr}}{a_1 b_1}\frac{\mathrm{d}^2}{\mathrm{d}{Y_1}^2}\left(\mu\frac{\mathrm{d}^2F_1}{\mathrm{d}{Y_1}^2}\right), \tag{B.1.147}$$

$$\frac{1}{a_1 b_1}\frac{\mathrm{d}^2T}{\mathrm{d}{Y_1}^2} + F_1\frac{\mathrm{d}T}{\mathrm{d}Y_1} = 0, \tag{B.1.148}$$

$$\text{on } Y_1 = 0: \quad T = 1, \quad F_1 = 0, \quad \frac{\mathrm{d}F_1}{\mathrm{d}Y_1} = 0, \tag{B.1.149}$$

$$\text{as } Y_1 \to \infty: \quad T, F_1 \text{ match to } T, F \text{ when } Y = \mathcal{O}(1). \tag{B.1.150}$$

To recover the full F_1 equation we must take $a_1 b_1 = \mathrm{Pr}$ and if F_1 is to match to F then we need $a_1 = b_1$. Therefore the viscous boundary layer scalings are

$$F = \mathrm{Pr}^{\frac{1}{2}}F_1, \quad Y = \mathrm{Pr}^{\frac{1}{2}}Y_1 \tag{B.1.151}$$

and the system to be solved is now

$$\frac{\mathrm{d}}{\mathrm{d}Y_1}\left(\left(\frac{\mathrm{d}F_1}{\mathrm{d}Y_1}\right)^2 - F_1\frac{\mathrm{d}^2F_1}{\mathrm{d}{Y_1}^2}\right) = \frac{\mathrm{d}^2}{\mathrm{d}{Y_1}^2}\left(\mu\frac{\mathrm{d}^2F_1}{\mathrm{d}{Y_1}^2}\right), \tag{B.1.152}$$

$$\frac{1}{\mathrm{Pr}}\frac{\mathrm{d}^2T}{\mathrm{d}{Y_1}^2} + F_1\frac{\mathrm{d}T}{\mathrm{d}Y_1} = 0, \tag{B.1.153}$$

$$\text{on } Y_1 = 0: \quad T = 1, \quad F_1 = 0, \quad \frac{\mathrm{d}F_1}{\mathrm{d}Y_1} = 0, \tag{B.1.154}$$

$$\text{as } Y_1 \to \infty: \quad T, F_1 \text{ match to } T, F \text{ when } Y = \mathcal{O}(1). \tag{B.1.155}$$

As we are interested in the large β limit another rescaling must be performed so that the behaviour of μ is consistent. Using

$$F_1 = a_2F_2, \quad Y_1 = b_2Y_2 \qquad (F_2, Y_2 = \mathcal{O}(1))$$

in (B.1.152–B.1.155) we find that we need $a_2 = b_2 = \mu_0^{\frac{1}{2}}$. The rescalings are now

$$F_1 = \mu_0^{\frac{1}{2}}F_2, \quad Y_1 = \mu_0^{\frac{1}{2}}Y_2 \tag{B.1.156}$$

and the system to be solved is

$$\frac{\mathrm{d}}{\mathrm{d}Y_2}\left(\left(\frac{\mathrm{d}F_2}{\mathrm{d}Y_2}\right)^2 - F_2\frac{\mathrm{d}^2F_2}{\mathrm{d}{Y_2}^2}\right) = \frac{\mathrm{d}^2}{\mathrm{d}{Y_2}^2}\left(\frac{\mu}{\mu_0}\frac{\mathrm{d}^2F_2}{\mathrm{d}{Y_2}^2}\right), \tag{B.1.157}$$

$$\frac{1}{\mu_0}\frac{1}{\mathrm{Pr}}\frac{\mathrm{d}^2T}{\mathrm{d}{Y_2}^2} + F_2\frac{\mathrm{d}T}{\mathrm{d}Y_2} = 0, \tag{B.1.158}$$

$$\text{on } Y_2 = 0: \quad T = 1, \quad F_2 = 0, \quad \frac{\mathrm{d}F_2}{\mathrm{d}Y_2} = 0, \tag{B.1.159}$$

$$\text{as } Y_2 \to \infty: \quad T, F_2 \text{ match to } T, F \text{ when } Y = \mathcal{O}(1). \tag{B.1.160}$$

The temperature T is fixed by the condition that it must match to the value in the thermal boundary layer and so in this region we have that $T = 1$. Thus (B.1.158) is satisfied and so we are concerned with (B.1.157) and the conditions upon F_2 in (B.1.159) and (B.1.160) only.

We may integrate the differential equation once with respect to Y_2; using the asymptotic behaviour to determine the integration constant and the fact that $\mu = \mu_0$ it

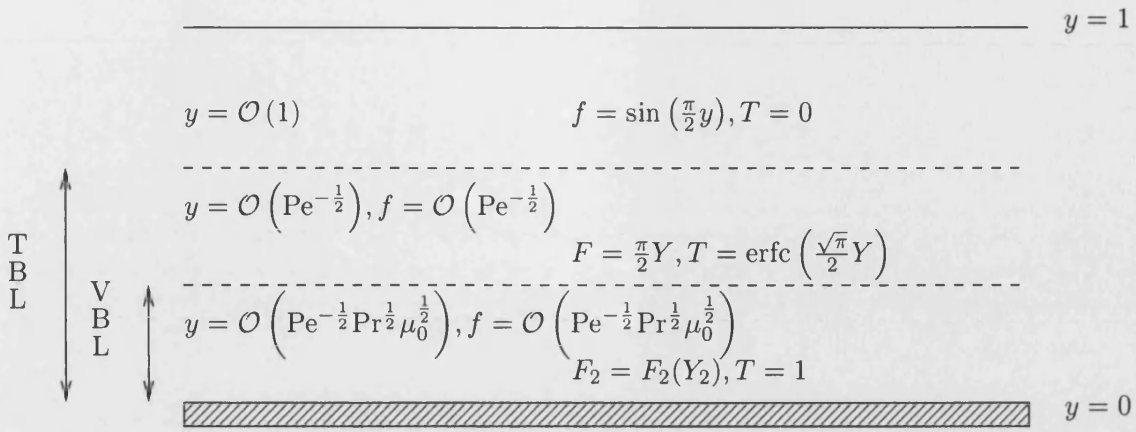

Figure B.1.5. Viscous (VBL) and thermal (TBL) boundary layer structure for Pe $\gg$ 1, Re $\gg$ 1, Pr $\ll$ 1 in the algebraic viscosity case. The TBL is of size $\mathcal{O}\left(\mathrm{Pe}^{-1/2}\right)$ and the smaller VBL is of size $\mathcal{O}\left(\mathrm{Pe}^{-1/2}\mathrm{Pr}^{1/2}\mu_0^{1/2}\right)$.

remains to find the solution of

$$\frac{\mathrm{d}^3F_2}{\mathrm{d}{Y_2}^3} = \left(\frac{\mathrm{d}F_2}{\mathrm{d}Y_2}\right)^2 - F_2\frac{\mathrm{d}^2F_2}{\mathrm{d}{Y_2}^2} - \frac{\pi^2}{4}, \tag{B.1.161}$$

$$\text{on } Y_2 = 0: \quad F_2 = 0, \quad \frac{\mathrm{d}F_2}{\mathrm{d}Y_2} = 0, \tag{B.1.162}$$

$$\text{as } Y_2 \to \infty: \quad F_2 \sim \frac{\pi}{2}Y_2. \tag{B.1.163}$$

Figure B.1.5 illustrates the structure of the boundary layers in this regime.

Pr $= \mathcal{O}(1)$, Algebraic viscosity

We are considering the (B.1.130–B.1.133) and wish to find the appropriate boundary layer equations in this case. Let

$$f = aF, \quad y = bY \qquad (F, Y = \mathcal{O}(1))$$

giving

$$\frac{a^2}{b^3}\frac{\mathrm{d}}{\mathrm{d}Y}\left(\left(\frac{\mathrm{d}F}{\mathrm{d}Y}\right)^2 - F\frac{\mathrm{d}^2F}{\mathrm{d}Y^2}\right) = \frac{a}{b^4}\frac{1}{\mathrm{Re}}\frac{\mathrm{d}^2}{\mathrm{d}Y^2}\left(\mu\frac{\mathrm{d}^2F}{\mathrm{d}Y^2}\right), \tag{B.1.164}$$

$$\frac{1}{\mathrm{Pe}}\frac{1}{b^2}\frac{\mathrm{d}^2T}{\mathrm{d}Y^2} + \frac{a}{b}F\frac{\mathrm{d}T}{\mathrm{d}Y} = 0, \tag{B.1.165}$$

subject to the conditions

$$\text{on } Y = 0: \quad T = 1, \quad F = 0 \quad F' = 0, \tag{B.1.166}$$

$$\text{as } Y \to \infty: \quad T \to 0, \quad aF \sim \frac{\pi}{2} bY. \tag{B.1.167}$$

The matching condition for F as $Y \to \infty$ has been determined by considering the Taylor expansion of the solution in the main region, $f(y) = \sin\left(\frac{\pi}{2}y\right)$, for small y. This also provides one condition upon the scalings, namely $a = b$. The second condition is that we need $ab\mathrm{Pe} = 1$. Therefore, the scalings for the boundary layer are

$$f = \mathrm{Pe}^{-\frac{1}{2}} F, \quad y = \mathrm{Pe}^{-\frac{1}{2}} Y \tag{B.1.168}$$

giving the boundary layer equations as

$$\frac{\mathrm{d}}{\mathrm{d}Y}\left(\left(\frac{\mathrm{d}F}{\mathrm{d}Y}\right)^2 - F\frac{\mathrm{d}^2F}{\mathrm{d}Y^2}\right) = \mathrm{Pr}\frac{\mathrm{d}^2}{\mathrm{d}Y^2}\left(\mu\frac{\mathrm{d}^2F}{\mathrm{d}Y^2}\right), \tag{B.1.169}$$

$$\frac{\mathrm{d}^2T}{\mathrm{d}Y^2} + F\frac{\mathrm{d}T}{\mathrm{d}Y} = 0, \tag{B.1.170}$$

subject to the conditions

$$\text{on } Y = 0: \quad T = 1, \quad F = 0 \quad F' = 0, \tag{B.1.171}$$

$$\text{as } Y \to \infty: \quad T \to 0, \quad F \sim \frac{\pi}{2} Y. \tag{B.1.172}$$

As $F = \pi Y/2$ satisfies the F equation, there is no need to introduce μ_0 at this time. However, the behaviour of F does not satisfy all of the wall boundary conditions; this will be corrected in a region closer to the wall. In spite of this, this means that we obtain the solution

$$T = \mathrm{erfc}\left(\sqrt{\frac{\pi}{4}} Y\right) \tag{B.1.173}$$

in this region.

We now need a region near the wall where we can obtain the correct behaviour for F. Introduce the scalings

$$F = a_1 F_1, \quad Y = b_1 Y_1, \quad T = c_1 T_1, \qquad (F_1, Y_1, T_1 = \mathcal{O}(1)).$$

In this region, $T_1 = 1$ and so $c_1 = 1$. To retain both terms in the F_1 equation we need to have $a_1 b_1 = \mu_0$ and in order to be able to match the F_1 behaviour to that of the F behaviour we require $a_1 = b_1$.

We have the following scalings in this near wall region

$$F = \mu_0^{\frac{1}{2}} F_1, \quad Y = \mu_0^{\frac{1}{2}} Y_1, \quad T = T_1, \tag{B.1.174}$$

and we must solve

$$\left(\frac{\mathrm{d}F_1}{\mathrm{d}Y_1}\right)^2 - F_1 \frac{\mathrm{d}^2 F_1}{\mathrm{d}{Y_1}^2} - \left(\frac{\pi}{2}\right)^2 = \mathrm{Pr} \frac{\mathrm{d}^3 F_1}{\mathrm{d}{Y_1}^3}, \tag{B.1.175}$$

subject to the conditions

$$\text{on } Y_1 = 0: \quad F_1 = 0 \quad F_1' = 0, \tag{B.1.176}$$

$$\text{as } Y_1 \to \infty: \quad F_1 \sim \frac{\pi}{2} Y_1. \tag{B.1.177}$$

It is possible to reduce this equation to one in which all the numbers are unity by means of the following transformation

$$\bar{Y} = \left(\frac{2\mathrm{Pr}}{\pi}\right)^{\frac{1}{2}} \eta, \quad \bar{F} = \left(\mathrm{Pr}\frac{\pi}{2}\right)^{\frac{1}{2}} G(\eta) \tag{B.1.178}$$

and then solve this numerically, i.e.

$$\frac{\mathrm{d}^3 G}{\mathrm{d}\eta^3} - \left(\frac{\mathrm{d}G}{\mathrm{d}\eta}\right)^2 - G\frac{\mathrm{d}^2 G}{\mathrm{d}\eta^2} = 1, \tag{B.1.179}$$

subject to

$$\text{on } \eta = 0: \quad G = 0, \quad \frac{\mathrm{d}G}{\mathrm{d}\eta} = 0, \tag{B.1.180}$$

$$\text{as } \eta \to \infty: \quad G \to \eta. \tag{B.1.181}$$

Figure B.1.6 illustrates the structure of the boundary layers in this regime.

Pr $\gg 1$, Algebraic viscosity

We introduce the rescalings

$$f = aF, \quad y = bY \qquad (F, Y = \mathcal{O}(1))$$

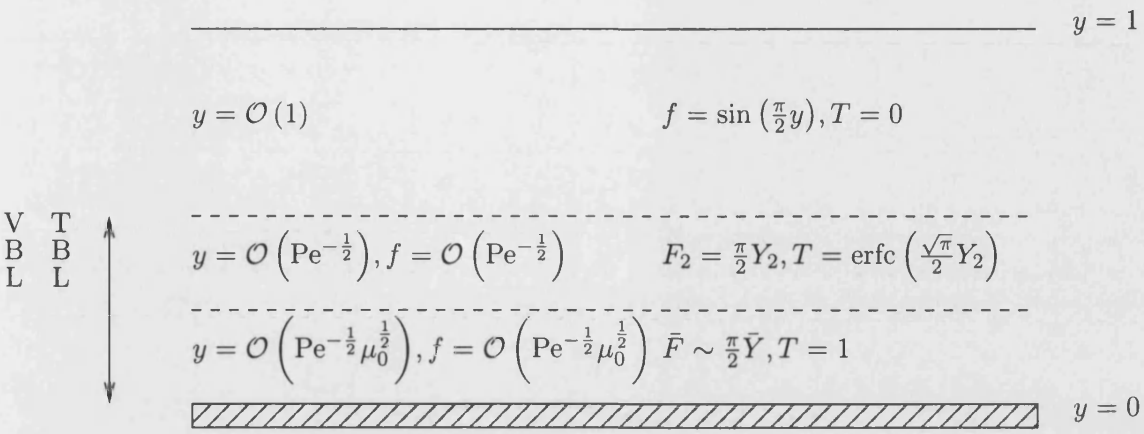

Figure B.1.6. Viscous (VBL) and thermal (TBL) boundary layer structure for Pe $\gg$ 1, Re $\gg$ 1, Pr $= \mathcal{O}(1)$ in the algebraic viscosity case. The layers are of comparable size in this case.

into (B.1.130–B.1.133) to get

$$\frac{a^2}{b^3}\frac{\mathrm{d}}{\mathrm{d}Y}\left(\left(\frac{\mathrm{d}F}{\mathrm{d}Y}\right)^2 - F\frac{\mathrm{d}^2F}{\mathrm{d}Y^2}\right) = \frac{a}{b^4}\frac{1}{\mathrm{Re}}\frac{\mathrm{d}^2}{\mathrm{d}Y^2}\left(\mu\frac{\mathrm{d}^2F}{\mathrm{d}Y^2}\right), \tag{B.1.182}$$

$$\frac{1}{\mathrm{Pe}}\frac{1}{b^2}\frac{\mathrm{d}^2T}{\mathrm{d}Y^2} + \frac{a}{b}F\frac{\mathrm{d}T}{\mathrm{d}Y} = 0, \tag{B.1.183}$$

subject to the conditions

$$\text{on } Y = 0: \quad T = 1, \quad F = 0 \quad F' = 0, \tag{B.1.184}$$

$$\text{as } Y \to \infty: \quad T \to 0, \quad aF \sim \frac{\pi}{2}bY. \tag{B.1.185}$$

In order to satisfy the asymptotic behaviour for F we must take $a = b$. As $1 \gg \frac{1}{\mathrm{Re}} \gg \frac{1}{\mathrm{Pe}}$ we expect to have a viscous boundary layer and then a thermal boundary layer contained within the viscous layer.

Within the viscous boundary layer we wish to retain the viscous term in the F equation and so this determines the viscous boundary layer scalings to be

$$f = \mathrm{Re}^{-\frac{1}{2}}F, \quad y = \mathrm{Re}^{-\frac{1}{2}}Y. \tag{B.1.186}$$

The system to be solved so far is

$$\frac{\mathrm{d}}{\mathrm{d}Y}\left(\left(\frac{\mathrm{d}F}{\mathrm{d}Y}\right)^2 - F\frac{\mathrm{d}^2F}{\mathrm{d}Y^2}\right) = \frac{\mathrm{d}^2}{\mathrm{d}Y^2}\left(\mu\frac{\mathrm{d}^2F}{\mathrm{d}Y^2}\right), \tag{B.1.187}$$

$$\frac{1}{\mathrm{Pr}}\frac{\mathrm{d}^2T}{\mathrm{d}Y^2} + F\frac{\mathrm{d}T}{\mathrm{d}Y} = 0, \tag{B.1.188}$$

subject to the conditions

$$\text{on } Y = 0: \quad T = 1, \quad F = 0 \quad \frac{\mathrm{d}F}{\mathrm{d}Y} = 0, \tag{B.1.189}$$

$$\text{as } Y \to \infty: \quad T \to 0, \quad F \sim \frac{\pi}{2}Y. \tag{B.1.190}$$

In order to prevent inconsistency in the $\beta \to \infty$ limit, a rescaling must be introduced into the F equation. Let us introduce the scalings

$$F = a_1F_1, \quad Y = b_1Y_1 \quad (F_1, Y_1 = \mathcal{O}(1))$$

and substituting them into the system of odes gives

$$\frac{a_1^2}{b_1^3}\frac{\mathrm{d}}{\mathrm{d}Y_1}\left(\left(\frac{\mathrm{d}F_1}{\mathrm{d}Y_1}\right)^2 - F_1\frac{\mathrm{d}^2F_1}{\mathrm{d}{Y_1}^2}\right) = \frac{a_1}{b_1^4}\frac{\mathrm{d}^2}{\mathrm{d}{Y_1}^2}\left(\mu\frac{\mathrm{d}^2F_1}{\mathrm{d}{Y_1}^2}\right), \tag{B.1.191}$$

$$\frac{1}{\mathrm{Pr}}\frac{1}{b_1^2}\frac{\mathrm{d}^2T}{\mathrm{d}Y^2} + \frac{a_1}{b_1}F\frac{\mathrm{d}T}{\mathrm{d}Y} = 0, \tag{B.1.192}$$

subject to the conditions

$$\text{on } Y_1 = 0: \quad T = 1, \quad F_1 = 0 \quad \frac{\mathrm{d}F_1}{\mathrm{d}Y_1} = 0, \tag{B.1.193}$$

$$\text{as } Y_1 \to \infty: \quad T \to 0, \quad a_1F_1 \sim \frac{\pi}{2}b_1Y_1. \tag{B.1.194}$$

Now if we wish to match the behaviour of F_1 as $Y_1 \to \infty$ then we must have $T = 0$ in this region (a thermal boundary layer will be required in order to satisfy the temperature boundary condition) and so $\mu = 1$ here[1]. Thus we will not need a μ_0 rescaling and so

$$F = F_1, \quad Y = Y_1 \tag{B.1.195}$$

[1] Alternatively, as $\frac{1}{\mathrm{Pr}} \ll 1$ we have that $\frac{1}{\mathrm{Pr}}\frac{\mathrm{d}^2T}{\mathrm{d}Y^2} = o(1)$. Then $F\frac{\mathrm{d}T}{\mathrm{d}Y} = 0$ and $F \neq 0$ which implies $T = 0$.

and we are then solving the differential equation

$$\frac{\mathrm{d}}{\mathrm{d}Y_1}\left(\left(\frac{\mathrm{d}F_1}{\mathrm{d}Y_1}\right)^2 - F_1\frac{\mathrm{d}^2F_1}{\mathrm{d}{Y_1}^2}\right) = \frac{\mathrm{d}^4F_1}{\mathrm{d}{Y_1}^4}, \tag{B.1.196}$$

with $T = 0$ and subject to the conditions

$$\text{on } Y_1 = 0: \quad F_1 = 0 \quad \frac{\mathrm{d}F_1}{\mathrm{d}Y_1} = 0, \tag{B.1.197}$$

$$\text{as } Y_1 \to \infty: \quad F_1 \sim \frac{\pi}{2}Y_1. \tag{B.1.198}$$

The viscous boundary layer is complemented by a thermal boundary layer which is contained within it. We wish to find the correct scalings for this region. Let

$$F_1 = a_2F_2, \quad Y_1 = b_2Y_2 \quad (F_2, Y_2 = \mathcal{O}(1))$$

and substitute this into (B.1.196–B.1.198) (with the reintroduction of μ and $T \neq 0$), giving

$$\frac{a_2^2}{b_2^3}\frac{\mathrm{d}}{\mathrm{d}Y_2}\left(\left(\frac{\mathrm{d}F_2}{\mathrm{d}Y_2}\right)^2 - F_2\frac{\mathrm{d}^2F_2}{\mathrm{d}{Y_2}^2}\right) = \frac{a_2}{b_2^4}\frac{\mathrm{d}^2}{\mathrm{d}{Y_2}^2}\left(\mu\frac{\mathrm{d}^2F_2}{\mathrm{d}{Y_2}^2}\right), \tag{B.1.199}$$

$$\frac{1}{\mathrm{Pr}}\frac{1}{b_2^2}\frac{\mathrm{d}^2T}{\mathrm{d}{Y_2}^2} + \frac{a_2}{b_2}F_2\frac{\mathrm{d}T}{\mathrm{d}Y_2} = 0, \tag{B.1.200}$$

subject to the conditions

$$\text{on } Y_2 = 0: \quad T = 1, \quad F_2 = 0 \quad \frac{\mathrm{d}F_2}{\mathrm{d}Y_2} = 0, \tag{B.1.201}$$

$$\text{as } Y_2 \to \infty: \quad T \text{ here matches to } T \text{ when } Y_1 = \mathcal{O}(\cdot), \tag{B.1.202}$$

$$F_2 \text{ matches to } F_1 \text{ when } Y_1 = \mathcal{O}(1).$$

If we perform a Taylor expansion of F_1 about $Y_1 = 0$ and then express it in terms of the new variables we obtain both a matching condition for $Y_2 \to \infty$ and a condition upon the boundary layer scales; namely that

$$a_2F_2 = \frac{1}{2}b_2^2Y_2^2\frac{\mathrm{d}^2F_1}{\mathrm{d}{Y_1}^2}(0), \tag{B.1.203}$$

and so $a_2 = b_2^2$.

We therefore have the following system

$$b_2^3 \frac{\mathrm{d}}{\mathrm{d}Y_2}\left(\left(\frac{\mathrm{d}F_2}{\mathrm{d}Y_2}\right)^2 - F_2\frac{\mathrm{d}^2F_2}{\mathrm{d}{Y_2}^2}\right) = \frac{\mathrm{d}^2}{\mathrm{d}{Y_2}^2}\left(\mu\frac{\mathrm{d}^2F_2}{\mathrm{d}{Y_2}^2}\right), \tag{B.1.204}$$

$$\frac{1}{\mathrm{Pr}}\frac{1}{b_2^2}\frac{\mathrm{d}^2T}{\mathrm{d}{Y_2}^2} + b_2F_2\frac{\mathrm{d}T}{\mathrm{d}Y_2} = 0, \tag{B.1.205}$$

subject to the conditions

$$\text{on } Y_2 = 0: \quad T = 1, \quad F_2 = 0 \quad \frac{\mathrm{d}F_2}{\mathrm{d}Y_2} = 0, \tag{B.1.206}$$

$$\text{as } Y_2 \to \infty: \quad T \text{ here matches to } T \text{ when } Y_1 = \mathcal{O}(1), \tag{B.1.207}$$

$$F_2 \sim \frac{1}{2}Y_2^2\frac{\mathrm{d}^2F_1}{\mathrm{d}{Y_1}^2}(0).$$

To retain both terms in the T equation we must take $b_2^3 = \frac{1}{\mathrm{Pr}}$, and so the thermal boundary layer scales are

$$F_1 = \mathrm{Pr}^{-\frac{1}{3}}F_2, \quad Y_1 = \mathrm{Pr}^{-\frac{2}{3}}Y_2. \tag{B.1.208}$$

The thermal boundary layer system of differential equations is

$$\frac{1}{\mathrm{Pr}}\frac{\mathrm{d}}{\mathrm{d}Y_2}\left(\left(\frac{\mathrm{d}F_2}{\mathrm{d}Y_2}\right)^2 - F_2\frac{\mathrm{d}^2F_2}{\mathrm{d}{Y_2}^2}\right) = \frac{\mathrm{d}^2}{\mathrm{d}{Y_2}^2}\left(\mu\frac{\mathrm{d}^2F_2}{\mathrm{d}{Y_2}^2}\right), \tag{B.1.209}$$

$$\frac{\mathrm{d}^2T}{\mathrm{d}{Y_2}^2} + F_2\frac{\mathrm{d}T}{\mathrm{d}Y_2} = 0, \tag{B.1.210}$$

subject to the conditions

$$\text{on } Y_2 = 0: \quad T = 1, \quad F_2 = 0 \quad \frac{\mathrm{d}F_2}{\mathrm{d}Y_2} = 0, \tag{B.1.211}$$

$$\text{as } Y_2 \to \infty: \quad T \to 0, \quad F_2 \sim \frac{1}{2}Y_2^2\frac{\mathrm{d}^2F_1}{\mathrm{d}{Y_1}^2}(0). \tag{B.1.212}$$

As the left hand side of (B.1.209) is small, we can replace it with zero to lowest order. We can now integrate the differential equation twice with respect to Y_2 and obtain the following equation, which replaces (B.1.209),

$$\mu\frac{\mathrm{d}^2F_2}{\mathrm{d}{Y_2}^2} = \frac{\mathrm{d}^2F_1}{\mathrm{d}{Y_1}^2}(0). \tag{B.1.213}$$

We must now introduce another rescaling to ensure consistency in the $\beta \to \infty$ limit.

Using the scalings

$$F_2 = a_3 F_3, \quad Y_2 = b_3 Y_3, \quad (F_3, Y_3 = \mathcal{O}(1))$$

the system (B.1.210–B.1.212), (B.1.213) becomes

$$\mu \frac{a_3}{b_3^2} \frac{\mathrm{d}^2 F_3}{\mathrm{d}Y_3^2} = \frac{\mathrm{d}^2 F_1}{\mathrm{d}Y_1^2}(0), \tag{B.1.214}$$

$$\frac{1}{b_3^2} \frac{\mathrm{d}^2 T}{\mathrm{d}Y_3^2} + \frac{a_3}{b_3} F_3 \frac{\mathrm{d}T}{\mathrm{d}Y_3} = 0, \tag{B.1.215}$$

subject to the conditions

$$\text{on } Y_3 = 0: \quad T = 1, \quad F_3 = 0, \quad \frac{\mathrm{d}F_3}{\mathrm{d}Y_3} = 0, \tag{B.1.216}$$

$$\text{as } Y_3 \to \infty: \quad T \to 0, \quad a_3 F_3 \sim \frac{1}{2} b_3^2 Y_3^2 \frac{\mathrm{d}^2 F_1}{\mathrm{d}Y_1^2}(0). \tag{B.1.217}$$

We need to take

$$\frac{a_3}{b_3^2} = \frac{1}{\mu_0}, \quad \frac{a_3}{b_3} = \frac{1}{b_3^2}$$

and this determines the scalings to be

$$F_2 = \mu_0^{-\frac{1}{3}} F_3, \quad Y_2 = \mu_0^{\frac{1}{3}} Y_3. \tag{B.1.218}$$

The thermal boundary layer system of differential equations, consistent in the limit $\beta \to \infty$, is

$$\frac{\mu}{\mu_0} \frac{\mathrm{d}^2 F_3}{\mathrm{d}Y_3^2} = \frac{\mathrm{d}^2 F_1}{\mathrm{d}Y_1^2}(0), \tag{B.1.219}$$

$$\frac{\mathrm{d}^2 T}{\mathrm{d}Y_3^2} + F_3 \frac{\mathrm{d}T}{\mathrm{d}Y_3} = 0, \tag{B.1.220}$$

subject to the conditions

$$\text{on } Y_3 = 0: \quad T = 1, \quad F_3 = 0, \quad \frac{\mathrm{d}F_3}{\mathrm{d}Y_3} = 0, \tag{B.1.221}$$

$$\text{as } Y_3 \to \infty: \quad T \to 0, \quad \mu_0^{-\frac{1}{3}} F_3 \sim \frac{1}{2} \mu_0^{\frac{2}{3}} Y_3^2 \frac{\mathrm{d}^2 F_1}{\mathrm{d}Y_1^2}(0). \tag{B.1.222}$$

We now consider the large β limit. As $Y_3 \to \infty$, $T \to 0$ and $\mu \to 1$; then (B.1.219)

gives the behaviour

$$\frac{\mathrm{d}^2F_3}{\mathrm{d}Y_3{}^2} \sim \mu_0 \frac{\mathrm{d}^2F_1}{\mathrm{d}Y_1{}^2}(0) \quad \therefore F_3 \sim d_1 Y_3 + \mathcal{O}(\mu_0) \quad \text{as } Y_3 \to \infty. \tag{B.1.223}$$

Substituting this behaviour into (B.1.220) and using the conditions (B.1.221) and (B.1.222) gives

$$T(Y_3) = \frac{2}{d_1\sqrt{\pi}} \operatorname{erfc}\left(\sqrt{\frac{d_1}{2}} Y_3\right) \tag{B.1.224}$$

which has the asymptotic behaviour

$$T \sim \frac{1}{\sqrt{2\pi d_1} Y_3} \mathrm{e}^{-\frac{d_1}{2}Y_3^2} \quad \text{as } Y_3 \to \infty. \tag{B.1.225}$$

The temperature behaviour now matches with that in the viscous boundary layer, but the flow behaviour fails to match with that in the viscous boundary layer. We require an intermediate layer in which it can be corrected. Introduce the scales

$$F_3 = a_4 F_4, \quad Y_3 = b_4 Y_4 \qquad (F_4, Y_4 = \mathcal{O}(1))$$

into (B.1.219–B.1.222). In this region, $T = o(1)$ and so $\mu \sim 1$. The system becomes

$$\frac{a_4}{b_4^2} \frac{\mathrm{d}^2F_4}{\mathrm{d}Y_4{}^2} = \mu_0 \frac{\mathrm{d}^2F_1}{\mathrm{d}Y_1{}^2}(0), \tag{B.1.226}$$

$$\frac{1}{b_4^2} \frac{\mathrm{d}^2T}{\mathrm{d}Y_4{}^2} + \frac{a_4}{b_4} F_4 \frac{\mathrm{d}T}{\mathrm{d}Y_4} = 0, \tag{B.1.227}$$

subject to the conditions

$$\begin{aligned} &\text{as } Y_4 \to 0: \quad F_4 \text{ matches to } F_3 \text{ when } Y_3 = \mathcal{O}(1), \\ &\qquad\qquad\quad T \text{ matches to } T \text{ when } Y_3 = \mathcal{O}(1), \end{aligned} \tag{B.1.228}$$

$$\begin{aligned} &\text{as } Y_4 \to \infty: \quad F_4 \text{ matches to } F_2 \text{ when } Y_2 = \mathcal{O}(1), \\ &\qquad\qquad\quad\ T \text{ matches to } T \text{ when } Y_2 = \mathcal{O}(1). \end{aligned} \tag{B.1.229}$$

The requirements upon T in this region fix $T = o(1)$. Thus $\mu \sim 1$ and so the T equation is satisfied. The F_4 matching conditions mean that

$$\begin{aligned} &\text{as } Y_4 \to 0: \quad F_4 \text{ matches to } F_3 \sim d_1 Y_3^2 + \frac{\mu_0}{2} \frac{\mathrm{d}^2F_1}{\mathrm{d}Y_1{}^2}(0) Y_3^2 \text{ when } Y_3 = \mathcal{O}(1). \\ &\text{as } Y_4 \to \infty: \quad F_4 \text{ matches to } F_1 \sim \frac{\pi}{2} Y_1 \text{ when } Y_1 = \mathcal{O}(1). \end{aligned}$$

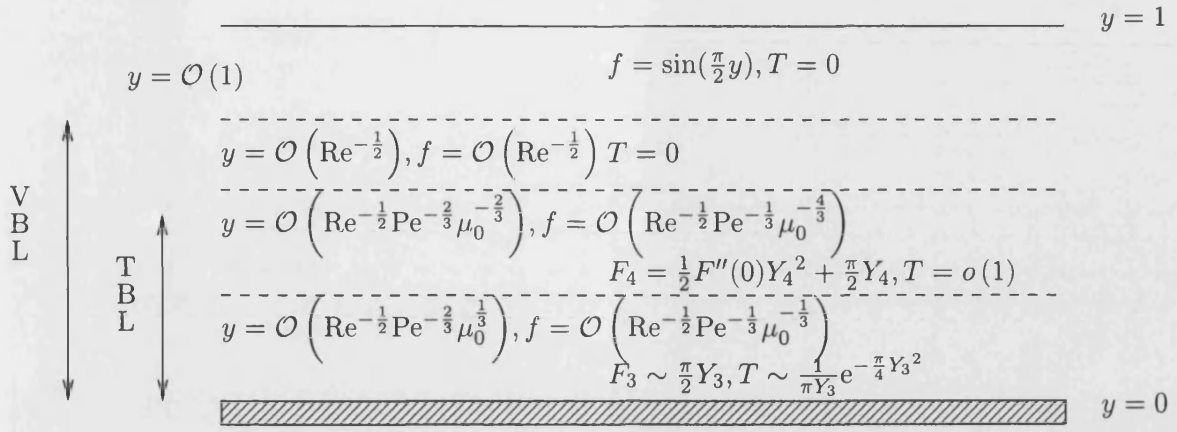

Figure B.1.7. Viscous (VBL) and thermal (TBL) boundary layer structure for Pe $\gg$ 1, Re $\gg$ 1, Pr $\gg$ 1 in the algebraic viscosity case. In this case the VBL is of size $\mathcal{O}\left(\mathrm{Re}^{-1/2}\right)$ and the thinner TBL is of size $\mathcal{O}\left(\mathrm{Re}^{-1/2}\mathrm{Pe}^{-2/3}\mu_0^{-2/3}\right)$.

This means that we must take $a_4 = \mu_0 b_4^2$ and $a_4 = b_4$, yielding the scales

$$F_3 = \frac{1}{\mu_0}F_4, \quad Y_3 = \frac{1}{\mu_0}Y_4. \tag{B.1.230}$$

In this transitory region, where $T = o(1)$, the differential equation to be solved is

$$\frac{\mathrm{d}^2 F_4}{\mathrm{d}{Y_4}^2} = \frac{\mathrm{d}^2 F_1}{\mathrm{d}{Y_1}^2}(0), \tag{B.1.231}$$

subject to the conditions

$$\text{as } Y_4 \to 0: \quad F_4 \text{ matches to } F_3 \text{ when } Y_3 = \mathcal{O}(1), \tag{B.1.232}$$

$$\text{as } Y_4 \to \infty: \quad F_4 \text{ matches to } F_1 \text{ when } Y_1 = \mathcal{O}(1). \tag{B.1.233}$$

This yields

$$F_4 = \frac{1}{2}\frac{\mathrm{d}^2 F_1}{\mathrm{d}{Y_1}^2}(0)Y_4^2 + d_5 Y_4 + d_6, \tag{B.1.234}$$

and matching to the prescribed behaviours determines the constants to be

$$d_5 = d_1 = \frac{\pi}{2}, \quad d_6 = 0.$$

Figure B.1.7 illustrates the structure of the boundary layers in this regime.

Bibliography

[BA81] J.F. Brady and A. Acrivos. Steady flow in a channel or tube with an accelerating surface velocity. An exact solution to the Navier-Stokes equations with reverse flow. *Journal of Fluid Mechanics*, 112:127-150, 1981.

[BAH87] R.B. Bird, R.C. Armstrong, and Ole Hassager. *Dynamics of Polymeric Liquids: Volume 1 - Fluid Mechanics.* Wiley, New York, 1987.

[Bat01] G. K. Batchelor. *An Introduction To Fluid Dynamics.* Cambridge University Press, Cambridge, 2001.

[Ber53] A.S. Berman. Laminar flow in channels with porous walls. *Journal of Applied Physics*, 24(9):1232–1235, 1953.

[Ber58] A.S. Berman. Laminar flow in an annulus with porous walls. *Journal of Applied Physics*, 29(1):71–75, 1958.

[BHW89] H.A. Barnes, J.F. Hutton, and K. Walters. *An Introduction to Rheology.* Rheology Series. Elsevier, Amsterdam, 1989.

[CK97] S.M. Cox and A.C. King. On the asymptotic solution of a high order nonlinear ordinary differential equation. *Proceedings of the Royal Society A*, 453:711–728, 1997.

[CK04] S.M. Cox and J.R. King. Large Reynolds number asymptotics of the Berman problem. *Studies In Applied Mathematics*, 3(113):217-243, 2004.

[CK05] S.M. Cox and J.R. King. Self-similar "stagnation point" boundary layer flows with suction or injection. *Studies In Applied Mathematics*, 115(1):73–107, 7 2005.

[Cox91a] S. Cox. Analysis of steady flow in channel with one porous wall or with accelerating walls. *SIAM Journal of Applied Mathematics*, 51:429–438, 1991.

[Cox91b] S.M. Cox. 2 dimensional flow of a viscous fluid in a channel with porous walls. *Journal of Fluid Mechanics*, 227:1–33, 1991.

[DB84] L. Durlofsky and J.F. Brady. The spatial stability of a class of similarity solutions. *Physics of Fluids*, 27(5):1068–1076, 1984.

[DD04] James P. Denier and Paul P. Dabrowski. On the boundary-layer equations for power-law fluids. *Proceedings of the Royal Society of London Series A*, 460:3143–3158, 2004.

[DM05] Chungtao Deng and D. Mark Martinez. Linear stability of a Berman flow in a channel partially filled with a porous medium. *Physics of Fluids*, 17(2), 2005.

[FG00] S. Ferro and G. Gnavi. Spatial stability of similarity solutions for viscous flows in channels with porous walls. *Physics of Fluids*, 12(4):797–802, 2000.

[FG02] S. Ferro and G. Gnavi. Effects of temperature dependent viscosity in channels with porous walls. *Physics of Fluids*, 14(2):839–849, 2002.

[HLM92] S.P. Hastings, C. Lu, and A.D. MacGillivray. A boundary value problem with multiple solutions from the theory of laminar flow. *SIAM Journal of Mathematical Analysis*, 32(1):201–208, 1992.

[KC01] J.R. King and S.M. Cox. Asymptotic analysis of the steady-state and time-dependent Berman problem. *Journal of Engineering Mathematics*, 39(1–4):87–130, 2001.

[LMH92] C. Lu, A.D. MacGillivray, and S.P. Hastings. Asymptotic behaviour of solutions of a similarity equation for laminar flow in channels with porous walls. *IMA Journal of Applied Mathematics*, 49:139–162, 1992.

[MD98] A. McAlpine and P.G. Drazin. On the spatio-temporal development of small perturbations of Jeffery-Hamel flows. *Fluid Dynamics Research*, 22:123–138, 1998.

[ML94] A.D. MacGillivray and C. Lu. Asymptotic solution of a laminar flow in a porous channel with large suction: a nonlinear turning point problem. *Methods and Applications of Analysis*, 1(2):229–248, 1994.

[Ock79] H. Ockendon. Channel flow with temperature-dependent viscosity and internal viscous dissipation. *Journal of Fluid Mechanics*, 93(4):737–746, 1979.

[OO77] H. Ockendon and J.R. Ockendon. Variable-viscosity flows in heated and cooled channels. *Journal of Fluid Mechanics*, 83(1):177–190, 1977.

[Rob76] W.A. Robinson. The existence of multiple solutions for the laminar flow in a uniformly porous channel with suction at both walls. *Journal of Engineering Mathematics*, 10(1):23–40, 1976.

[Sel55] J.R. Sellars. Laminar Flow in Channels with Porous Walls at High Suction Reynolds Numbers. *Journal of Applied Physics*, 26(4):489–490, 1955.

[Ste96] J.F. Steffe. *Rheological Methods in Food Process Engineering.* Freeman Press, East Lansing, MI 48823, USA, 2nd edition, 1996.

[SW78] Francis M. Skalak and Chang-Yi Wang. On the nonunique solutions of laminar flow through a porous tube or channel. *SIAM Journal of Applied Mathematics*, 34(3):535–544, 1978.

[Tan00] R.I. Tanner. *Engineering Rheology*, volume 52. Oxford University Press, Oxford, 2nd edition, 2000.

[TBZD91] C.L. Taylor, W.H.H. Banks, M.B. Zaturska, and P.G. Drazin. 3 dimensional flow in a porous channel. *Quarterly Journal of Mechanics and Applied Mathematics*, 44:105–133, 1991.

[Ter64] R.M. Terrill. Laminar flow in a Uniformly Porous Channel. *Aeronautical Quarterly*, 15:299–310, 1964.

[Ter65] R. M. Terrill. Laminar flow in a Uniformly Porous Channel with Large Injection. *Aeronautical Quarterly*, 16:323–332, 1965.

[Yua56] S.W. Yuan. Further Investigation of Laminar Flow in Channels with Porous Walls. *Journal of Applied Physics*, 27(3):267–269, 1956.

[ZB03] M.B. Zaturska and W.H.H. Banks. New solutions for flow in a channel with porous walls and/or non-rigid walls. *Fluid Dynamics Research*, 33(1-2):57–71, 2003.

[ZDB88] M.B. Zaturska, P.G. Drazin, and W.H.H. Banks. On the flow of a viscous fluid driven along a channel by suction at porous walls. *Fluid Dynamics Research*, 4(3):151–178, 1988.